



**Joined Thesis**  
From  
**The University of Lille & KU Leuven**

Dissertation presented in partial fulfilment of the requirements for the degree of:

**Doctor of Science: Chemistry**  
Sciences de la matière, du rayonnement et de l'environnement (SMRE)

**Doctor of Engineering Science (PhD): Chemical Engineering**  
Science, Engineering & Technology (Arenberg), Faculty of Engineering Science

**Michaël Lalanne-Tisé**

**Surface initiated organocatalyzed ring-opening polymerization as a tool for grafting polymers on nanocelluloses.**

**Polymérisation par ouverture de cycle organocatalysée initiée en surface comme outil de greffage de polymères sur nanocelluloses.**

Defended on the: 27/02/2023 in presence of the examination committee

**Chair:**

Mr Jean Berlamont, Emeritus Professor, KU Leuven (Belgium)

Mme Lydie Pelinski, Professor, Lille University (France)

**Referees:**

Ms Sophie Guillaume, Directrice de recherche, Rennes University (France)

Ms Gaëlle Morandi, Maître de conférences, Insa de Rouen Normandie (France)

**Examiners:**

Mr Louis Pitet, Assistant professor, Hasselt University (Belgium)

Ms Aurélie Taguet, Maître de conférences, Ecole des Mines d'Alès (France)

Mr Michiel Dusselier, Associate Professor, KU Leuven (Belgium)

**Direction:**

Mr Philippe Zinck, Professor, Lille University (France)

Mr Wim Thielemans, Professor, Ku Leuven (Belgium)

**Co-Direction:**

Ms Audrey Favrelle Huret, Maître de conférence, Lille University (France)





## Acknowledgement

I would like to first give my thanks to my supervising team: Prof. Wim Thielemans, Prof. Philippe Zinck, and Dr. Audrey Favrelle-Huret for their invaluable help over these last four years. Thank you Wim for your endless support, your kindness and your guidance, be it for scientific related things, handling a PhD, or future career perspective. Despite being quite busy, your door was always open and you have always found the right words to put an ease to whatever was troubling me. Many thanks to Philippe, for your never-failing availability in times of need, your teachings even in the lab, and for your continuous stream of advice and suggestions. You always had ideas regarding the work and I learned a lot about organic catalysis under your supervision. Lastly, thank you Audrey for your help, especially with teaching, and for your different perspective, and for being very thorough on reviewing my written work. I am glad they gave me the chance to work on this collaborative project, and the opportunity to work between different teams with different views helped me to broaden my appreciation for research.

My thanks also go to Dr. Sophie Guillaume and Dr. Gaëlle Morandi for accepting to be part of my thesis committee as referees, Dr. Louis Pitet, Pr. Dr. Michiel Dusselier, and Dr. Aurélie Taguet for their role as examiners, as well as Pr. Jean Berlamont and Pr. Lydie Pelinski for their role as chair during the first and second defense respectively. Thank you for giving your time to thoroughly examine my work and for your future feedback.

I would like to thank the Initiatives for Science, Innovation, Territories and Economy (I-SITE) Lille Nord – Europe for financially supporting this project over four years allowing it to become a joined PhD.

I would like to thank Prof. João P. Prates Ramalho for all of his work on the DFT. His contribution gave us a lot of insight on the some of the reactions and it was a great help. I hope we can someday meet in person in order to give you proper thanks.

Many thanks to Catarina who has been around during these last two years and has always been a great support and helped me through thick and thin, and has heard me rambling over countless hours at this point. I thank you for your patience, as much as I like to say you do not have much of it, and for all your advice, as you have never been one to shy away from listening and helping. You have been good company both in and out of the workplace, and while being friend with your

colleagues is certainly not a requirement to work, it sure made finishing all of this a lot easier. For your endless help, your time, and your presence in all situations, you have my deepest gratitude and appreciation. You have been a great colleague, and an even greater friend.

To all of my colleagues of the SusMat group: thank you for all of your help, especially throughout the first part of this work. I wish I had spent more time there during the second half of my PhD, but it was always pleasant to come there and interact with the group, you all have contributed to make campus Kulak a great work environment. I will definitely keep a lot of fond memories there, and team building time were always a blast. To Sam, thank you for being such a knowledgeable person and sharing it so willingly, for your help around the lab, and in particular for all of your help with the analyses throughout, I have learned a lot thanks to you. Thank you to Reeta as well who was a great help for a lot of things related to working with cellulose, which was quite new to me. Thank you to Maarten for introducing me to the topic and for some of his preliminary work which helped me get started. Elise, thank you for giving your time to run analyses for me and for answering all of my frequent inquiries regarding the state of the EA and TGA. Lastly, thank you to all the people in Kulak I have spent time with, and in particular those of you I shared an office with, you all made my stay nothing but enjoyable.

Thank you to all of my colleagues from UCCS, both past and present, that all have contributed in one way or another these last four years. Special thanks to Xavier, who despite joining the group late, I shared a lot of good memories with, and who was always down to help and to spend some quality time outside of the office. You have been a great source of support throughout this last year, and know that you will always find a friend in me shall you need my help. I hope we will cross paths again, which may be difficult considering you cannot stay in place for long. Another person I would like to thank is Kifah, who has also contributed greatly to making the atmosphere around our office a pleasant one for the amount of time mine and his stay overlapped. Lastly, I would also like to thank all of the other members of the group in C3, both past and present, with which I have spent a lot of time and shared the task of making sure everything in the lab runs smoothly. All of them have made working there fun and all of the help I have received there has been priceless.

Maja, thank you for your support over the last years, the distance has been a bit difficult to deal with at times but you have been there for support when I needed you regardless. Your

encouragement and belief in me have been very helpful and contributed greatly to keeping me going forward, and we both know looking at the future positively is not always my strong suit.

Lastly, I would like to thank my family, whose support has always been something I could rely on. To my parents, for which I know scientific research is foreign territory, I thank you for always encouraging me to pursue whatever I wanted to do, and giving me time to question myself when I needed to. Thank you to my sister as well, you certainly talk about your work more than I do, but you have always been a great moral support.

To all of the people I may have not mentioned by name here, know that your help over the last four years was not any less appreciated, and I have greatly enjoyed meeting and interacting with so many of you.

## Résumé

La cellulose, polysaccharide naturel le plus abondant, a connu un regain d'intérêt au cours du 21<sup>ème</sup> siècle grâce à la recherche d'alternatives aux matériaux issus de l'industrie pétrolière. En particulier, les nanoparticules de cellulose ont fait l'objet de beaucoup de travaux grâce à leurs propriétés prometteuses en tant que renfort pour les composites. Cependant, des étapes de modification sont souvent nécessaires afin de pouvoir utiliser la nanocellulose avec les matrices polymères les plus courantes à cause de problèmes d'incompatibilité et de dispersion du renfort nanocellulosique. Dans ce contexte, l'objectif des travaux présentés porte sur la modification de la nanocellulose par greffage de polymères d'intérêt tel que des polyesters et polycarbonates.

Le greffage de poly(lactide) sur des nanofibrilles de cellulose (NFC) a d'abord été étudié. Le « grafting from » par polymérisation par ouverture de cycle a été choisi et réalisé par organocatalyse, principalement avec la 4-diméthylaminopyridine (DMAP), une base organique. En effectuant la polymérisation du lactide initiée par les groupements hydroxyles en surface des NFC, l'influence des conditions de la réaction sur le taux de greffage de poly(lactide) sur la cellulose a pu être étudiée de façon quantitative, avec un maximum à 24% en masse, et une méthodologie a pu être établie. L'utilisation d'un catalyseur organique a permis une élimination facile de ce dernier, contrairement aux catalyseurs métalliques.

La deuxième partie des travaux effectués a porté sur le greffage de poly(triméthylène carbonate) sur des nanocristaux de cellulose (NCC), toujours par « grafting from » par polymérisation par ouverture de cycle organocatalysée. Dans un premier temps, une étude sur l'efficacité de différents catalyseurs organiques connus pour leur capacité à polymériser le triméthylène carbonate (TMC) a été conduite afin de déterminer le meilleur choix pour le greffage sur la cellulose. Suite à cette étude, la 1,5,7-triazabicyclo[4.4.0]dec-5-ène (TBD), une base organique, a été utilisée pour le reste de l'étude, et a permis l'obtention de matériaux composés jusqu'à 74% en masse de greffons dans des conditions douces. En plus d'être une valeur élevée pour ce type de greffage si l'on s'en réfère à la littérature, c'est aussi à notre connaissance le premier exemple de NCC possédant des greffons polycarbonate.

En parallèle, une étude théorique DFT a été menée en collaboration avec le professeur João P. Prates Ramalho (U. Evora, Portugal) pour élucider le mécanisme de polymérisation du TMC par différents catalyseurs. Cette étude a permis de montrer que le mécanisme par liaisons H avec

activation de l'alcool a une barrière d'activation bien plus basse qu'un mécanisme d'attaque nucléophile du catalyseur, confirmant les résultats expérimentaux obtenus.

Une autre collaboration a été réalisée avec un doctorant du laboratoire, Nouaamane El Idrissi, qui a pu produire des NCC possédant des groupements TBD greffés. Ceux-ci ont pu être utilisés en tant que catalyseurs supportés de polymérisation du TMC. Bien que la catalyse avec la TBD non-supportée semble plus rapide, la polymérisation du TMC par catalyse supportée sur NCC a fonctionné, avec toutefois un taux de greffage beaucoup plus faible.

Enfin, la dernière partie des travaux concerne le greffage de copolymères sur les NCC en utilisant la méthodologie développée auparavant avec la TBD comme organocatalyseur. En utilisant des NCC greffés poly(TMC) comme substrat de départ, une polymérisation par ouverture de cycle de différents esters cycliques a permis le greffage de blocs de différentes natures sur les NCC, ce qui est une première à notre connaissance. Des copolymères statistiques ont également pu être greffés en réalisant une copolymérisation de deux monomères initiée par les groupements hydroxy des NCC natifs. Certains matériaux ont été obtenus avec plus de 80% de greffons en masse.

La méthodologie établie avec la TBD est un outil très polyvalent car elle permet l'obtention de matériaux avec des compositions et des propriétés différentes, en utilisant des conditions similaires.

## Abstract

Cellulose, the most abundant natural polysaccharide on the planet, has known a surge in interest at the turn of the 21st century due to the increasing demand in alternative to petroleum based chemistry. In particular, cellulose nanoparticles have been the topic of a great amount of work due to their valuable properties as reinforcing filler in composite material. However, additional steps are often necessary in order to use nanocellulose with typical polymer matrixes due to compatibility issues and dispersibility of the nanofiller. In this context, the objective of the work presented is the modification of nanocellulose by grafting different polymers of interest such as polyesters and polycarbonates on it.

The grafting of poly(lactide) on cellulose nanofibrils (CNF) was first studied. A “Grafting from” approach by ring-opening polymerization was selected for our work and catalyzed by an organic base catalyst, mainly 4-dimethylaminopyridine (DMAP). By polymerizing lactide initiated by CNF surface hydroxy as initiator, the importance of the reaction parameters on the grafting of poly(lactide) (PLA) on cellulose could be studied quantitatively, with a maximum of 24 wt%, and a methodology could be developed. The use of an organic catalyst also allowed for an easy removal during purification, unlike metal catalyst which are known to be very difficult to remove from the finished material.

The second part of the study was devoted to the grafting of poly(trimethylene carbonate) moieties on cellulose nanocrystals (CNC), once again by grafting from organocatalyzed ring-opening polymerization. First, a study on the efficiency of different organic catalysts reported to polymerize trimethylene carbonate (TMC) was conducted in order to select the best one for the rest of the work. Following this study, 1,5,7-triazabicyclo[4.4.0]dec-5-ene (TBD), an organic base, was our choice to conduct the rest of the experiments as it worked best for grafting of poly(trimethylene carbonate) (PTMC), and materials made of up to 74% grafts by weight could be obtained in mild conditions. Not only was this result particularly impressive when compared to similar work reported in the literature, it is also to our knowledge the first case of CNC grafted with polycarbonate.

In parallel to this, a density-functional theory (DFT) study was conducted in collaboration with professor João P. Prates Ramalho (U. Evora, Portugal) to understand the mechanism behind the polymerization of TMC with different catalyst. This study showed that the H-bond mechanism

with alcohol activation had a much lower activation barrier than the nucleophilic attack mechanism, confirming the experimental results obtained.

Another collaborative work was done with another PhD in our laboratory, Nouaamane El Idrissi, who produced CNC grafted with TBD moieties. These CNCs were used as catalyst for the polymerization of TMC. While the polymerization with unsupported TBD seemed faster, polymerization of TMC by supported catalysis on CNC occurred, albeit with a much lower amount of grafting.

Lastly, the methodology developed with TBD as an organocatalyst during the previous experiments was used in order to graft copolymers on CNC. By first using PTMC-grafted CNCs as the starting substrate, ring-opening polymerization with different cyclic esters resulted in CNCs grafted with block copolymers of different nature, for the first time by ROP to the best of our knowledge. Statistical copolymeric grafts could also be obtained by copolymerizing two monomers on the hydroxy group of native CNCs. Some of the material obtained contained more than 80% graft content by weight.

The methodology established throughout this with TBD proved to be quite interesting due to its versatility, as material of different nature and properties could be obtained with similar conditions.

## Table of Content

Acknowledgement.....	I
Résumé.....	IV
Abstract.....	VI
List of Abbreviations.....	XII
List of Figures.....	XIV
List of Tables.....	XIX
<b>Introduction.....</b>	<b>1</b>
<b>I. Bibliography.....</b>	<b>5</b>
I.1. Cellulose.....	5
I.1.1. Generalities.....	5
I.1.2. Cellulose nanomaterials.....	9
I.1.2.1. Cellulose nanofibrils.....	11
I.1.2.2. Cellulose nanocrystals.....	14
I.1.3. Other polysaccharides.....	16
I.2. Synthetic polymers considered in this work.....	19
I.2.1. Polyesters.....	19
I.2.1.1. Poly(lactic acid).....	19
I.2.1.2. Poly( $\epsilon$ -caprolactone) and Poly( $\delta$ -valerolactone).....	24
I.2.2. Polycarbonates.....	25
I.2.2.1. Generalities.....	25
I.2.2.2. Aliphatic PC.....	26
I.3. Organocatalyzed ring-opening polymerization.....	30
I.3.1. Ring-opening polymerization general concepts.....	30
I.3.2. Aminopyridines, amidines and guanidine.....	37
I.3.3. Immortal polymerization.....	44

I.4.	Polysaccharide-based polymer material.....	45
I.4.1.	Non-grafted material.....	46
I.4.2.	Surface grafting .....	48
<b>II.</b>	<b>Materials and Methods .....</b>	<b>56</b>
II.1.	Materials .....	56
II.1.1.	Cellulose .....	56
II.1.2.	Solvents .....	57
II.1.3.	Catalysts.....	57
II.1.4.	Reagents.....	57
II.2.	Purification.....	58
II.3.	Polymerization methods.....	59
II.4.	Characterization techniques .....	63
II.5.	Grafting and conversion calculation .....	65
II.6.	DFT methodological details.....	67
<b>III.</b>	<b>Organocatalyzed ring-opening polymerization of lactide from the surface of cellulose nanofibrils .....</b>	<b>69</b>
III.1.	Introduction .....	69
III.2.	Results and discussion.....	71
III.2.1.	SI-ROP modification of lyophilized CNF .....	71
III.2.2.	SI-ROP modification of never dried CNF .....	75
III.3.	Conclusion.....	82
<b>IV.</b>	<b>DFT investigations on the ring-opening polymerization of trimethylene carbonate catalyzed by N-heterocyclic bases .....</b>	<b>84</b>
IV.1.	Introduction .....	84
IV.2.	Results and discussion.....	86
IV.2.1.	TBD catalyzed ring-opening polymerization of TMC.....	86

IV.2.2.	DMAP catalyzed ring-opening polymerization of TMC .....	91
IV.3.	Conclusion.....	98
<b>V.</b>	<b>Cellulose nanocrystals modification by grafting from ring-opening polymerization of a cyclic carbonate .....</b>	<b>99</b>
V.1.	Introduction.....	99
V.1.	Results and discussion .....	102
V.1.1.	PTMC grafting on the surface of CNCs .....	102
V.1.1.1.	Catalyst screening.....	102
V.1.1.2.	Influence of experimental parameters for the TBD catalyzed grafting .....	105
V.1.2.	Characterization of the poly(trimethylene carbonate)-grafted CNC as a function of the grafting ratio .....	110
V.1.3.	ROP of TMC by CNC-Supported TBD trial experiments .....	124
V.2.	Conclusion .....	128
<b>VI.</b>	<b>Block and Statistical Copolymer Grafted CNC by organocatalysis.....</b>	<b>131</b>
VI.1.	Introduction .....	131
VI.2.	Results and discussion.....	134
VI.2.1.	PTMC/PLLA Copolymers .....	134
VI.2.1.1.	Block Copolymers.....	136
VI.2.1.2.	Statistical Copolymers.....	141
VI.2.1.3.	Differential scanning calorimetry (DSC) .....	144
VI.2.1.1.	Degrafting / depolymerization of the modified CNCs .....	147
VI.2.2.	Poly(methyl metacrylate) (PMMA) grafting with phosphazene.....	149
VI.2.1.	Poly( $\epsilon$ -caprolactone) (PCL) grafting .....	152
VI.2.2.	PTMC/PVL Copolymers .....	154
VI.2.3.	PTMC/PLA/PVL terpolymers .....	158
VI.1.	Conclusion.....	161

<b>VII. General conclusion and Perspectives .....</b>	<b>163</b>
<b>VIII. Annexes .....</b>	<b>167</b>
VIII.1. Elemental analysis.....	167
VIII.2. NMR spectra .....	171
VIII.3. Infrared .....	176
VIII.4. XPS Data .....	177
VIII.5. Size exclusion chromatography .....	183
<b>IX. References .....</b>	<b>185</b>

## List of Abbreviations

Abbreviation	Description
AFM	<i>Atomic force microscopy</i>
ATRP	<i>Atom transfer radical polymerization</i>
BE	<i>Binding energy</i>
BEMP	<i>2-(tert-butylimino)-2-(diethylamino)-1,3-dimethylperhydro-1,3,2-diazaphosphorinane</i>
BnOH	<i>Benzyl alcohol</i>
CAB	<i>Cellulose acetate butyrate</i>
CL	<i>Caprolactone = <math>\epsilon</math>-caprolactone</i>
CNC(s)	<i>Cellulose nanocrystal(s)</i>
CNF(s)	<i>Cellulose nanofibrils(s)</i>
DBU	<i>1,8-diazabicyclo[5.4.0]undec-7-ene</i>
DCM	<i>Dichloromethane</i>
DMAP	<i>4-dimethylaminopyridine</i>
DP	<i>Degree of polymerization</i>
DS	<i>Degree of substitution</i>
DSC	<i>Differential scanning calorimetry</i>
EA	<i>Elemental analysis</i>
EtOH	<i>Ethanol</i>
eV	<i>Electron volt</i>
FT-IR	<i>Fourier-transform infrared spectroscopy</i>
L-LA	<i>L-lactide</i>
MALDI	<i>Matrix-assisted laser desorption/ionization</i>
MMA	<i>Methyl methacrylate</i>
MeOH	<i>Methanol</i>
mTBD	<i>7-methyl-1,5,7-triazabicyclo[4.4.0]dec-5-ene</i>
NMR	<i>Nuclear magnetic resonance</i>
PBuOH	<i>4-pyrenebutanol</i>
PCL	<i>Poly(<math>\epsilon</math>-caprolactone)</i>
PEGME	<i>Poly(ethylene glycol) methyl ether</i>
PLA	<i>Poly(lactic acid) (from polycondensation) = Poly(lactide) (from ROP)</i>
PET	<i>Poly(ethylene terephthalate)</i>
PMDETA	<i>N,N,N',N'',N''-pentamethyldiethylenetriamine</i>
PMMA	<i>Poly(methyl methacrylate)</i>
PTMC	<i>Poly(trimethylene carbonate)</i>
PVL	<i>Poly(valerolactone) = poly(<math>\delta</math>-valerolactone)</i>
ROP	<i>Ring-opening polymerization</i>
Rpm	<i>Rotations per minute</i>

RT	<i>Room temperature</i>
SEC	<i>Size exclusion chromatography</i>
SEM	<i>Scanning electron microscopy</i>
SI-ROP	<i>Surface-initiated ring-opening polymerization</i>
TBD	<i>1,5,7-triazabicyclo[4.4.0]dec-5-ene</i>
tBuP <sub>4</sub>	<i>N,N,N',N',N'',N''-hexamethyl-N''-[N-(2-methyl-2-propanyl)-P,P-bis{[tris(dimethylamino)phosphoranylidene]amino}phosphorimidoyl]phosphorimidic triamide</i>
TEM	<i>Transmission electron spectroscopy</i>
TGA	<i>Thermogravimetric analysis</i>
TMC	<i>Trimethylene carbonate</i>
UCCS	<i>Unité de catalyze et de chimie du solide</i>
VL	<i>Valerolactone = <math>\delta</math>-valerolactone (no other VL described)</i>
WAXS	<i>Wide-angle X-ray scattering</i>
XPS	<i>X-ray photoelectron spectroscopy</i>

## List of Figures

Figure 1: Cellulose chemical structure.....	5
<b>Figure 2:</b> Examples of modification of cellulose to introduce different functional group by hydroxy chemistry.....	7
<b>Figure 3:</b> Number of research documents published since 2006 by year according to Scopus database using "Nanocellulose" as a keyword.....	9
<b>Figure 4:</b> Number of research documents published since 2006 by subject area according to Scopus database using "Nanocellulose" as a keyword.....	10
<b>Figure 5:</b> TEM image of CNF. Scale bar corresponding to 0.5 $\mu$ m. Reprinted (adapted) with permission from: Wang, W.; Sabo, R. C.; Mozuch, M. D.; Kersten, J. Y.; Zhu, J. Y.; Jin, Y. Physical and Mechanical Properties of Cellulose Nanofibril Films from Bleached Eucalyptus Pulp by Endoglucanase Treatment and Microfluidization. Journal of Polymers and the Environment 2015, 23 (4), 551–558. Copyright (2022) Springer Science Business Media New York. ....	13
<b>Figure 6:</b> Schematic representation of acid hydrolysis of cellulose fiber into cellulose nanocrystals.....	14
<b>Figure 7:</b> Positively stained electron micrograph of cotton cellulose crystallites taken from the anisotropic phase. Scale bar corresponding to 400 nm. Reprinted (adapted) with permission from: Fleming, K.; Gray, D.; Prasannan, S.; Matthews, S. Cellulose Crystallites: A New and Robust Liquid Crystalline Medium for the Measurement of Residual Dipolar Couplings. J. Am. Chem. Soc. 2000, 122 (21), 5224–5225. Copyright (2022) American Chemical Society. ....	15
<b>Figure 8:</b> Chemical structure of amylopectin. ....	17
Figure 9: Chemical structure of chitin.....	18
<b>Figure 10:</b> Conversion of carbon dioxide and water into lactic acid through multiple natural steps. ....	19
<b>Figure 11:</b> Most common route for the production of PLA.....	20
<b>Figure 12:</b> chemical structure of the different stereoisomers of lactide and their resulting polymers.....	22
<b>Figure 13:</b> chemical structure of $\epsilon$ -caprolactone, $\delta$ -valerolactone, and their corresponding polymers. ....	24
<b>Figure 14:</b> Chemical structure of Bisphenol A polycarbonate (BPA-PC).....	25
<b>Figure 15:</b> Different pathways to obtain polycarbonates. a: reaction of diol with phosgene. b: transcarbonatation reaction, step 1 and 2 repeated with the product multiple times to lead to a polymer. c: ring-opening polymerization of cyclic carbonate. d: copolymerization of epoxy and CO <sub>2</sub> . ....	26
<b>Figure 16:</b> Reaction of oxetane and CO <sub>2</sub> to obtain TMC, as described in the work of Baba, Kashiwagi, and Matsuda <sup>108</sup> . ....	28
<b>Figure 17:</b> Polymerization of five-membered cyclic carbonate resulting in a poly(ether-co-carbonate). ....	28
<b>Figure 18:</b> General mechanism of ring-opening polymerization.....	30
<b>Figure 19:</b> Nucleophilic activated monomer mechanism (AMM) of organocatalyzed ROP.....	31
<b>Figure 20:</b> Activated chain-end mechanism (ACEM) of organocatalyzed ROP. ....	32
<b>Figure 21:</b> Example of some organic catalysts reported for the ROP of cyclic esters. <b>MSA:</b> methane sulfonic acid, <b>TfOH:</b> trifluoromethanesulfonic acid, <b>Tf<sub>2</sub>NH:</b> bis(trifluoromethane)sulfonimide, <b>t-BuP<sub>4</sub>:</b> <i>N,N,N',N',N'',N'''</i> -hexamethyl- <i>N'''</i> -[N-(2-methyl-2-propanyl)-P,P	

bis{[tris(dimethylamino)phosphoranylidene]amino}phosphorimidoyl}phosphorimidic triamide, <b>BEMP</b> : 2-( <i>tert</i> -butylimino)-2-(diethylamino)-1,3-dimethylperhydro-1,3,2-diazaphosphorinane. ....	33
<b>Figure 22</b> : Chemical structure of pyridine and guanidine organic ROP catalysts and their associated $pK_{aH^+}$ . <sup>144</sup> .....	37
<b>Figure 23</b> : Dual activation mechanism by hydrogen bonding of TBD for the ROP of cyclic ester in the presence of a protic co-initiator.....	43
<b>Figure 24</b> : Illustration of the distinction between “classical living” and “immortal” ROP process. Reprinted from Publication Dalton transactions : an international journal of inorganic chemistry, 39, Nouredine Ajellal, Jean-François Carpentier, Clémence Guillaume, Sophie M. Guillaume, Marion Helou, Valentin Poirier, Yann Sarazin and Alexander Trifonov., Metal-catalyzed immortal ring-opening polymerization of lactones, lactides and cyclic carbonates., Pages No. 8363, Copyright (2022), with permission from Royal Society of Chemistry.....	44
<b>Figure 25</b> : Extreme high resolution scanning electron microscopy (XHR-SEM) micrographs cryo-fractured cross sections of (A) CAB matrix and its nanocomposites with (B) wt%, (C) 12wt% CNCs (D) a detailed view of the nanocomposites with 12wt% CNCs. Reprinted from Publication Composites Science and Technology, 71, Gilberto Siqueira,Aji P. Mathew, Kristiina Oksman, Processing of cellulose nanowhiskers/cellulose acetate butyrate nanocomposites using sol–gel process to facilitate dispersion, Pages No. 7, Copyright (2022), with permission from Elsevier. ....	47
<b>Figure 26</b> : Schematic representation of the "grafting onto" and “grafting from” method of surface modification of polysaccharides. ....	49
<b>Figure 27</b> : Synthesis of Polysaccharide Nanocrystals-g-polystyrene by ATRP. Reprinted (adapted) with permission from: Morandi, G.; Heath, L.; Thielemans, W. Cellulose Nanocrystals Grafted with Polystyrene Chains through Surface-Initiated Atom Transfer Radical Polymerization (SI-ATRP). <i>Langmuir</i> 2009, 25 (14), 8280–8286. Copyright (2022) American Chemical Society. ....	50
<b>Figure 28</b> : Chemical structure of $\beta$ -cyclodextrin.....	53
<b>Figure 29</b> : Surface-Initiated Ring-Opening Polymerization (SI-ROP) of <i>rac</i> -Lactide from the surface of cellulose nanofibrils using 4-dimethylaminopyridine (DMAP) as catalyst and dichloromethane (DCM) as solvent.....	59
<b>Figure 30</b> : General reaction scheme of the ring-opening polymerization of cyclic esters (or carbonates) co-initiated by the hydroxy groups present on the surface of cellulose nanocrystals and catalyzed by an organic base. ....	61
<b>Figure 31</b> : Chemical structure of DMAP, DBU and TBD. ....	72
<b>Figure 32</b> : FT-IR spectra of cellulose nanofibrils (CNF) and modified CNF with different amount of grafting after purification by Soxhlet extraction corresponding to entries in <b>Table 5</b> . ....	73
<b>Figure 33</b> : Carbon 1s X-ray Photoelectron Spectroscopy (XPS) scan of modified cellulose nanofibrils using different amounts of 4-dimethylaminopyridine. ....	74
<b>Figure 34</b> : Graphical representation of the grafting percent of PLA on cellulose with different sets of parameters. Numbers correspond to entries in <b>Table 6</b> . ....	77
<b>Figure 35</b> : FT-IR spectra of unmodified cellulose nanofibrils (a) and PLA-grafted CNF (entry 15 in <b>Table 6</b> ) using the “never-dried” method (b). ....	79

<b>Figure 36:</b> Carbon 1s XPS scan of modified cellulose nanofibrils (CNF) obtained from never dried CNFs, with different entries corresponding to the samples in <b>Table 6</b> .....	80
<b>Figure 37:</b> <sup>1</sup> H NMR spectra of crude mixture after reaction in DMSO-d <sub>6</sub> . Crude product separated from modified CNF corresponding to entry 15 in <b>Table 6</b> (300 MHz) .....	82
<b>Figure 38:</b> N-heterocyclic bases catalysts considered in this study. From left to right, 4-dimethylaminopyridine (DMAP), 1,5,7-Triazabicyclo[4.4.0]dec-5-ene (TBD) .....	84
<b>Figure 39:</b> Schematic representation of the nucleophilic (upper part) and the alcohol activation / H-bond mechanism (bottom part) for the ring-opening polymerization of TMC catalyzed by an N-heterocyclic base and co-initiated by an alcohol .....	85
<b>Figure 40:</b> Optimized geometry structures of the species involved in the TBD catalyzed ring-opening polymerization for the TMC – H-bond / alcohol activation mechanism .....	86
<b>Figure 41:</b> Free energy profile for the TBD catalyzed ring-opening polymerization of TMC – H-bond / alcohol activation mechanism .....	87
<b>Figure 42:</b> Free energy profile for the nucleophilic mechanism of the TBD catalyzed ring-opening polymerization of TMC .....	88
<b>Figure 43:</b> Optimized geometry structures of the species involved in the nucleophilic mechanism for the TBD catalyzed ring-opening polymerization of TMC .....	90
<b>Figure 44:</b> Optimized geometry structures of the species involved in the first step of the H-bond mechanism for the DMAP catalyzed ring-opening polymerization of TMC .....	91
<b>Figure 45:</b> Free energy profile for the H-bond / alcohol activation pathway of the DMAP catalyzed ring-opening polymerization of TMC .....	92
<b>Figure 46:</b> Optimized geometry structures of the species involved in the second step of the H-bond / alcohol activation mechanism of the DMAP catalyzed ring-opening polymerization of TMC .....	93
<b>Figure 47:</b> Free energy profile for the nucleophilic path of the DMAP catalyzed ring-opening polymerization of TMC .....	94
<b>Figure 48:</b> Optimized geometry structures of the species involved in the first and second steps for the nucleophilic mechanism of the DMAP catalyzed ring-opening polymerization of TMC. The structure of a possible bicyclo intermediate species (BICY1) is also displayed (bottom) .....	95
<b>Figure 49:</b> Optimized geometry structures of the species involved in the final steps step of the nucleophilic mechanism of the DMAP catalyzed ring-opening polymerization of TMC .....	97
<b>Figure 50:</b> Structure of the organocatalysts used in this study. pKaH <sup>+</sup> values in acetonitrile <sup>144</sup> .....	102
<b>Figure 51:</b> FT-IR spectra of unmodified cellulose nanocrystals (CNC) and grafted one with different graft content after purification by Soxhlet extraction. PTMC of 15,400 g.mol <sup>-1</sup> extracted from Soxhlet and purified by precipitation .....	111
<b>Figure 52:</b> <sup>1</sup> H NMR spectra of the crude mixture after quenching with benzoic acid and separation of CNC in CDCl <sub>3</sub> (300 MHz) .....	112

<b>Figure 53:</b> Carbon 1s X-ray photoelectron spectroscopy (XPS) scan of cellulose nanocrystals grafted with different poly(trimethylene carbonate content). Grafted CNCs corresponding to reference in <b>Table 10</b> : entry 21 (23%) entry 23 (41%), entry 18 (64%), entry 17 (74%).....	114
<b>Figure 54:</b> X-ray photoelectron spectroscopy (XPS) scan of unmodified CNC (red) and 74% grafted CNC (green) in the region of Nitrogen 1s peak. ....	115
<b>Figure 55:</b> X-ray photoelectron spectroscopy (XPS) scan of unmodified cellulose nanocrystals in the region of Sulfur 2p peak. ....	115
<b>Figure 56:</b> Contact angle of a water droplet on the surface of CNC modified with different polycarbonate content. Grafted CNCs corresponding to reference in <b>Table 10</b> : entry 15 (9%) entry 21 (23%), entry 4 (51%), and entry 17 (74%).....	116
<b>Figure 57:</b> Differential Scanning Calorimetry (DSC) graphs of CNC, poly(trimethylene carbonate) (PTMC) and modified CNC during the second heating at 10°C/min. . Grafted CNCs corresponding to reference in <b>Table 10</b> : entry 21 (23%), entry 4 (51%), and entry 17 (74%).....	117
<b>Figure 58:</b> Thermogram of PTMC non-grafted polymer and grafted CNCs, each polymer and CNC of the same color coming from the same reaction. ....	119
<b>Figure 59:</b> Thermograms of unmodified and grafted CNCs from 30 to 600°C as well as pure PTMC. Grafted CNCs corresponding to reference in <b>Table 10</b> : entry 21 (23%) entry 23 (41%), entry 18 (64%), entry 17 (74%). ....	120
<b>Figure 60:</b> MALDI-MS spectra for entry 25 and 29, (A) global mass spectrum, (B) magnification from m/z 1,500 to m/z 1,700 and (C) comparison between experimental data and theoretical isotopic models. ....	123
<b>Figure 61:</b> FT-IR spectra of TBD-fuctionnalised CNCs before and after polymerization of TMC .....	126
<b>Figure 62:</b> <sup>1</sup> H NMR spectra of the crude mixture after quenching with benzoic acid and separation of CNC in CDCl <sub>3</sub> (300 MHz).....	128
<b>Figure 63:</b> Carbon 1s X-ray photoelectron spectroscopy (XPS) normalized spectrogram of unmodified CNCs and PLLA-grafted CNCs. Grafted CNCs corresponding to entry 2 in <b>Table 15</b> .....	135
<b>Figure 64:</b> Carbon 1s X-ray photoelectron spectroscopy (XPS) normalized spectrogram of unmodified CNCs, PLLA and PTMC blocks grafted CNCs. Modified CNCs corresponding to entries 3 to 7 in <b>Table 16</b> and entry 26 in <b>Table 10</b> . ....	138
<b>Figure 65:</b> FT-IR spectra of copolymer-grafted CNC and non-grafted PTMC and PLLA. ....	140
<b>Figure 66:</b> <sup>1</sup> H NMR spectra of the crude mixture obtained after equimolar reaction of TMC and L-lactide with BnOH as initiator (entry 8, <b>Table 17</b> ) TBD and Toluene at 110°C for 60 seconds in CDCl <sub>3</sub> (300 MHz). Crossed signals correspond to THF as the NMR can be carried out right after quenching of the reaction. ....	142
<b>Figure 67:</b> Carbon 1s X-ray photoelectron spectroscopy (XPS) normalized spectrogram of unmodified CNCs and P(L-LA-stat-TMC) grafted CNCs. Modified CNCs corresponding to entry 9 to 11 in <b>Table 17</b> and entry 3 in <b>Table 16</b> . ....	143
<b>Figure 68:</b> DSC thermograms of PTMC, PLLA, unmodified CNCs, and grafted CNCs between -80°C and 180°C. ....	145
<b>Figure 69:</b> DSC thermograms of PTMC, PLLA, unmodified CNCs, and grafted CNCs between -80°C and 180°C. ....	146

<b>Figure 70:</b> <sup>1</sup> H NMR spectra of the crude mixture of grafted CNCs (corresponding to entry 7, <b>Table 16</b> ) in the presence of TBD and toluene at 110°C for 60 seconds in CDCl <sub>3</sub> (300 MHz). .....	147
<b>Figure 71:</b> <sup>1</sup> H NMR spectra of the crude mixture of grafted CNCs (corresponding to entry 9, <b>Table 17</b> ) in the presence of TBD and toluene at 110°C for 60 seconds in CDCl <sub>3</sub> (300 MHz). .....	148
<b>Figure 72:</b> Carbon 1s X-ray photoelectron spectroscopy (XPS) normalized spectrogram of unmodified CNCs and PMMA-grafted CNCs. Grafted CNCs corresponding to entry 17 in <b>Table 18</b> .....	151
<b>Figure 73:</b> Carbon 1s X-ray photoelectron spectroscopy (XPS) normalized spectrogram of unmodified CNCs, PTMC-CNCs and PCL grafted PTMC-CNCs. PCL-grafted CNCs corresponding to entry 21 in <b>Table 19</b> .....	153
<b>Figure 74:</b> DSC thermograms of PTMC-grafted CNCs and PCL-grafted PTMC-CNCs between -80°C and 180°C. ....	154
<b>Figure 75:</b> Carbon 1s X-ray photoelectron spectroscopy (XPS) normalized spectrogram of unmodified CNCs, PVL and PTMC copolymer grafted CNCs. Modified CNCs corresponding to entry 23 to 25 in <b>Table 20</b> .....	156
<b>Figure 76:</b> DSC thermograms of unmodified CNCs, and PVL/PTMC grafted CNCs between -80°C and 180°C....	157
<b>Figure 77:</b> <sup>1</sup> H NMR spectra of the crude mixture after polymerization with TMC, <i>L</i> -lactide and δ-valerolactone corresponding to corresponding to entry 28 ( <b>Table 21</b> ) in CDCl <sub>3</sub> (300 MHz). .....	159
<b>Figure 78:</b> Carbon 1s X-ray photoelectron spectroscopy (XPS) normalized spectrogram of unmodified CNCs and modified CNCs corresponding to entries 26 to 28 in <b>Table 21</b> . .....	160
<b>Figure 79:</b> DSC thermograms of unmodified of grafted CNCs corresponding to reactions in <b>Table 21</b> between -80°C and 180°C.....	161
<b>Figure 80:</b> <sup>1</sup> H NMR spectra of 4-dimethylaminopyridine in DMSO-d <sub>6</sub> (300 MHz). .....	171
<b>Figure 81:</b> <sup>1</sup> H NMR spectra of lactide in DMSO-d <sub>6</sub> (300 MHz). .....	172
<b>Figure 82:</b> <sup>1</sup> H NMR spectra of TBD in CDCl <sub>3</sub> (300 MHz). .....	173
<b>Figure 83:</b> <sup>1</sup> H NMR spectra of TMC in CDCl <sub>3</sub> (300 MHz). .....	174
<b>Figure 84:</b> <sup>1</sup> H NMR spectra of ε-CL in CDCl <sub>3</sub> (300 MHz). .....	175
<b>Figure 85:</b> SEC analyses data of the non-grafted copolymer obtained from reaction 26 in <b>Table 20</b> . .....	183
<b>Figure 86:</b> SEC analyses data of the non-grafted copolymer obtained from reaction 28 in <b>Table 20</b> . .....	184
<b>Figure 87:</b> SEC analyses data of the non-grafted copolymer obtained from reaction 27 in <b>Table 20</b> . .....	184

## List of Tables

<b>Table 1:</b> Non-exhaustive table of example of ROP reaction found in the literature performed with the organic catalyst described in <b>Figure 21</b> with their associated protic initiators and solvents .....	34
<b>Table 2:</b> Non-exhaustive list of cyclic esters and carbonate polymerized by TBD in different conditions found in the literature. All reaction performed at RT except for the polymerization of TMC in bulk (110 °C). .....	40
<b>Table 3:</b> Mechanical data from tensile tests of PCL composite reinforced with unmodified and PCL-grafted CNF. Data from the work of Lönnberg <i>et al.</i> , 2011. ....	52
<b>Table 4:</b> Ring-opening polymerization of <i>rac</i> -lactide initiated from the surface of freeze-dried CNF in the presence of DBU/TBD in DCM for 48 hours at 35 °C. ....	71
<b>Table 5:</b> Ring-opening polymerization of <i>rac</i> -lactide initiated from the surface of freeze-dried CNF in the presence of DMAP in DCM for 48 hours at 35 °C. ....	72
<b>Table 6:</b> Ring-opening polymerization of <i>rac</i> -lactide initiated from the surface of never-dried CNF in the presence of DMAP in DCM. ....	76
<b>Table 7:</b> Experimental results. Reactions conducted for 1h at room temperature in 2 mL CH <sub>2</sub> Cl <sub>2</sub> . TMC / Catalyst / Initiator = 100/1/1. ....	98
<b>Table 8:</b> Ring-opening polymerization of TMC initiated from the surface of CNC in the presence of various organocatalysts at 25 °C in THF. ....	103
<b>Table 9:</b> Ring-opening polymerization of TMC initiated in different solvents on the surface of CNC in the presence of TBD over 5 hours, 25 °C, at a ratio of TMC/Catalyst/OH of 500/1/50. Solvent added outside the glovebox under inert atmosphere. ....	105
<b>Table 10:</b> Ring-opening polymerization of TMC initiated from the surface of CNC in the presence of TBD in THF for 5 hours. ....	107
<b>Table 11:</b> intensity ratio of C6-OH and C3-OH peak to C-O-C in FT-IR for unmodified cellulose and grafted cellulose. Grafted CNCs corresponding to reference in <b>Table 10</b> : entry 21 (23%), entry 20 (47%), and entry 19 (57%), entry 17 (74%). ....	110
<b>Table 12:</b> The calculated sample crystallinity based on WAXS measurements for all samples. ....	121
<b>Table 13:</b> Ring-opening polymerization of TMC using TBD-grafted CNC as catalyst, at 25 °C in THF for 5 hours. ....	124
<b>Table 14:</b> Water and elemental composition for unmodified CNCs and TBD-grafted CNCs before and after reaction. ....	127
<b>Table 15:</b> Ring-opening polymerization of <i>L</i> -LA initiated from the surface of CNC using TBD and DMAP, at 25 °C in THF. ....	135
<b>Table 16:</b> Ring-opening polymerization of <i>L</i> -LA initiated from the surface of PTMC-grafted CNCs using TBD, at 25 °C in THF over 1 hour. Full conversion was reached for all reactions. ....	137
<b>Table 17:</b> Ring-opening copolymerization of <i>L</i> -LA and TMC initiated from the surface of CNCs using TBD, at 25 °C in THF over 5 hours. ....	141

<b>Table 18:</b> Ring-opening polymerization of MMA initiated from the surface of CNC using tBu-P <sub>4</sub> , at 25 °C in THF. ....	150
<b>Table 19:</b> Ring-opening polymerization of ε-CL initiated from the surface of PTMC-grafted CNCs (20: 73 wt%, 21: 59%).....	152
<b>Table 20:</b> Ring-opening copolymerization of δ-VL on the surface of unmodified and PTMC-grafted CNCs using TBD, at 25 °C in THF.....	155
<b>Table 21:</b> Ring-opening copolymerization of TMC, δ-VL and L-LA initiated from the surface of CNCs using TBD, at 25 °C in THF.....	158
<b>Table 22:</b> EA and TGA data obtained for samples in <b>Table 4:</b> Ring-opening polymerization of <i>rac</i> -lactide initiated from the surface of freeze-dried CNF in the presence of DBU/TBD in DCM for 48 hours at 35 °C. ....	167
<b>Table 23:</b> EA and TGA data obtained for samples in <b>Table 5:</b> Ring-opening polymerization of <i>rac</i> -lactide initiated from the surface of freeze-dried CNF in the presence of DMAP in DCM for 48 hours at 35 °C. ....	167
<b>Table 24:</b> EA and TGA data obtained for samples in <b>Table 6:</b> Ring-opening polymerization of <i>rac</i> -lactide initiated from the surface of never-dried CNF in the presence of DMAP in DCM. ....	167
<b>Table 25:</b> EA and TGA data obtained for samples in <b>Table 8:</b> Ring-opening polymerization of TMC initiated from the surface of CNC in the presence of various organocatalysts at 25 °C in THF.....	168
<b>Table 26:</b> EA and TGA data obtained for samples in <b>Table 9:</b> Ring-opening polymerization of TMC initiated in different solvents on the surface of CNC in the presence of TBD over 5 hours, 25 °C, at a ratio of TMC/Catalyst/OH of 500/1/50. Solvent added outside the glovebox under inert atmosphere.....	168
<b>Table 27:</b> EA and TGA data obtained for samples in <b>Table 10:</b> Ring-opening polymerization of TMC initiated from the surface of CNC in the presence of TBD in THF for 5 hours.....	168
<b>Table 28:</b> EA and TGA data obtained for samples in <b>Table 13:</b> Ring-opening polymerization of TMC using TBD-grafted CNC as catalyst, at 25 °C in THF for 5 hours.....	169
<b>Table 29:</b> EA and TGA data obtained for samples in <b>Table 15:</b> Ring-opening polymerization of L-LA initiated from the surface of CNC using TBD and DMAP, at 25 °C in THF. ....	169
<b>Table 30:</b> EA and TGA data obtained for samples in <b>Table 16:</b> Ring-opening polymerization of L-LA initiated from the surface of PTMC-grafted CNCs using TBD, at 25 °C in THF over 1 hour. Full conversion was reached for all reactions. ....	169
<b>Table 31:</b> EA and TGA data obtained for samples in <b>Table 18:</b> Ring-opening polymerization of MMA initiated from the surface of CNC using tBu-P <sub>4</sub> , at 25 °C in THF.....	170
<b>Table 32:</b> EA and TGA data obtained for samples in <b>Table 19:</b> Ring-opening polymerization of ε-CL initiated from the surface of PTMC-grafted CNCs (20: 73 wt%, 21: 59%).....	170
<b>Table 33:</b> EA and TGA data obtained for samples in <b>Table 20:</b> Ring-opening copolymerization of δ-VL on the surface of unmodified and PTMC-grafted CNCs using TBD, at 25 °C in THF. ....	170
<b>Table 34:</b> EA and TGA data obtained for samples in <b>Table 21:</b> Ring-opening copolymerization of TMC, δ-VL and L-LA initiated from the surface of CNCs using TBD, at 25 °C in THF.....	170
<b>Table 35:</b> FT-IR signals detected for unmodified and modified CNFs, with their corresponding functions.....	176

<b>Table 36:</b> Xray Photoelectron Spectroscopy data obtained for different signals, material analyzed corresponding to <b>Table 5</b> .....	177
<b>Table 37:</b> Xray Photoelectron Spectroscopy data obtained for different signals, material analyzed corresponding to <b>Table 6</b> .....	178
<b>Table 38:</b> Xray Photoelectron Spectroscopy data obtained for different signals, material analyzed corresponding to <b>Table 10</b> .....	179
<b>Table 39:</b> Xray Photoelectron Spectroscopy data obtained for different signals, material analyzed corresponding to <b>Table 16</b> .....	180
<b>Table 40:</b> Xray Photoelectron Spectroscopy data obtained for different signals, material analyzed corresponding to <b>Table 17</b> .....	181
<b>Table 41:</b> Xray Photoelectron Spectroscopy data obtained for different signals, material analyzed corresponding to <b>Table 18</b> .....	181
<b>Table 42:</b> Xray Photoelectron Spectroscopy data obtained for different signals, material analyzed corresponding to <b>Table 19</b> .....	181
<b>Table 43:</b> Xray Photoelectron Spectroscopy data obtained for different signals, material analyzed corresponding to <b>Table 20</b> .....	182
<b>Table 44:</b> Xray Photoelectron Spectroscopy data obtained for different signals, material analyzed corresponding to <b>Table 21</b> .....	182

## Introduction

All across the globe, the shortcomings of our current means of production and our economy are subject to a lot of debate, and it is clear that viable alternatives need to be found in many areas touching our daily lives. While renewable energy is on a lot of people's mind, many other fields of study are looking closely for means to become more sustainable. Among these, polymers cover a large portion of the global production for material, and can be used in a wide array of applications, from low-cost plastic bags to high end specialized materials such as sensors for biomedical applications<sup>1</sup>. However, most of the current production of polymers is still derived from non-renewable, petroleum based chemistry. This production has been optimized over the years, and competing with it for new technologies can be hard without a lot of added values other than being "greener". This means transitioning towards renewable material requires overcoming a few challenges, such as cost efficiency, which is particularly important for low-end applications, and high degree of tunability/modifications, which matters for a lot of high-end applications.

As such, polysaccharides have received a tremendous amount of attention as they can be obtained through various ways using biomass, and lead to very different materials depending on their structures<sup>2</sup>. Cellulose, the most abundant of them all, is quickly becoming a major research topic, as this naturally occurring polymer can be found in large quantities anywhere on the planet from various sources such as plants, animals, or even bacteria<sup>3</sup>. In its native form, cellulose is a glucopyranose chain with a very high degree of polymerization ( $>10,000$ ), high average molecular weight ( $M_w > 1,800,000 \text{ g}\cdot\text{mol}^{-1}$ ), and is a promising material with remarkable properties. To push its possible applications even further, natural fibers can be refined into two types of nanoparticles: nanocrystals (CNC), crystalline and shorter rod like particles, and nanofibers (CNF), long semi-crystalline fibers with a very high aspect ratio. The very high potential for such material has led to a large amount of research on it, with a large portion dedicated to their use as reinforcing nanofillers in polymers<sup>4</sup>. This approach to composite as the advantage of requiring a smaller amount of filler to affect the polymer's property greatly due to the high surface area of the nanofillers. Nanocellulose also offers other benefits when used in composites such as biodegradability, low cost and energy of production, low density, and reactive surface area (due to high OH density). The promising characteristics of such a combination has been demonstrated two decades ago by Favier *et al.* who reported the successful preparation of nanocellulose composite material with great

mechanical properties<sup>5</sup>. These benefits however come with several challenges, as the use of nanocellulose for composites requires a good dispersion of the filler in the polymer, which is often difficult to achieve. Indeed, cellulose is a highly hydrophilic material with great moisture absorption, which makes it difficult to disperse into hydrophobic polymer matrices. Therefore, using nanocellulose as a reinforcement for composites without additional steps is rather limiting, with mostly aqueous or polar environments being suitable<sup>6</sup>.

Among the different methods developed for the modification of nanocellulose, polymer grafting is a promising approach as it improves the interfacial compatibility between the polymer matrix used and the reinforcing fibers, as well as the dispersibility of the latter. By grafting chains of the same nature as the matrix, a perfect compatibility at the interface can be obtained. In addition, if the graft has a sufficient molecular weight, entanglement between the modified filler and the matrix could be obtained, which should potentially improve the mechanical properties<sup>7</sup>. This modification method for cellulose has already been reported successfully, with examples such as the work of Morandi *et al.* which used atom transfer radical polymerization from the surface of cellulose nanocrystals to obtain polystyrene grafted cellulose<sup>8</sup>. In another example, Habibi *et al.* produced poly( $\epsilon$ -caprolactone) grafts on cellulose nanofibrils. The resulting modified cellulose was then used to make a nanocomposite which showed improved properties when compared to a similar one using unmodified CNF<sup>9</sup>. As can be seen in the literature, ring-opening polymerization is a popular way to obtain polymer-grafted nanocellulose as it can be used with various lactones, some of which can be biosourced, and results in biocompatible and biodegradable polymers similarly to cellulose. This approach could therefore lead to fully biocompatible and biodegradable composites. However, one major drawback to using this type of modifications is that they are often making use of metal catalysts such as stannous ones. These metal catalyst, while efficient, can be a detriment to the use of the material obtained in some applications such as electronic or biomedical, and completely removing them from the polymer after reaction can be difficult. Therefore, the use of small organic molecules as catalysts for these reactions can be a good alternative, as they can be removed more easily, and can present other advantages such as reacting at lower temperatures<sup>10</sup>. Thankfully, the organocatalyzed ring-opening polymerization (ROP) of heterocycles, particularly containing oxygens, has been studied to a great extent in the last few decades<sup>11,12</sup>. In particular, N-heterocyclic bases have showed great catalytic activity and control when used for ROP, and most often require

the use of an alcohol co-initiator<sup>12</sup>. Despite the countless reports of their use for polymerization, such catalytic systems are still underused for the purpose of functionalizing polysaccharides.

Given this context, we have chosen to conduct this research on the surface modification of nanocellulose by polymer grafting, using a “grafting from” approach employing organic catalysts. This research is based on a project funded by the Initiatives for Science, Innovation, Territories and Economy (I-SITE) Lille Nord – Europe, from Research Foundation Flanders (grant G0C6013N), KU Leuven (grant C14/18/061) and from the European Union’s European Fund for Regional Development, Flanders Innovation & Entrepreneurship, and the Province of West-Flanders for financial support in the Accelerate project (Interreg Vlaanderen-Nederland program).

This work will be presented as a collection of publications, due to a large portion of the work produced being published, or in the process of being published. Some modifications may have been done on the original paper to fit the format of the manuscript better. Due to this format, some redundancy may occur, for which the author apologizes.

In Chapter 1, the state of the art of the relevant fields of study for this work will be presented in the form of a review to contextualize the rest of the work presented.

In Chapter 2, all the material and methods from different part of the work will be presented and compiled for clarity and to avoid unnecessary repetitions.

Chapter 3 will present the surface modification of cellulose nanofibrils by grafting lactide using organocatalyzed ROP, mainly using 4-dimethylaminopyridine (DMAP) with two different methods of CNF preparation. This work is issued from a publication in *Carbohydrate Polymer* with some additions and modifications.

Lalanne-Tisné, M.; Mees, M. A.; Eyley, S.; Zinck, P.; Thielemans, W. Organocatalyzed Ring-opening Polymerization of Lactide from the Surface of Cellulose Nanofibrils. *Carbohydrate Polymers* **2020**, *250*, 116974.

<https://doi.org/10.1016/j.carbpol.2020.116974>

Chapter 4 will be introducing the ROP of trimethylene carbonate (TMC) by computational study of the reaction with some organic catalyst in order to elucidate the mechanism of such reactions. This work is issued from a publication in *Catalysts*.

Lalanne-Tisné, M.; Favrelle-Huret, A.; Thielemans, W.; Prates Ramalho, J. P.; Zinck, P. DFT Investigations on the Ring-Opening Polymerization of Trimethylene Carbonate Catalyzed by Heterocyclic Nitrogen Bases. *Catalysts* **2022**, *12* (10), 1280.

<https://doi.org/10.3390/catal12101280>.

Chapter 5 will be developing on the polymerization of trimethylene carbonate by producing PTMC-grafted CNCs using organocatalyzed ROP, with 1,5,7-triazabicyclo[4.4.0]dec-5-ene (TBD) as the main catalyst in the first part. A second part will present some trials using CNC-supported TBD produced by another PhD student, Nouaamane El Idrissi, for the polymerization of TMC . The first part of this work is issued from a publication in Carbohydrate Polymer with some additions and modifications.

Lalanne-Tisné, M., Eyley, S., De Winter, J., Favrelle-Huret, A., Thielemans, W., & Zinck, P. (2022). Cellulose nanocrystals modification by grafting from ring-opening polymerization of a cyclic carbonate. *Carbohydrate Polymers*, *295*, 119840.

<https://doi.org/10.1016/j.carbpol.2022.119840>

Chapter 6 has been written in a similar format as a journal article in order to fit the format on this dissertation better and will explore the grafting of multiple polymers on CNC making use of the method developed in chapter 5 in order to produce copolymer grafts.

Lastly, a conclusion of the work that has been produced throughout this thesis will be given, and perspectives on how to develop the work further and its future uses will be given.

## I. Bibliography

Due to the ever-growing need to find alternatives to fossil fuel-based materials, a lot of research has been done to find viable renewable resources for the production of polymers, either by making use of biomass derived polymers, or by obtaining biosourced monomers. For the latter, this also requires the development of efficient catalytic systems to have a good control over the properties of the resulting polymer and to be appealing economically. The following chapter will therefore serve as an introduction to polysaccharides, an abundant source of biobased polymers, and particularly on cellulose and its potential use as a nanofiller for composite materials. Different polymeric material of interest will then be described, as well as some of the organic catalytic system that have been developed over the years to obtain them. Lastly, the combination of polysaccharides with different polymers reported in the literature will be explored to showcase the benefits of it, what has been done in the past, and what could be explored further.

### I.1. Cellulose

#### I.1.1. Generalities

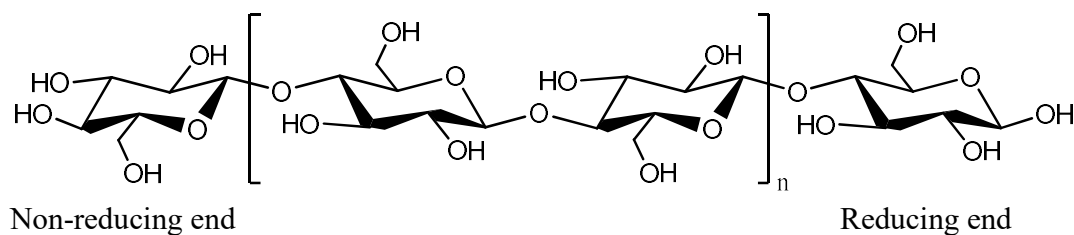


Figure 1: Cellulose chemical structure.

Cellulose is one of the most abundant polymers on the planet, with an annual production estimated at  $10^{12}$  metric tons. It is considered a practically inexhaustible source for the increasing demand of environmentally friendly products. Cellulose has been used for many purposes over the ages, such as for ropes and sails in the past, and much more advanced applications in the present. The word *cellulose* was first used in 1839 in a report of the French Academy of Sciences to describe the work of Anselm Payen who discovered a fibrous material left behind after multiple chemical treatments of plant material<sup>13</sup>. For the most part, its main used source has been wood, but cellulose can also be obtained from many other plants in large quantities such as flax and cotton. Plants however are not the only organisms producing cellulose, as tunicates, small marine invertebrates, are able to

produce cellulose, as are some bacteria, *i.e.* *Acetobacter xylinum*. These different sources of cellulose each produce a different unique structure, where bacteria produce a fine fibrous network under the right conditions<sup>13</sup>, whereas tunicate produce rod like cellulose materials<sup>5</sup>. Natural fibers coming from plants are more complicated, as cellulose is randomly mixed with lignin and pectin in the primary cell wall, while the secondary cell wall contains crystalline cellulose microfibrils with pectin and hemicellulose<sup>14</sup>. As a chemical raw material, cellulose has been used since the end of the 19<sup>th</sup> century to produce synthetic fibers<sup>15</sup>. The structure of cellulose is constituted of repeating  $\beta$ -D-glucopyranose units covalently linked together by  $\beta$ 1-4 glycosidic linkages through acetal functions to form a semi-crystalline polymer (Figure 1). This results in a long, linear chain bearing three hydroxy group per repeating unit. Each unit is rotated at a 180° angle compared to adjacent units to accommodate for the preferred bond angle of the acetal oxygen  $\beta$ 1-4 bridge. The length of cellulose chains varies greatly with the source, wood pulp having a degree of polymerization ranging from 300 to 1,700, while cotton ranges from 800 to 10,000. The characteristic properties of cellulose such as hydrophilicity, chirality, and degradability are highly dependent on its structure, and so is the reactivity of its multitude of OH groups. These hydroxy groups are also responsible for the extensive intra- and intermolecular hydrogen bonding, resulting in different structures and crystallinities. All of this means it can be complicated to give general statements on the properties of cellulose, as they can vary extensively from one type of cellulose to another<sup>13</sup>. One aspect that all types of cellulose have in common is their insolubility in water and most solvents. This means that some of the industrial production of cellulose is done in its swollen state under heterogeneous reactions. The reactivity of the hydroxy groups is in those cases determined by the hydrogen bond-breaking capability of the reaction media, and by the swelling of the cellulose due to the solvent<sup>16</sup>.

This means transferring usual organic chemistry reactions done on hydroxy groups to cellulose is not an easy task, and to this day a large amount of work is still to be done to fully understand the different aspects affecting modification reactions on cellulose. A great body of research exists on modification of cellulose through hydroxy group chemistry developed over the years, spanning a large range of target applications. The most industrially relevant cellulose ester produced, cellulose acetate, is produced using an excess of anhydride acetic in acetic acid, with sulphuric acid as the catalyst<sup>17</sup>. Cellulose functionalized with aliphatic, aromatic, and bulky esters are also available using acyl chlorides, or by activating carboxylic acids *in-situ* with carbonyldiimidazole or tosyl-

chloride under homogeneous acylation conditions. This leads to a wide range of degree of substitution on the cellulose, with different possible substituent and different properties available (**Figure 2**)<sup>18</sup>. Another possible route to produce cellulose is to dissolve cellulose in dimethylacetamide/LiCl and to add solid NaOH particles to the mixture. This leads to the formation of a gel at the interface between the solution and the solid particles, a process called induced phase separation. Sodium monochloroacetate is then added, which produces carboxymethyl cellulose<sup>18</sup>.

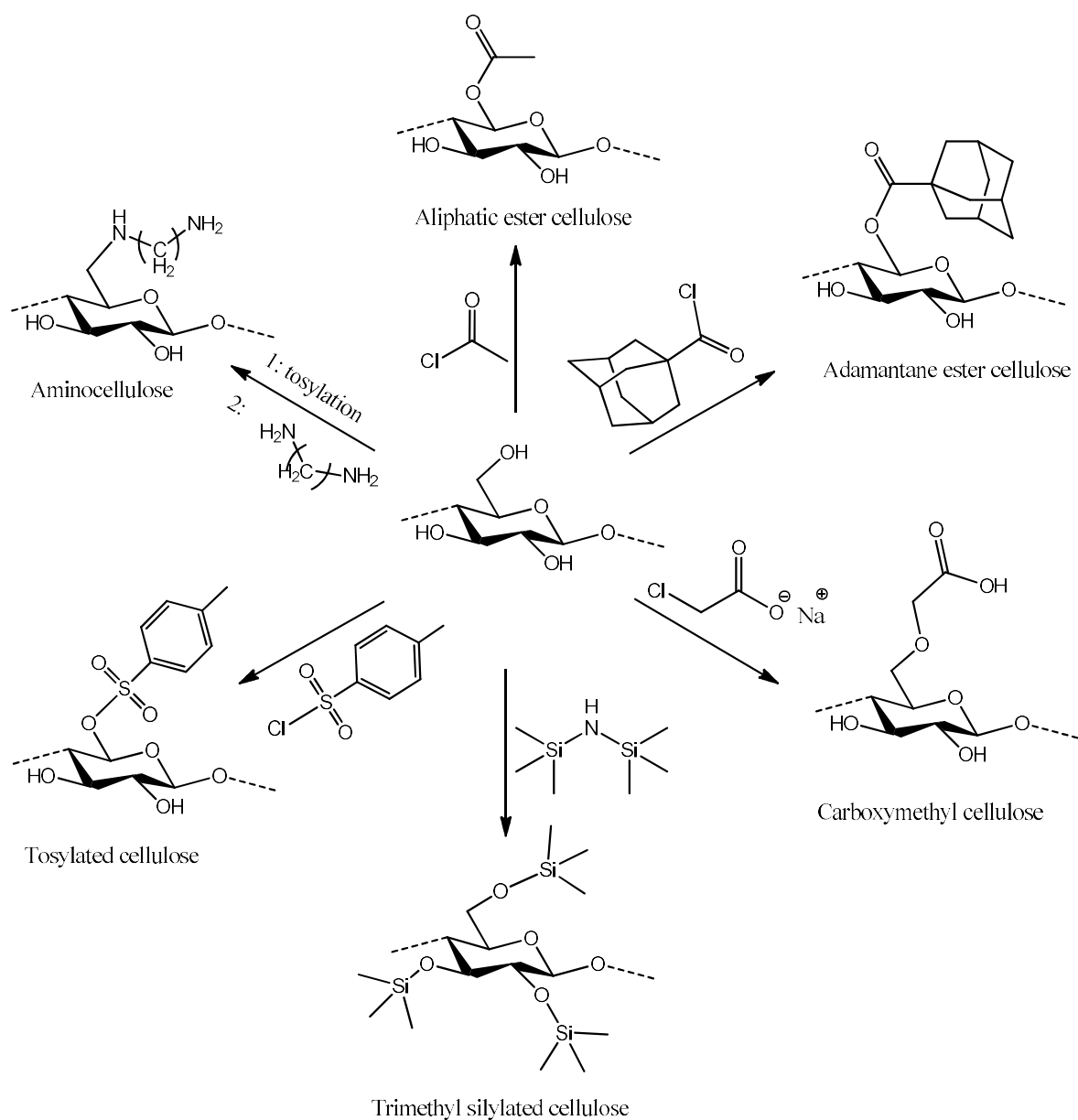


**Figure 2:** Examples of modification of cellulose to introduce different functional group by hydroxy chemistry.

Silyl cellulose has also been investigated because silylation of typical polar protic groups leads to materials with an important increase in thermal stability and also suppress hydrogen bonds, making it soluble in various organic solvents. Furthermore, silyl ethers are easy to cleave under acidic conditions, making these groups useful as a protective group<sup>19</sup>. Silylation can for example be done using hexamethyldisilazane in ammonia which results in the complete conversion of all hydroxy groups into O-trimethylsilyl (OTMS) groups<sup>20</sup>.

Another useful modification is sulfonation of cellulose as it is an interesting way to unlock other chemical pathways to modify cellulose than reactions involving alcohol moieties, *e.g.* the use of sulfonic acid chlorides to attach a nucleofuge to cellulose. Sulfonated cellulose also has some interesting properties that differ from pure cellulose and is useful for other applications<sup>21</sup>. Lastly, another modification that has been studied is the synthesis of aminocellulose, which can be obtained through different pathways. One is to react cellulose tosylate with 1,4-phenylenediamine (PDA) under specific conditions to obtain PDA-cellulose. This specific modification can be used as a polymer carrier capable of immobilizing enzymes, an interesting prospect for fiber-optical biosensors<sup>22</sup>. Aliphatic diamino groups can also be introduced instead with diaminoalkanes, using a nucleophilic substitution ( $S_N2$ ) of cellulose tosylate derivatives<sup>23</sup>. Overall, cellulose can be modified in many different ways through its hydroxy groups, but the reactions are not always straightforward because of the lack of good non-modifying solvents for cellulose and its strong hydrogen bonding network.

As mentioned previously, a wide variety of sources exists for cellulose such as plants, tunicates, fungi, and bacteria. However, due to the high amount of biomass waste from plants produced by different industries, most of the commercially used cellulose comes from wood or agricultural waste. This raw product contains more than just cellulose, and materials such as lignin and hemicellulose are also present. In plant material, cellulose is one of the main constituents of the cell walls, being responsible for mechanical strength due to its organized architecture. These walls are composed of several layers, each only a couple microns thick<sup>24</sup>. Each layer has a different chemical composition and structure and plays different roles. In the primary cell wall, cellulose is in the form of microfibrils that are oriented in a crossed pattern, whereas microfibrils of the secondary wall are aligned and densely packed. The secondary cell wall contains a large amount of cellulose fibers and has a varying degree of thickness mostly dependent on the source material<sup>25</sup>.

The microfibrils themselves are composed of smaller elementary fibrils, which are key to the production of nanocellulose.

### I.1.2. Cellulose nanomaterials

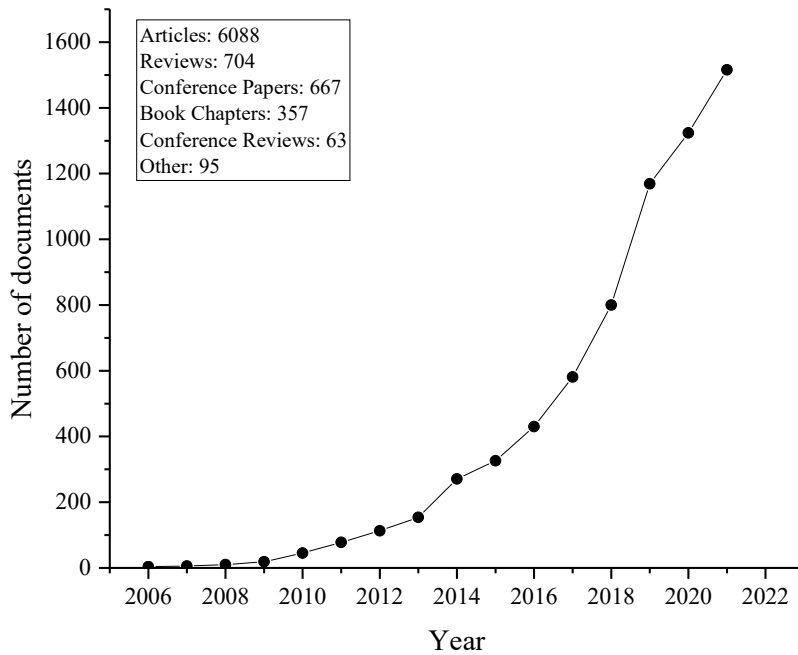


**Figure 3:** Number of research documents published since 2006 by year according to Scopus database using "Nanocellulose" as a keyword.

As mentioned previously, cellulose has been used for ages in many different ways. However, in recent years, a revolution was the discovery of cellulose nanofibers, and reliable ways to obtain it in a controlled fashion. Nanocellulose research started in earnest more than 20 years ago with the work of Favier *et al.* using cellulose whiskers as reinforcing fiber<sup>5</sup>. Since this article was published, an enormous amount of research has focused on using nanocellulose as reinforcement in composites, with entire research groups dedicated to it, yearly conferences being held, and thousands of papers published covering different aspects (**Figure 3** and **Figure 4**). One of the reasons is that while cellulose harvested directly from plant matter has its uses, it does not possess the properties, functionality, durability, malleability, and uniformity required for a higher degree of engineering. Therefore being able to extract and control cellulose morphology and use it in materials design at the nanoscale presents a significant advantage<sup>26</sup>.

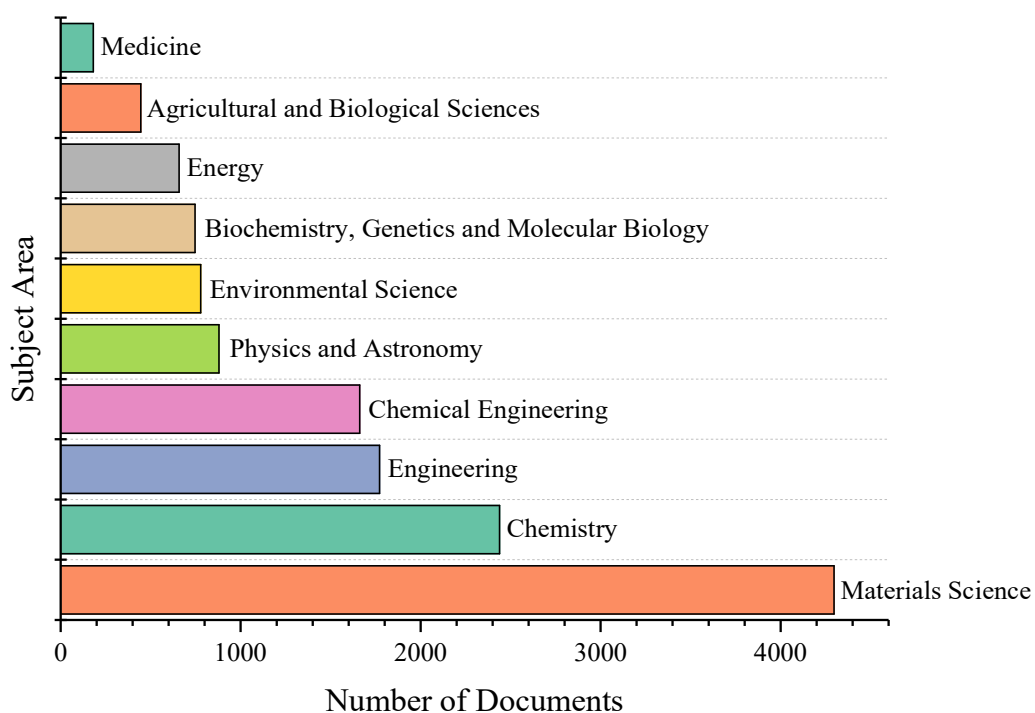


**Figure 4:** Number of research documents published since 2006 by subject area according to Scopus database using "Nanocellulose" as a keyword.

Nanocellulose can be found in the literature under different names, especially at the advent of the research effort. Generally speaking, nanocellulose refer to either two kinds of cellulose: “nanofibrils” or “nanocrystals”. Cellulose nanofibrils are long semi-crystalline nanoparticles with dislocated domains separating crystalline phases. On the other hand, nanocrystals refers to shorter, rod like crystalline nanoparticles obtained by removing the connecting non-crystalline regions from the nanofibrils, and are sometimes referred to as nanowhiskers. The cellulose crystals are also found under the name “microcrystals” despite their dimensions in the nanoscale<sup>4</sup>. For the rest of this document, cellulose nanofibrils (CNF) and cellulose nanocrystals (CNC) will be used exclusively to talk about those entities to avoid any possible confusion, and the term nanocellulose (NC) will be used as a general term to describe both of them.

### I.1.2.1. Cellulose nanofibrils

Cellulose nanofibrils (CNF), sometimes referred to as micro fibrillated cellulose (MFC), but not to be mistaken with cellulose microfibrils which have larger cross-sectional dimensions, were first described in 1983 by Turbak *et al.*<sup>27</sup>, and by Herrick *et al.*<sup>25</sup>. By using soft wood pulp and passing it through a homogenizer, they obtained fibers with a cross-section in the nanometer range. These nanofibrils are semi-crystalline and form a highly entangled network. Due to their very narrow nature, they possess a high aspect ratio, and can have a thickness between 5 and 50 nm, the wider ones representing aggregates of multiple fibers<sup>28</sup>. In order to produce CNF, multiple steps are required, and the process has been studied extensively over the year. However, common to every method, cellulose is first turned into a purified pulp by cooking and bleaching in order to separate it from hemicellulose and lignin. While wood is the go-to material for extraction of CNF, it has also been prepared out of cellulose from wheat or soy<sup>29</sup>, beet pulp<sup>30,31</sup>, potato pulp<sup>32</sup>, stems of cacti<sup>33</sup>, and many other sources.

One of the most important steps, *i.e.* separating the fibers through mechanical disintegration, can be done with dried material as well as in water. However, dry disintegration is usually avoided as it can be quite destructive and shreds fibers rather than separate them. This in turn produces shorter CNF, lowers crystallinity and aspect ratio, leading to reduced mechanical properties.

A widely used technique for the production of CNF is homogenization, a high-pressure process that disintegrates the larger fibrils into their smaller individual component. This process has been developed using mostly two different apparatus: homogenizers and microfluidizers. As described earlier, the first production of CNF by Turbak *et al.*<sup>27</sup> was carried out with a Manton-Gaulin homogenizer. This mechanical method used impact and shear forces to separate the individual nanofibrils, and the fibrillation of cellulose was carried out without any preliminary chemical treatment such as hydrolysis<sup>34</sup>, carboxylation<sup>35</sup> or quaternization<sup>36</sup>. A common alternative method developed later for disintegration was the use of a microfluidizer, a process first reported by Zimmermann *et al.*<sup>37</sup> in which a pulp suspension was first mixed at very high speed (24,000 rpm) and then passed through a microfluidizer at very high pressure (1000 bar). This resulted in fibers with a short width of 20-100 nm and a length of several microns. Similarly to homogenization, this method was also used to yield CNF without any pre-treatment. However, the lack of pre-treatment for both methods remained the main barrier for commercial process as homogenization alone

required a large amount of energy (over 70 MW/h for a ton of material)<sup>38</sup>. Thanks to the development of different pre-treatment methods, the high power consumption has been reduced down to 2 MW h/t, leaving clogging issues when using long fibers as the main hurdle for up-scaling homogenization in industry<sup>39</sup>.

Other than homogenization, grinding is also commonly used in the production of cellulose nanofibrils, usually starting from a fiber suspension passed through a grinder multiple times<sup>40</sup>. This method also makes use of shear force by using multiple disks between which the cellulose layers are separated. A major benefit of this method compared to homogenization is that the distance between the stones can be adjusted to avoid clogging. Some improvements to this method have been investigated such as adding a filler like calcium carbonate that can act as an additional source of grinding<sup>41</sup>. The CNF and mineral composite created this way is usually used in the paper industry, and its successful industrialization is a proof of its efficiency<sup>42</sup>.

While the techniques described previously cover a large portion of the production of CNFs, “non-conventional” methods exist as well, and are quite numerous. Refining is a method mostly used in the paper industry and can be used as a single means of producing CNF, or as a pre-treatment as well. In this method, cellulose fibers are swollen and peeled off of the cell wall in an aqueous solution, which makes the fibrils easier to access for further modifications<sup>43</sup>. Extrusion, while common for the production of various synthetic polymers, is also used to make CNFs as it produces shear force and high pressure as well. One of the main benefit of extrusion is that a much higher concentration of CNF can be used at once (up to 40% vs. 10% using most traditional methods). Moreover, it can be used at the same time as melting polymers, producing *in-situ* composites. However, this method is not without difficulties, and tuning the conditions to generate enough force to separate the fibrils without reaching cellulose degradation can be quite difficult<sup>44</sup>. Blending has also been used successfully by Uetani and Yano to produce homogeneous CNF in size with a width of 20 nm in just 30 minutes. However, the concentration used was very low, with optimal results obtained for 0.7 wt% of cellulose pulp<sup>38</sup>. Sonication is also a viable technique to produce CNFs at very high frequency (>20 kHz) producing differences in pressure and vacuum bubbles. This technique works by producing shear hydrodynamically to delaminate the fibers, which as described before is a key factor in the production of nanofibrils<sup>45</sup>. Lastly, some other methods for

mechanical separation of the fibers exist such as cryocrushing<sup>30</sup>, steam explosion<sup>46</sup>, ball milling<sup>47</sup>, and aqueous counter collision<sup>48</sup>.

As mentioned before pure mechanical disintegration is not cost effective and is a major drawback for the mass production of CNF, and most of the methods described before are used only after a pre-treatment. Pretreatment methods are designed to facilitate the separation of the cellulose layer, typically by swelling the layers in the cell wall, or by surface modification of the fibers to reduce their interaction, or to create repulsive forces between them. Such methods include hydrolysis<sup>34</sup>, carboxylation<sup>49,50</sup>, and sulfonation<sup>36</sup>, among others.

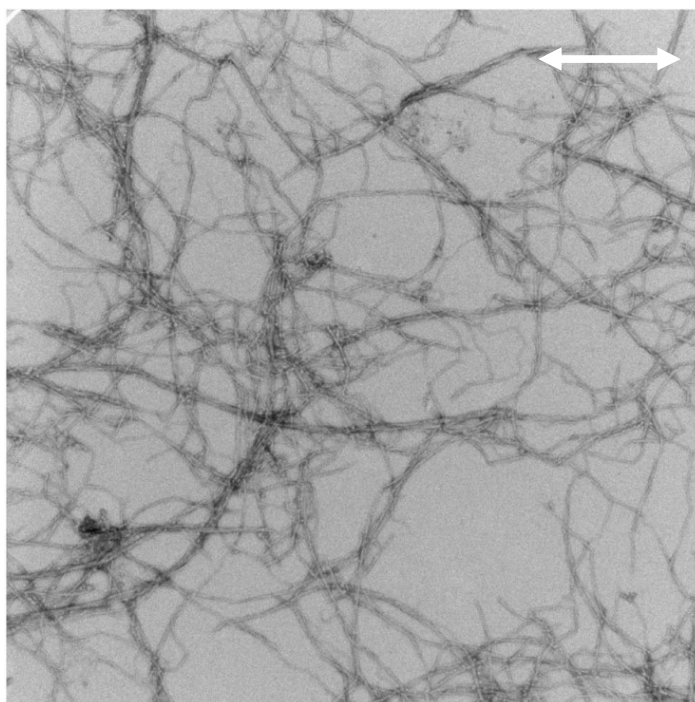


**Figure 5:** TEM image of CNF. Scale bar corresponding to 0.5 $\mu$ m. Reprinted (adapted) with permission from: Wang, W.; Sabo, R. C.; Mozuch, M. D.; Kersten, J. Y.; Zhu, J. Y.; Jin, Y. Physical and Mechanical Properties of Cellulose Nanofibril Films from Bleached Eucalyptus Pulp by Endoglucanase Treatment and Microfluidization. *Journal of Polymers and the Environment* 2015, 23 (4), 551–558. Copyright (2022) Springer Science Business Media New York.

As there are many different sources and methods to produce them, the morphology of CNFs can vary greatly. Typically, CNFs prepared purely by mechanical treatment have a larger diameter to those of CNFs obtained with a pre-treatment, as shown by Atomic Force Microscopy (AFM) by Aulin et al<sup>51</sup>. For CNFs produced after an optimal pre-treatment, a diameter in the 2-5nm range can be obtained, likely the width of an elementary fibril, obtainable in a variety of way such as a

combination of TEMPO-oxidation followed by blending<sup>52</sup>. The length of the fibrils is usually difficult to measure, due to their very high aspect ratio, as too high a magnification does not show the fibrils in their entirety, and too low a magnification makes them not visible anymore due to their very small diameter. However, it is usually agreed that they can be up to several microns in length (**Figure 5**), but comparison of their length for each method used is difficult.

#### I.1.2.2. Cellulose nanocrystals

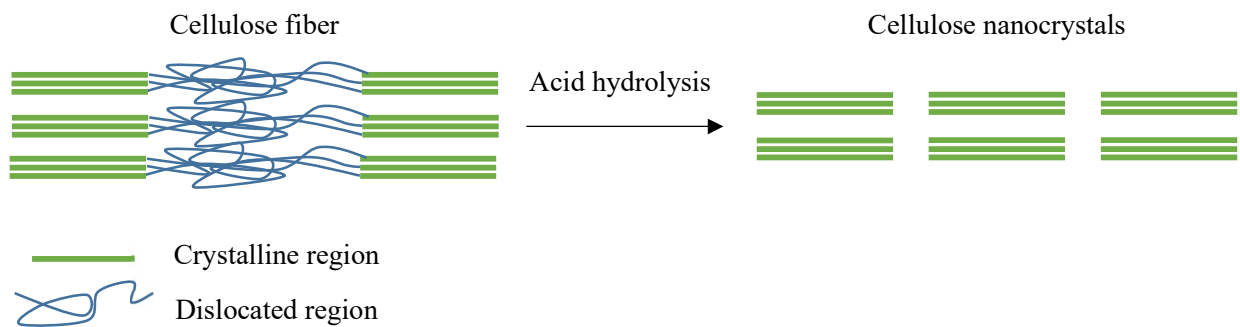


**Figure 6:** Schematic representation of acid hydrolysis of cellulose fiber into cellulose nanocrystals

Cellulose nanocrystals, unlike cellulose nanofibrils, are obtained by removing the non-crystalline portion of natural cellulose fibers (**Figure 6**). This is typically done using strong acids and is a very destructive process resulting in the cleavage of bonds in the glycosidic chains that cellulose is made of. The first report of nanocrystalline cellulose was made 70 years ago by Rånby who degraded cellulose fiber with sulphuric acid<sup>53</sup>. While this acid has been studied and used the most, hydrochloric acid has also seen substantial usage<sup>26,54</sup>, and uses of phosphoric and hydrobromic acid have also been reported<sup>55,56</sup>. The hydrolysis reaction produces CNCs due to an important difference in free volume between non-crystalline regions. In this region, the degree of polymerization (DP) decreases very quickly, as opposed to crystalline regions, where even prolonged exposure to acid shows only a minor reduction of DP. Due to this difference, the acid can penetrate the dislocated regions more easily, while the crystalline regions take much longer to go through hydrolysis<sup>57</sup>. Selecting the right acid for this step is important as each of them affect the properties of the final CNCs. Sulfuric acid introduces a negatively charged surface on the CNCs due to the grafting of sulfate moieties during the hydrolysis, stabilizing the suspension of CNCs in water by electrostatic repulsions. The same effect is observed for nanocrystals produced with phosphoric acid, as a result of phosphate group grafting. Sulfate groups however can be detrimental for high end-applications

as a high amount of surface sulfate groups can lead to a loss of thermostability for the nanocrystals, lowering the degradation temperature of the material significantly<sup>58</sup>. If the nanocrystals are instead prepared by hydrochloric acid hydrolysis, they retain their thermal stability, however they will lack stabilizing groups on the surface leading to unstable suspensions and eventually flocculation<sup>55</sup>.

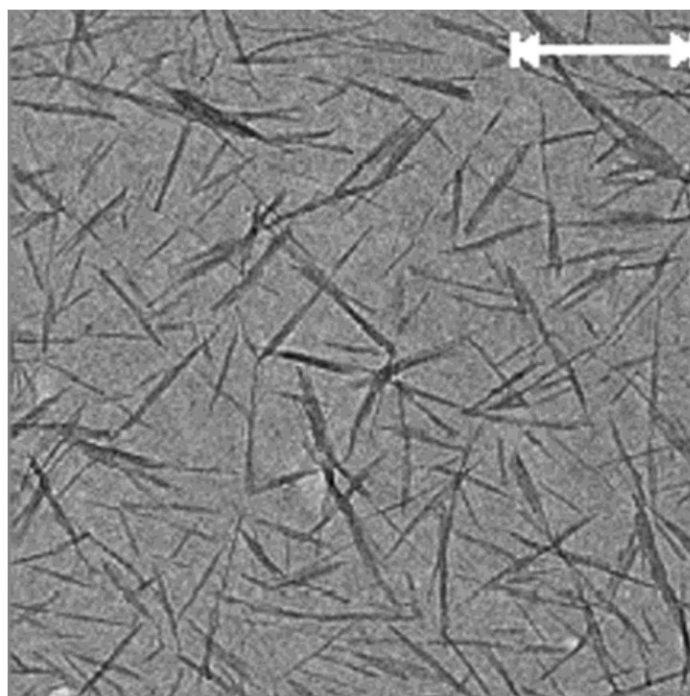


**Figure 7:** Positively stained electron micrograph of cotton cellulose crystallites taken from the anisotropic phase. Scale bar corresponding to 400 nm. Reprinted (adapted) with permission from: Fleming, K.; Gray, D.; Prasannan, S.; Matthews, S. Cellulose Crystallites: A New and Robust Liquid Crystalline Medium for the Measurement of Residual Dipolar Couplings. *J. Am. Chem. Soc.* 2000, 122 (21), 5224–5225. Copyright (2022) American Chemical Society.

While all CNCs have a characteristic rod-like shape (**Figure 7**), their dimensions can vary greatly depending on the source of the cellulose and the hydrolysis conditions. Some studies have investigated the effect of time and temperature for a given hydrolysis reaction, and it was found that a higher crystallinity was obtained for hydrolysis conducted at higher temperature for a shorter amount of time<sup>59</sup>. The dimensional heterogeneity due to the diffusion-controlled nature of the hydrolysis can be reduced for a given reaction by filtration or centrifugation<sup>60,61</sup>. AFM is one of the main techniques used to study the dimensions of nanocrystals, as it can give information about the size of the particles down to a tenth of a nanometer rather quickly. Moreover, it has been shown to give good measurements on their mechanical properties such as stiffness or adhesion<sup>62</sup>. Average

dimensions obtained from different sources has been studied to a great length by different research groups, but the typical width for CNCs is a couple of nanometers. The length of these needle-like CNCs varies to a much greater degree, from tens of nanometers to a few microns. A summary of those results can be found in several review articles, such as the work of Habibi *et al.*<sup>54</sup> which groups the characteristics of many different kinds of CNCs sources. In the case of cotton, which is one of the most commonly used starting material used for the production of CNCs due to its high cellulose content and purity, the typical width measured is 5-10 nm while the length spans from 100 to 300 nm. Another aspects that can vary with regards to the morphology of CNCs is the shape of the cross section of the crystals. As an example, CNCs obtained from bacteria or tunicate are reported to be ribbon-like in shape, whereas those obtained from plant have never shown such shapes and are thought to display a flat uniplanar axial orientation<sup>60,63</sup>.

The mechanical properties of cellulose nanocrystals have also been studied extensively due to the high interest of using them as reinforcing fillers in polymer matrixes. While many measurements have been done to determine the modulus of CNCs, the obtained values do not always concur. It is generally agreed however that the axial Young's modulus of cellulose nanocrystals is in theory similar to that of Kevlar, and at least higher than that of steel. In the case of a perfect crystal, the value for the Young modulus is 167.5 GPa<sup>64</sup>. The best results for reinforcement with cellulose nanocrystals are obtained when cellulose can be mixed with other materials and processed by solvent casting after they were well dispersed, which is quite limiting as unmodified cellulose is well dispersed in a limited list of solvents (usually protic solvents such as water and alcohols). Dispersion of CNCs into individual particles is particularly important for their use as reinforcement in composite, as this is key to maximizing mechanical performances, hence the use of surface modification of CNCs to achieve a better dispersion into organic solvents.

### I.1.3. Other polysaccharides

Starch is a natural polysaccharide, insoluble in water at lower temperatures, that stores energy in the form of easily hydrolysable glucose chains. It is present in various parts of plants, mainly in the stem, roots, seeds and leaves, and exists in the form of granules measuring 2 to 100  $\mu\text{m}$  with various possible shapes<sup>2</sup> (**Figure 8**). Starch is composed of amylose, a linear chain of  $\alpha$ -1,4-glucose, and amylopectin, chains of  $\alpha$ -1,4-glucose heavily branched with 1,6 linking happening every 20-30 anhydroglucose units<sup>65</sup>. Amylose is the smaller of the two polymers with a molecular weight

between  $10^4$  and  $10^5$ , and a DP of 250-1,000<sup>66</sup>. Amylopectin is one of the largest naturally occurring molecules with molecular weight far superior to amylose at  $10^6$  to  $10^8$  corresponding to a DP of 5,000-50,000.

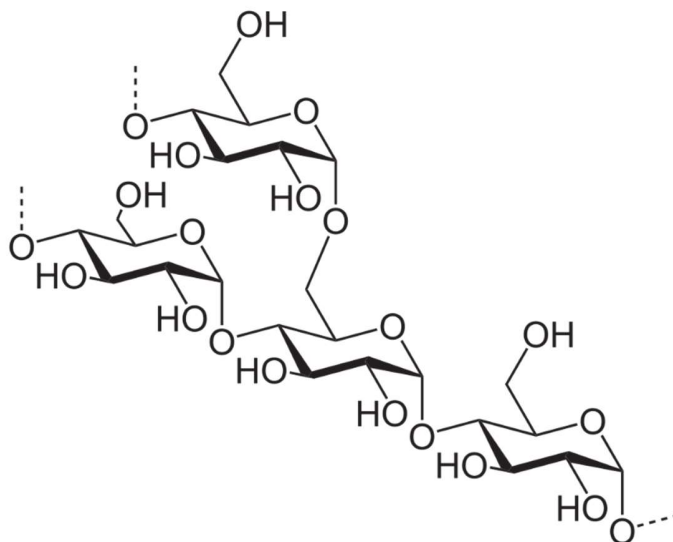


**Figure 8:** Chemical structure of amylopectin.

Typical starch contains 20-30% amylose and 70-80% amylopectin<sup>67</sup>. Commercial starch is usually made from corn or wheat, but potato, tapioca, rice, or manioc can be used as well. The fact that starch is cheap, relatively easy to modify physically and chemically, and possesses all the typical polysaccharide benefits (renewable, biodegradable) make it a very good candidate for food packaging applications<sup>68</sup>. Another interesting property of starch is its ability to turn into a thermoplastic when shear is applied in the presence of a plasticizer such as water, oil, or glycerol. This thermoplastic starch is already available commercially<sup>69</sup>, and can be processed by moulding, extrusion and blow moulding into more refined material<sup>70</sup>. However, while starch has been widely studied, it still has two disadvantages to using it for packaging: moisture absorption and poor mechanical properties. Starch also does not have any antimicrobial or antioxidant properties.

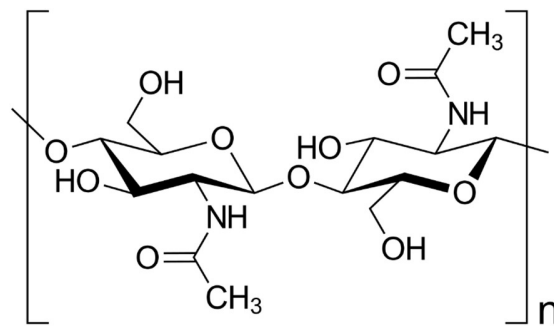


Figure 9: Chemical structure of chitin.

Chitin is a structural material present in many living organisms, mainly crustaceans, but also insects and fungi (Figure 9). Depending on the ratio of monomers, it is named chitin or chitosan, with chitin being a ratio acetamidation/acetylation superior to 50%. Just like starch, chitin is insoluble in water, but also in most common solvents which is still a major limitation<sup>71</sup>. It is however possible to turn chitin into chitosan under high alkaline conditions and a high temperature, with the resulting chitosan soluble in acidic media such as aqueous HCl and acetic acid. Chitin can be obtained as a waste of the food industry in the range of 10<sup>11</sup> tons per year, but only 150,000 tons of chitin is made available for commercial use<sup>72</sup>. Like starch, one of the most promising applications for chitosan resides in food packaging due to its incredible properties: biocompatibility, non-toxicity, edibility, antibacterial properties, and biodegradability. Chitosan film also possesses good mechanical properties, and selective permeability to carbon dioxide and dioxygen. Their main drawback resides in their high water affinity, which significantly reduces their barrier properties. To counteract this, many strategies have been studied such as blending it with other polysaccharides or cross-linking the chitosan chains to decrease its water affinity. Chitosan has therefore been investigated by many research groups as an active, anti-microbial packaging coupled with more typical polymers used in packaging such as poly(ethylene terephthalate) (PET)<sup>73</sup>. So far, neat chitosan has been extensively researched as packaging for fruit, as it prevents the decay of fruit when applied as a thin coating from solution<sup>74</sup>. However, food packaging is far from being the only application for chitosan, as its interesting properties have found uses in other fields, some of which are highly specialized. For example, chitosan fibers have been used to reinforce chitosan-based nerve conduits, an artificial means of helping nerve regeneration. *In vitro* tests were performed, and chitosan proved to be non-toxic to neuro-2a cells, and reinforced conduits showed significantly improved mechanical properties, and preliminary *in vivo* testing seemed to

show compatibility of those conduits with the surrounding tissues<sup>75</sup>. Overall, chitosan is a very promising material for biomedical applications, and it has also been studied for use in cartilage engineering<sup>76</sup>, intervertebral disc tissue engineering<sup>77</sup>, and substrate for cell growth<sup>78</sup>.

## I.2. Synthetic polymers considered in this work

### I.2.1. Polyesters

Synthetic polyesters were first developed in the 20<sup>th</sup> century as coatings by combining acids and alcohols. A large amount of work was carried out by Carothers who reported different polyesters of various sizes from dicarboxylic acids and diols. Some of this work was the precursor for many commercial polyesters produced today by starting to optimize polycondensation, one of the common polymerization methods for the production of polyesters<sup>79</sup>. In this work, we limited ourselves to the ring-opening polymerization of cyclic lactones and carbonates from cellulose nanocrystals. The subsequent sections will therefore be limited to the polymers and polymerization techniques used in this work as reviewing all other polymers and techniques would be a substantial task, with much of it outside of the scope of this thesis.

#### I.2.1.1. Poly(lactic acid)

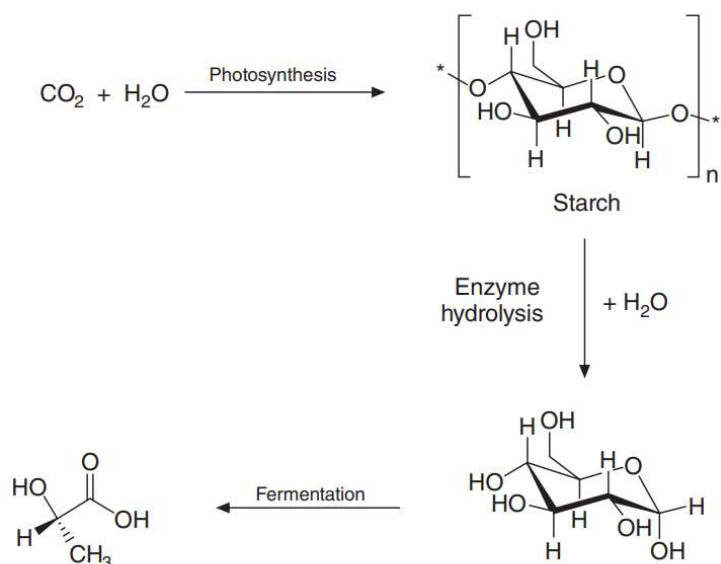


**Figure 10:** Conversion of carbon dioxide and water into lactic acid through multiple natural steps.

Poly(lactic acid), or polylactide (PLA), is currently one of the most widely researched polyester on the planet due to its biodegradability, biocompatibility, and the potential renewability of its monomer, which is commercially produced from natural sources. Indeed, conventional synthetic polymers are often petroleum based, lactic acid however, can be obtained from crops through fermentation. Starch, readily produced by plants in the cell wall for energy storage, can be extracted and converted to sugar which turns into lactic acid under bacterial fermentation (**Figure 10**)<sup>80</sup>.

Not only does this make lactic acid a renewable resource, the process is also economically viable as sugar is a cheap and abundant resource. Corn, currently the cheapest sugar source, is produced in enormous quantities in the United States, and the production of half a million ton of PLA requires less than 1% of the annual US corn production<sup>81</sup>. Therefore, unlike some other renewable resources, lactic acid has a good economic potential already, and optimization of the fermentation processes is still pursued. Lastly, lactic acid production can be carried out all over the world as it not limited to corn but rather relies on starch-containing crops, which are numerous and spread throughout the world.

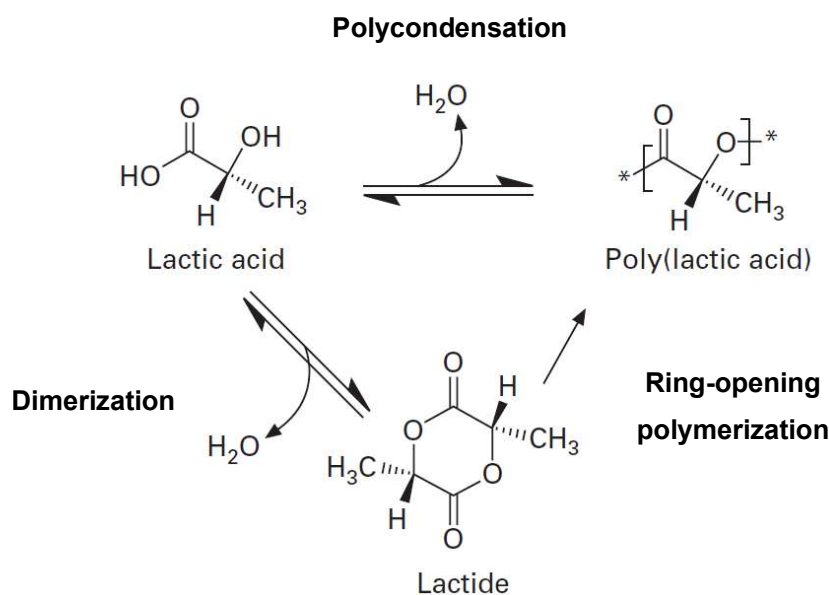


**Figure 11:** Most common route for the production of PLA.

From lactic acid, PLA can be obtained by two different routes: either the polymerization of lactic acid by condensation, making poly(lactic acid), or by ring-opening polymerization after forming the cyclic intermediate lactide, producing poly(lactide) (**Figure 11**). Polycondensation under high

vacuum and temperature to remove the water formed and to move the equilibrium of the reaction was first developed by Carothers<sup>79</sup>. However this method did not yield very high molecular weight polymers, and it had other drawbacks such as the need for large reactors and unwanted racemization of the product. This method however proved useful to make oligomers for the preparation of adhesives, as cross linking was made possible with the proper choice of additives<sup>82</sup>. As an alternative way of producing higher molecular weight PLA by condensation, azeotropic solution polymerization was studied under different conditions. By using an azeotrope, the pressure required for the synthesis could be lowered significantly, and the separation of PLA with the solvent was also made easier. After careful optimization of the process, PLA with a molecular weight above 50,000 g.mol<sup>-1</sup> could be achieved<sup>83</sup>. Another method of condensation that has been reported to obtain high molecular PLA consists of a melt/solid condensation, as described by Moon *et al.*<sup>84</sup>. This two-step process consists of a first melt-polycondensation to obtain a PLA of 20,000 g.mol<sup>-1</sup>. After cooling down and recovery of the PLA, the polymer is submitted to a heat treatment above the glass transition temperature ( $T_g$ ) of the polymer but below its melting temperature ( $T_m$ ) to obtain a higher crystallinity. The reaction is then continued at higher temperature but still in solid state, to yield a very high molecular weight PLA (up to 500,000 g.mol<sup>-1</sup>).

The most common way to obtain high molecular weight poly(lactide) in a controlled manner is to turn first lactic acid into lactide (**Figure 11**), which can be accomplished under mild condition and solvent free by water removal. The product is then purified by distillation at high temperatures, and can be readily polymerized by ring-opening polymerization (ROP), which can be done in bulk or solution, and by cationic, anionic and coordination mechanism. A specific look at the ring-opening polymerization reaction will be given later for additional details.

Due to PLA's popularity, there has been a many studies on the properties of PLA. PLA is a biodegradable material, which is one of the primary reasons for its popularity. It is however not biodegradable under ambient temperature and conditions, and requires other factors for its degradation to occur. *In vivo*, PLA is readily hydrolyzed, both with and without the help of enzymes. It is therefore biodegradable under physiological conditions, which contributed to its biocompatibility<sup>85</sup>. In addition, the degradation of PLA under composting conditions also leads to its hydrolysis, but this requires elevated temperatures (60 °C) to occur, and is helped by microorganisms<sup>86</sup>.

While some of PLA's properties are often compared to other common thermoplastic, PLA fibers are one of the only fibers that are able to be processed by melting that can be made from renewable sources. With regards to its thermal properties, PLA is rigid at room temperature due to its  $T_g$  being in the 55-65 °C range, and in this state it can either be amorphous or semi-crystalline depending on its thermal history and stereochemistry. For semi-crystalline PLA, the melting point can vary between 130 °C to 180 °C depending on the ratio of D and L isomers in the polymer (Figure 12). Overall, PLA thermal properties can vary greatly depending on the structure of the polymer and the molecular weight. When compared to other thermoplastics, PLA is considered fairly easy to use for thermal processing due its average  $T_g$  and  $T_m$ , but these are also a limiting factor compared to poly(ethylene terephthalate) (PET) for some applications<sup>87</sup>.

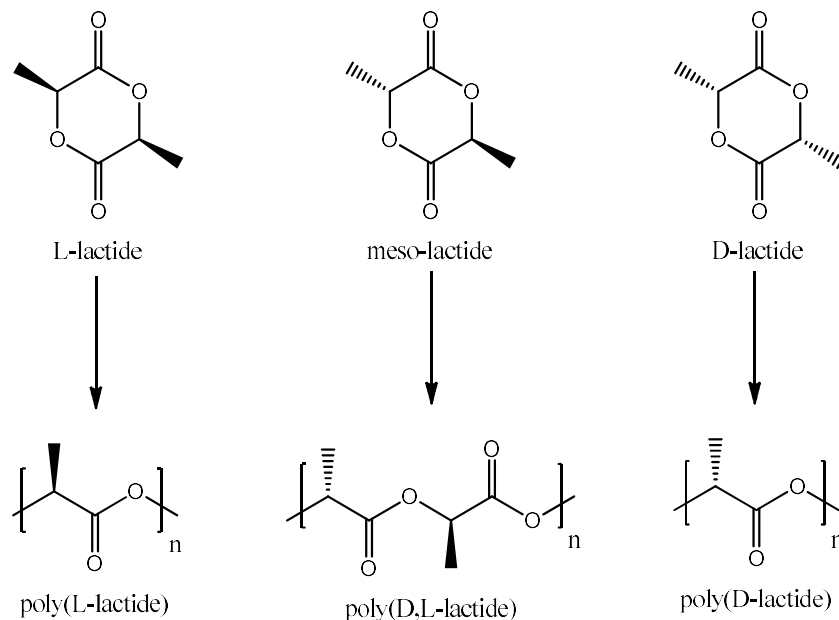


**Figure 12:** chemical structure of the different stereoisomers of lactide and their resulting polymers.

PLA mechanical properties can also vary greatly, from a softer material to a very stiff one. To achieve the later one, semi-crystalline PLA is preferred as the crystalline part gives the polymer a much higher tensile strength and modulus, at respectively 50 MPa and 3 GPa. However, stiff PLA is brittle with a fairly low elongation at break, typically under 5%<sup>88</sup>. While the thermal properties of PLA are dependent on a multitude of factors, its mechanical properties depend almost exclusively on the stereochemistry of the chain and its length. Poly(L-Lactide) for example has

been reported to have double its modulus when its molecular weight increases from 50.000 to 100.000 g.mol<sup>-1</sup>, and a tensile strength multiplied more than tenfold going from 50.000 to 200.000 g.mol<sup>-1</sup> <sup>89,90</sup>. This means that by having a good control over the microstructure of PLA by using the different lactide isomers and/or stereoselective catalysts, as well as the degree of polymerization, specific mechanical properties can be achieved which is critical for some applications.

Due to the possibility to tune PLA's mechanical and thermal properties over a wide range, and its ease of processing, it is not surprising that PLA has found uses in many applications. Among these, packaging has seen the largest share of the market for several years, but the medical field and use in textiles field have been steadily increasing over the years as well<sup>83</sup>.

For packaging, PLA has seen success due to its barrier properties which have been reported to be very good for most gases<sup>91</sup>. This gives PLA the properties that are needed for packing fresh products as it acts as a barrier to the outside, preserving the product, while also retaining flavor and aroma inside. As an added advantage, it is also easily heat-sealable. More recently, more advanced applications in packaging have been studied such as active packaging, a concept in which the material used as packaging can have interactions with the product inside and help with, for example, preserving the product inside from degradation<sup>92</sup>. This novel approach makes use of similar concepts that can be found in medicine, using the slow release of active species that can be "stored" inside the polymer. These species can help in various aspects such as O<sub>2</sub> capture, regulating moisture, act as antioxidants to slow down degradation, or even help with antimicrobial properties<sup>93</sup>.

In the biomedical field, it is PLA's biocompatibility and biodegradability that are its most interesting attributes. It has a very wide range of uses, and wound management is a very common one. In fact, PLA makes for great bioresorbable suture and temporary implant material, as it can be employed to mend a certain area until it heals and then degrades over time<sup>94</sup>. Due to the breakage of the ester bonds by hydrolysis, PLA-based devices can erode in the body, slowly releasing entrapped compounds such as hormones and proteins, while the products of degradation are naturally turned into non-toxic species eliminated by the body. One last example of a very promising application in this field is tissue engineering. Because PLA degrades over time, they have attracted a lot of interest as a growing support for transplants. Different cell types have been investigated, and muscle tissue, and bone have successfully been grown<sup>95</sup>.

The production of PLA fibers has also found many uses in industry. Nowadays fiber production is a very large market where more than 50% of the total fiber production is synthetic, largely dominated by PET. One of the benefits of PLA is that it can be made as both a yarn, similar to wool, or produced as a filament, which can be used to produce clothing with different feel, sometimes close to natural fibers such as cotton. Due to its interactions with water, PLA fiber-made clothing exhibit fast moisture spreading and drying, making them ideal for sportswear, and tests *vs.* PET fabric have shown improved comfort for people wearing them. The main drawbacks from such fabric is its degradation by hydrolysis, which can be problematic under dyeing conditions, and the melting point of typical PLA yarn at 170 °C which can be a problem with unaware consumers ironing their clothing. Other than clothing PLA fibers can be used to make a variety of homeware such as pillows, carpets, mattresses and other similar fabric items<sup>81</sup>.

Overall, PLA is a very promising material with a wide range of applications, and its biodegradability, biocompatibility, and availability of its monomer from renewable source can easily explain the great interest it has generated. However, some of its mechanical and thermal properties, while sometime advantageous, can also be detrimental to some applications, hence the vast number of works conducted to improve it.

#### 1.2.1.2. Poly( $\epsilon$ -caprolactone) and Poly( $\delta$ -valerolactone)

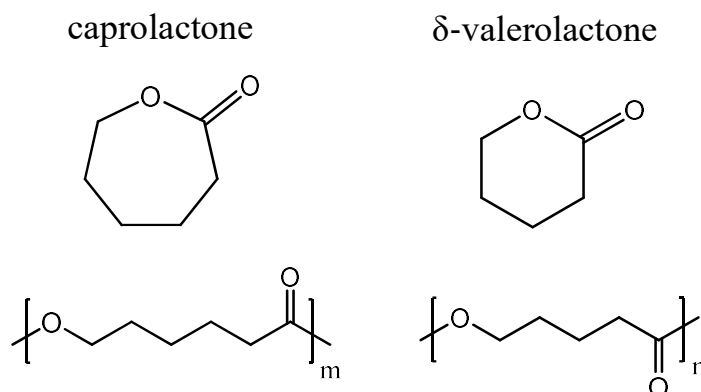


**Figure 13:** chemical structure of  $\epsilon$ -caprolactone,  $\delta$ -valerolactone, and their corresponding polymers.

Poly( $\epsilon$ -caprolactone), or PCL (**Figure 13**), is a biodegradable aliphatic polymer which has found significant uses in the biomedical field. It is usually obtained by ring-opening polymerization of  $\epsilon$ -caprolactone in the presence of a catalyst, stannous compound being quite common for this

reaction. Once the polymer is obtained, it is a semi-crystalline material with a very low glass transition temperature at around  $-60\text{ }^{\circ}\text{C}$ , and a melting point around  $60\text{ }^{\circ}\text{C}$ . It is degraded by hydrolysis in much the same way as poly(lactide) does, but this process is even slower which makes it a material of choice for long term *in vivo* devices. Perhaps one of the main uses for PCL, as it has relatively poor mechanical properties on its own, resides in its compatibility with other polymers. A lot of work has been done on blending it with other common polymers to tune their properties, or copolymerizing it, both giving very different results<sup>96</sup>. Such copolymers have seen a lot of use for biomedical applications, where they can be employed to make amphiphilic copolymers for drug delivery, or scaffolds for tissue engineering<sup>97,98</sup>.

Valerolactone, more specifically  $\delta$ -valerolactone (**Figure 13**), is a lactone that has also gathered a lot of attention as it can be derived from biomass and can be turned into poly( $\delta$ -valerolactone) (PVL), a polymer with many potential applications. While this monomer can be prepared by a Baeyer-Villiger oxidation of cyclopentanone, it is an expensive and hazardous reaction. Therefore dehydrogenation of pentane-1,5-diol has been developed, which can start from furfuryl alcohol, a biomass derived product<sup>99</sup>.  $\delta$ -Valerolactone can be polymerized by ring-opening polymerization, which will be described in more details further in I.3. Due to its close resemblance to poly( $\epsilon$ -caprolactone), PVL is used in similar applications and is also often used along with other polymers to tune their properties. It is particularly interesting as a biomedical material<sup>100</sup>.

## I.2.2. Polycarbonates

### I.2.2.1. Generalities

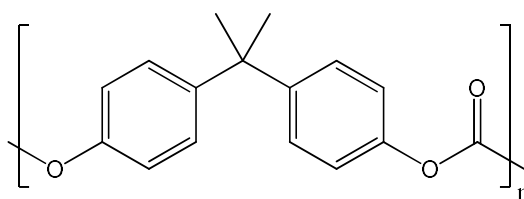


**Figure 14:** Chemical structure of Bisphenol A polycarbonate (BPA-PC)

Polycarbonates is an important group of polymers which possess a O-CO-O group in the main chain and are generally divided into two groups with vastly different properties: aromatic and aliphatic polycarbonates. The most economically important one was discovered in the year 1953 at Bayer by Schnell, Bottenbruch and Krimm and is now known as Bisphenol A Polycarbonate

(BPA-PC) (**Figure 14**). Interestingly, it was also synthesized later the same year independently by Fox at General Electric<sup>101</sup>. A few years after, the product was commercialized and had a great success due its impressive toughness, glass-like transparency and high heat resistance, which made BPA-PC a great alternative to PET. While other bisphenol polycarbonates have been produced, none of them have had the same success BPA-PC had, which is still widely used and occupies the largest portion of the polycarbonate market<sup>102</sup>.

Aliphatic polycarbonates are quite different and were already explored by Carothers years prior along with his work on polyesters, who produced low molecular weight low melting point polycarbonate. However, due to high demand for stronger material at the time, they did not know the success that their aromatic homologues had. But due to their other very interesting properties, they would eventually see a lot of interest for different uses as detailed below.

#### 1.2.2.2. Aliphatic PC

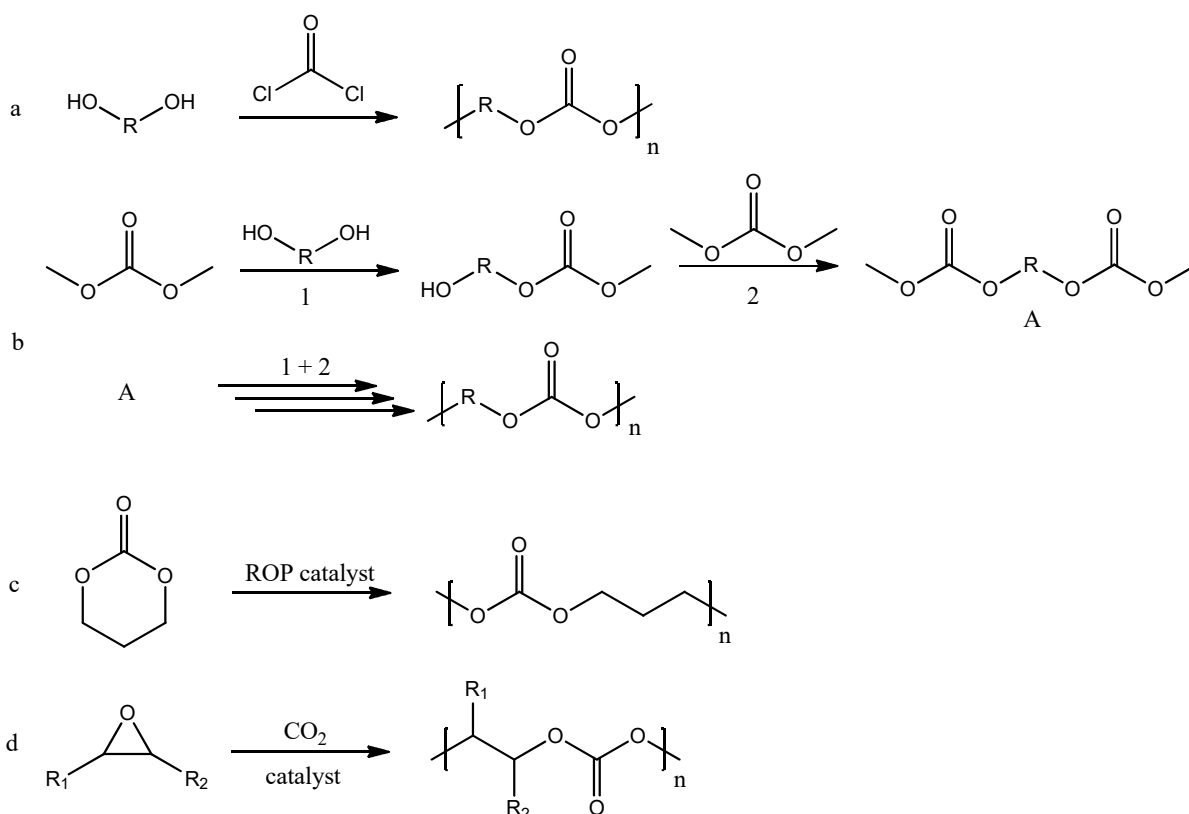


**Figure 15:** Different pathways to obtain polycarbonates. a: reaction of diol with phosgene. b: transcarbonatation reaction, step 1 and 2 repeated with the product multiple times to lead to a polymer. c: ring-opening polymerization of cyclic carbonate. d: copolymerization of epoxy and  $\text{CO}_2$ .

Aliphatic polycarbonates can typically be obtained in four different ways (Figure 15): first the polymerization of diols in the presence of phosgene, a similar reaction that can be used to obtain BPA-PC. A second method is to react diols with dialkyl carbonates in the presence of a transcarbonatation catalyst, as was done by Carothers. Ring-opening polymerization of cyclic carbonate can also be performed, a method that has seen a lot of interest in recent years thanks to the many ways to produce cyclic carbonate that have been developed<sup>101</sup>. Lastly, the copolymerization of epoxides along with CO<sub>2</sub> has also been developed as an efficient and greener way to obtain aliphatic polycarbonates<sup>103</sup>.

Multiple methods exist in order to obtain cyclic carbonate, with five and six-membered cycles being the most commonly produced. As mentioned before, phosgene can be used to produce polycarbonates in the presence of diol, and it can also be used to make cyclic carbonates. However, due to phosgene high toxicity, other methods are preferred. One of the most promising method is to use CO<sub>2</sub> insertion into a cyclic ether, which is most commonly catalyzed by a Lewis acid or a base. However, these reactions require high temperature and pressure which can limit their commercial applications<sup>104</sup>. Due the potential to reduce CO<sub>2</sub> during their synthesis, a lot effort has been put towards developing different catalytic systems that reduce the high temperature and pressure requirements of the current CO<sub>2</sub> insertion method.

For five-membered cyclic carbonates, organometallic compounds such as methyltin tribromide and butanestannic acids were reported to be good at turning CO<sub>2</sub> and oxirane into their cyclic counterpart under mild conditions. Organoantimonies have also been reported to produce cyclic carbonates, with the added benefit of not being able to initiate the polymerization of the oxirane, unlike organotins<sup>105</sup>. Ammonium salts have also been used successfully at the industrial scale to prepare five-membered cyclic carbonates<sup>106</sup>. Lastly electrochemical procedures have also been studied to obtain cyclic carbonates at room temperature and atmospheric pressure in an electrolysis cell with dimethylformamide (DMF) and potassium bromide<sup>107</sup>. In addition to the few examples given, many other systems have been developed showing the great interest that using CO<sub>2</sub> to produce monomer has<sup>104</sup>.

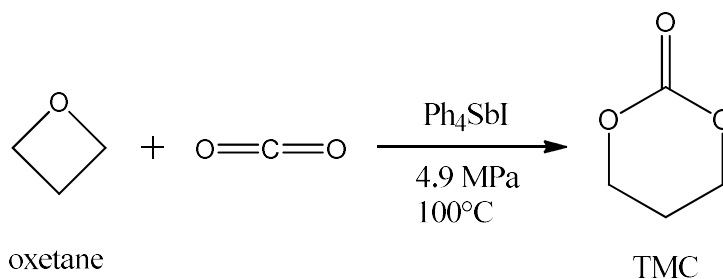


**Figure 16:** Reaction of oxetane and CO<sub>2</sub> to obtain TMC, as described in the work of Baba, Kashiwagi, and Matsuda<sup>108</sup>.

Six-membered cyclic carbonates, much like their five-membered cyclic cousin, can also be produced from a cyclic ether (this time oxetane) and CO<sub>2</sub>. However, this tends to be much less efficient and has led to fewer studies. This problem can be attributed to the instability of the six-membered cyclic carbonate, for which polymerization is heavily favored<sup>109</sup>. Nevertheless, due to the importance of these monomers, and in particular 1,3-dioxan-2-one, or trimethylene carbonate (TMC), some work has been done to try to produce these valuable monomers using CO<sub>2</sub>. Pioneering this reaction, Baba, Kashiwagi and Matsuda reported the reaction of oxetane with CO<sub>2</sub> at 4.9 MPa catalyzed by Ph<sub>4</sub>SbI with a 96% yield<sup>108</sup> (Figure 16). This group would later improve the reaction efficiency further to the point of a quantitative yield by using Bu<sub>3</sub>SnI and hexamethylphosphoramide (HMPA) as the catalytic system<sup>110</sup>. Lastly, their methodology was used to produce substituted six-membered cyclic carbonates, with mono-substituted species giving a much better yield than di-substituted cyclic carbonates. This work opened the door to a lot research and several catalytic system have been developed since to try to improve the synthesis of di-substituted TMC species<sup>111</sup>.

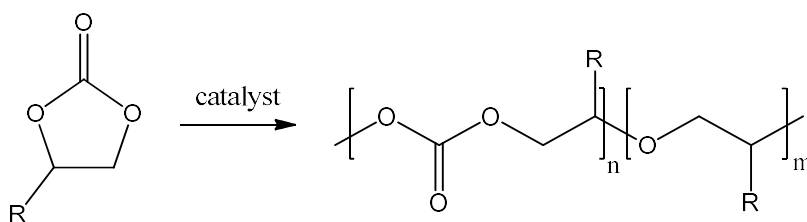


**Figure 17:** Polymerization of five-membered cyclic carbonate resulting in a poly(ether-co-carbonate).

With regard to the polymerization of cyclic carbonate, five-membered ring are much harder to polymerize, but some success has been reported with metal alkoxides and metal alkyls. However,

this reaction often occurs at high temperature (170 °C) and under those conditions, the polymerization involves a partial decarboxylation thus giving a poly(ether-co-carbonate), with up to 50% carbonate units under the best conditions (Figure 17)<sup>112</sup>. More recently however, reports of the polymerization of cyclohexene carbonate (CHC) has been done by coordination-insertion ROP with a wide variety of catalysts, and pure isotactic PCHC was obtained from enantiopure (R,R)-CHC with no decarboxylation. For six-membered cyclic carbonates, polymerization is much easier and usually done via a ring-opening mechanism. A lot of work has been carried out using metal catalysts based on aluminum and zinc<sup>113,114</sup>, but increasing interest in organocatalysis has made cyclic esters and carbonates prime candidates to find new catalytic system, which will be described in section 1.3.

For applications, aliphatic polycarbonates present much of the same benefits as PLA does when it comes to biodegradability and biocompatibility<sup>115,116</sup>. However, mechanical properties can vary greatly depending on the structure of the main chain, therefore different polycarbonates have different expected applications such as textiles, microelectronics, packaging and biomedical applications<sup>117</sup>. They are also particularly interesting material to use with other polymers in copolymers<sup>118</sup> which can help with their weak mechanical strength. It is interesting to note that for medical applications they offer a very good alternative to PLA which is sometime too hard and brittle to be used. For *in vivo* applications in particular, PLA degradation also generates acid species which can affect pH locally and is thought to be a potential source of inflammation. Aliphatic polycarbonates such as poly(trimethylene carbonate) on the other hand are very flexible and do not generate acidic species by decomposition, giving it the edge on PLA<sup>119</sup>.

Due to the increasing number of potential applications for polyesters and aliphatic polycarbonates, a high control over the structure of the polymer is important to target specific properties and tailor each material to each application. Therefore, the need for efficient and well controlled catalytic systems to develop such material is needed.

### I.3. Organocatalyzed ring-opening polymerization

#### I.3.1. Ring-opening polymerization general concepts

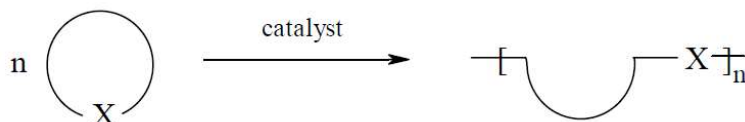


**Figure 18:** General mechanism of ring-opening polymerization

According to IUPAC, a ring-opening polymerization is defined as “a polymerization in which a cyclic monomer yields a monomeric unit which is acyclic or contains fewer cycles than the monomer”<sup>120</sup> (**Figure 18**). The first example of ring-opening polymerization (ROP) reported dates back the early 20<sup>th</sup> century, with the work of Leuch on polypeptides<sup>121</sup>. However, ROP was studied properly to get a better understanding of its mechanism and thermodynamics only around 1950<sup>122</sup>. Quickly this gained a lot of attraction to manufacture polyesters, and some early work aimed at developing medical materials such as surgical implants and tissues repair<sup>123</sup>. Polyesters synthesized via ROP have since then been considered for a very wide range of applications as mentioned earlier<sup>124</sup>.

In most cases, the driving force behind ROP reactions is the strain created by the ring configuration, and the steric considerations associated with it. Along with this comes the chain-ring equilibrium, making initial monomer concentration an important factor, as well as temperature<sup>125</sup>. It is also worth noting that with very few exceptions, this type of polymerization does not generate any small molecules as a secondary product. As stated by the IUPAC definition, all ROPs have in common a cyclic monomer, but the exact reason why the polymerization occurs can vary depending on ring size, type of bonds, and heteroatoms present. For example, three atoms rings such as oxirane have an important ring strain which leads to an enthalpy-driven polymerization. On the contrary, some rings with carbonate moieties polymerize via an entropy-driven mechanism because of the increased rotational freedom of these groups in a linear chain<sup>126</sup>.

Catalysis for ring-opening polymerization is dominated for the most part by metal catalysts. For reactions which have been very well optimized, the catalyst is commonly used at a low ratio of catalyst to monomer of 1 to 10<sup>6</sup> or higher, in which case removal of the catalyst is rarely needed. However, the production of specialty polymers has not been optimized to such an extent and may

require higher concentrations of catalyst, which can require an intense purification process to avoid hazards if toxic metals or ligands are used. This also limits the applications for polymers obtained in such a way as some sensitive fields such as microelectronic which prohibit the use of some metallic species, while only a few metals are considered safe for medical applications. This in turn has paved the way for the development of organocatalyzed polymerization, which also presents other benefits such as a different reactivity, less sensibility to impurities in some cases, and the possibility to work under milder conditions for some reactions, as will be showcased further.

To understand the mechanism of ring-opening polymerization performed by organic catalyst, three general mechanisms have been described in the literature under which most reactions fit. The “Activated monomer mechanism” (AMM) is a mechanism in which the active specie (the catalyst) first activates the monomer in order to proceed to the opening of the ring. In the case of a nucleophilic attack on an ether or other similar monomer (ester, carbonate), the nucleophile operates through a direct attack on the electronegative carbon neighboring the oxygen atom, resulting in the formation of a zwitterionic intermediate (**Figure 19**).

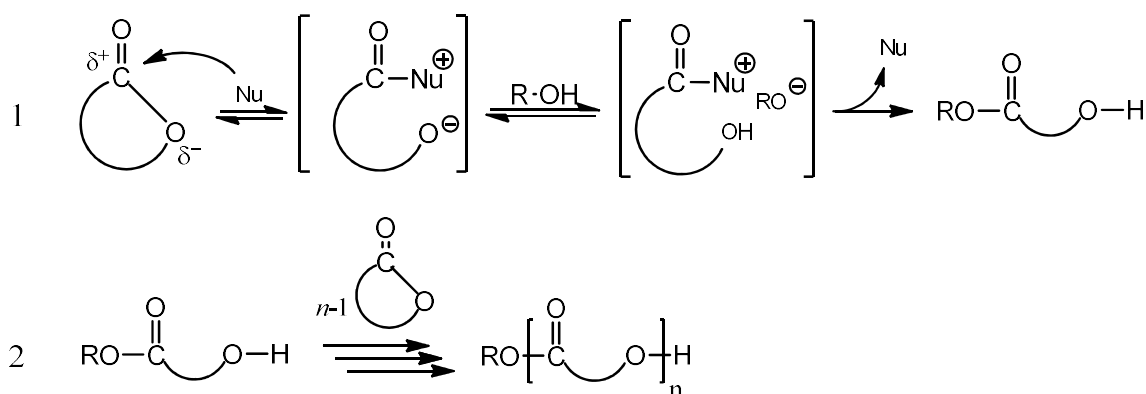


**Figure 19:** Nucleophilic activated monomer mechanism (AMM) of organocatalyzed ROP.

An alcohol initiator is then used to protonate this intermediate and the alkoxide takes the place of the catalyst, which is regenerated. Propagation proceed through a similar mechanism, with the now opened ring acting as the alcohol initiator<sup>127</sup>. Electrophilic AMM is the polymerization mechanism that occurs with Lewis or Brønsted acids. In this latter case, the catalyst activation of the monomer proceeds through protonation of the heteroatom. The activated monomer is then attacked by the alcohol initiator acting as a nucleophile and the acid is regenerated<sup>128</sup>.

A second type of mechanism is the “Activated chain end mechanism” (ACEM). In this case, the alcohol initiator (which ends up being the chain end) is activated by a base, often by hydrogen bonding, which favors the attack on the monomer (**Figure 20**). The propagation can then be done by the hydroxy-terminated product obtained and subsequent reactions of ring-opening of the monomer<sup>129</sup>. The last mechanism found for organocatalyzed ROP is a “Dual activation of the monomer and initiator”. This particular mechanism has been reported for specific catalysts such as guanidines and 4-(dialkylamino)pyridines which will be explored in section I.3.2.

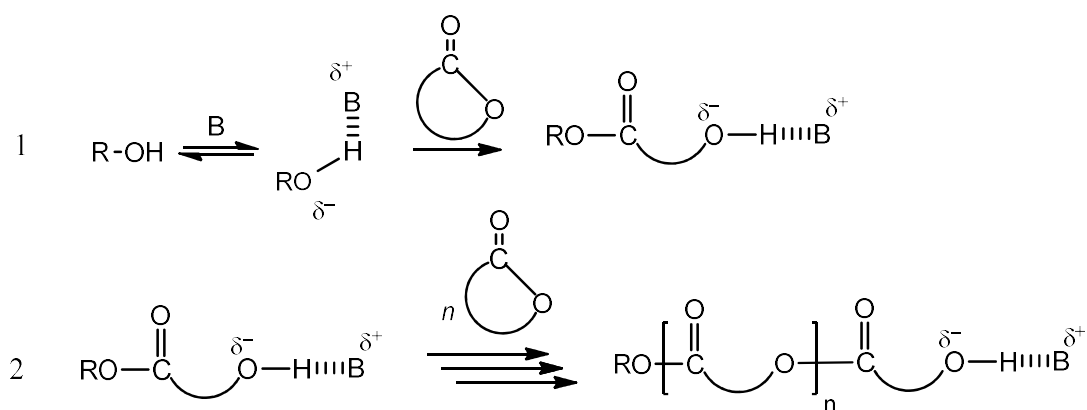


**Figure 20:** Activated chain-end mechanism (ACEM) of organocatalyzed ROP.

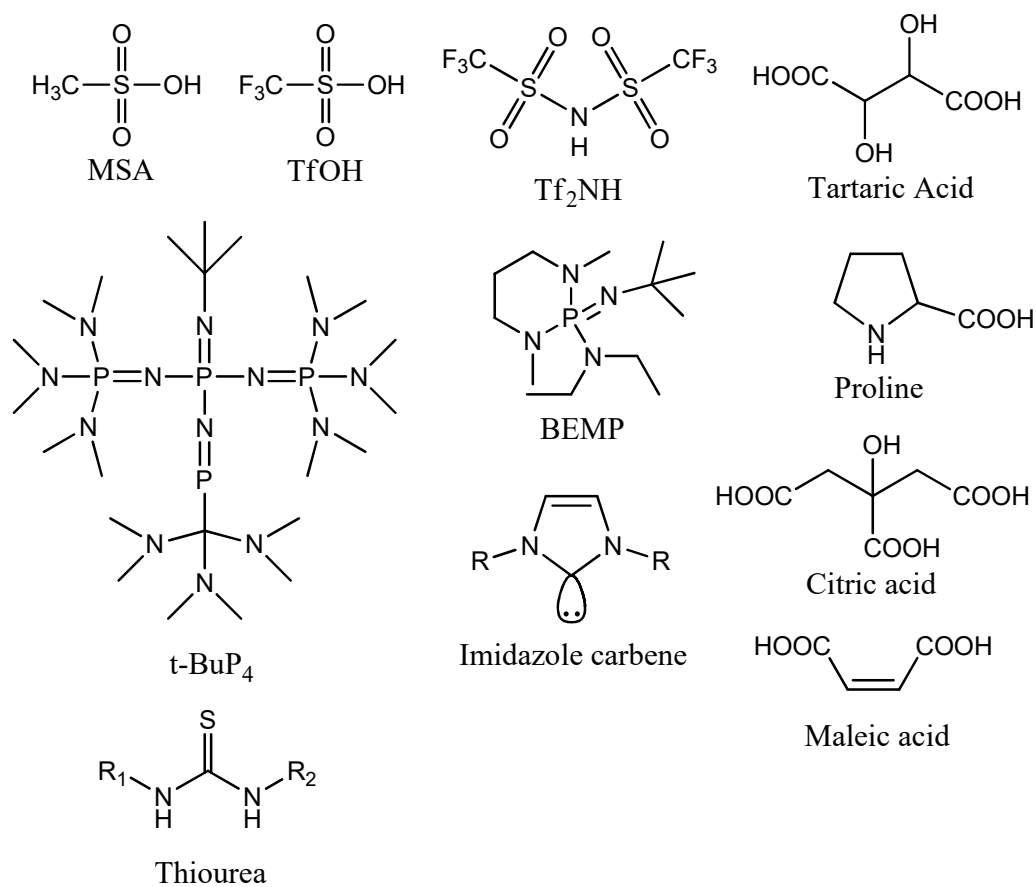


**Figure 21:** Example of some organic catalysts reported for the ROP of cyclic esters. **MSA:** methane sulfonic acid, **TfOH:** trifluoromethanesulfonic acid, **Tf<sub>2</sub>NH:** bis(trifluoromethane)sulfonimide, **t-BuP<sub>4</sub>:** *N,N,N',N'',N''',N''''*-hexamethyl-*N'''*-[*N*-(2-methyl-2-propanyl)-*P*]-*P* bis{[tris(dimethylamino)phosphoranylidene]amino}phosphorimidoyl]phosphorimidic triamide, **BEMP:** 2-(*tert*-butylimino)-2-(diethylamino)-1,3-dimethylperhydro-1,3,2-diazaphosphorinane.

**Table 1:** Non-exhaustive table of example of ROP reaction found in the literature performed with the organic catalyst described in **Figure 21** with their associated protic initiators and solvents

	Lactide	$\epsilon$ -caprolactone	$\delta$ -valerolactone	Trimethylene carbonate
MSA		Pentanol (DCM, toluene) <sup>130</sup> EtOH (toluene) <sup>131</sup>		H <sub>2</sub> O/pentanol (toluene) <sup>132</sup>
TfOH	Pentanol (DCM) <sup>133</sup> Water (DCM) <sup>133</sup>	Pentanol (DCM, toluene) <sup>130</sup> EtOH (toluene) <sup>131</sup>		H <sub>2</sub> O/pentanol (toluene) <sup>132</sup>
Tf <sub>2</sub> NH		EtOH (toluene) <sup>131</sup>	Ph(CH <sub>2</sub> ) <sub>3</sub> OH (DCM) <sup>134</sup>	
Tartaric acid		BnOH (bulk) <sup>135</sup>	BnOH (bulk) <sup>135</sup>	
Citric acid		BnOH (bulk) <sup>135</sup> CNC (bulk) <sup>136</sup>	BnOH (bulk) <sup>135</sup>	
Proline		BnOH (bulk) <sup>135</sup>	BnOH (bulk) <sup>135</sup>	
t-BuP <sub>n</sub>	PBuOH (toluene) <sup>137,138</sup>	MeOH (toluene) <sup>139</sup>	PBuOH (bulk) <sup>137</sup>	
BEMP	PBuOH (toluene) <sup>137</sup> BnOH (toluene) <sup>137</sup>	PBuOH (bulk) <sup>137</sup>	BnOH (bulk) <sup>137</sup> PBuOH (bulk) <sup>137</sup>	BnOH (bulk) <sup>117</sup>
Thiourea	PBuOH (DCM) <sup>140,141</sup>	PBuOH (benzene) <sup>141</sup>	PBuOH (benzene) <sup>141</sup>	BnOH (DCM) <sup>141</sup> PBuOH (DCM) <sup>142</sup>
Imidazole carbene	BnOH (THF <sup>143,144</sup> , DCM <sup>145</sup> , toluene <sup>146</sup> ) PBuOH (THF <sup>143,144</sup> , DCM <sup>147</sup> )	BnOH (THF) <sup>143,144</sup> PBuOH (THF) <sup>143</sup>	BnOH (THF) <sup>144</sup>	BnOH (THF) <sup>148</sup>
DMAP	BnOH (Bulk <sup>149</sup> , DCM <sup>149</sup> ) EtOH (DCM) <sup>150</sup> Cyclodextrin (DCM) <sup>150</sup>	Chitosan (water) <sup>151</sup>		BnOH (bulk) <sup>117</sup>
TBD	PBuOH (DCM) <sup>141</sup>	PBuOH (DCM) <sup>141</sup>	PBuOH (DCM) <sup>141</sup>	BnOH (bulk <sup>117</sup> , DCM <sup>149</sup> )
mTBD	PBuOH (DCM) <sup>141</sup>	PBuOH (DCM) <sup>141</sup>	PBuOH (DCM) <sup>141</sup>	BnOH (DCM) <sup>149</sup>
DBU	PBuOH (DCM) <sup>141</sup>	PBuOH (DCM) <sup>141</sup>	PBuOH (DCM) <sup>141</sup>	BnOH (DCM) <sup>149</sup>

For the polymerization of ester and carbonates, a multitude of organic catalysts (**Figure 21, Table 1**) have been explored since the resurgence of interest in the domain after Hendrick *et al.* reported the ring-opening polymerization of lactide catalyzed by 4-dimethylaminopyridine<sup>12</sup>. Acids were first reported for the polymerization of cyclic ethers, however this reaction is often subject to chain transfer, both by intramolecular or intermolecular reactions when progressing through an ACEM mechanism. This is due to the fact that the nucleophilic heteroatoms along the growing chain compete with the monomer. To avoid this problem the AMM mechanism can be prioritized over ACEM, which was made possible using acids such as BF<sub>3</sub>, a protic co-initiator and a low concentration of monomer. This method however was not able to generate polymers with a high molecular weight, and even under optimal condition the total suppression of ACEM was difficult to achieve.

This type of reaction was nevertheless carried out for the polymerization of cyclic esters<sup>152</sup>. Sulfonic acids in particular has seen a lot of usage and polymerization carried out with methyl sulfonic acid (MSA) and trifluoromethanesulfonic acid (TfOH) have been reported to give polymers with a narrow distribution and a molecular weight of 10,000 g.mol<sup>-1</sup><sup>130</sup>. Sulfonimides, at first used for the polymerization of acrylic monomers, have also been used successfully for the ring-opening of cyclic esters using bis(perfluoroalkanesulfonyl)imides catalysts, as demonstrated by Oshimura, Tang and Takatsu in 2011<sup>131</sup>. The last group of acids that has seen some use as organic catalyst of ROP reactions are carboxylic acids, both synthetic and natural ones, which are of particular interest due to their potential for solvent-free reactions. Due to their overall lower reactivity, these acids can also be used in the presence of various functional groups without the risk of side reactions. Among such catalysts, a wide range has been studied and examples include tartaric acid, maleic acid, citric acid, and proline to name but a few<sup>153</sup>. Acids overall show a great potential for organocatalyzed ROP as there is a wide variety of them, and many can be used to prepare common cyclic esters such as lactones, lactide, and cyclic carbonates. However, many of these reactions require a great control over many parameters to avoid back-biting, and the molecular weight obtained for most reactions is relatively low, with very few exceeding 20,000 g.mol<sup>-1</sup>.<sup>12</sup>

Another family of organic catalysts that has seen some use for the ROP of heterocycles are phosphazenes (**Figure 21**), which mostly act as a strong deprotonating agent. The first ROP done

with such catalyst was performed by Molenberg and Möller who made poly(ethylene glycol) from ethylene oxide using  $t\text{-BuP}_4$ <sup>154</sup>. Similar catalysts were later used for ROP of esters, with BEMP showing the best efficiency, however at the cost of control, which was observed due to transesterification at high conversion of lactide. BEMP was also used with great success for the polymerization of cyclic carbonates in the group of Carpentier and Guillaume, showing high catalytic activity in bulk and producing poly(trimethylene carbonate) (PTMC) with an average molecular weight as high as 48,500  $\text{g}\cdot\text{mol}^{-1}$ . Branched polycarbonates using different protic initiators were also reported using the same catalytic system<sup>117</sup>.

N-heterocyclic carbenes (NHC) used for ring-opening polymerization is a relatively recent discovery, first reported in 2002. Multiple lactones and lactide were successfully polymerized in a controlled manner under mild conditions with the help of a protic source<sup>143</sup>. This work was then followed by several reports with different NHCs, and polycarbonates such as PTMC were also obtained successfully with good control and short reaction times. The mechanism of polymerization by carbenes is a topic that has been heavily debated, and both computational and experimental data point towards a combination AMM and ACEM in the presence of a protic initiator<sup>155</sup>.

A functional group well known for activating carbonyl groups is thiourea thanks to its excellent hydrogen bonding capabilities. This has naturally led to the use of thiourea derivatives for the catalysis of the ROP of cyclic esters. Some work done on lactide showed that monocomponent thiourea yielded a very good conversion and had a high selectivity with very few side reactions, but the reaction was overall slow. The high selectivity and low amount of transesterification of the thiourea-based system is due to its mechanism: a dual activation of the monomer and the initiator by hydrogen bonding. For the best result, this typically requires the presence of an amine group on the thiourea (or addition of an amine for a dual-catalytic system)<sup>140</sup>.

The last groups of catalysts, which will be grouped for the purpose of this dissertation, will be described in more details as they are of particular interest for the work that has been done throughout this thesis.

### I.3.2. Aminopyridines, amidines and guanidine

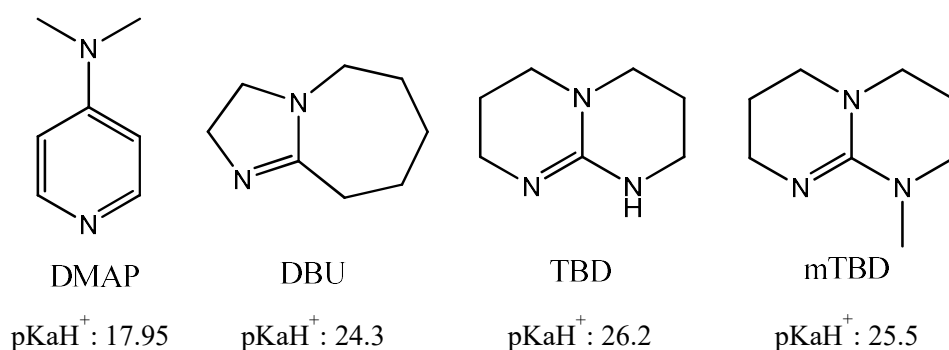


**Figure 22:** Chemical structure of pyridine and guanidine organic ROP catalysts and their associated pKaH<sup>+</sup>.<sup>144</sup>

Aminopyridines, amidines and guanidines are three groups of nitrogen bases used for organic catalysis of polymerization. While these families of catalysts are different, they have in common to act either as a base or as a nucleophile, usually through similar mechanisms. As one of the first reported organocatalyst for polymerization reactions, 4-dimethylaminopyridine (DMAP) (**Figure 22**) has seen many different uses since the first report of Nederbeg *et al.* in 2001<sup>149</sup>. In their work, they used DMAP to polymerize lactide in the presence of various protic sources to act as co-initiator, leading to PLA with a controlled molecular weight and a low dispersity, either in solvent or in bulk at higher temperature. During this work, one of the main drawbacks of DMAP was identified: a relatively high catalyst loading was required for optimal conversion, with ratios from 0.1 to 4 equivalents of the alcohol initiator being used. The reaction was also relatively slow, often requiring more than 24 hours, especially given the concentration of catalyst used. Despite this, DMAP proved to be a very good catalyst leading to a controlled polymerization, as shown by the overall close values obtained for the experimental and theoretical degree of polymerization (DP) in different conditions, in addition to a low dispersity (<1.2)<sup>149</sup>. The mechanism for this reaction was discussed, and an activated monomer mechanism was first proposed where DMAP would act as a nucleophile and attack the carbonyl of the monomer. However, density functional theory (DFT) studies conducted by Bonduelle *et al.* indicated that the hydrogen bonding capacity of DMAP leads to a lower energy requirement for ACEM where the catalyst would first activate the alcohol<sup>156</sup>. Interestingly, despite the low amount of transesterification observed for the work described previously, purposeful chain scission of PLA using DMAP was performed in 2001 by

Nederberg *et al.* in the presence of an alcohol with a great control over the end result. Using size exclusion chromatography (SEC) and NMR, they showed that both high ( $M_n = 100,000 \text{ g.mol}^{-1}$ ) and low molecular weight PLA ( $M_n = 12,000 \text{ g.mol}^{-1}$ ) would undergo transesterification in the presence of DMAP and an excess of alcohol. The molecular weight obtained after the reaction was shown to be consistent with alcohol to polymer ratio used to the reaction, showing the great control over the transesterification. Using this procedure, star and block copolymers were obtained by using polyols such as pentaerythritol and end capped poly(ethylene oxide), again with good control and dispersity in the 1.1 to 1.7 range, showing the potential for such reactions<sup>157</sup>. A couple years later, the use of DMAP for the polymerization of cyclic carbonates was reported as well by Brignou *et al.* who first created seven-membered cyclic carbonates from renewable diols. Multiple catalysts were used for the polymerization of  $\beta$ - and  $\alpha$ -substituted monomers and DMAP was reported to work for  $\beta$ -methyl-tetramethylene carbonate but only at high temperature (110 °C), in which case a polymer with narrow dispersity (1.2) was readily obtained after 60 minutes of reaction in bulk. Interestingly, 1,5,7-triazabicyclo[4.4.0]dec-5-ene (TBD) was used for the same reactions and the same observation could be made with regards to the high temperatures required for the reaction to occur, even when tested in solvent. Similar results were obtained but with a superior conversion for TBD over DMAP<sup>158</sup>. The ROP of multiple six-membered cyclic carbonates was also reported in a different work by Helou *et al.* using DMAP. Conversion at 60 °C was again lower at 50%, but almost quantitative conversion could be obtained in under 15 minutes at temperatures of 110 °C and above. In addition, only a small amount of transcarbonatation was observed despite the high temperatures used, which was indicated by the only slightly broader molecular weight distribution and correlation between experimental and theoretical number average molecular weight. In comparison to the ROP of lactide described earlier, it is interesting to note that this reaction required only short reaction times (15 minutes) and with a sub-stoichiometric ratio of DMAP/OH (1/5)<sup>117</sup>. The capacity of DMAP to polymerize both TMC and lactide has led to the copolymerization of these monomers. In 2013, the work of Guerin *et al.* compared many different catalytic systems, both metal and organic-based, including DMAP with interesting results. The authors reported the sequential synthesis of block copolymers by using alcohol terminated PTMC and using it as the co-initiator in the presence of lactide and DMAP. Reactions starting from both a low average molecular weight PTMC (2,300  $\text{g.mol}^{-1}$ ) and a higher one (15,300  $\text{g.mol}^{-1}$ ) were performed with different amounts of lactide as well. The first reaction showed a much higher conversion (70%)

and led to an almost 50/50 ratio of PTMC/PLA by weight. The second reaction showed a much lower conversion (30%) despite the increased reaction time (4h vs. 24h), and led to a polymer with excess of PTMC (79/21 vs. lactide ratio). A one-pot/two-step approach was also investigated and a very high conversion (100% for TMC, 90% for *L*-LA) at 130 °C was obtained after 10h, giving a copolymer with a narrow dispersity (1.3)<sup>159</sup>.

Amidine and guanidine-based catalysts make use of the excellent catalytic properties demonstrated by many naturally occurring nitrogen-containing compounds. When compared to DMAP, they are overall stronger bases (pKaH<sup>+</sup> given in **Figure 22**<sup>160</sup>) due to the delocalization of charge of their corresponding acid over multiple nitrogen atoms. 1,8-Diazabicyclo[5.4.0]undec-7-ene (DBU) is an amidine that has been documented as a good catalysts for the polymerization of lactide. In 2006, Lohmeijer *et al.* compared the results obtained for various amidines and guanidines and obtained very satisfactory results for the ROP of lactide with DBU in the presence of an alcohol initiator. Total conversion could be obtained in one to two hours, and polymers with average molecular weight over 80,000 g.mol<sup>-1</sup> were described with narrow molecular weight distribution (<1.1)<sup>141</sup>. DBU has since then been used in other studies to polymerize lactide, with a variety of conditions explored. For example, Brown *et al.* reported the polymerization of lactide without the use of a protic source and using DBU as a nucleophile. Their results showed that in a solvent reaction, DBU was able to polymerize lactide at room temperature in dichloromethane, and up to 85% conversion was obtained after 60 minutes. Compared to reactions performed with a protic initiator, the average molecular weight was increased significantly (56,000 vs. 17,000 g.mol<sup>-1</sup>), but an increase in dispersity was also observed (1.63 vs. 1.13). Despite the lower conversion, this work showed that DBU could in fact polymerize lactide through a nucleophilic mechanism without the need for a protic initiator<sup>161</sup>. Coulembier *et al.* attempted to use previous reported results for the polymerization of lactide to produce copolymers of lactide and TMC using a eutectic melting process in the presence of benzyl alcohol (BnOH). However, the result of a 50/50 mixture polymerization led to pure PLLA, which was attributed to the very fast polymerization of lactide. This would lead to the growing PLLA chain nucleating and crystallizing outside of the melt, preventing the inclusion of TMC units. To solve this problem, the mixture was solubilized once PLLA formed, and then a gradient copolymer with PTMC could be obtained with 63% conversion of TMC, and an overall dispersity of 1.6<sup>162</sup>. As with DMAP, the use of DBU in combination with other catalysts was also explored. For example, Miao *et al.* investigated the polymerization of *rac*-

lactide with and without a salt, and noticed a reduced dispersity when using (*R*)-(+)-binaphthyl-diyl hydrogen phosphate (BNPH)/salt, and the authors were able to use only 0.1 equivalents of catalyst to induce polymerization<sup>163</sup>.

The mechanism of ROP catalyzed by DBU has been debated for a while, in particular for lactide. With the vast number of studies conducted using this combination of catalyst and monomer, finding a “unified” mechanism was difficult. However, in 2016 Sherck, Kim and Won reviewed the state of the art and proposed a mechanism. Mechanistic studies led to the conclusion that nucleophilic activation of the monomer was unlikely, and a ketene aminal was hypothesized to be the active chain end in this polymerization. They concluded that proper control over the molar ratio was the key to obtain a living polymerization<sup>164</sup>.

**Table 2:** Non-exhaustive list of cyclic esters and carbonate polymerized by TBD in different conditions found in the literature. All reaction performed at RT except for the polymerization of TMC in bulk (110 °C).

Monomer	M / Catalyst / I	Initiator	Solvent	Time	Conversion (%)	$\bar{M}_w$
<i>L</i> -LA <sup>[a]</sup>	100/0.1/1	Pyrenebutanol	CH <sub>2</sub> Cl <sub>2</sub>	20 s	99	1.2
<i>L</i> -LA <sup>[a]</sup>	500/0.5/1	Pyrenebutanol	CH <sub>2</sub> Cl <sub>2</sub>	1 min	95	1.1
$\delta$ -VL <sup>[a]</sup>	100/0.5/1	Pyrenebutanol	C <sub>6</sub> D <sub>6</sub>	30 min	91	1.1
$\epsilon$ -CL <sup>[a]</sup>	50/0.25/1	Pyrenebutanol	C <sub>6</sub> D <sub>6</sub>	5h	76	1.1
$\epsilon$ -CL <sup>[a]</sup>	100/0.5/1	Pyrenebutanol	C <sub>6</sub> D <sub>6</sub>	5h	72	1.2
$\delta$ -DL <sup>[b]</sup>	60/0.3/1	1,4-benzenedimethanol	Bulk	10h	80	1.2
TMC <sup>[c]</sup>	50/1/1	BnOH	CH <sub>2</sub> Cl <sub>2</sub>	15min	99	1.3
TMC <sup>[c]</sup>	100/1/1	BnOH	CH <sub>2</sub> Cl <sub>2</sub>	1h	99	1.3
TMC <sup>[c]</sup>	250/1/1	BnOH	CH <sub>2</sub> Cl <sub>2</sub>	6h	99	1.3
TMC <sup>[d]</sup>	500/1/5	BnOH	Bulk	5min	99	1.5

[a] From Lohmeijer *et al.*, 2006<sup>141</sup>. [b] From Martello *et al.*, 2012<sup>165</sup>. [c] From Nederberg *et al.*, 2007. [d] From Helou *et al.*, 2010.

When it comes to guanidines, 1,5,7-triazabicyclo[4.4.0]dec-5-ene (TBD) is certainly the most referenced one and has been used extensively for the polymerization of cyclic esters and carbonates. In their 2006 work mentioned previously, Lohmeijer *et al.* also studied the ROP of lactide using TBD<sup>141</sup>. With a low catalyst loading (0.1%), *L*-lactide was fully converted in one minute with the help of a protic initiator in solvent at room temperature. Two reactions were reported, one with a 100 monomer/initiator ratio and another with a 500 monomer/initiator ratio, and both reactions reached near full conversion in a minute or less, with a dispersity under 1.2. Interestingly, not quenching the reaction for several minutes after full conversion increased the

dispersity, but only from 1.06 to 1.23, showing that the rate of transesterification for such a very active system was much lower than similarly active catalyst like carbenes. Unlike many other organic catalysts however, TBD was also reported to be able to readily convert lactones such as  $\delta$ -VL and  $\epsilon$ -CL. At room temperature and in deuterated benzene, PVL was obtained in 30 minutes with conversions up to 91% and a narrow dispersity ( $<1.1$ ). Similar reactions were also performed on  $\epsilon$ -CL but with longer reaction time, as is common for this monomer. After 5 to 8 hours, PCL was obtained, once again with narrow dispersity, but with lower conversion at a maximum of 76%. Still, these reactions obtained with low catalyst loading showed the potential of TBD as a ROP catalyst as it was able to readily polymerize various cyclic esters that other similar catalyst such as 7-methyl-1,5,7-triazabicyclo[4.4.0]dec-5-ene (mTBD) and DBU could not<sup>141</sup>. TBD has been investigated with other lactones such as  $\delta$ -decalactone ( $\delta$ -DL), a monomer that can be obtained from renewable sources. Using a diol as initiator, an equilibrium for the conversion around 80% was reached in bulk at RT, giving a polymer with a low dispersity ( $<1.25$ ). Using the same method, ABA triblock could be obtained by adding a solution of *D,L*-Lactide after the polymerization of  $\delta$ -DL reached equilibrium, leading to a well-defined triblock (PLA-block-PDL-block-PLA) with two different glass transition temperatures ( $-51$  and  $54$  °C), characteristic of immiscible polymer phases<sup>165</sup>. Another use for TBD that was studied by Meimoun *et al.* is the epimerization and chain scission of lactide. In toluene at  $105$  °C, a nucleophilic attack of the catalyst was suggested, leading to oligolactide with a TBD end-chain that would undergo hydrolyzation during quenching. With increasing concentration of catalyst, the average molecular weight of the starting polymer was shown to decline, and the final polymer chain could be up to 20 times shorter (with 5 equivalents of TBD) over 48h<sup>166</sup>.

Naturally, TBD was also investigated for the ROP of cyclic carbonates, where it once again was shown to be a very efficient catalyst. First, Nederberg *et al.* conducted the polymerization of TMC in dichloromethane at room temperature with BnOH as initiator, which led to full conversion in 15, 60 and 360 minutes for a targeted DPs of 50, 100 and 250, respectively. Despite the very high activity of the catalysts, the experimental DP obtained were all under 5% of the theoretical DPs, and a rather low dispersity was measured (1.31). In comparison to the other catalysts tested, only 1,3-diisopropyl-4,5-dimethyl-imidazol-2-ylidene (a carbene) showed higher activity, but the resulting polymer had a high dispersity ( $>2$ )<sup>148</sup>. The polymerization of TMC was also reported by Helou *et al.* in bulk, where TBD was again noted to have a very high activity, and PTMC could be

obtained with total conversion within minutes at 110 °C in the presence of BnOH. Lower temperatures (30 °C) were also used and required more time (30 minutes), but quantitative results could still be obtained. In all the reactions reported, a great control over the targeted DP could be obtained by using the proper monomer/initiator ratio, allowing for a low amount of catalyst<sup>117</sup>.

The much higher catalytic activity of TBD for the ROP of cyclic ester when compared to catalysts such as DBU was explained by a dual activation mechanism (**Figure 23**). This was supported by DFT calculations, showing that the dual activation of the monomer and the alcohol via hydrogen bonding was much more favorable energetically<sup>167</sup>. However, similar studies have not been conducted for the polymerization of carbonates.

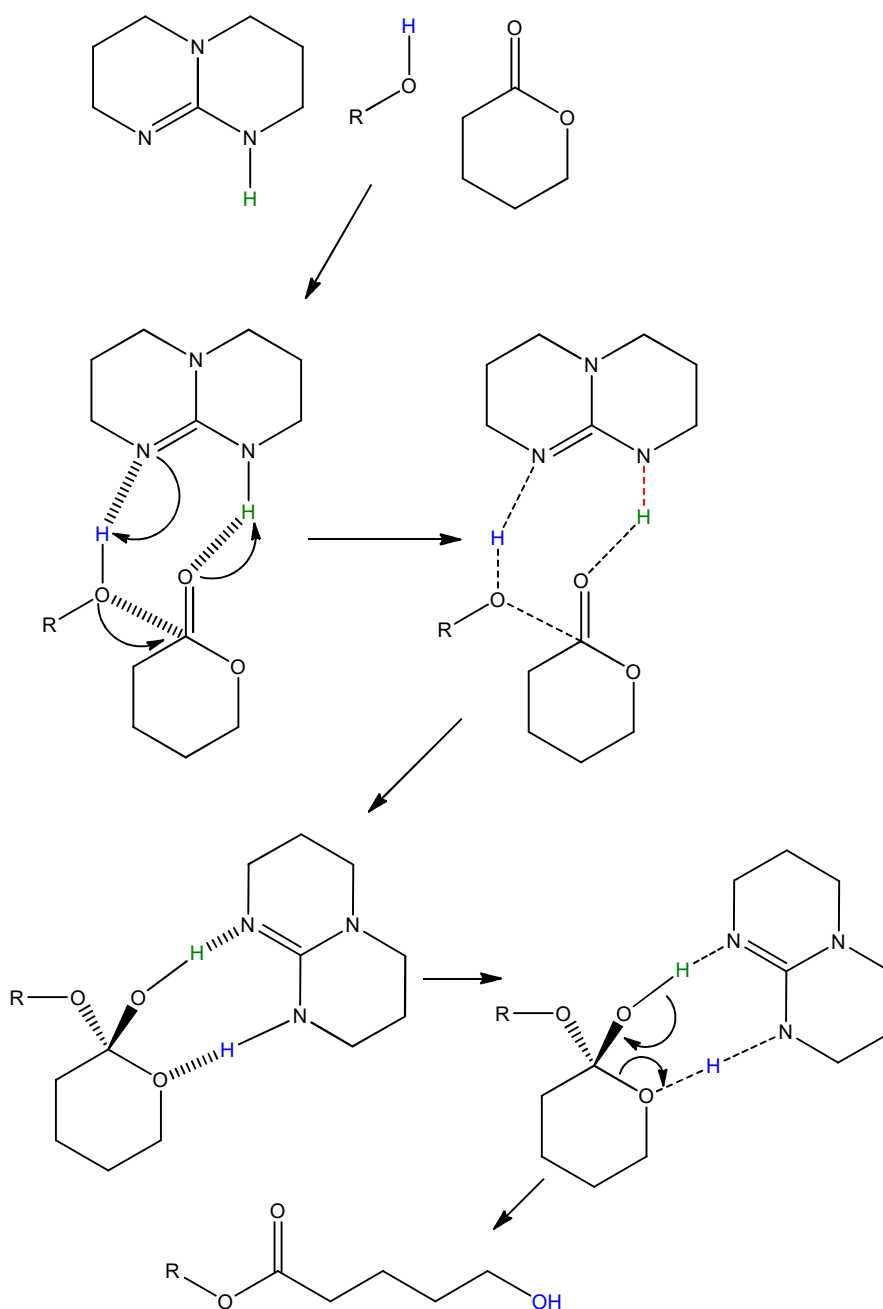


**Figure 23:** Dual activation mechanism by hydrogen bonding of TBD for the ROP of cyclic ester in the presence of a protic co-initiator.

Nevertheless, organic catalysts are very powerful tools for the polymerization of cyclic monomers, and the use of a protic source to control the polymerization not only allows for smaller catalyst quantities, but also results in interesting chain ends for the resulting polymer.

### I.3.3. Immortal polymerization

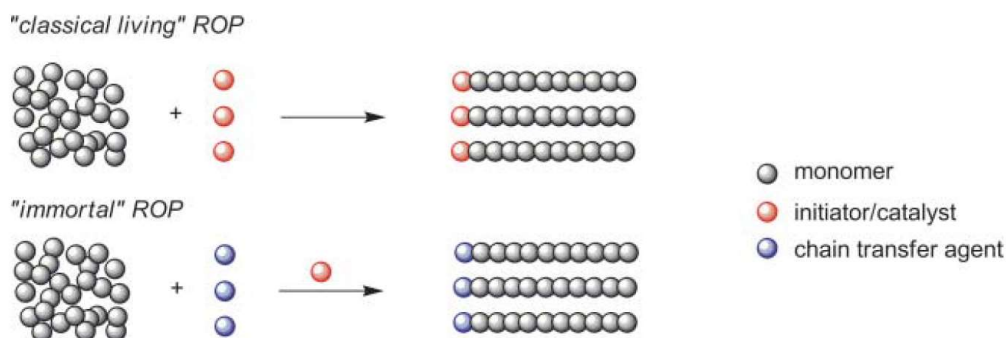


**Figure 24:** Illustration of the distinction between “classical living” and “immortal” ROP process. Reprinted from Publication Dalton transactions : an international journal of inorganic chemistry, 39, Nouredine Ajellal, Jean-François Carpentier, Clémence Guillaume, Sophie M. Guillaume, Marion Helou, Valentin Poirier, Yann Sarazin and Alexander Trifonov., Metal-catalyzed immortal ring-opening polymerization of lactones, lactides and cyclic carbonates., Pages No. 8363, Copyright (2022), with permission from Royal Society of Chemistry.

The concept of immortal polymerization was first reported by Inoue in 1985 for the polymerization of epoxides with aluminum porphyrins<sup>168</sup>. It is a polymerization that leads to a narrow molecular weight distribution, a constant number of growing chains throughout the reaction, and a predictable degree of polymerization defined by the ratio of monomer to initiator is reachable. These are also attributes of living polymerization, however both types of reaction possess some key differences (**Figure 24**). When first described, Inoue noticed that immortal polymerization could be performed under various conditions, including the presence of protic or acidic species, without leading to the termination of growing chains. This was different than what was observed at the time for the polymerization of the same monomer (epoxide) in living condition with alkali metals. What would once lead to the termination of a chain (acids) took on the role of a transfer agents in the polymerization catalyzed by aluminum porphyrins. Inoue noted that in this reaction, the transfer reaction was much faster than the propagation, which lead to a low dispersity but a higher amount of chains formed than the number of porphyrins initiators. When tested with methanol, it was observed that the number of polymer molecules formed during the reaction corresponded to the number of methanol molecules, confirming the observations made so far<sup>168</sup>.

This reaction was further researched by Inoue and co-workers and led to the development of the immortal ring-opening polymerization of various cyclic monomers of interest by Ajellal *et al.* in 2010. Based on the work done on porphyrin, this research group developed multiple metal

complexes showing the characteristics of immortal polymerization. By using different alcohol as co-initiators, they were able to use catalytic quantities of the metal species and target desired DPs by changing the ratio of monomer/OH. Yttrium-based catalysts were used for the polymerization of *rac*-LA to great success, and ratios of up to 1,000/1/50 (for LA/Cat/OH) readily produced polymers with low dispersity and high end-group fidelity. No presence of cyclic oligomers was detected, confirming the immortal character of this reaction. Similar reactions were also conducted on *rac*- $\beta$ -butyrolactone, which proved to be more difficult, in particular with more than 5 equivalents of alcohol. Zinc complexes however showed a much better potential for the polymerization of the same monomer. Polymerization of TMC was also studied extensively, and many different metals were shown to lead to the immortal polymerization of this cyclic carbonate with great success. While some conditions such as bulk reaction revealed the presence of a small amount of transcarbonatation, great control over the final polymer was still observed and no decarboxylation was noticed<sup>169</sup>. The same concept would later be applied to the organocatalyzed polymerization of TMC using previously described organocatalysts such as DMAP, TBD and BEMP<sup>117</sup>. A clear benefit of these catalysts, other than the usual advantage of organic catalyst over metallic ones mentioned earlier, is that they are all commercially available. Substituted six-membered cyclic carbonates could also be polymerized, again with a great control over the polymer obtained. The ability to control the polymerization with a protic initiator was also used to great extent by creating different polymer architecture with diols and triols. Narrow dispersity (<1.6) and predictable molecular weight could be obtained with both diols and triols using BEMP as the catalyst, and no drop in reactivity was noticed when compared to reaction using BnOH. Overall, this shows the great versatility of immortal polymerization, in particular for the ROP of cyclic carbonates with tuneable chain ends.

#### I.4. Polysaccharide-based polymer material

Polysaccharides can make for a great addition to polymer matrices in order to obtain a biphasic material with interesting mechanical properties. Therefore a large body of research exists on the production of polymer materials containing a small amount of polysaccharide as filler, with or without extra modification steps<sup>170-172</sup>.

#### I.4.1. Non-grafted material

The most straightforward method to obtaining polysaccharide-reinforced composites is to mix the filler into the polymer matrix without any extra steps. A good example is the work of Alemdar and Sain who used wheat straw nanofibers in combination with a starch-based thermoplastic in 2007<sup>29</sup>. The CNF used were prepared with both a chemical and mechanical treatment and determined to have dimension of 10-80 nm in width and a few microns in length. Due to the similar composition of starch and cellulose, no compatibility problems were encountered, and scanning electron microscopy (SEM) showed a good dispersion of the fibers in the thermoplastic matrix. Tensile tests were used to demonstrate the improvements in mechanical properties and the tensile modulus was increased by up to 145% using 10% of nanofibers, showing a good stress transfer from the matrix to the reinforcement. The storage modulus also increased significantly, going from 112 MPa to 308 MPa, again with 10% nanofibers. Lastly, the glass transition temperature was also measured and was seen to increase with the addition of the CNF, which could be attributed to the interfacial interactions between the matrix and the filler. This work shows the potential for nanocellulose as reinforcement when there is no compatibility issues with the polymer and the fibers are well separated and dispersed<sup>29</sup>.

Because of the limitation of using only polymers readily compatible with polysaccharides, some work has been done on trying to circumvent that restriction. An idea that was explored was the use of surfactant, which are used to reduce the interfacial energy at the interface between the polymer matrix and the reinforcing fiber. In the work of Bondeson and Oksman, a PLA composite was produced by extrusion in the presence of cellulose nanocrystals and acid phosphate esters referred to as Beycostat A B209. This technique proved to have few challenges, as the surfactant used was not completely miscible in the melted PLA and was also a source of PLA degradation at higher concentrations. In spite of this, some interesting results were shown with this method, most notably the increase of tensile modulus in the presence of CNCs was negligible going from 2.65 GPa to 2.69 GPa, but adding 5% of surfactant increased it further to 3.10 GPa. When increasing the amount of surfactant used, elongation at break decreased at first from 19.5 to 3.1%, but increased above 100% when using 20% of surfactant. Dynamic mechanical analysis (DMA) also showed a decrease of the softening temperature under these conditions<sup>173</sup>.

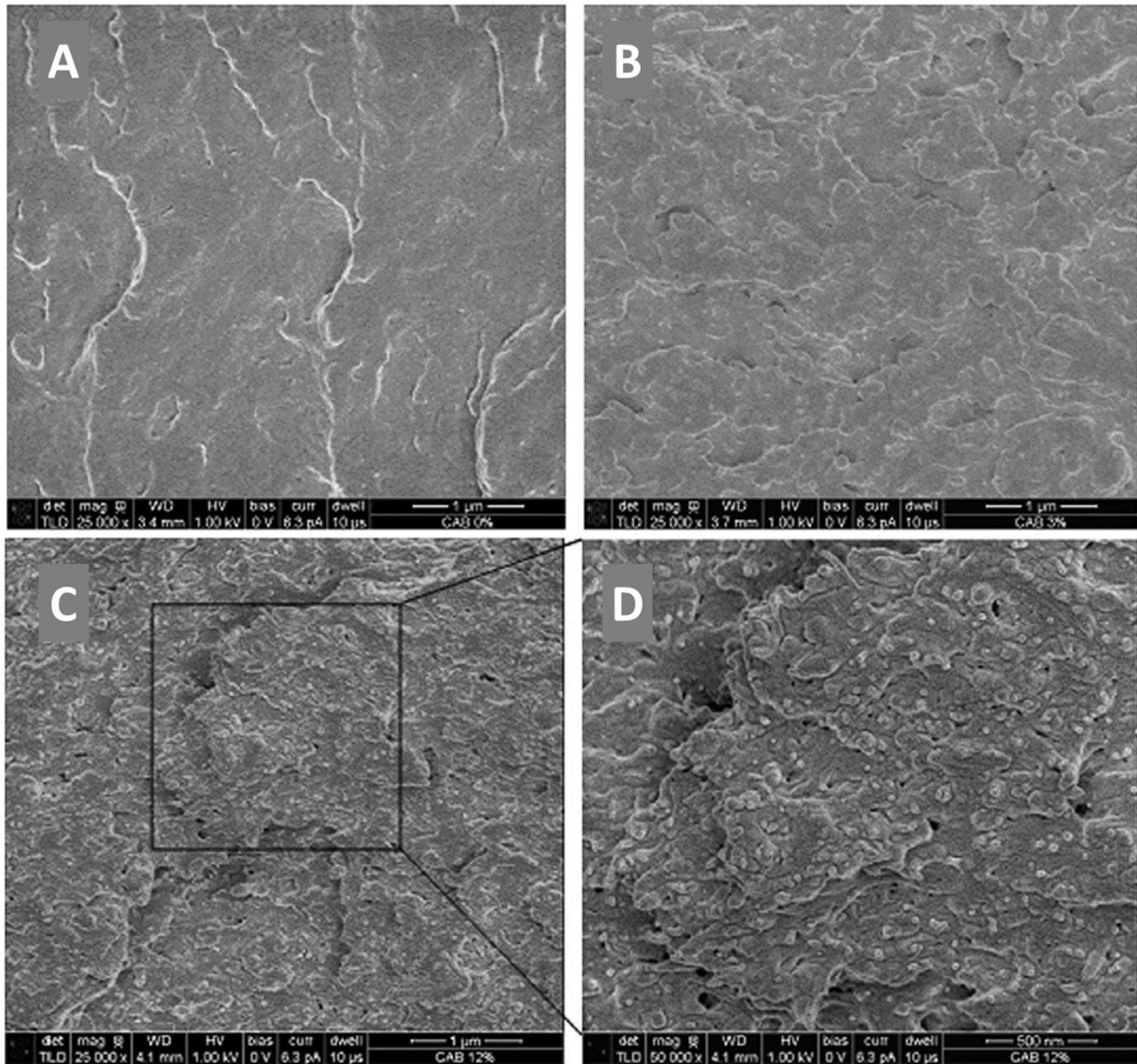


**Figure 25:** Extreme high resolution scanning electron microscopy (XHR-SEM) micrographs cryo-fractured cross sections of (A) CAB matrix and its nanocomposites with (B) wt%, (C) 12wt% CNCs (D) a detailed view of the nanocomposites with 12wt% CNCs. Reprinted from Publication Composites Science and Technology, 71, Gilberto Siqueira, Aji P. Mathew, Kristiina Oksman, Processing of cellulose nanowhiskers/cellulose acetate butyrate nanocomposites using sol-gel process to facilitate dispersion, Pages No. 7, Copyright (2022), with permission from Elsevier.

Another great example of nanocellulose-based composite was presented by Siqueira *et al.* in 2011<sup>174</sup>. Cellulose acetate butyrate (CAB) was prepared by a sol-gel process which acted as a solvent exchange method to eliminate water. With this method, a mixture in ethanol of CAB (dissolved) and CNC gel could be obtained. After dispersing the nanocrystals, the suspension could then be cast into a Petri dish to obtain films after evaporation in a vacuum oven. Three different

films were made with 3, 6, 9 and 12% CNC content, and ultra-high resolution SEM was used to show the dispersion of the nanofillers in the CAB films and differences in appearance to the neat CAB film. Traces of the fillers could be seen in the form of small white dots which increased in number with the concentration of the filler (**Figure 25**). This showed that the nanocrystals could be dispersed successfully in the matrix without the need for surface modification or surfactant in a non-hydrosoluble polymer. Stress-strain measurements were conducted and showed a significant increase of the strength of the material with increasing cellulose content, with a maximum for 9 wt% filler content at 8.7% vs. 5.4% neat CAB. As for the Young's modulus, an increase from 1.26 GPa to 2.30 GPa was observed. It was noted that the transparency of the material was not affected, making this method an interesting option to obtain clear high stiffness and strain at break materials<sup>174</sup>.

#### I.4.2. Surface grafting

To increase the range of polymers that can be reinforced with polysaccharide nanofillers, a surface grafting approach has also been explored by many research groups, with the potential to obtain very high compatibility between the filler and the polymer matrix by grafting polymer chains of similar nature on the filler. Different approaches can be used to obtain grafts, the most common methods being the “grafting onto” and the “grafting from” for the modification of polysaccharides. In the “grafting onto” method, an already synthesized polymer, usually end-capped with a reactive group, is attached onto the polysaccharide backbone using the surface hydroxy group (**Figure 26**). Prior modification of the surface hydroxy can also be done to give access to other types of chemistry and potentially increase the reactivity. This method's main advantage is the ability to control the chain length of the polymer grafts onto the polysaccharide backbone. However, this is not the preferred way of obtaining grafted polysaccharides as the steric hindrance created by the grafted chain can limit the availability of other reactive groups on the surface, therefore yielding a low grafting density<sup>175</sup>.

An example of such grafting reaction was reported by Thielemans *et al.* in 2006 in which starch nanocrystals were grafted with either stearic acid chloride using triethylamine, or poly(ethylene glycol) methylether (PEGME) chains using a tin catalyst. The modified starch showed interesting results, in particular in contact angle measurements with water. An angle of 35° was measured for the unmodified starch, whereas the contact angle for stearate grafted starch and PEGME grafted

starch were  $102^\circ$  and  $66^\circ$  respectively. Sufficient grafting was characterized by X-ray photoelectron spectroscopy (XPS) and Fourier-transform infrared spectroscopy, and the crystallinity of the starch was not affected as determined by X-ray diffraction. Interestingly, stearate moieties were shown to form a crystalline shell around the starch, resulting in a hydrophobic shell around the hydrophilic starch core. The PEGME-starch structure was different, most likely due to the stronger interactions between the graft and the starch as noted by the authors. Both modifications lead to a clear modification of the surface properties of the starch nanoparticles due to the reduction in hydrogen bonding between starch molecules<sup>176</sup>.

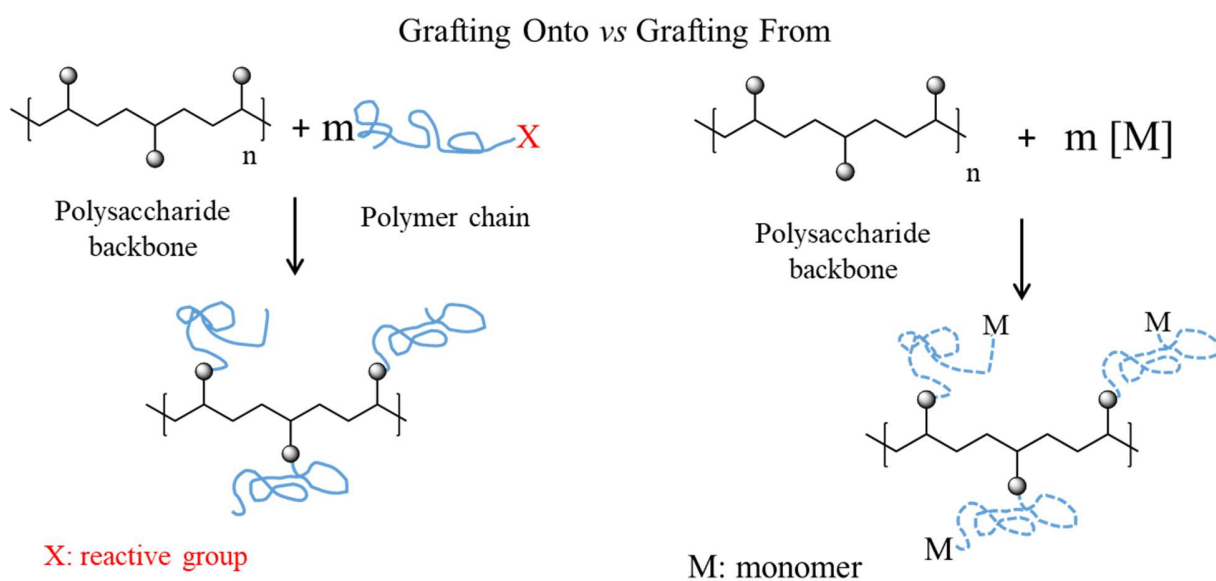


**Figure 26:** Schematic representation of the "grafting onto" and "grafting from" method of surface modification of polysaccharides.

Another approach to grafting polymer chains onto polysaccharides is to use a "grafting from" process. In this method, the polymer is formed in the presence of the polysaccharide which commonly acts as the initiator for the polymerization (**Figure 26**). Similarly to the "grafting onto" method, a modification of the polysaccharide surface OH can be done to allow for different polymerization methods to be used. Due to the growth of the polymer chain on the surface, the steric hindrance encountered in the "grafting onto" method is usually not as prominent as long as the rate of initiation is much faster than the rate of propagation (*i.e.* all chains grow at the same time). This can therefore yield a fairly high polymer graft density<sup>4,177</sup>.

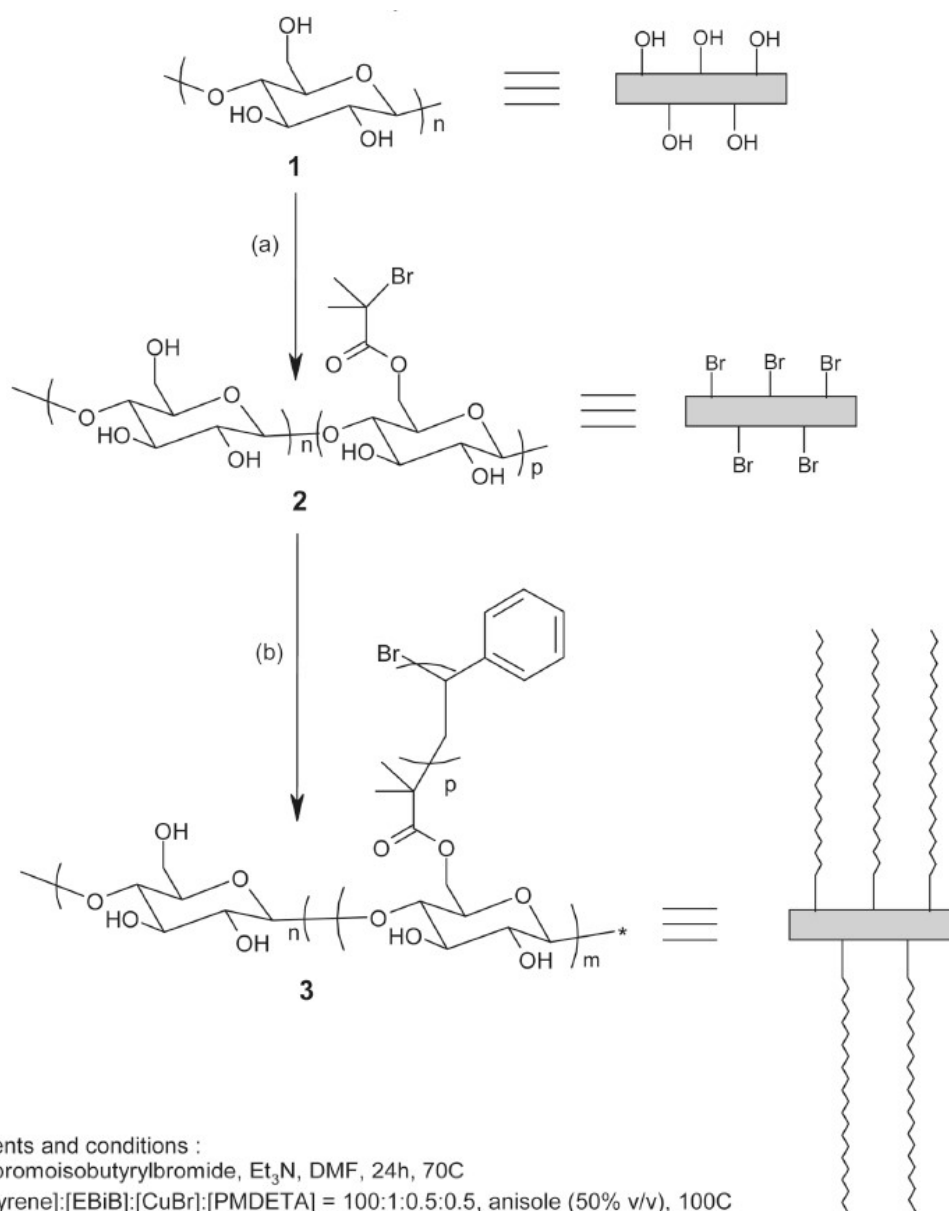


**Figure 27:** Synthesis of Polysaccharide Nanocrystals-g-polystyrene by ATRP. Reprinted (adapted) with permission from: Morandi, G.; Heath, L.; Thielemans, W. Cellulose Nanocrystals Grafted with Polystyrene Chains through Surface-Initiated Atom Transfer Radical Polymerization (SI-ATRP). *Langmuir* 2009, 25 (14), 8280–8286. Copyright (2022) American Chemical Society.

In 2009, Morandi *et al.* employed a “grafting from” approach to functionalize cellulose nanocrystals with polystyrene chains. Atom transfer radical polymerization (ATRP) was employed for this grafting reaction, and allowed for a good control of the polymerization<sup>8</sup>. After an extra step

of modification to introduce bromide moieties on the surface (about 35% of the surface hydroxy were modified), copper bromide was used along with styrene, anisole, ethyl-2-bromoisobutyrate, and *N,N,N',N',N''*-pentamethyldiethylenetriamine (PMDETA) to start the polymerization (**Figure 27**). By following the kinetics of the reaction and analyzing the non-grafted polymer produced in SEC, the controlled character of the reaction was confirmed. FT-IR, XPS and elemental analysis (EA) confirmed the presence of grafts after purification and showed a quantity of grafts on the surface of the nanocrystals of up to 20 wt%. Water contact angle measurements showed a good coverage of the PS layer with an angle of 94° vs. 43° for the unmodified cellulose nanocrystals. Lastly, the modified cellulose showed great results for the absorption of 1,2,4-trichlorobenzene, making it potentially interesting for some specific applications<sup>8</sup>.

Ring-opening polymerization is also commonly used for “grafting from” modification of polysaccharides, in particular due to its use with bio-based and/or biodegradable monomers. It is for this very reason that poly( $\epsilon$ -caprolactone) in combination with cellulose has gained some attention, with the potential to create an all biodegradable composite material. Lönnberg *et al.* reported the grafting of PCL on cellulose nanofibrils, called microfibrillated cellulose (MFC) in this case<sup>178</sup>. This nanocellulose was obtained from bleached sulfite softwood pulp and had a carboxymethylation pretreatment leading to a degree of substitution of 0.089, and was then suspended in acetone, then toluene by solvent exchange. This reaction was performed using tin octoate Sn(Oct)<sub>2</sub> at 2 wt%/monomer and in the presence of a small quantity of BnOH. Bionanocomposites were produced with a PCL of 80,000 g.mol<sup>-1</sup> mixed with different quantities of unmodified and modified CNF in THF, then dried and pressed in a hot plate to obtain different films. Various grafting contents were reported (22, 30 and 78%), and improved dispersibility in organic solvent (namely THF) was observed with increasing PCL content. Mechanical tests of the composites were performed and at a low CNF content (3 wt%), PCL-grafted CNF showed a much better retention of the ductility of PCL than their unmodified counterpart which showed very low elongation before breaking (**Table 3**). The elastic modulus also increased for the composite compared to neat PCL, regardless of the grafting of CNF. At higher CNF loading (10 wt%), elongation at break dropped significantly for all cases, but composites with grafted CNF had a slightly higher elongation at break. Interestingly, elastic modulus was this time affected by the grafting of the filler, and the best result was achieved with the most grafted CNF (78%).

**Table 3:** Mechanical data from tensile tests of PCL composite reinforced with unmodified and PCL-grafted CNF. Data from the work of Lönnberg *et al.*, 2011.

Composite	CNF content (wt%)	Maximum stress $\sigma_{\max}$ (MPa)	Elongation at break (%)	Elastic modulus (MPa)
PCL		$22 \pm 4.3$	$880 \pm 200$	$190 \pm 18$
unmodified CNF	3	$17 \pm 0.1$	$16.1 \pm 2.5$	$256 \pm 24$
PCL-grafted CNF (28 wt%)	3	$21 \pm 1.2$	$690 \pm 71$	$229 \pm 16$
PCL-grafted CNF (70 wt%)	3	$20 \pm 2.5$	$435 \pm 270$	$257 \pm 14$
PCL-grafted CNF (78 wt%)	3	$22 \pm 2.3$	$495 \pm 150$	$230 \pm 3.4$
unmodified CNF	10	$18 \pm 1.1$	$13.2 \pm 3.2$	$260 \pm 42$
PCL-grafted CNF (28 wt%)	10	$20 \pm 0.2$	$16.9 \pm 2.3$	$287 \pm 34$
PCL-grafted CNF (70 wt%)	10	$24 \pm 0.8$	$21.2 \pm 4.4$	$276 \pm 24$
PCL-grafted CNF (78 wt%)	10	$27 \pm 0.7$	$18.3 \pm 1.2$	$326 \pm 29$

Despite all of the examples described above as well as many more found in the literature<sup>175</sup> all using metal-based catalyst, work has also focused on the use of organocatalysis to obtain similar materials. As described previously metallic species can be difficult to remove from the final material, and sometimes have to be used in rather high amount (2 wt%) for the grafting on polysaccharide to be successful. In addition, many metallic catalyst are very sensitive to water, which makes their use with polysaccharide difficult due to their hygroscopic nature. In comparison, the use of a naturally occurring and benign acid has been reported for the ROP of caprolactone on CNCs by Labet *et al.* in 2011<sup>179</sup>. In this work, the effect of different parameters on the grafting reaction was studied in order to optimize it, an aspect sometime neglected of the grafting of polymers on cellulose in favor of studying the material obtained. With optimized parameters, a grafting content of up to 58 wt% PCL could be obtained (determined by EA) using citric acid, and the success of the reaction was also confirmed by FT-IR and XPS. Water contact angle measurement were also performed and showed the increase in hydrophobicity of the modified CNCs with increasing graft length, going from 40° for unmodified CNCs to more than 70° with 60% PCL. This work showed that with some optimization, a high amount of grafting could be achieved with no solvent and a natural, benign acid, proving that organic catalysis can sometime achieve similar results to that of metal catalysis, or even better ones<sup>136</sup>.

While cellulose is one of the most popular polysaccharide, chitosan has also been functionalized by surface polymer grafting. One such example is the work of Feng and Dong in 2006 who used ROP as a way of grafting poly( $\epsilon$ -caprolactone) on chitosan<sup>151</sup>. For this reaction, water was used as

a swelling agent and DMAP was selected as the catalyst of choice. High amounts of grafts were obtained, with an increase of up to 400% by weight, and interestingly, FT-IR and  $^1\text{H-NMR}$  showed a high selectivity for the amino groups as the hydroxy groups were reported not to participate in the initiation of the reaction. Wide-angle X-ray diffraction was used to determine the crystallinity of the modified chitosan and it was shown that in these conditions, the PCL grafts limited the ability of the chitosan backbone to form crystalline structure, and that the grafts themselves were purely amorphous.

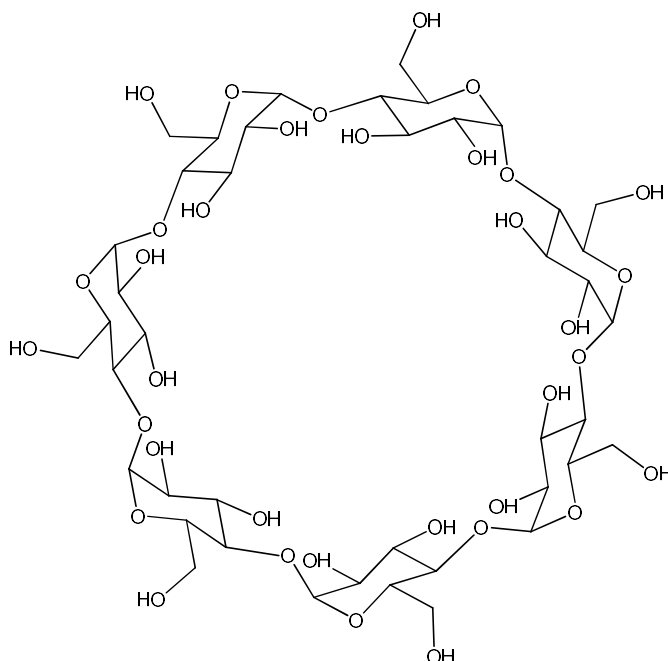


**Figure 28:** Chemical structure of  $\beta$ -cyclodextrin

Better described as an oligosaccharides rather than a polysaccharide, cyclodextrins (**Figure 28**) have also been used for “grafting from” polymerization as was described in the work of Miao *et al.* in 2011. In this study, DMAP was employed as the organic catalyst of lactide ROP. Due to the particular structure of the cyclodextrins, star shaped polymers could be obtained with a controlled degree of polymerization. The different hydroxy groups of the cyclodextrin could also be selectively protected to control the number of growing chains on the surface of the carbohydrate. Moreover, the reaction could be performed in bulk, with relatively short reaction time (30 minutes) and a low dispersity ( $<1.1$ ), and showed results superior to those of similar reactions performed with  $\text{Sn}(\text{Oct})_2$ . In addition, this work shows that due to their different reactivity, organic catalyst

can open the door to never obtained before material, as this work was the first report of a  $\beta$ -cyclodextrin modified on all 21 positions, showing interesting perspective for the use of such systems with polysaccharide such as cellulose<sup>150</sup>.

While much less studied than polyester, polycarbonates have also been used to graft polymers on the surface of polysaccharides. For example, starch granules were successfully grafted with trimethylene carbonate moieties as reported by Samuel *et al.* in 2013. In a one step process, PTMC was synthesized in the presence of starch particles with the help of an organic catalyst such as TBD or phosphazene bases. High conversion of the monomer could be obtained with the organic catalyst within 20 minutes and with a very low catalyst concentration. In comparison, similar reactions performed with Sn(Oct)<sub>2</sub> did not lead to the conversion of TMC under the same conditions. A low degree of substitution was calculated (0.9% for the highest), likely due to the reactivity of only surface OH, and the DP calculated of the PTMC graft ranged from 2 to 12 which was attributed to the presence of propane-1,3-diol (PPD) formed by TMC hydrolysis. Nonetheless, the modified starch particles showed a good dispersion when used in a PTMC matrix as shown by SEM, and retained their spherical shape showing the compatibility of the two phases. Due to the biocompatibility of PTMC, such material produced in a simple one step process, using an organic catalyst, have the potential to be suited for many applications<sup>180</sup>.

PTMC grafts were also reported on the surface of cellulose by Pendergraph *et al.* who performed the polymerization of TMC using TBD and DBU as catalysts. In this work the polysaccharide used were cellulose fibers in the form of a filter paper. The polymerization occurred readily and high conversion was obtained, very quickly with TBD which showed a much higher reactivity and reached full conversion under 10 minutes. Water contact angle measurement were performed on the modified filter paper, and an increased hydrophobicity after surface grafting was shown. SEM images were used to observe the filter paper post reaction, and a smoother and less porous surface was observed when compared to the unmodified filter paper. Due to the biocompatibility of TMC, easy and quick grafting method on the surface of cellulose without any metal impurities could be relevant for biomedical application.

As demonstrated by some of the work than has been reported in the literature, there is a clear potential and demand for polymer-grafted polysaccharide surfaces and particles. Moreover, much of the work done on the surface modification of polysaccharide by polymer grafting has been done

using metallic species, and organic catalysis has showed to be a viable alternative for all the reasons mentioned before such as ease of removal, mild operating conditions, and different reactivity. However, some aspects of these reactions such as the influence of different parameters are still not well understood and reported, and a thorough study of the chemistry and methodology for the synthesis of such materials is often overlooked. In particular, while polyesters have been well studied, polycarbonates have received much less attention despite their high potential for many applications due to sharing a large number of advantages with polyesters of interest. Therefore, producing nanofillers grafted with polycarbonate moieties would be interesting to obtain new composites, as this has never been done before with aliphatic polycarbonates. Due to the multiple advantages it presents, organocatalysis would be preferred for such reactions. Trimethylene carbonate, the most simple of the six-membered cyclic carbonates, seems like a natural choice for this type of work. The mechanism behind the polymerization of this monomer with organic bases has also not been determined by quantitative study before, therefore DFT could provide useful information. Lastly, very little work has been done on the grafting of copolymer on nanocellulose, and surface initiated ROP copolymerization has yet to be studied.

## II. Materials and Methods

In order to avoid redundancy between different chapters, all of the materials, methods, characterization techniques and details regarding calculation have been put into this chapter together. Some products may have been obtained from different suppliers and used differently in some parts due to the collaborative nature of the work done between the two research teams.

### II.1. Materials

#### II.1.1. Cellulose

Cellulose nanofibrils were obtained from SAPPI and received as a 1% suspension in water and were used as the initiator for the reaction. This product is available commercially under the brand name Valida. CNFs were first frozen using liquid nitrogen, and then freeze-dried for four days at -56 °C with a Thermo Heto PowerDry PL6000, under a vacuum of 2 mbar. After lyophilization, the CNFs were Soxhlet-extracted with ethanol for 24 hours to remove any impurities adsorbed on the surface of the cellulose fibers<sup>179</sup>. The CNFs were subsequently dried at 40 °C for 24h, under vacuum at around 3 mbar.

Cotton nanocrystals were prepared by acid hydrolysis of cotton wool for 35 min at 45 °C in a 64 wt% aqueous H<sub>2</sub>SO<sub>4</sub> solution while stirring constantly<sup>181</sup>. Deionized water was used to wash the resulting suspension by three successive centrifugations at 10,000 rpm and 10 °C for 40 min, replacing the supernatant with deionized water each time. Dialysis under continuous tap water flow was then used to remove residual free acids and neutralize the CNCs. After 48 h, the pH of the eluent was checked to be neutral and a homogeneous dispersion of cotton nanocrystals in water was obtained using a Branson sonicator at 10% amplitude for 2 minutes. The dispersion was subsequently filtered over a fritted glass filter no. 2, and stirred overnight with Amberlite MB-6113 resin to remove non-H<sub>3</sub>O<sup>+</sup> cations. The dispersion was sonicated one last time, frozen in liquid nitrogen, and freeze-dried using a Heto PowerDry PL6000 apparatus from Thermo Scientific under a vacuum of 2 mbars. In addition to this procedure commonly followed in the literature to prepare cellulose nanocrystals, a further purification was performed to remove surface adsorbed impurities onto the nanocrystal surface<sup>166</sup>. After freeze-drying, the cotton nanocrystals were Soxhlet extracted for 24h using ethanol as a solvent. The nanocrystals were subsequently dried in a vacuum oven (0.5 bar) at 50 °C and then dried further under ultra-high vacuum (Pfeiffer DCU 100) at 10<sup>-6</sup> bars

for up to five days. The glassware used for the drying process was then tightly closed, filled with argon, and stored in a glovebox.

### II.1.2. Solvents

Chapter 3: Dichloromethane (analytical reagent grade) was obtained from Van Waters Rogers (VWR) and used as both the reaction solvent and for purification, acetone and ethanol (technical grade) were purchased from Acros Organics and were used for purification.

Chapters 4, 5, and 6: dichloromethane and ethanol (analytical reagent grade) used for purification were obtained from Carlo Erba. Dichloromethane, toluene and tetrahydrofuran (THF) used in reactions were obtained from Sigma Aldrich and purified through alumina column (Mbraun SPS).

### II.1.3. Catalysts

4-Dimethylaminopyridine (DMAP, 99%) was purchased from Sigma Aldrich and used as received for the work presented in Chapter 3, and purified as described in paragraph II.2 for the rest of the work.

2-*tert*-Butylimino-2-diethylamino-1,3-dimethylperhydro-1,3,2-diazaphosphorine (BEMP, 98%) was obtained from Acros Organics.

*N,N,N',N'',N''',N'''*-hexamethyl-*N'''*-[*N*-(2-methyl-2-propanyl)-*P,P*-bis{[tris(dimethylamino)phosphoranylidene]amino}phosphorimidoyl]phosphorimidic triamide (tBuP<sub>4</sub>, 0.8M in hexane ) was provided by Sigma Aldrich.

1,8-Diazabicyclo[5.4.0]undec-7-ene (DBU, 99%) was bought from Alpha Aesar and 1,5,7-triazabicyclo[4.4.0]dec-5-ene (TBD, >98%) from TCI.

BEMP, tBuP<sub>4</sub>, DBU and TBD were introduced, opened, and stored in a glovebox and used as received.

### II.1.4. Reagents

*Rac*-Lactide (*rac*-LA) was obtained from Fisher Scientific (99%) and used as received.

Benzoic acid (99%) was obtained from Sigma Aldrich and used as received.

*L*-lactide (*L*-LA) monomer (assay > 99.5% and water content < 0.02%) was provided by Purac Biochem (Netherlands) and stored into a glovebox to avoid moisture and used as received.

Trimethylene carbonate (TMC, 99.5%) was purchased from Actual Chemicals and purified by recrystallisation as described in paragraph II.2. Sulfuric acid (97%) was obtained from VWR and calcium hydride was purchased from Acros Organics. Cotton wool was obtained from Fischer Scientific.

$\epsilon$ -Caprolactone (CL) (99%, Acros Organics),  $\delta$ -valerolactone (VL) (98%, TCI), methyl methacrylate (MMA) (99%, Fisher scientific), and benzyl alcohol (99%, Sigma Aldrich) were all distilled over calcium hydride and stored in a glovebox before use.

## II.2. Purification

### **Recrystallisation of TMC**

In a double Schlenk tube with a central filter, trimethylene carbonate (99%) was added into one side as well as calcium hydride and a stir bar. The system was then closed, placed under vacuum and filled with argon. The vacuum/argon process was repeated three times to ensure an inert atmosphere was achieved. THF was then added through a rubber septum, and the monomer, calcium hydride and solvent mixture were stirred at 40 °C for 48 hours. The dissolved monomer was then poured through the central filter into the second Schlenk tube to be recrystallized in an ice bath. The solid obtained was dried under vacuum, and then placed in a glovebox for later use.

### **Purification of DMAP**

DMAP was placed under an inert atmosphere in a Schlenk tube after which dry toluene was added. The mixture was heated to 85 °C under vacuum to remove water by azeotropic distillation. Once all the toluene was evaporated, the process was repeated twice, then DMAP was left under vacuum to dry overnight. The dry DMAP was transferred into a sublimation apparatus inside the glovebox, which was then taken out and placed into an oil bath at 85 °C. Liquid nitrogen was placed inside the cold finger (glassware), and DMAP was put under vacuum. Once sublimation was over, all of the glassware was put in the glovebox, and the catalyst was removed from the cold finger, collected, and stored inside the glovebox.

### II.3. Polymerization methods

#### Surface-initiated ring-opening polymerization (SI-ROP) from lyophilized cellulose nanofibrils (Chapter III)

Surface modification of the freeze-dried CNFs was performed in a 100 mL three-necked round bottom flask under an inert atmosphere (argon) while stirring continuously. First CNFs and *rac*-lactide were introduced in the flask, placed under vacuum, and flushed with argon for 15 minutes. Molar ratio of initiator were calculated considering one primary hydroxy group per glucopyranose unit ( $162 \text{ g}\cdot\text{mol}^{-1}$ )<sup>177</sup>. Then dichloromethane (DCM) was added and the mixture was left to stir for another 15 minutes. Finally, DMAP was introduced and the mixture was heated to 35 °C. A condenser was connected to the round bottom flask to avoid gas build-up and pressure increase in the flask. For all those reactions, the temperature was set to 35 °C, and the monomer/OH ratio was set at 30/1, considering one available OH per glucopyranose unit. The catalyst loading was gradually increased from 0.5 eq to 5eq/OH.

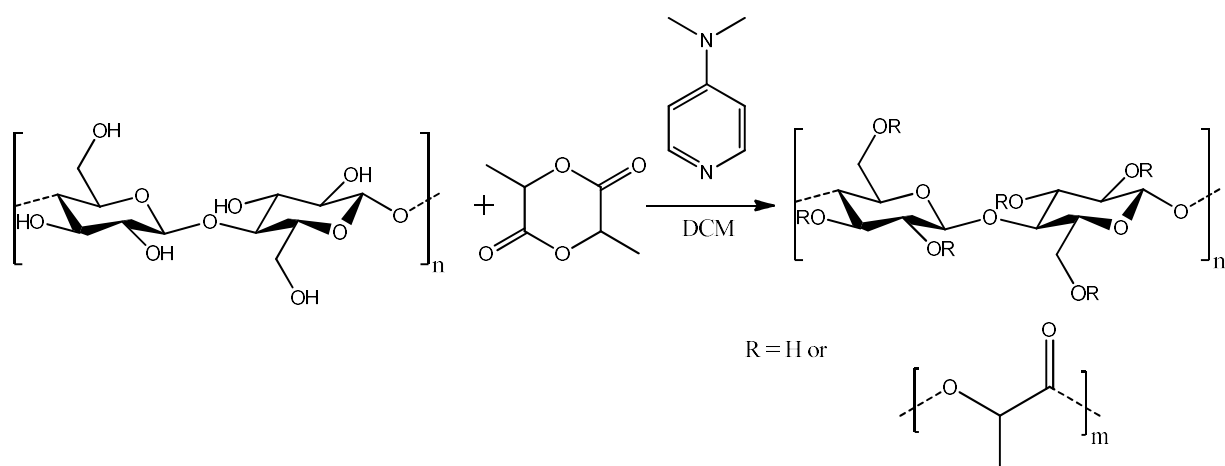


**Figure 29:** Surface-Initiated Ring-Opening Polymerization (SI-ROP) of *rac*-Lactide from the surface of cellulose nanofibrils using 4-dimethylaminopyridine (DMAP) as catalyst and dichloromethane (DCM) as solvent.

After 48 hours, the reaction mixture was filtered over a cellulose Soxhlet extraction thimble and purified by Soxhlet extraction with dichloromethane for 24 hours to remove non-grafted polymer. An additional Soxhlet extraction with ethanol was performed for 24 hours to remove DMAP from the surface of cellulose. The modified nanofibrils were subsequently dried under vacuum for 24 hours at 40 °C and a pressure of 3 mbar. The reaction scheme for SI-ROP is presented in **Figure 29**.

### SI-ROP from never-dried CNF dispersion (Chapter III)

A known amount of 1 wt% CNF/H<sub>2</sub>O dispersion was poured in a 1L round bottom flask and mixed with an equal part of ethanol. The resulting suspension was filtered through a large cellulose Soxhlet extraction thimble and purified by Soxhlet extraction with acetone (8h) to remove water from the cellulose. The CNF were then further purified by Soxhlet extraction with ethanol (24h) and then with DCM (6,5h). Care was taken to always keep the CNF in the extraction thimble in a wet state to avoid drying-induced aggregation. The cellulose nanofibrils obtained were then mixed with additional DCM to obtain a 1% suspension of CNFs in DCM. Surface modification of cellulose was performed in a 100 mL three-necked round bottom flask under inert atmosphere (argon) while stirring continuously. Catalyst (DMAP, DBU or TBD) was first introduced in the flask connected to a condenser and flushed with argon for 15 minutes. Ten mL of the cellulose dispersion in DCM was then added and stirred with the catalyst to allow it to adsorb to the surface of cellulose. Molar ratio of initiator were calculated considering one primary hydroxy group per glucopyranose unit (162 g.mol<sup>-1</sup>)<sup>177</sup>. Five mL of pure dichloromethane was then added to the mixture, followed by *rac*-lactide. During all these experiments, the temperature was tested between 25 °C and 39 °C, the monomer/cellulose ratio was in a range between 1/1 to 30/1. The catalyst loading was in a range of 0.5 eq to 3 eq/OH. The reaction was subsequently heated to the desired reaction temperature and stopped after 24 hours.

The mixture was first filtered through a cellulose Soxhlet extraction thimble and then purified by DCM Soxhlet extraction for 24h to remove non-grafted polymer formed during the reaction. Another 24 hours, an ethanol Soxhlet extraction was then carried out to clean cellulose of all the impurities still on its surface, especially catalyst traces. Finally, the solid was dried under vacuum at 40 °C and a pressure of 3 mbar for 24 hours. Non-grafted polymer was recovered from the dichloromethane Soxhlet extraction and dried for SEC and NMR analysis.

### Ring-opening polymerization on CNC surface (Chapter V)

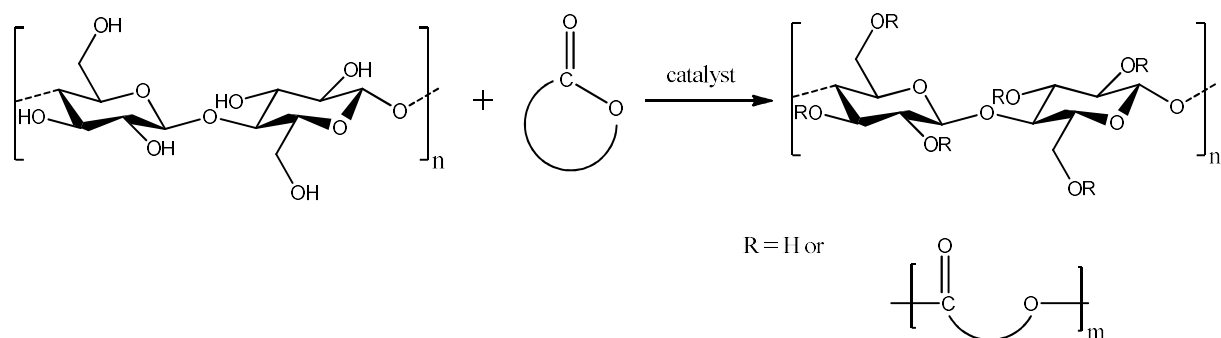


**Figure 30:** General reaction scheme of the ring-opening polymerization of cyclic esters (or carbonates) co-initiated by the hydroxy groups present on the surface of cellulose nanocrystals and catalyzed by an organic base.

All experiments were carried out under inert atmosphere and prepared in a glovebox unless stated otherwise.

In a typical reaction, a stirring bar was placed in a small glass tube reactor, along with a specified amount of CNCs. Molar ratio of initiator were calculated considering one primary hydroxy group per glucopyranose unit ( $162 \text{ g}\cdot\text{mol}^{-1}$ )<sup>177</sup>. THF (2 mL) was added as well as monomer(s) and the mixture was stirred for 30 minutes to disperse the CNCs and solubilize the monomer(s). The catalyst was then added while stirring and the reactor was taken out of the glovebox and placed in an oil bath set at a given temperature. After the desired duration, the reaction was quenched using benzoic acid and dichloromethane addition, and the mixture was filtered through a Soxhlet extraction thimble. A sample of the filtered crude mixture was taken for  $^1\text{H}$  NMR analysis, and the modified CNCs were purified by Soxhlet extraction twice, first with dichloromethane (24 hours), and then with ethanol (24 hours). The modified nanocrystals were then dried under vacuum on a Schlenk line ( $< 1 \text{ mbar}$ ) for 24 hours.

The non-grafted polymer produced as a side reaction was recovered from the first Soxhlet extraction mixture after evaporation of the dichloromethane and precipitated in cold methanol. The methanol was then filtered and the polymer obtained was dried under vacuum on a Schlenk line ( $< 1 \text{ mbar}$ ) for 24 hours.

## **Ring-opening copolymerization on CNC surface (Chapter V & VI)**

Copolymer-grafted CNCs were made using TMC and a variety of lactones. To obtain these modified CNCs, three different methods were used.

### Multistep block copolymer grafting

To obtain these modified CNCs, multiple polymerization reactions were done, with a complete purification and characterization after each of them.

The first reaction was a grafting of PTMC on the surface of the CNCs carried out as described in the previous section. The purified modified CNCs were analyzed, then dried under ultra-high vacuum at  $10^{-6}$  bars for up to five days. The dried modified cellulose was then stored in a glovebox.

The second reaction was carried out using the same general procedure described in the previous section. For this reaction, molar ratio of initiator were still calculated based on one primary hydroxy per glucopyranose unit ( $162 \text{ g}\cdot\text{mol}^{-1}$ ), however graft wt% of the modified cellulose used as the substrate was taken into account. As an example, 100 mg of modified CNCs grafted with 60 wt% polymer would therefore be considered only 40 mg of cellulose, corresponding to 0.24 mmol of glucopyranose unit and primary hydroxy. Calculation aside, the reaction, purification and analyses were carried out as described in the previous section.

### Statistical copolymer grafting

These modified CNCs were obtained using the same polymerization method described in the previous section, but multiple monomers were added at the same time during the initial solubilization in THF step. The rest of the procedure was carried out as described in the previous section.

### Block copolymerization grafting

This third method to obtain block copolymer grafts on CNCs differs from the first one as this procedure was done as a “one pot” reaction using a sequential addition of monomers. The first polymerization was carried out using the same general procedure described previously. After the desired amount of time was reached, the glass tube reactor was re-introduced into the glovebox rather than quenching. More THF (2 mL) was added to help solubilize the mixture, which was left

stirring for a minute. Then, an addition of the second monomer to the mixture was done. The rest of the procedure was carried out as described in the previous section.

### **Ring-opening polymerization of trimethylene carbonate**

TMC, the catalyst of choice, and 2 mL dichloromethane were added in a glass tube reactor and let at room temperature for a desired duration. The reaction was then quenched with a solution of benzoic acid in dichloromethane. The resulting product was precipitated in methanol, filtered and dried for 24 hours under vacuum.

### **Depolymerization of polymers grafted on the surface of CNCs**

In a Schlenk tube, 100 mg of polymer-grafted CNCs and 5.45 mg TBD were introduced and placed under vacuum at 1 mbar for about 1 minute. The tube was then filled back with argon, and then put under vacuum once more. The vacuum-argon cycle was repeated for a total of three times. Dried toluene was then added to the tube and the mixture was heated and stirred at 110 °C. The reaction was stopped after the desired duration by addition of an excess of benzoic acid.

#### **II.4. Characterization techniques**

Elemental composition (C, H, N, and S) was measured with a Thermo Scientific FLASH 2000 elemental analyzer (EA), using about 1 mg of dry sample. The standard used for calibration was 2,5-bis(5-*tert*-butyl-2-benzo-oxazol-2-yl)thiophene (BBOT, Elemental Microanalysis, UK. Vanadium pentoxide was used to aid sulphur determination. All values reported are the average of three measurements (or two in case of an outlier).

Thermogravimetric analysis (TGA) was performed using a Netzsch TG 209 F3 Tarsus. Around 2 mg of sample were placed in an aluminum-(III)-oxide pan and heated from 30 to 600 °C at a ramp rate of 10 °C/min under argon flow. Water content of the various samples was determined as the difference between the initial mass and the stabilized mass around 100 °C. The determined water content was taken into account in the determination of the level of surface modification to correct H content based on elemental composition results in line with our earlier reported procedure<sup>182</sup>.

Infrared spectra were measured using a Bruker ALPHA Fourier-transform Infrared Spectroscopy (FT-IR) spectrophotometer. Measurements were carried out in attenuated total reflection (ATR)

mode with a diamond-ATR. Spectra were acquired as the sum of 16 scans over a frequency ranging from 4,000 to 400  $\text{cm}^{-1}$ .

X-ray photoelectron spectroscopy (XPS) was carried out by Samuel Eyley from KU Leuven (Belgium). Surface-sensitive analysis of modified nanocellulose was carried out by XPS on a Kratos Axis Supra photoelectron spectrometer using a monochromated Al  $K\alpha$  ( $h\nu = 1486.7$  eV, 5 mA) X-ray source, hybrid (magnetic/electrostatic) optics, and a hemispherical analyzer with a pass energy of 160 eV for survey spectra and 20 eV for high resolution spectra. Analyses were performed on cellulose disk obtained by pressing the samples under six bars. Spectra were acquired under charge neutralization conditions using an electron flood gun within the field of the magnetic lens, and were charge corrected to aliphatic carbon at 285.0 eV. Spectra were processed in CasaXPS with Tougaard 2-parameter backgrounds used for integration and  $LA(\alpha, m)$  lineshapes corresponding with a Voigtian function with Lorentzian exponent  $\alpha$  and Gaussian width  $m$  used for fitting high resolution spectra. Empirical relative sensitivity factors supplied by Kratos Analytical (Manchester, UK) were used for quantification.

Size Exclusion Chromatography (SEC) was carried out by Aurélie Malfait from the University of Lille (France). The number-average molecular weight ( $M_n$ ) and the dispersity ( $\mathcal{D}_M$ ) of the crude product were determined by SEC in tetrahydrofuran (THF) at 40 °C at a flow rate of 1  $\text{mL}\cdot\text{min}^{-1}$ . Sample concentration was of 2g/l,  $M_n$  and  $\mathcal{D}_M$  were determined from the Refractive Index (RI) signal using a calibration curve based on polystyrene (PS) standards from Polymer Standards Service on a Waters apparatus equipped with Waters Styragel columns HR2, HR3, HR5 and HR5E.

NMR was used on some crude product after reaction to characterize the non-grafted polymer formed and evaluate the presence or not of unreacted monomer.  $^1\text{H}$  NMR spectra were recorded on AVANCE III HD 300 Bruker spectrometer (7.1 Tesla) at room temperature in deuterated dimethyl sulfoxide or deuterated chloroform (0.6 mL). The main signals used for the determination of conversion for PTMC characterization are the following:

PTMC ( $^1\text{H}$ ,  $\text{CDCl}_3$ ): 4.45 (t, 4H,  $\underline{\text{CH}_2}\text{OCOO}\underline{\text{CH}_2}\text{CH}_2$  - monomer), 4.23 (t, 4H,  $-\text{O}\underline{\text{CH}_2}\text{CH}_2\underline{\text{CH}_2}\text{OCO}$  - polymer), 2.14 (qi, 2H,  $\text{CH}_2\text{OCOOCH}_2\underline{\text{CH}_2}$  - monomer), 2.04 (qi,  $\text{CH}_2\text{OCOOCH}_2\underline{\text{CH}_2}$  - polymer)

Additional NMR spectra to be used as reference are provided in annex VIII.2.

Contact angle measurements were performed with water on a DSA 100 apparatus (KrEuss GmbH), placed on top of an antivibration table (Micro 60, Halcyonics). An ultrapure water droplet with a volume of 100pL was dispensed by a piezo dozer. During the experiment, images of the droplet profile were recorded and the resulting image was analyzed using a Young–Laplace profile. The samples were prepared as follows: the CNCs were placed in a die between two optically polished pellets. The die was pressed at 10 bars using a KBr press, resulting in a smooth sample surface. No liquid penetration into the sample was noticed during experimental determination of the contact angle for the first 10 seconds after deposition, except for pure cellulose nanocrystals, for which the contact angle was determined immediately after drop deposition.

Wide angle X-ray scattering (WAXS) was carried out by Samuel Eyley from KU Leuven (Belgium). WAXS was performed on a Xenocs Xeuss 2.0 C laboratory beamline with a monochromated copper  $K\alpha$  source, collimated with ultra-low dispersion optics to give a beam diameter of 1 mm at the sample. The samples were mounted between two Kapton windows. Scattering images were collected on a DECTRIS Eiger 1M detector.

Positive-ion Matrix assisted LASER Desorption/Ionization-Mass Spectrometry (MALDI-MS) experiments were carried out by Julien De Winter from the University of Mons (Belgium). The measurements were performed using a Waters QToF Premier mass spectrometer equipped with a Nd:YAG laser operating at 355 nm (third harmonic) with a maximum output of 65  $\mu$ J delivered to the sample in 2.2 ns pulses at 50 Hz repeating rate. Time-of-flight mass analysis was performed in the reflectron mode at a resolution of about 10 k ( $m/z$  569). All samples were analyzed using trans-2-[3-(4-*tert*-butylphenyl)-2-methylprop-2-enylidene]malononitrile (DCTB) as a matrix. Polymer samples were dissolved in THF to obtain 1 mg.mL<sup>-1</sup> solution. Additionally, 40  $\mu$ L of 2 mg.mL<sup>-1</sup> NaI solution in acetonitrile was added to the polymer solution.

## II.5. Grafting and conversion calculation

### **% Grafting content**

Grafting percentage was evaluated using the mass fraction of carbon, hydrogen, and oxygen, and comparing the elemental composition of unmodified and grafted nanocellulose. Water content, determined by TGA, was taken into account for the mass fraction of O and H for every measurement. Nitrogen content was measured, but only traces were detected, with values similar

to the detection limit for the device. Moreover, modified NCs had a similar amount of nitrogen as unmodified NCs, therefore it was considered negligible for the purpose of calculating graft content, and indicates the organocatalyst was removed from the modified samples by the purification procedure.

Unmodified NC composition used for this calculation was provided by elemental analysis of the starting product, while the following graft composition was used for each species:

PLLA composition:  $C_6H_8O_4$  (50.0% carbon, 5.6% H, 44.4% O)

PTMC composition:  $C_4H_6O_3$  (47.1% carbon, 5.9% H, 47.0% O)

PVL composition:  $C_5H_8O_2$  (60.0% carbon, 8.0% H, 32.0% O)

PCL composition:  $C_6H_{10}O_2$  (63.2% carbon, 8.8% H, 28.0% O)

PMMA composition:  $C_5H_8O_2$  (60.0% carbon, 8.0% H, 32.0% O)

The calculation used was similar to solving the following system of equation:

$$\%C_{\text{sample}} = x\%C_{\text{Polym}} + y\%C_{\text{NC}}$$

$$\%H_{\text{sample}} = x\%H_{\text{Polym}} + y\%H_{\text{NC}}$$

Where  $\%C_{\text{sample}}$ ,  $\%C_{\text{NC}}$ ,  $\%H_{\text{sample}}$ ,  $\%H_{\text{NC}}$  were obtained by elemental analysis, and  $\%C_{\text{Polym}}$ ,  $\%H_{\text{Polym}}$  were known from their chemical composition.

This was done using a python script taking into account the measured elemental composition of unmodified and modified NCs, as well as their water content as determined by TGA. The method also took into account standard deviation of detected elements, and used a minimization matrix as well.

Both EA and TGA were done at the same time to obtain an accurate value of the quantity of water present in the sample that were analyzed at the time of the elemental analysis. The starting nanocellulose was run through EA and TGA again for every series of measurement to obtain more accurate results when comparing with the modified cellulose samples.

### **Conversion calculation**

Conversion was calculated based on  $^1\text{H}$  NMR data and polycarbonate grafting described previously.

$$C = m_{\text{reacted}} / m_{\text{total}}$$

C was the conversion, and  $m_{\text{total}}$  the mass of monomer introduced at the beginning of the reaction

$m_{\text{reacted}}$  was the mass of reacted monomer and calculated using the following formula:

$$m_{\text{reacted}} = m_{\text{grafted}} + m_{\text{non-grafted polymer}}$$

$m_{\text{grafted}}$  was the mass of monomer turned into grafts, and was calculated from the wt% grafts using the following formula:

$$m_{\text{grafted}} = (m_{\text{CNC}} \times \text{wt}\%_{\text{graft}}) / (100 - \text{wt}\%_{\text{graft}})$$

Using the crude sample after quenching, a “visible conversion” was calculated based on integration of  $^1\text{H}$  NMR spectra signals for TMC and PTMC. Using this,  $m_{\text{non-grafted polymer}}$  could be calculated using the following formula:

$$m_{\text{non-grafted polymer}} = (m_{\text{total}} - m_{\text{grafted}}) \times \text{visible conversion}$$

Grafting yield was calculated as the ratio of monomer grafted / monomer total.

## II.6. DFT methodological details

The DFT calculation work was done by Pr. João P. Prates Ramalho from the University of Evora (Portugal).

We adopt a simple model with methanol as initiator, trimethylene carbonate (TMC) as a cyclic carbonate and TBD and DMAP as organocatalysts. All calculations in this study were conducted with the Gaussian 16 program package<sup>183</sup>.

Geometries of the chemical relevant species were obtained by density functional theory (DFT) from optimizations using the hybrid meta-GGA exchange–correlation functional M06-2X<sup>184</sup> together with the 6-31+G(d,p) basis set. In all calculations solvent effects were taken into account by using the SMD continuum solvation model<sup>185</sup> with the parameters of dichloromethane.

Frequency analysis confirmed optimized geometries as energy minimum by the non-existence of imaginary frequencies or as transition states by the existence of a sole imaginary frequency that links reactants and products along the reaction coordinate.

The stability of the different species was established by calculating their Gibbs energy in solution which were used to describe the reaction profiles. Due to the well-known limitations of the harmonic oscillator model for low-frequency vibrational modes the thermal corrections were calculated by means of the quasiharmonic oscillator approximation, with the vibrational frequencies smaller than  $100\text{ cm}^{-1}$  being raised to  $100\text{ cm}^{-1}$ <sup>186</sup>. Atomic charges were calculate by fitting the molecular electrostatic potential with the Breneman and Wiberg<sup>187</sup> CHELPG scheme.

### III. Organocatalyzed ring-opening polymerization of lactide from the surface of cellulose nanofibrils

#### III.1. Introduction

After playing an important role in the advent of the chemical industry and being replaced by petroleum-based alternatives, carbohydrate polymers have again regained an increasing amount of attention. Polysaccharides have been the focus of a large amount of work as the biggest fraction of renewable biomass, with cellulose being the most common biopolymer on the planet with an estimated annual production of well over  $10^{10}$  tons<sup>54</sup>. Cellulose has many potential uses, and can be made into nanomaterials such as cellulose nanofibrils (CNF)<sup>188,189</sup> and cellulose nanocrystals (CNC)<sup>54,189</sup>. CNF are micron-length fibers that possess remarkable properties such as a high aspect ratio (width of 4 to 20 nm, length of up to several microns), a high stiffness with a Young's modulus superior to 110 GPa, and a low density of  $1.6 \text{ g/cm}^3$ ,<sup>171</sup> capable of forming a network structure. Unlike CNFs, cellulose nanocrystals do not contain dislocated non-crystalline sections as the dislocated regions are removed during an acid hydrolysis, making their length smaller and crystallinity higher<sup>191</sup>. Their high abundance, stiffness, and high aspect ratio make CNFs and cellulose nanocrystals good candidates for use in composite materials as reinforcements<sup>4</sup>. Moreover, nanocellulose can be produced at an industrial scale<sup>192,193</sup>. Because of the lower aspect ratio of CNCs when compared to CNFs, CNFs have a greater potential as reinforcing fiber and impact modifier in composites<sup>194</sup>, yet they have not received the same amount of attention as CNCs when it comes to surface modification<sup>195</sup>. Using CNFs and CNCs in polymer matrices comes with a few challenges; the compatibility between hydrophobic polymer matrices and hydrophilic cellulose is limited, and the dispersion of nanomaterials in polymer can be quite poor. This in turn diminishes the achievable mechanical strength improvements of the composite material as these depend on individualization of the reinforcing fibers. Hence, some research has been carried out on the surface modification of nanocellulose to enhance their dispersibility and to improve the compatibility of cellulose nanomaterials with hydrophobic polymer matrices. Their surface hydroxy groups allow for a wide array of chemical modifications and these could thus be used to change the nanocellulose surface energy to increase compatibility with polymer matrices<sup>196,197</sup>. Examples of modifications reported in the literature include non-covalent modification such as

surfactant adsorption<sup>173,198</sup>, but also covalent surface reactions such as sulfonation<sup>36,199</sup>, oxidation<sup>200,201</sup>, acetylation<sup>202,203</sup>, etherification<sup>204</sup>, silylation<sup>205</sup>, and amidation<sup>206</sup>.

The combination of a biodegradable, biocompatible, and bio-based polymer with CNFs could lead to an all-biodegradable and biocompatible composite material made completely from renewable materials. Polylactide (PLA), a polyester that can be obtained from 100% renewable sources, is therefore an interesting candidate<sup>207</sup>. In addition, PLA is non-toxic and biocompatible, allowing it to be used in many fields such as food-contact and biomedical applications<sup>208</sup>. Combining cellulose fibers with PLA could thus lead to materials with a larger range of mechanical properties opening up a wider range of possible applications than those now achievable<sup>209</sup>. Using the same monomer to graft on the cellulose as the polymer matrix should provide the best possible compatibility between matrix and reinforcing fiber<sup>7</sup>.

Cellulose and other polysaccharides with PLA grafts have mostly been reported using a “grafting from” approach<sup>150,210–212</sup>, but “grafting onto” methods have also been used successfully to produce similar materials<sup>213</sup>. In the case of lactide and other similar cyclic monomers, the “grafting from” approach makes use of ring-opening polymerization (ROP), using the polysaccharide hydroxy groups as initiating sites along with a catalyst, often tin(II) octoate ( $\text{SnOct}_2$ )<sup>210</sup> or 4-dimethylaminopyridine (DMAP)<sup>150,213</sup>. ROP reactions initiated from the surface of nanocellulose have been performed in solution and in bulk under a wide variety of conditions<sup>136,213</sup>. A previous report of PLA-grafted cellulose nanofibrils using the “grafting from” approach and  $\text{SnOct}_2$  achieved a grafting of around 20w% of PLA<sup>211</sup>.

Metal-based catalysts, and in particular tin-based catalysts, have been used for a long time to perform ring-opening polymerization of lactides, both for homogeneous PLA synthesis and for the grafting from carbohydrates as described previously. However, some metal catalysts can be toxic, requiring additional steps for removal implying an increased cost for sensitive applications such as biomedical applications. Even these steps in general do not fully remove the metal catalysts in the presence of cellulose, making trace pollution a potential problem<sup>214</sup>.

Organic catalysis is an interesting alternative to metal-based catalysis, as the use of small, easily removed, organic molecules with different reactivities can be very beneficial to some applications. In particular, this has been heavily investigated in the last few decades for the ROP of lactide<sup>11,155,215</sup>. A wide range of organocatalysts can be used including N-heterocyclic carbenes<sup>216</sup>,

pyridine-based compounds<sup>150,213</sup>, guanidine<sup>141,167</sup>, and nucleobases such as adenine<sup>217</sup>. Most of these have received thorough studies for the ROP of lactide and were proven to be competitive with metal-based catalysts.

While ROP of lactide initiated from polysaccharide hydroxy groups is well documented, and organocatalyzed ROP has been studied in great details, the SI-ROP of lactide from nanocelluloses catalyzed by an organic compound has not received as much attention. In addition, the surface modification of cellulose nanocrystals has been reported more often than surface modification on nanofibrils, with little work done on studying the influence of different parameters on the reaction of polymerization initiated from nanocellulose surfaces. Where such studies have been carried out, they proved to be quite valuable in bringing insights in the SI-ROP reaction of and enabled optimization of the modification reaction<sup>136</sup>. Furthermore, while formation of non-grafted polymer is also expected as trace water cannot be fully excluded from the reaction mixture, little is known about the competition between water-initiated polymerization and polymerization from the nanocellulose surface. We report herein an investigation of the influence of experimental parameters on the grafting efficiency of lactides in the DMAP catalyzed CNF hydroxy groups initiated ROP reaction to start developing the insights needed to optimize these reactions.

## III.2. Results and discussion

### III.2.1. SI-ROP modification of lyophilized CNF

**Table 4:** Ring-opening polymerization of *rac*-lactide initiated from the surface of freeze-dried CNF in the presence of DBU/TBD in DCM for 48 hours at 35 °C.

Entry	Catalyst	<i>rac</i> -Lactide / Catalyst / OH <sup>[a]</sup>	Poly(lactide) grafting <sup>[b]</sup> (wt%)
1	DBU	30/0.5/1	0
2	DBU	30/2.5/1	0
3	DBU	30/5/1	0
4	TBD	50/1/1	0
5	TBD	50/3/1	0
6	TBD	50/6/1	0
7	TBD	50/10/1	7
8	DMAP	30/0.5 /1	6
9	DMAP	30/5/1	17

[a] Ratio calculated based on primary hydroxy group of CNF (1/glucose unit) [b] Determined by elemental analysis (calculation based on hydrogen content (%H) and carbon content (%C)) and corrected for adsorbed water using TGA.

The effect of reaction temperature, catalyst loading, and monomer-to-cellulose ratio on the SI-ROP of lactide from the surface of freeze-dried CNF was investigated in order to optimize and control CNF functionalization. The reactions were carried out in DCM for 48h at 35 °C. Some preliminary work was done to test 1,8-diazabicyclo[5.4.0]undec-7-ene (DBU) and 1,5,7-triazabicyclo[4.4.0]dec-5-ene (TBD) as catalyst for this reaction (**Figure 31**).

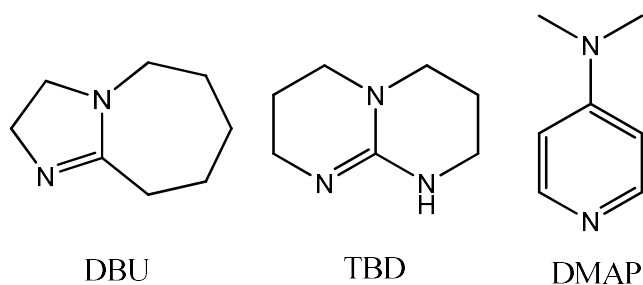


**Figure 31:** Chemical structure of DMAP, DBU and TBD.

As can be seen from **Table 4**, DBU did not provide grafted CNF, whereas TBD did, but only reaching 7% with a large amount of catalyst. This could be attributed to the generally higher activity of these catalyst, making the initiation and polymerization on residual water occur much faster, therefore limiting the grafting. As opposed to DBU and TBD, DMAP leads to superior grafting above 10% when using higher amount of it (5eq), but also led to grafted CNFs when using a small catalyst loading (0.5eq). Therefore, DMAP was selected and further explored for the rest of the experiments.

**Table 5:** Ring-opening polymerization of *rac*-lactide initiated from the surface of freeze-dried CNF in the presence of DMAP in DCM for 48 hours at 35 °C.

Entry	<i>rac</i> -Lactide / DMAP / OH <sup>[a]</sup>	Grafted PLA (wt%) <sup>[b]</sup>
8	30/0.5 /1	6
10	30/1/1	6
11	30/1.5/1	8
12	30/2/1	8
13	30/2.5/1	11
14	30/3/1	19
15	30/4/1	12
9	30/5/1	17

[a] Ratio calculated based on primary hydroxy group of CNF (1/glucose unit) [b] Determined by elemental analysis (calculation based on hydrogen content (%H) and carbon content (%C)) and corrected for adsorbed water using TGA.

At a fixed temperature and reaction time (35 °C and 48 hours), the PLA content of grafted cellulose nanofibrils increased with the amount of catalyst, and reached a maximum for 3 equivalents of catalyst per surface hydroxy group (**Table 5**). Water present during the reaction competes with cellulose nanofibrils surface hydroxy groups to initiate the polymerization reaction, thus resulting in non-grafted polymer formation. This side reaction is important due to the hydrophilic nature of cellulose. It is further exemplified at DMAP amounts above 3 equivalents of the surface hydroxy groups, where the grafted PLA content on the CNF dropped, indicating that a higher catalyst amount leads to a faster initiation by water. In addition, DMAP has been reported to go through both a nucleophile and a H-bond mechanism for the polymerization of lactide, and the nucleophile mechanism occurs at higher loading of catalyst ( $>2$  eq)<sup>162</sup>. Therefore a ratio [CNF]/[DMAP] of 3 appears to be optimal for CNF surface modification. This catalytic ratio is in the range of values reported in the literature for DMAP-catalyzed non-grafted polymerization of lactide and for the ROP of lactide from polysaccharides<sup>149,150,188</sup>.

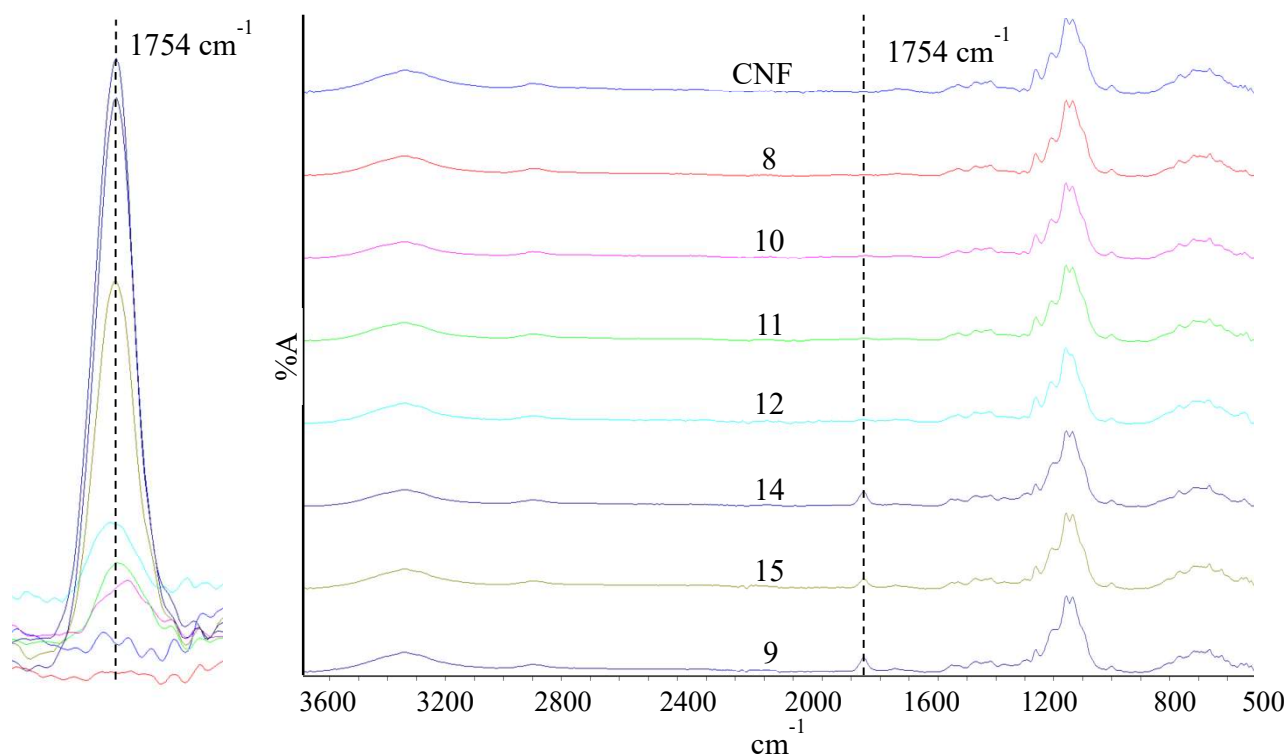


**Figure 32:** FT-IR spectra of cellulose nanofibrils (CNF) and modified CNF with different amount of grafting after purification by Soxhlet extraction corresponding to entries in **Table 5**.

In addition to elemental analysis, successful modification was confirmed by FT-IR (**Figure 32**). The spectra of the product closely resembled that of cellulose as expected. The appearance of a band at  $1754\text{ cm}^{-1}$  is characteristic of polylactide stretching frequencies for  $\nu(\text{C}=\text{O})$  and confirms successful esterification on the CNF surface, as well as a signal at  $1451\text{ cm}^{-1}$  and  $1090\text{ cm}^{-1}$ , which are typical for PLA<sup>150,217</sup>. As shown in the magnification in **Figure 32**, the relative intensity of the carbonyl signal in modified CNF increased with increasing amount of catalyst, reaching a maximum for 3 equivalent of catalyst/surface hydroxy, in line with the trend observed for the calculated amount of PLA obtained from elemental analysis (EA). This confirms the trend in surface modification and the maximum amount of PLA grafted on the surface of cellulose for 3 equivalents of catalyst.

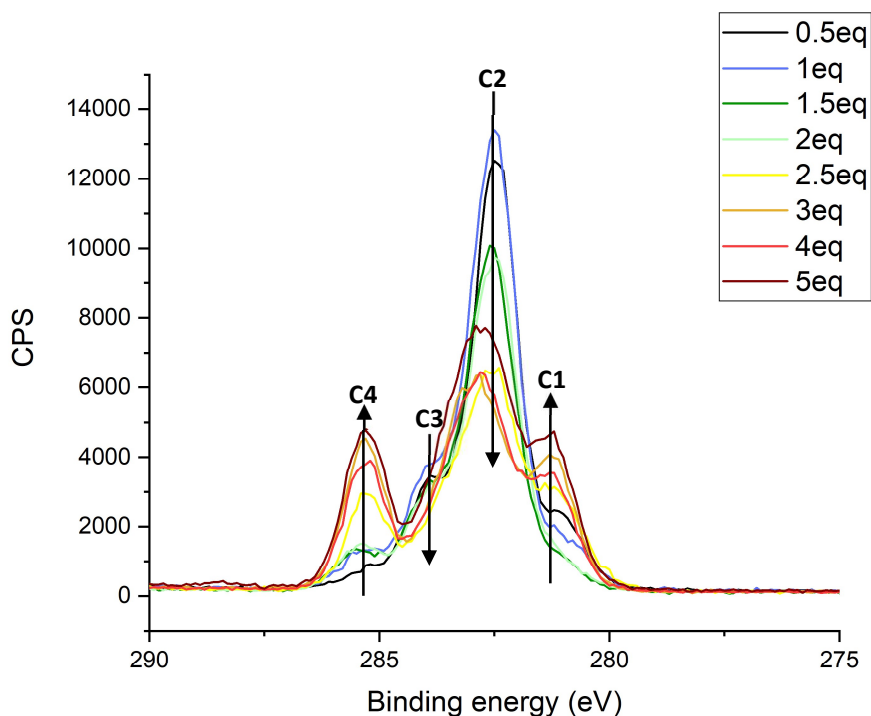


**Figure 33:** Carbon 1s X-ray Photoelectron Spectroscopy (XPS) scan of modified cellulose nanofibrils using different amounts of 4-dimethylaminopyridine.

X-ray Photoelectron Spectroscopy (XPS) gives even more information on the surface composition and the chemical environment of the CNFs. In **Figure 33**, C1 is the aliphatic carbon contribution at 285eV, which initially increases with the amount of catalyst used. C2 and C3 correspond to C-O (at 286.41eV) and O-C-O (287.45eV) contribution respectively and both decreased with an

increasing amount of PLA grafted on the surface of cellulose. C4 is the O-C=O contribution visible at 289.16eV, which increased with the amount of modification on the fiber in agreement with C1. Both C4 and C1 are not present for unmodified cellulose, confirming modification after purification of the CNF. All the positions reported for the different contributions are in agreement with earlier reported results for poly( $\epsilon$ -caprolactone) grafted on nanocellulose<sup>179</sup>. XPS data thus confirmed the results obtained by elemental analysis and FT-IR, with the most amount of modification detected for 3 equivalents of catalyst.

### III.2.2. SI-ROP modification of never dried CNF

Using the results obtained from the previous experiments, a different protocol was tested using never-dried CNF. Indeed, working with lyophilized CNF requires freeze-drying, giving CNF that are more difficult to redisperse and that require the use of more solvent than never-dried CNF suspensions to obtain a homogeneous reaction mixture. Therefore, different methods for preparing CNF dispersions in DCM, from a 1% water dispersion, were tested. The results of the DMAP-catalyzed ROP grafting reactions are reported in **Table 6**. This method gave a product that was easier to characterize after drying (powder-like) and showed in general a superior quantity of PLA grafting on CNF, particularly at lower amounts of catalyst (*e.g.* comparing entries 10 and 11 in **Table 5** to entry 10 in **Table 6**).

Using a ratio of lactide/CNF/catalyst of 30/1/3, two similar reactions were performed at 39 °C over 24h, one using freeze-dried CNF and the other never-dried CNF. After using elemental analysis and thermogravimetric analysis (TGA), the grafting obtained from freeze-dried cellulose was 13% (entry 16, **Table 6**), while never dried cellulose grafting reached 24% (entry 15, **Table 6**). As the result found for never-dried cellulose was comparable to better grafting obtained using freeze-dried cellulose over 48h, experiments using never-dried cellulose were performed over 24h. Using never-dried CNF suspensions in DCM, we also investigated the effect of temperature, monomer amount, and monomer/initiator ratio.

**Table 6:** Ring-opening polymerization of *rac*-lactide initiated from the surface of never-dried CNF in the presence of DMAP in DCM.

Entry	T ( °C)	<i>rac</i> -Lactide/CNF	Eq DMAP/CNF	Grafted PLA (wt%) <sup>[a]</sup>
1	25	1	0.5	7
2	25	1	3	13
3	25	15	1.75	7
4	25	30	0.5	16
5	25	30	3	18
6	32	1	1.75	5
7	32	15	0.5	9
8	32	15	1.75	11
9	32	15	3	9
10	32	30	1.75	12
11	39	1	0.5	6
12	39	1	3	17
13	39	15	1.75	12
14	39	30	0.5	18
15	39	30	3	24
16 <sup>[b]</sup>	39	30	3	13

[a] Determined by elemental analysis (calculation based on hydrogen content (%H) and carbon content (%C)) and corrected for adsorbed water using TGA. [b] reaction with freeze-dried CNFs

Grafting onto CNF ranged from 5% to 24%: Overall an increase in catalyst ratio from 0.5 eq to 3 eq led to an increase in the amount of PLA grafted onto CNF, irrespective of the temperature (comparing entry 1 to 2 and 12 to 11) or the quantity of lactide (comparing entry 1 to 2 and 5 to 4). As described previously, the polymerization reaction initiated from the surface of CNF takes place in competition with the non-grafted polymerization initiated by residual water. While DMAP is known to work better at higher quantities for ROP initiated by hydroxy groups<sup>141</sup>, the presence of a small amount of water means more catalyst is needed to ensure a proper initiation from the nanofibril surface. At higher temperatures but low monomer amount (entry 11 and 12, **Table 6**), the increase in DMAP content has more of an impact on the amount of PLA grafted which increased by 11%, compared to a 5% increase at lower temperature. This is likely due to a faster polymerization of lactide at higher temperatures, but initiation being preferred for water as it is more mobile and available than cellulose OH groups, resulting in non-grafted polymerization being heavily favored. An opposite effect is observed at lower temperatures and a high lactide amount (entry 5 and 4, **Table 6**): an increase in the quantity of DMAP did not make a noticeable difference

in the surface-grafted quantity of PLA (2%). If polymerization on cellulose “starts late” due to initiation on water being faster, but there is a lot more monomer available and propagation is slower, then grafting on cellulose still has time to occur. In that regard, adding more DMAP to ensure initiation on cellulose can happen quickly does increase the amount of grafting found, but only by a small margin.

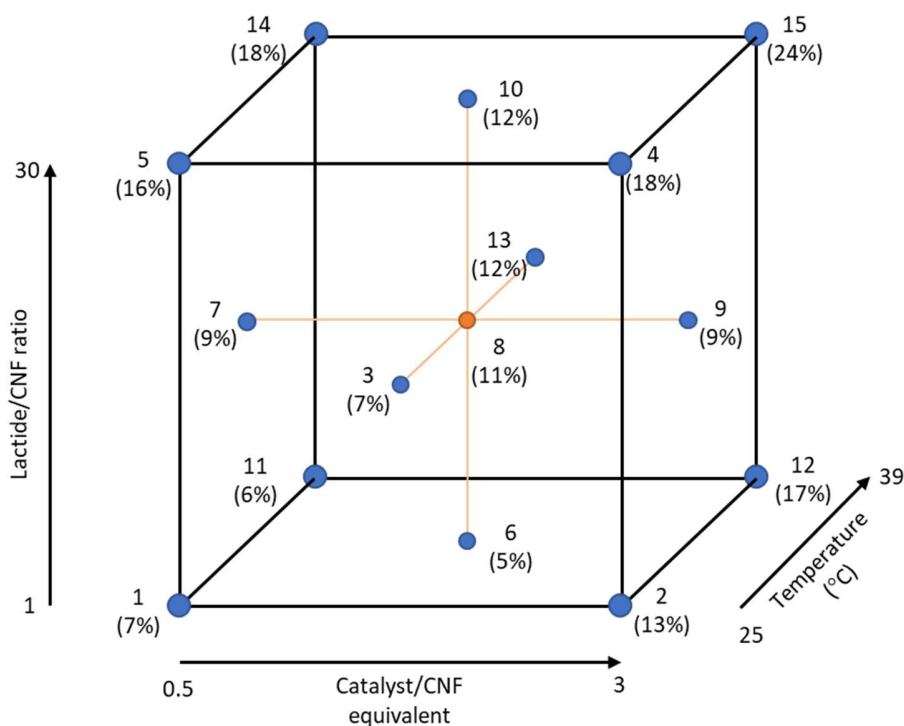


**Figure 34:** Graphical representation of the grafting percent of PLA on cellulose with different sets of parameters. Numbers correspond to entries in **Table 6**.

An increase in temperature (entry 1 to 11, 2 to 12, 5 to 14 and 4 to 15, **Table 6**) in general led to a greater amount of grafted PLA on the CNF, similarly to an increase in catalyst amount. However this effect was more pronounced for higher catalyst amounts (6% increase), as increasing the temperature from 25 to 39 °C when only 0.5 eq of DMAP was used (entry 1 vs. 11, 2 vs. 12, 5 vs. 14 and 4 vs. 15) did not make a significant difference (2% increase) in the amount of PLA grafted on the CNFs, irrespective of amount of monomer. While increasing the temperature was beneficial to the amount of PLA grafting, it may also lead to faster polymerization, while the lower amount of catalyst may lead to a slower initiation on CNF surface hydroxy, both of which favor water-initiated non-grafted polymerization.

Finally, the effect of the monomer quantity was studied. When comparing the results of entry 1 vs. 5, 2 vs. 4, 11 vs. 14, 12 vs. 15 and 6 vs. 10, the PLA weight content on modified CNF increased significantly with increasing amounts of lactide in the reactive medium. This particular effect was more pronounced for a smaller quantity of catalyst, leading to an increase of 9% (entries 1 to 5) and 12% (entries 11 to 14) in PLA grafting. Comparatively, increasing the monomer amount at higher DMAP loading increased the PLA amount on CNF by 5% (entries 2 to 4) and 7% (entries 12 to 15) respectively. This result agrees with the previous observations, showing that a small amount of catalyst favors initiation by residual water, which then will quickly turn the monomer into non-grafted polymer. When more lactide is added to the reaction medium, this effect is mitigated as more monomer takes longer to react away allowing for surface-grafting on the nanocellulose. Comparing all reactions, the monomer amount comes out as the most influential parameter, as an increase in *rac*-lactide always led to the most significant increase in grafting amount on CNF. However, increasing the amount of catalysts can achieve comparable results, especially at higher temperatures. This can be more advantageous as the amount of catalyst needed to yield such result is significantly less than the amount of monomer required, as an increase by a factor 6 for the quantity of catalysts can yield similar amount of grafting as an increase by a factor 30 for the quantity of monomer.

Reactions with intermediate values for all parameters were also performed to verify the trends. While those observations stayed true for most experiments, some specific combinations gave low PLA grafting onto cellulose, meaning some parameter combinations do not favor grafting, but rather water-initiated non-grafted polymerization. In particular, increasing the temperature was detrimental to PLA grafting on CNF for low DMAP and lactide quantities, explained by the temperature increasing the speed of non-grafted polymerization.

Compared to the results for freeze-dried CNF, solvent-exchanging CNF allows for a higher maximum grafting efficiency, and significantly better results are obtained for reactions performed with less than 3 eq of catalysts, all the while requiring shorter reaction times. In addition, elemental analysis showed no significant retention of DMAP in the grafted CNF, indicating a near complete removal of the catalyst from the product.

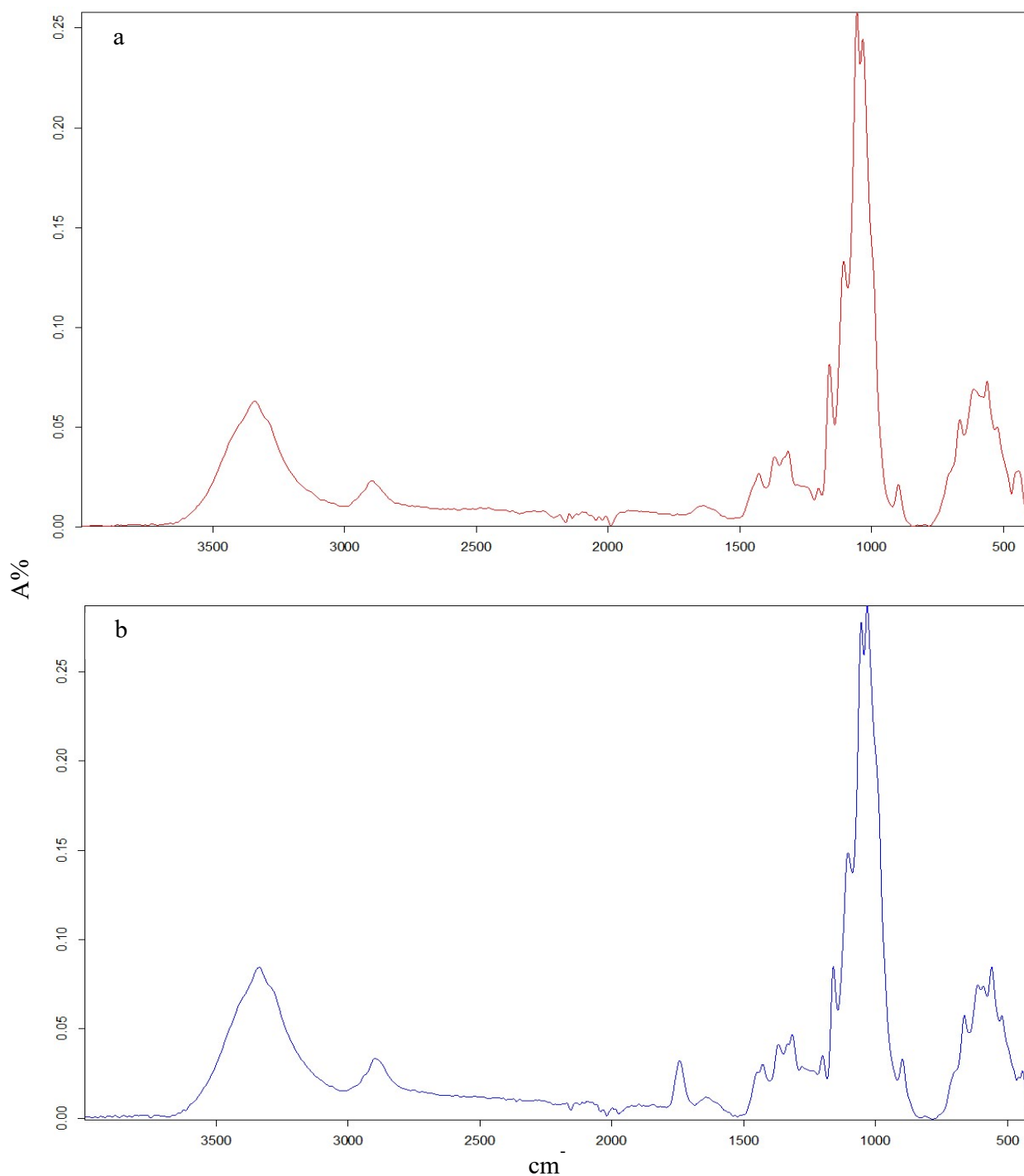


**Figure 35:** FT-IR spectra of unmodified cellulose nanofibrils (a) and PLA-grafted CNF (entry 15 in **Table 6**) using the “never-dried” method (b).

FT-IR (**Figure 35**) analysis showed a band around  $1750\text{ cm}^{-1}$ , characteristic of a stretching frequency for  $\nu(\text{C}=\text{O})$ . A characteristic ester band is seen at  $1454\text{ cm}^{-1}$  and is more important for

the cellulose with a higher PLA content. As shown in the magnification the carbonyl signal increase, following the same trend as the amount of grafting calculated using EA. Comparing the spectra obtained using the freeze-dried CNF, the overall signal is similar, and the relative intensity of the ester band is similar for samples with equal PLA content calculated with EA.

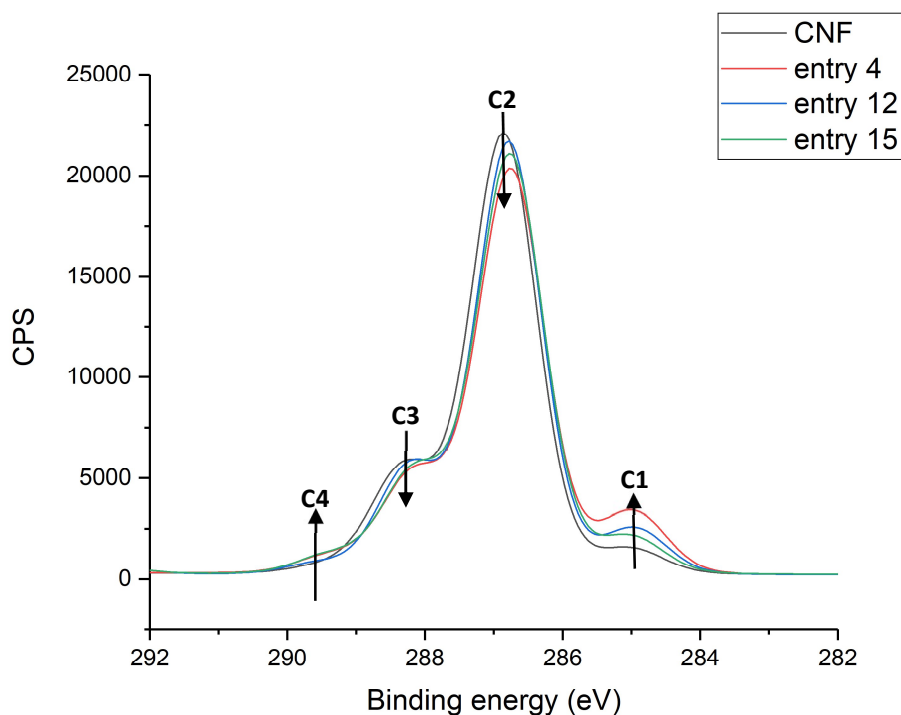


**Figure 36:** Carbon 1s XPS scan of modified cellulose nanofibrils (CNF) obtained from never dried CNFs, with different entries corresponding to the samples in **Table 6**.

X-ray photoelectron spectroscopy (**Figure 36**), shows the aliphatic carbon contribution C1 increasing for modified CNF compared to non-modified ones due to the methyl-bearing lactide units grafted on the cellulose. The same conclusion can be made for the C4 contribution, related to O-C=O visible at 289.54 eV present only on the grafts. When comparing the XPS results for the never dried CNF to the one in **Figure 33**, the same peaks can be seen. However, increases are more pronounced for samples prepared with freeze-dried cellulose, despite EA showing higher grafting for never-dried CNF. A plausible explanation could be that XPS is a surface analysis, only revealing the composition of the top 10 nm of the material. Freeze-dried CNF is more aggregated in the reaction mixture and in the final product. The majority of grafting will thus occur on the surface of aggregated CNF particles, leading to a stronger signal in XPS, yet a lower EA amount. The well-dispersed CNF form a powdery product however, and it is likely that the better dispersion

leads to a better separation of the fibrils, giving more surface area for the graft to occur and better overall spread of the grafts over the CNF.

To confirm that lactide polymerization did occur during the reaction and determine the potential length of the PLA chains obtained, size exclusion chromatography (SEC) was used to determine the length of the non-grafted polymer separated from the CNF during the Soxhlet extraction. Overall, the results showed that short oligomeric chains were obtained, with a number average molecular weight between 600 and 1,400 g/mol, confirming the successful polymerization reaction and the presence of chains initiated by water. As a complementary approach to determine polymerization of lactide, NMR was used on some crude samples separated from CNF, similar to the one used for SEC analysis. Samples separated from CNF with different % of grafting (according to EA) were analyzed and compared to the spectra of DMAP and *rac*-lactide (**Figure 80** and **Figure 81**)

Characteristic doublet are observed at 8.16 and 6.72 ppm, corresponding to protons on the pyridine ring of DMAP. Additionally, a singlet corresponding to CH<sub>3</sub> moieties of DMAP is also observed at 3.01 ppm. As the analysis was performed on crude product separated from cellulose, the presence of catalyst was expected.

Complex signals can be observed between in the region 4.86-5.21 ppm and 4.10-4.24 ppm. This corresponds to the proton in the polymerized lactide chain. Protons closer to chain ends have a different chemical shift, which leads to two complex multiplets. Due to the short length of the oligomer produced, protons next to chain ends have a strong signal in NMR. A similar phenomenon can be observed between 1.16 and 1.49 ppm, which corresponds to methyl protons.

Interestingly, the signal for lactide in DMSO, particularly for the proton in the six-membered ring, is not observed around 5.43 ppm where a quartet should be in the presence of *rac*-lactide (**Figure 81**). This shows that while the grafting measured on CNF is low, and only short oligomers are produced, the full conversion of monomer does occur.

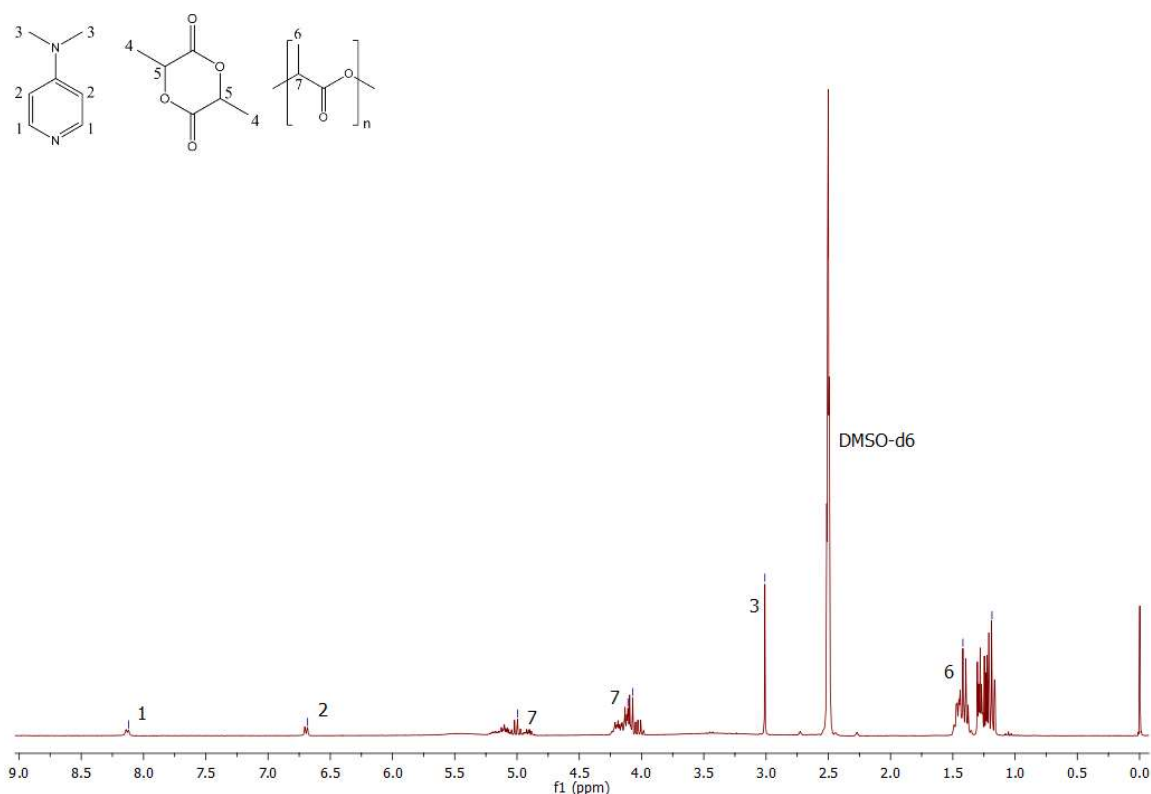


**Figure 37:** <sup>1</sup>H NMR spectra of crude mixture after reaction in DMSO-d<sub>6</sub>. Crude product separated from modified CNF corresponding to entry 15 in **Table 6** (300 MHz).

<sup>1</sup>H NMR (DMSO-d<sub>6</sub>, 300 MHz) δ (ppm) 5.43 (q, 2H), 1.44 (d, 6H)

Overall using never-dried CNF with DMAP and *rac*-lactide has been the more promising grafting method. While both methods used for freeze-dried and never-dried CNF are different, and a quantitative comparison cannot be done, the second method used shows more promising results, in particular when trying to use lower quantities of catalyst. It also does not require freeze-drying, a method that can at times take several days, and leads to a better dispersed state of cellulose which is overall easier to analyze.

### III.3. Conclusion

We performed SI-ROP of *rac*-lactide using an organocatalyst, 4-dimethylaminopyridine (DMAP), and CNFs as the initiator. The effect of different parameters on the reaction were investigated as well as the interaction between these parameters on the modification of cellulose. The highest modification amount was achieved for never-dried CNF suspensions transferred into DCM by solvent exchange, as opposed to the more common lyophilization procedure. The highest grafting

was obtained for a DMAP/CNF of 3/1, 3 g of *rac*-lactide, a reaction time of 24 h at 39 °C under inert atmosphere. The amount of modification was similar to earlier reports using tin(II) octoate as the catalyst in solution at 90 °C or in bulk at 120 °C<sup>211</sup>, while we used a simple one-step reaction and an organic catalyst under mild conditions. In addition, most of the catalyst could be removed from the final product, showcasing one of the main benefit of using an organic catalyst. We were also able to elucidate the effect of changing parameters on the effect of residual water interference of the grafting reaction.



The mechanisms involved in the ring-opening polymerization of cyclic esters catalyzed by *N*-heterocyclic bases have been widely studied in the literature<sup>100,156,164,167,217,223–226</sup> and nicely reviewed recently<sup>227</sup>. Two main mechanisms have been shown to occur: a nucleophilic attack of the catalyst on the carbonyl moieties of the monomer, and a basic activation of a protic co-initiator followed by a nucleophilic attack. The latter mechanism is generally preferred to the monomer nucleophilic activation by the catalyst, as soon as a protic co-initiator is present in the reactive medium. In the case of bases such as TBD, an additional H-bond activation of the carbonyl moieties of the cyclic ester has been advanced to occur.

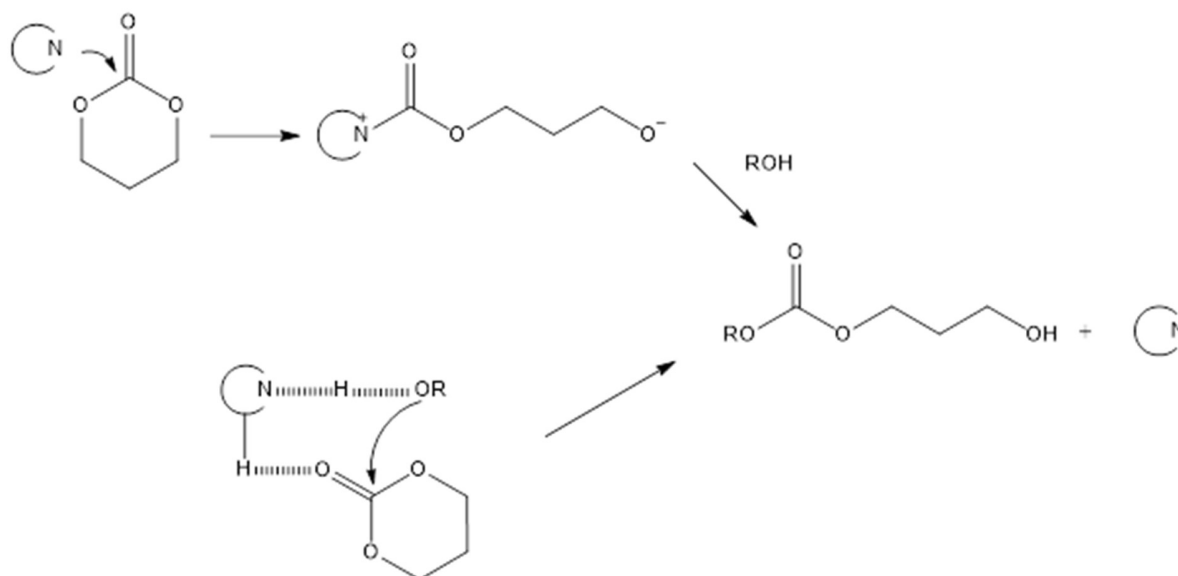


**Figure 39:** Schematic representation of the nucleophilic (upper part) and the alcohol activation / H-bond mechanism (bottom part) for the ring-opening polymerization of TMC catalyzed by an *N*-heterocyclic base and co-initiated by an alcohol.

Regarding the ring-opening polymerization of cyclic carbonates, coordination insertion mechanisms have been well discussed on the basis of DFT studies for various metal based catalysts<sup>114,228–232</sup>. Theoretical mechanistic insights of organocatalyzed ring-opening polymerizations were in turn devoted to rationalize the polymerization of a *N*-substituted eight-membered carbonate ring<sup>233</sup>, to support regioselectivity results of the polymerization of carbohydrate based carbonates<sup>234–236</sup> or to explain the absence of reactivity observed using a Brønsted pair as catalyst<sup>237</sup>. As far as we know, the discrimination between the alcohol activation pathway and the direct nucleophilic mechanism of the organocatalyzed ring-opening polymerization of cyclic carbonates catalyzed by performant heterocyclic nitrogen bases, as

represented in **Figure 39**, has never been discussed in the literature. We report in this contribution a DFT investigation of those two mechanisms for the ring-opening polymerization of TMC catalyzed by TBD and DMAP as case studies, and corroborate the findings by experimental results.

## IV.2. Results and discussion

### IV.2.1. TBD catalyzed ring-opening polymerization of TMC

We started our investigation with the H-bond / alcohol activation pathway for the TBD catalyzed ring-opening polymerization of TMC co-initiated by methanol. The reaction progresses with two transition states (**Figure 40** and **Figure 41**). It is initiated with the formation of a complex with two hydrogen bonds, one between the tertiary amine catalyst nitrogen and the alcohol hydroxy and the second between the TMC carbonyl oxygen and the catalyst protonated nitrogen. That activates the alcohol and the carbonate, leading to the addition to the carbonyl carbon and hydrogen transfer from the alcohol to the TBD catalyst. The structure is presented in **Figure 40**.

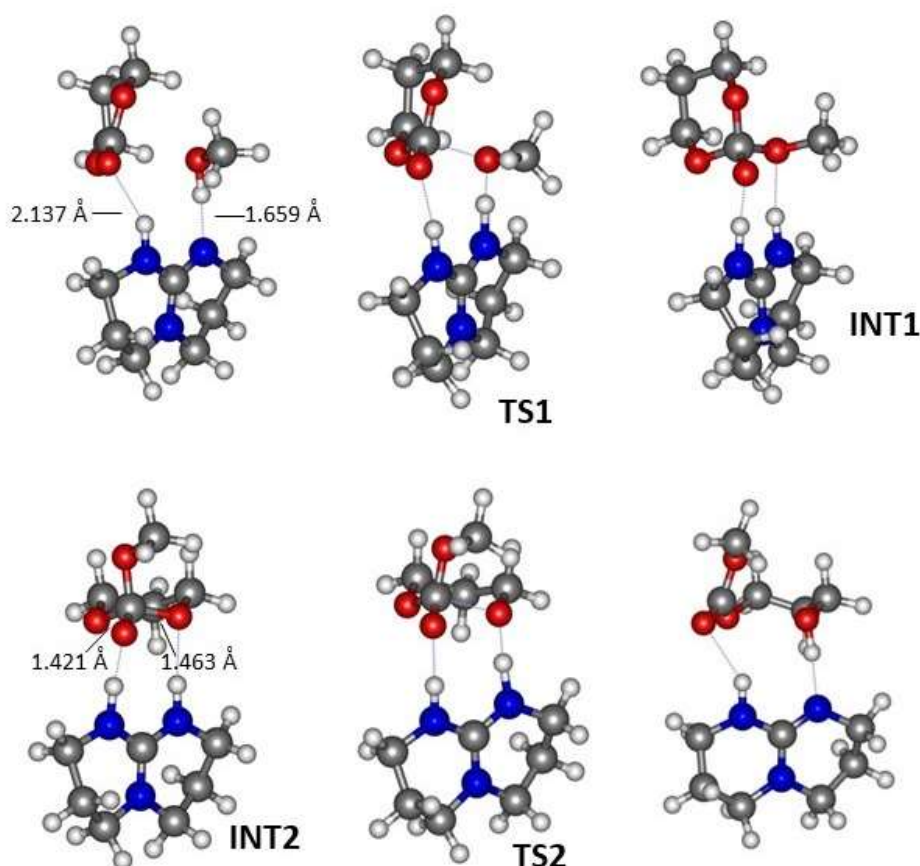


**Figure 40:** Optimized geometry structures of the species involved in the TBD catalyzed ring-opening polymerization for the TMC – H-bond / alcohol activation mechanism.

This bifunctional activation mechanism leads to an intermediate with a tetrahedral carbon due to the formation of a new oxygen-carbon bond. Remarkably, the **INT1** intermediate consists of two charged moieties ( $-0.52e$  the carbonate moiety and  $+0.52e$  the protonated TBD moiety) stabilized both by hydrogen bonding and Coulombic interaction. In the second step a new intermediate adduct **INT2** is formed where a hydrogen bond now activates one of the TMC endocyclic oxygen, giving rise to a slightly elongated bond ( $1.463 \text{ \AA}$ , compared with  $1.421 \text{ \AA}$  of the other endocyclic C-O bond) that, through **TS2** and concomitant transferring the TBD hydrogen to the endocyclic oxygen, opens the TCM ring and regenerates the TBD catalyst.

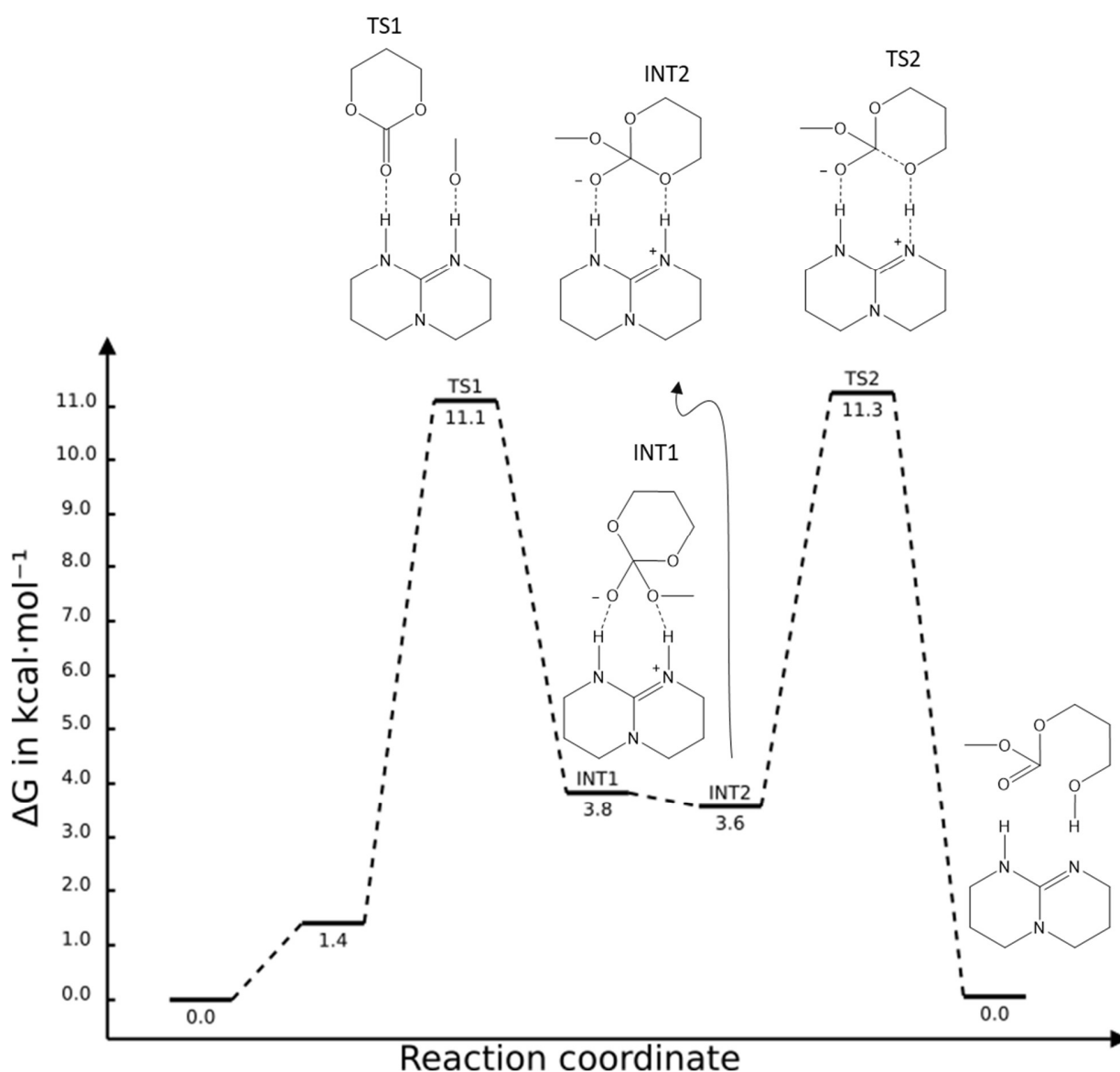


**Figure 41:** Free energy profile for the TBD catalyzed ring-opening polymerization of TMC – H-bond / alcohol activation mechanism.

Considering the free energy profile depicted in **Figure 41**, a barrier height of 11.3 kcal.mol<sup>-1</sup> for the ring-opening of the TMC molecule is the rate-limiting step of this mechanism, slightly higher than initial activated nucleophilic attack, the with a barrier height of 11.1 kcal.mol<sup>-1</sup>, suggesting high plausibility for this mechanism.

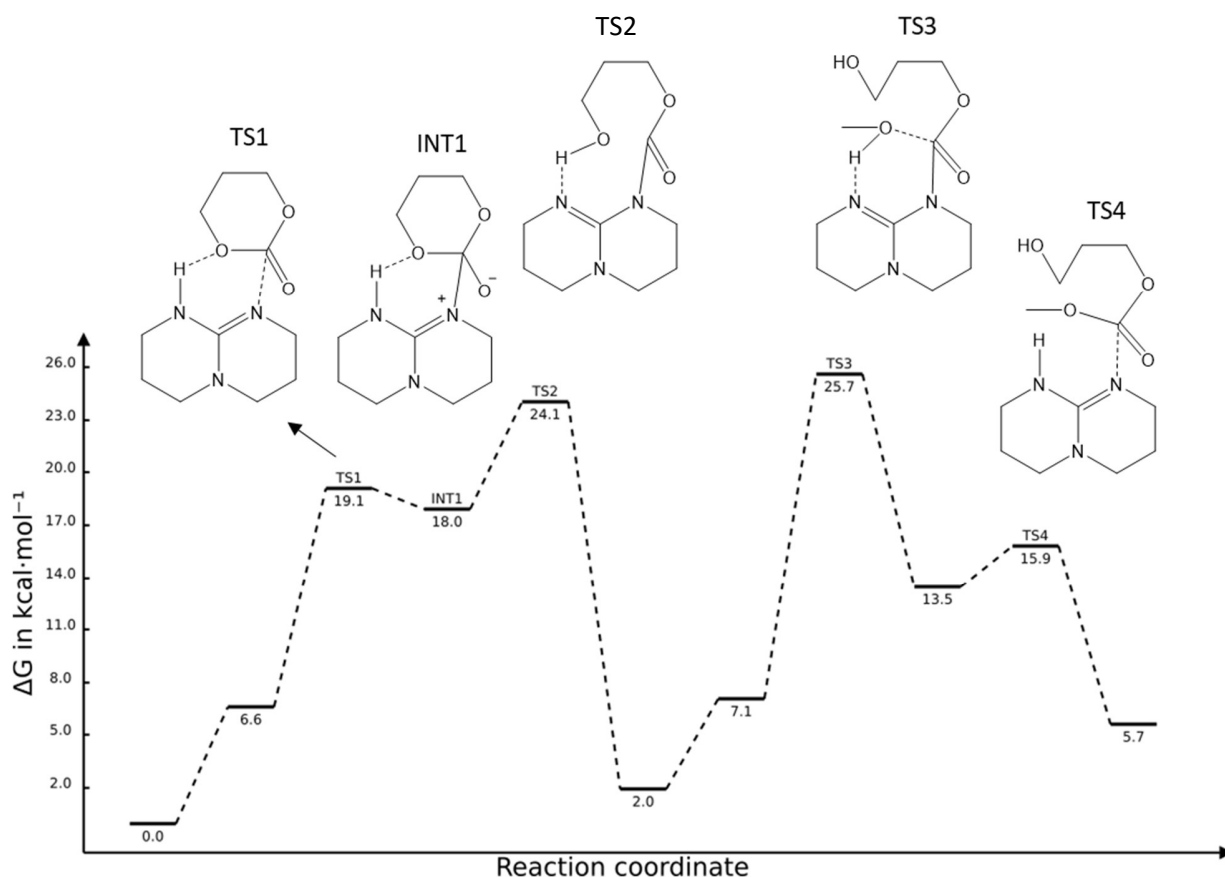


**Figure 42:** Free energy profile for the nucleophilic mechanism of the TBD catalyzed ring-opening polymerization of TMC.

The free energy profile for the nucleophilic mechanism is presented in **Figure 42**. A nucleophilic attack of the N-heterocyclic TBD catalyst to the carbonyl group of TMC occurs on the first reaction step. It involves activation of one of the TMC endocyclic oxygen through hydrogen bonding to the TBD leading to the zwitterionic tetrahedral intermediate **INT1** (**Figure 43**). The formed nitrogen-carbon bond (1.604 Å) is elongated as well as the endocyclic C-O bond (1.449 Å) corresponding to the oxygen that shares a hydrogen bond with the TBD catalyst. This intermediate presents a partial charge of -0.81e on the carbonyl oxygen, -0.66e on endocyclic oxygen ester involved in the hydrogen bond and -0.55e on the other endocyclic oxygen ester. The ring-opening step proceeds

through **TS2**, with a hydrogen transfer from the TBD to the hydrogen-bonded oxygen resulting the formation of an end-capped carbonate.

The reaction follows with a catalyzed attack of the alcohol on the carbonyl group (**TS3**) and hydrogen transfer of the alcohol hydrogen to the TBD catalyst, which is the rate-limiting step in this mechanism. The associated barrier height of 25.7 kcal.mol<sup>-1</sup> for this mechanism is significantly higher than the 11.3 kcal.mol<sup>-1</sup> obtained for the H-bond / alcohol activation pathway, suggesting that the latter preferentially occurs in the presence of TBD. At this point the elongated nitrogen-carbon bond (1.587 Å) that connects the TBD catalyst with the carbonate moiety promptly dissociates with a small energy barrier corresponding to **TS4**, leading to the separated product and release of the catalyst.

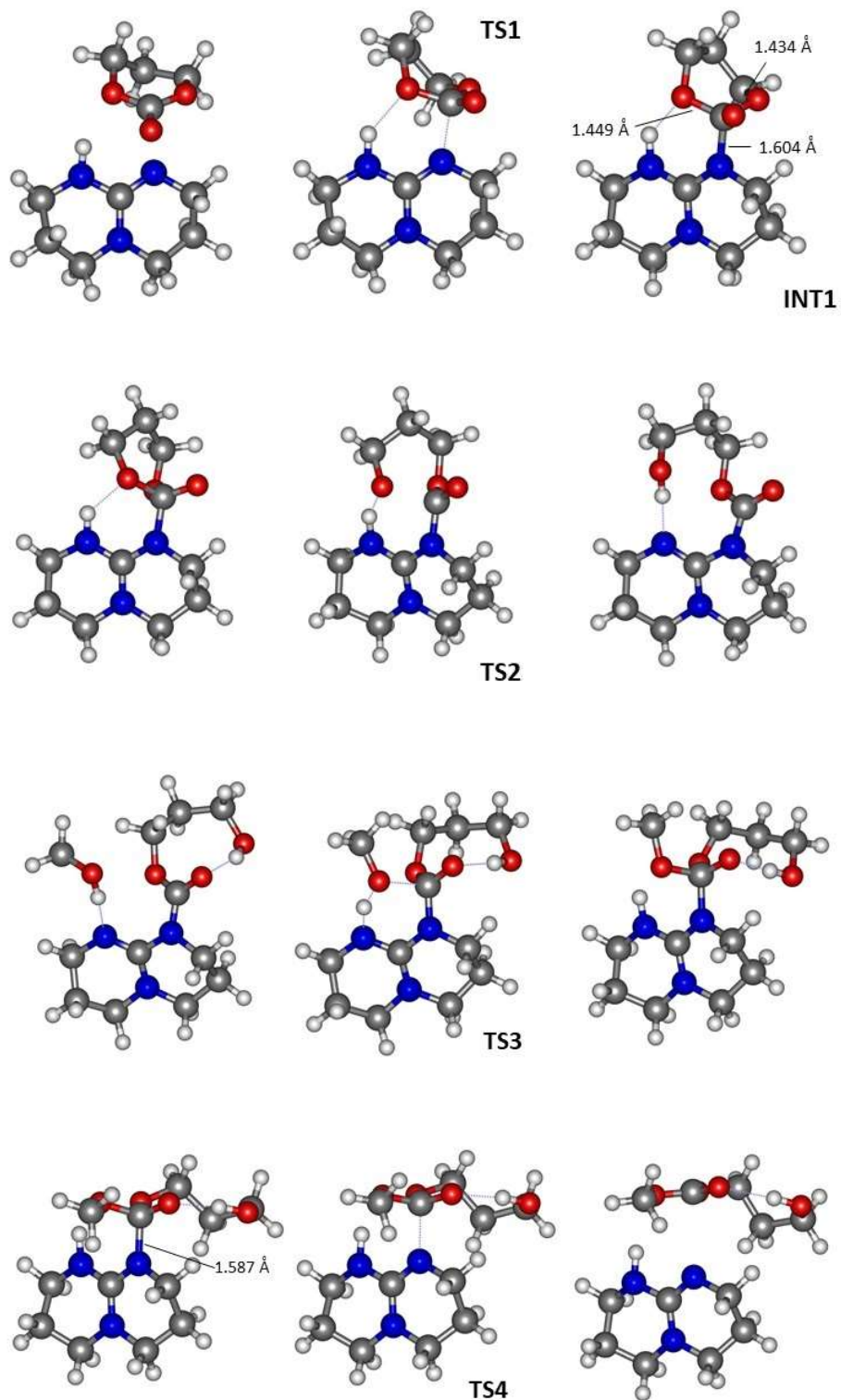


**Figure 43:** Optimized geometry structures of the species involved in the nucleophilic mechanism for the TBD catalyzed ring-opening polymerization of TMC.

#### IV.2.2. DMAP catalyzed ring-opening polymerization of TMC

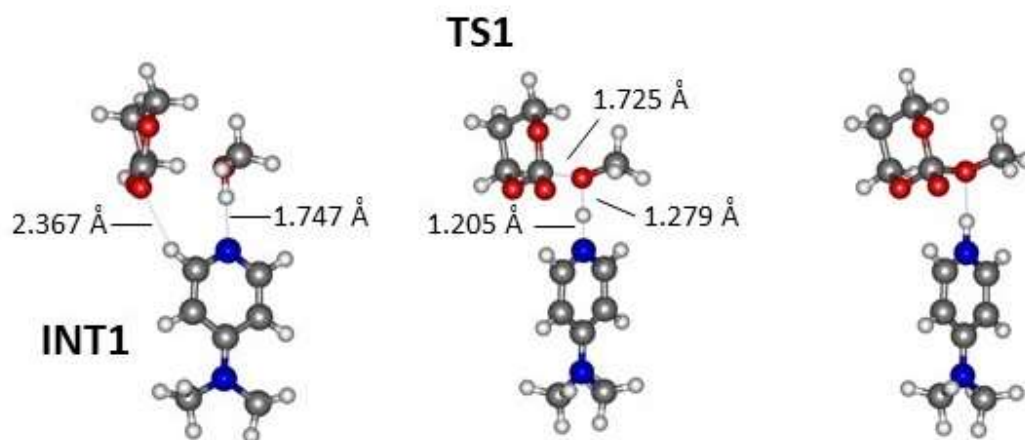


**Figure 44:** Optimized geometry structures of the species involved in the first step of the H-bond mechanism for the DMAP catalyzed ring-opening polymerization of TMC.

The first step of the H-bond / alcohol activation mechanism in the presence of DMAP is shown in **Figure 44**. The reaction starts with an intermediate **INT1** with a weak nonclassical hydrogen bond of the TMC carbonyl oxygen and one hydrogen atom of the DMAP pyridinium ring (O...H 2.367 Å) and a hydrogen bond of the alcohol with the basic nitrogen of DMAP (N-H 1.747 Å), which activates the alcohol oxygen leading to the addition to carbonyl carbon and the hydrogen transfer to DMAP. The free energy profile of this reaction is given in **Figure 45**.

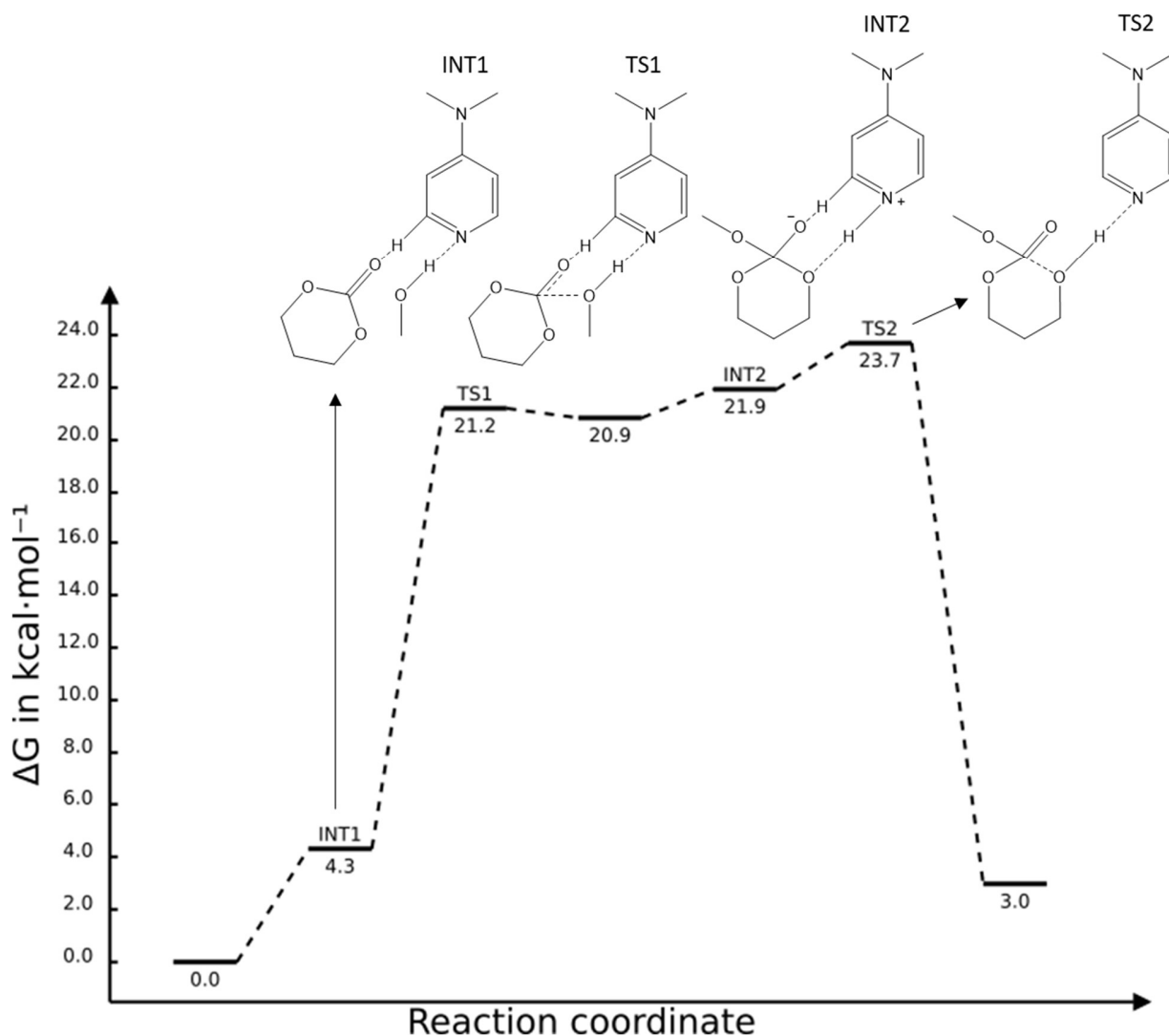


**Figure 45:** Free energy profile for the H-bond / alcohol activation pathway of the DMAP catalyzed ring-opening polymerization of TMC.

With the hydrogen transferred to the DMAP nitrogen and the methoxy oxygen bonded to the TMC carbonyl carbon, an ion-pair character intermediate (**INT2** see **Figure 46**) with the negative charge mainly located in the TCM oxygens (-0.88e for the carbonyl oxygen, -0.57e and -0.61e for the ester endocyclic oxygens and -0.48e for the methoxy exocyclic oxygen) and a positively (0.74e) charged DMAP ring, is formed. In addition, the DMAP hydrogenated nitrogen interacts with one of the endocyclic TMC oxygens (O...H 1.724 Å) and the TMC carbonyl oxygen with a close ortho-hydrogen atom of the DMAP pyridinium ring, forming a weak nonstandard hydrogen bond (O...H 2.213 Å), resulting in a slight elongation of the oxygen bond with the carbonyl carbon (1.470 Å,

compared with 1.432 Å for the other carbonyl carbon endocyclic oxygen bond) that leads to **TS2**. The barrier of 23.7 kcal.mol<sup>-1</sup> for this step, makes this the rate-determining step for this mechanism. Finally, a subsequent transfer of the DMAP hydrogen back to TMC conducts to the TMC ring opening.

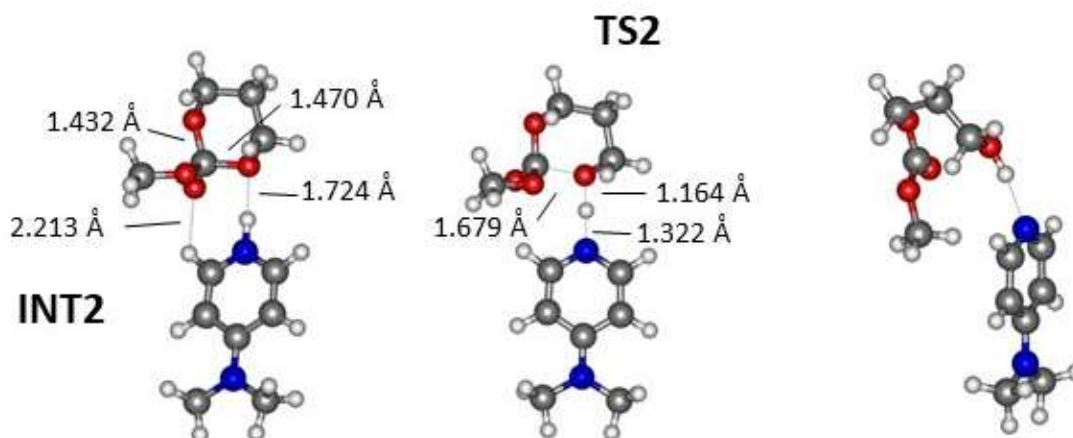


**Figure 46:** Optimized geometry structures of the species involved in the second step of the H-bond / alcohol activation mechanism of the DMAP catalyzed ring-opening polymerization of TMC.

The free energy profile for the nucleophilic mechanism is presented in **Figure 47**. The reaction starts with an initial formation of a zwitterionic nature tetrahedral intermediate (**INT1**, see **Figure 48**), only slightly more stable than that of the previous transition state **TS1**. This intermediate possesses an elongated N-C bond (1.659 Å) linking the DMAP pyridinium ring and the carbonyl carbon, and presents a partial charge of 0.48e on the DMAP ring, -0.61e on the endocyclic oxygen ester closest to the hydrogen ring, -0.58e on the other endocyclic oxygen ester, and -0.79e on the carbonyl oxygen. The ring-opening follows through **TS2** to the linear zwitterionic intermediate **INT2**. In the open ring intermediate the charges modify to 0.61e on the DMAP pyridinium ring, -1.17e on the endocyclic oxygen, -0.56e on the carbonyl oxygen, and -0.43e on the terminal oxygen. It is interesting to note that the zwitterionic tetrahedral intermediate **INT1** is more stable than the ring-opened zwitterion **INT2**, as tetrahedral zwitterionic intermediates are not usually considered as stable species in zwitterionic polymerization reactions<sup>225</sup>. Actually a similar situation has been reported by Waymouth's calculations on the zwitterionic ring-opening polymerization of  $\delta$ -valerolactone<sup>100</sup>.

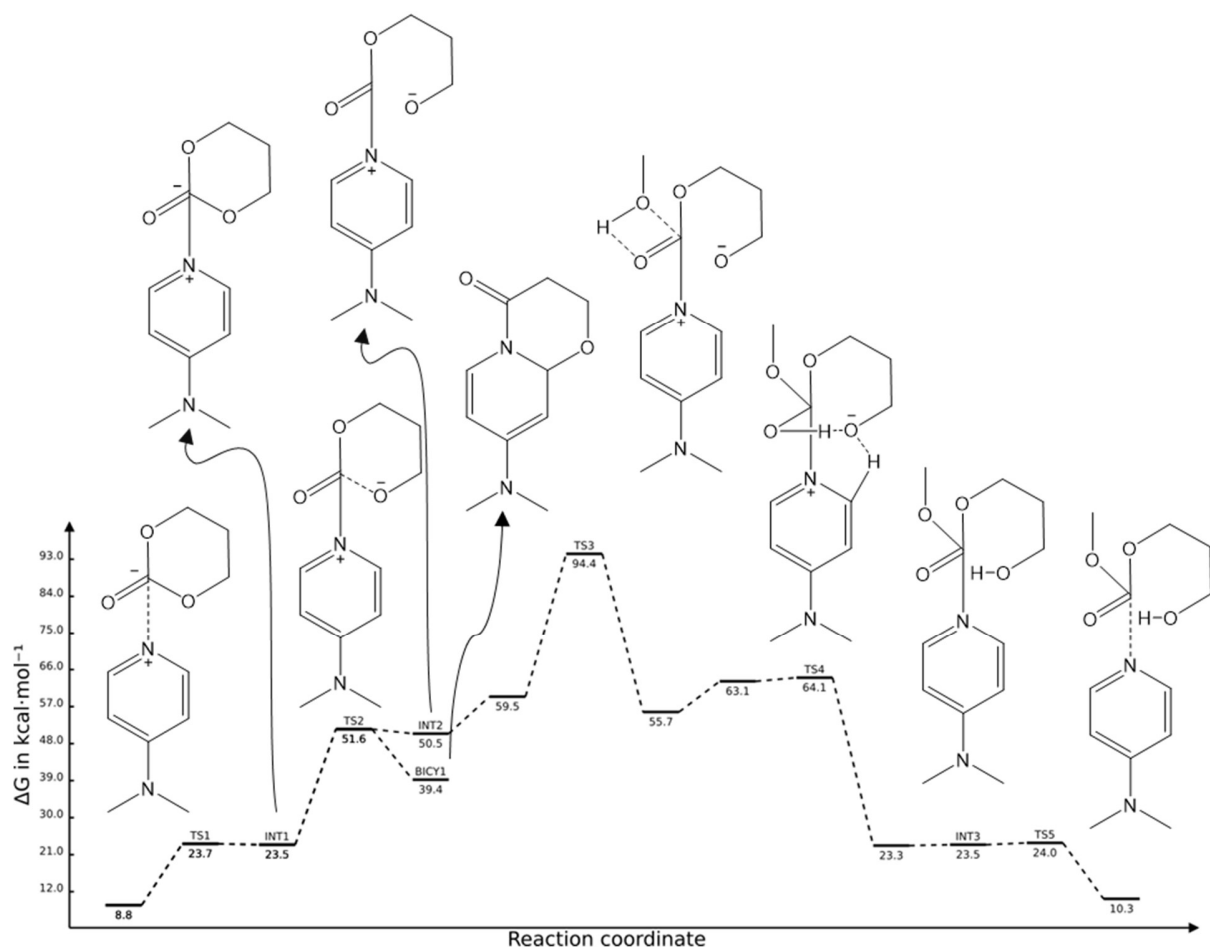


**Figure 47:** Free energy profile for the nucleophilic path of the DMAP catalyzed ring-opening polymerization of TMC.

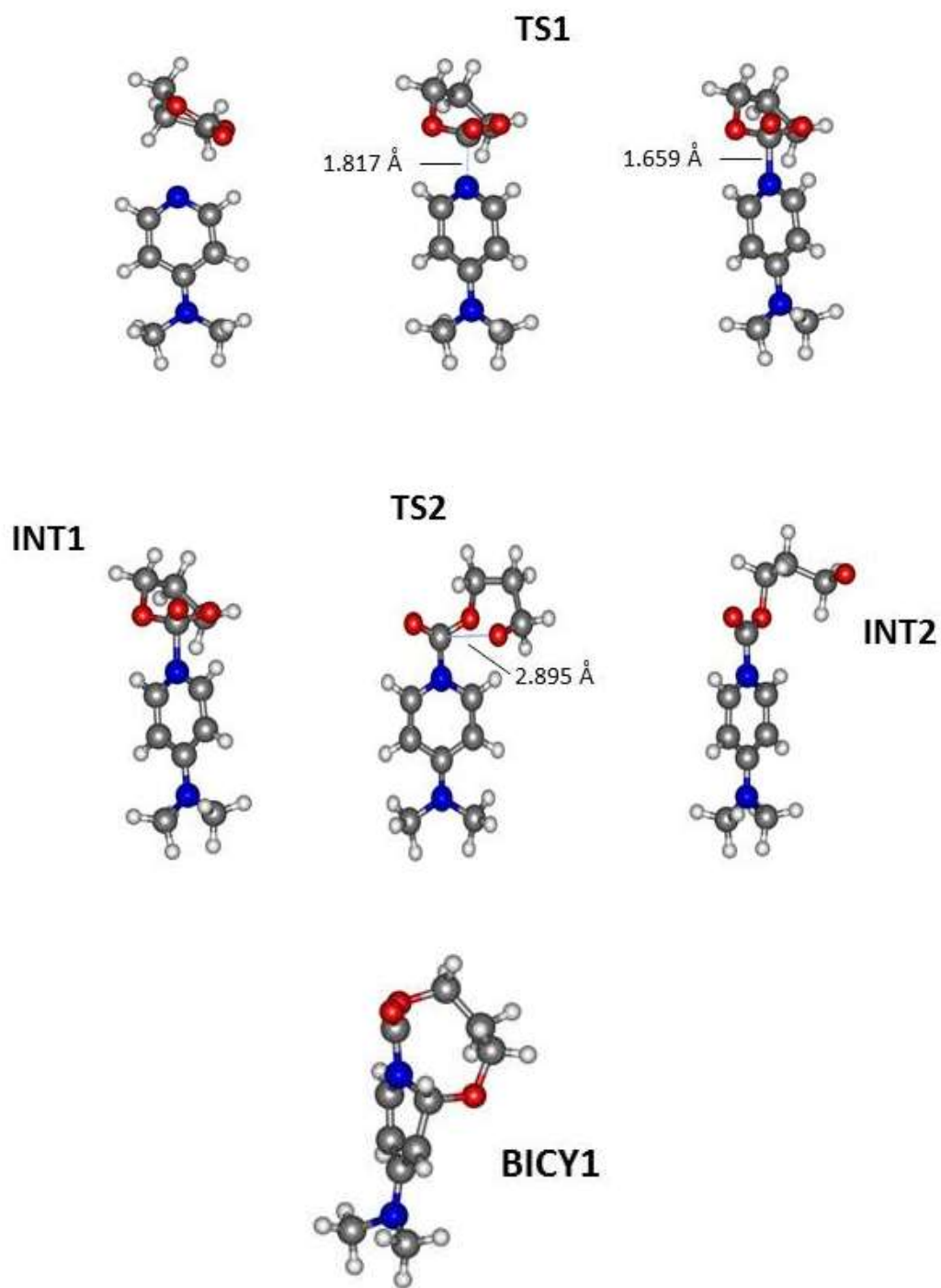


**Figure 48:** Optimized geometry structures of the species involved in the first and second steps for the nucleophilic mechanism of the DMAP catalyzed ring-opening polymerization of TMC. The structure of a possible bicyclo intermediate species (BICY1) is also displayed (bottom).

This ring-opened zwitterionic intermediate is a highly reactive species and one can speculate that it might react with other TMC molecules leading to the formation of polymers of ring open TMC molecules as was suggested by Waymouth for polymerization of  $\delta$ -valerolactone<sup>100</sup>. Other possible intermediates are neutral bicyclo species like **BICY1**. Actually, this bicyclo species is 10.8 kcal.mol<sup>-1</sup> more stable, when compared with the open zwitterion (**INT2**) and 16.1 kcal.mol<sup>-1</sup> less stable than the **INT1** intermediate. The reaction then proceeds with methanol addition to the carbon carbonyl with the oxygen bonding to the carbon and concomitant hydrogen transfer to the carbonyl oxygen. This transition state (**TS3**) has a high barrier becoming the rate-limiting step of this mechanism, with a value of 90.3 kcal.mol<sup>-1</sup>. The H-bond / alcohol activation mechanism, with an energy barrier of 23.7 kcal.mol<sup>-1</sup>, is thus more prone to occur in the presence of DMAP.

The ring opened zwitterion is finally stabilized by a hydrogen transfer through a small energy barrier (Scheme 2), with the formation of **INT3** intermediate (see **Figure 49**) where the negative charge is mainly located on the carbonyl oxygens (-0.75e for the carbonyl oxygen and -0.55e and -0.52e for the ester oxygens) closer to the positively (0.48e) charged DMAP ring. Finally, the **INT3** complex, that possesses an extended N-C bond of 1.594 Å promptly dissociates into products through the transition state **TS5** with a tiny barrier of 0.50 kcal.mol<sup>-1</sup> relative to **INT3**, leading to the reaction products. The calculated free energy profiles indicate that the H-bonding mechanism possesses a lower barrier when compared with the nucleophilic mechanism, and hence is more favorable.

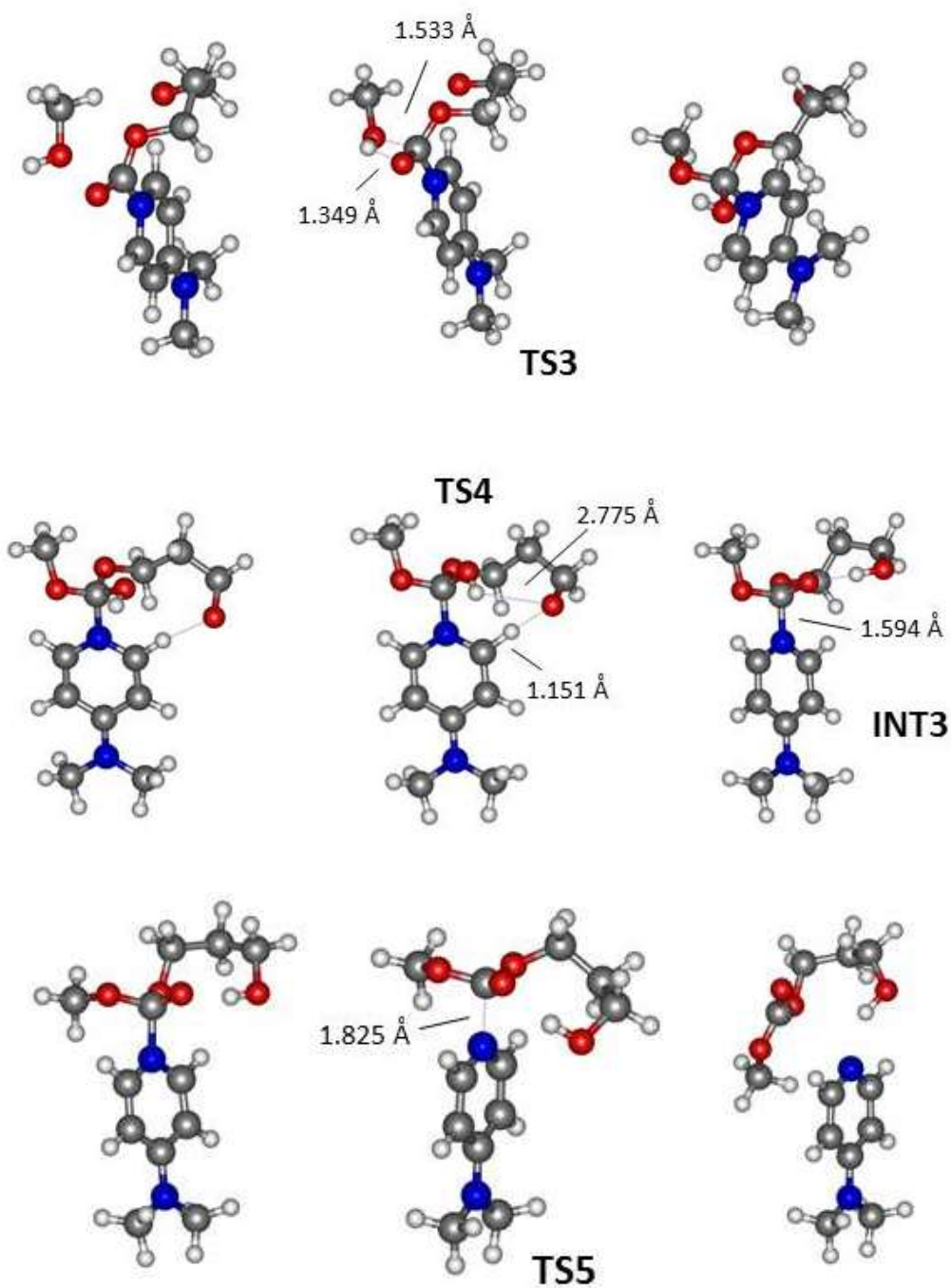


**Figure 49:** Optimized geometry structures of the species involved in the final steps of the nucleophilic mechanism of the DMAP catalyzed ring-opening polymerization of TMC.

## Experimental confrontation

Regarding the more favorable H-bond / alcohol activation mechanism, the highest energy barrier for TBD is 9.3 kcal.mol<sup>-1</sup>, which is lower than the one for DMAP, found at 16.3 kcal.mol<sup>-1</sup>. This corroborates well with the activity of the polymerizations of TMC mediated with these catalysts reported **Table 7**. In 1h at room temperature in dichloromethane, the reaction is quantitative using TBD, while only 19% conversion is reached using DMAP.

**Table 7:** Experimental results. Reactions conducted for 1h at room temperature in 2 mL CH<sub>2</sub>Cl<sub>2</sub>. TMC / Catalyst / Initiator = 100/1/1.

Catalyst	Conv <sup>[a]</sup> (%)	M <sub>n</sub> <sup>[b]</sup> (g/mol)	Đ <sub>M</sub> <sup>[c]</sup>
DMAP	19	5 500	1.7
TBD <sup>[d]</sup>	> 99	9 900	1.3

[a] determined by <sup>1</sup>H NMR. [b] Number average molecular weight determined by size exclusion chromatography. [c] Dispersity of the non-grafted polymer determined by size exclusion chromatography. [d] after reference<sup>148</sup>.

### IV.3. Conclusion

We have investigated in this study using computational methods the mechanisms of the ring-opening polymerization of TMC catalyzed by DMAP and TBD and co-initiated by methanol. For both catalysts, a mechanism based on the activation of the alcohol co-initiator by the C=N moieties together with a H-bond between a proton of the catalyst and the carbonyl moieties of the monomer was found to lead to significantly lower energy barriers than the direct nucleophilic attack of the heterocyclic nitrogen molecule on the carbonate monomer, 11.3 and 25.7 vs. 23.7 and 90.3 kcal.mol<sup>-1</sup> for TBD and DMAP, respectively. For both catalysts, we found the ring-opening of the TMC molecule as the rate-limiting step, slightly higher than initial activated nucleophilic attack. The calculations also indicate TBD as a more efficient catalyst than DMAP, probably due to its polyfunctionality that allows a simultaneous alcohol and carbonyl activation via conventional H-bonding on two different sites. The lower energy barriers found for TBD vs. DMAP were corroborated by ring-opening polymerization experiments conducted in dichloromethane at 25 °C.

## V. Cellulose nanocrystals modification by grafting from ring-opening polymerization of a cyclic carbonate

### V.1. Introduction

Polysaccharides, and in particular cellulose, have experienced a rejuvenation of interest in recent years after being slowly replaced by petroleum alternatives during the 20<sup>th</sup> century in many applications. With the increasing concern over sustainability of many aspects of chemistry and materials science, the surge of interest in these materials is unsurprising as they constitute the bigger fraction of biomass<sup>54</sup>. Cellulose nanoparticles in particular have received a lot of attention due to native cellulose availability and their interesting properties such as a high aspect ratio, high Young modulus, and low density<sup>190</sup>. Both cellulose nanofibrils (CNF) and cellulose nanocrystals (CNC) have been widely studied as fillers for composite materials since the work of Favier *et al.* in 1995 who reported on the first composites reinforced with cellulose nanocrystals<sup>5</sup>. Incorporation of nanocellulose into a polymer matrix has since been studied extensively and has the potential, especially when combined with biodegradable polymers, to produce strong yet fully biodegradable materials. To this end, carbonates are of particular interest, as aliphatic polycarbonates are highly valuable polymers with a very large scope of applications, most notably in textiles, biomedical, and packaging<sup>238,239</sup>. As an additional benefit to being biodegradable<sup>218</sup>, aliphatic polycarbonates have also been obtained from renewable sources making them valuable as a potential alternative to petroleum-based polymers<sup>117</sup>. To produce high performance composite materials, using nanocellulose directly as an additive to polymers has proven to give less than ideal results due to the highly hydrophilic nature of cellulose and its tendency to aggregate. These issues typically lead to a lower than expected mechanical strength and ductility as these are highly dependent on the dispersion of the reinforcing fiber in the polymer matrix and on the strength of the interface<sup>197</sup>.

To find solutions, a large body of work has been carried out on the surface modification of cellulose nanocrystals, typically using the hydroxy groups<sup>196</sup> *via* acetylation<sup>240</sup>, carbamation<sup>241</sup>, esterification<sup>242</sup>, etherification<sup>243</sup>, silanization<sup>244</sup>, amidation<sup>206</sup>, and polymer grafting by different methods. While “grafting onto” polymerization, *i.e.* the process of grafting a pre-synthesized polymer chain to the surface of cellulose can be successful<sup>245</sup>, the “grafting from” method is usually the preferred pathway to cellulose modification with polymers as it is better controlled and avoids problems such as steric hindrance<sup>175</sup>. The “grafting from” approach has been used to combine many

type of polymers with cellulose such as polylactones<sup>9,136</sup> and polylactide<sup>246</sup>. In the case of polymer grafting, the main goal is usually to increase the compatibility between the cellulose fibers and a polymer matrix<sup>176</sup>. Polylactones and polylactide have received a lot of attention due to their potential in biomedical application as they can undergo hydrolysis *in vivo*<sup>124</sup>. However, polyester hydrolysis generates carboxylic acids, which can be a significant drawback<sup>247</sup>. Polycarbonates demonstrate much of the same advantages as polyesters when it comes to their degradation *in vivo*<sup>248</sup> but they do not generate acidic products during hydrolysis<sup>249</sup>. Despite their potential use, however, polycarbonate grafting has not seen much attention, with only some work on grafting on cellulose filter paper<sup>250</sup>, synthesis of isosorbide-based polycarbonates (PC) in the presence of cellulose nanocrystals<sup>251</sup>, and grafting of poly(trimethylene carbonate) on starch<sup>180</sup>. To our knowledge, the grafting of aliphatic polycarbonates from the surface of cellulose nanocrystals has never been reported before.

To exert control over final properties, it is important to have a well-controlled polymerization reaction. Therefore, the choice of a catalytic system with a high activity and a high level of control is a primary concern. In the case of aliphatic polycarbonates, ring-opening polymerization (ROP) is currently the main approach as it leads to a living polymerization, therefore satisfying the criteria listed before, *i.e.* high level of control<sup>152,252</sup>. State of the art ROP allows for the use of many catalysts, including non-toxic metal centers like zinc. However the presence of catalyst traces in the material produced is unwanted for many applications, and metal catalysts are known for being hard to remove completely from polymeric materials<sup>10</sup>. “Immortal” ring-opening polymerization is an approach that has been used for carbonate polymerization and which allows for the use of a small amount of catalyst along with a co-initiator in the form of a protic source. This co-initiator determines the number of chains growing, which gives control over the chain length no matter the quantity of catalyst used while keeping a high catalytic activity<sup>113</sup>. This approach can also be carried out metal free, as many advances in organocatalysis have led to the emergence of a wide variety of ROP catalysts<sup>11,117</sup>. While not all these systems are as efficient as metallic catalysts, some are very promising and have shown a high degree of control. In the case of aliphatic carbonates, and in particular trimethylene carbonate (TMC), base catalysts have been reported to produce polycarbonates with low dispersity<sup>253</sup>. Catalysts of interest include amines (dimethylethanolamine, 4-dimethylaminopyridine-DMAP), guanidines (1,5,7-triazabicyclo[4.4.0]dec-5-ene-TBD), amidines (1,8-diazabicyclo[5.4.0]undec-7-ene-DBU), and

phosphazenes (2-*tert*-butylimino-2-diethylamino-1,3-dimethylperhydro-1,3,2-diazaphosphorine-BEMP) among others<sup>117,141</sup>. While ring-opening polymerization of trimethylene carbonate with organic catalysts has been studied extensively in the last decade, small protic molecules such as benzyl alcohol were mostly used as the co-initiator<sup>117</sup>. Therefore, using cellulose nanocrystals as the protic source to graft polycarbonate is an interesting perspective. Understanding of the reaction and the influence of different parameters would be valuable to increase the general efficiency of polymer grafting on cellulose, a process with a generally low yield<sup>246</sup>.

Supported catalysis, similarly to organocatalysis, has seen a lot of development in recent years to try to obtain more sustainable catalytic systems, which could also be of interest for the polymerization of TMC<sup>254</sup>. Nano-catalysis is a new approach to catalysis that has seen a lot of development in the last few decades and that tries to combine the advantages of both heterogeneous and homogeneous catalysis. Homogeneous catalysis presents the advantage of a very high activity due to the high coverage and mobility of the catalyst, whereas heterogeneous catalysts can more easily be recovered<sup>255</sup>. In essence, this method corresponds to a particular case of heterogeneous catalysis in which the catalyst has an extremely high surface area due to the nano-sized particles used, and has been shown to have homogeneous catalyst like surface area<sup>256</sup>. The catalytic activity of these type of supported catalysis depends on a lot of parameters such as the particle size and its distribution, the support-metal interaction and the properties of the substrate<sup>257</sup>. Supported organic catalyst have been explored, with inspiration coming from enzymatic catalysis: a highly selective catalytic group on a substrate with a specific structure. To this day, silica is a common substrate used for supported catalysis, in no small part due to the existence of mesoporous silica, a very high surface area nanomaterial. Moreover, silica's high density of surface hydroxy groups facilitates its functionalisation which is an important factor for supported catalysis<sup>258</sup>. Cellulose nanocrystals share these characteristics with mesoporous silica, but are also made from native cellulose which has the benefit of being renewable. They have been reported to undergo surface modification in many different ways, which makes them ideal candidates as a substrate for supported catalysis<sup>259-261</sup>.

To our knowledge, trimethylene carbonate has never been grafted on the surface of cellulose nanocrystals before, hence this chapter will first focus on the synthesis of poly(trimethylene carbonate) grafted cellulose nanocrystals *via* ring-opening polymerization and investigate the



**Table 8:** Ring-opening polymerization of TMC initiated from the surface of CNC in the presence of various organocatalysts at 25 °C in THF.

Entry	Catalyst	TMC / Catalyst / OH <sup>[a]</sup>	Time	Grafting <sup>[b]</sup>	Conversion <sup>[c]</sup>	Grafting Yield <sup>[d]</sup>	$M_n$ non-grafted polymer <sup>[e]</sup>	$\bar{D}_M$ <sup>[f]</sup>
			(h)	(wt%)	(%)	(%)	(g.mol <sup>-1</sup> )	
1.	Blank	500/0/50	5	2	4	0.3	NA	NA
2.	TBD	500/1/50	5	51	99	16.5	19,700	1.8
3.	BEMP	500/1/50	3	24	45	5.0	35,400	1.9
4.	BEMP	500/1/50	5	35	52	8.6	33,500	1.8
5.	BEMP	500/1/50	16	37	52	9.3	33,500	1.8
6.	DMAP	500/0.5/50	5	13	6	2.4	n.d.	n.d.
7.	DMAP	500/2/50	5	3	7	0.5	n.d.	n.d.
8.	DMAP	500/5/50	5	12	6	2.2	2,100	1.2
9.	DBU	500/1/50	3	18	9	3.5	n.d.	n.d.
10.	DBU	500/1/50	5	12	8	2.2	n.d.	n.d.

[a] Primary hydroxy group of CNC (1 /glucose unit) [b] Determined by elemental analysis (calculation based on hydrogen content (%H) and carbon content (%C)) and corrected for adsorbed water using TGA. [c] Calculated via <sup>1</sup>H NMR to determine monomer/polymer ratio and corrected to include monomer grafted [d] Ratio of initial monomer to monomer grafted. [e] Number-average molecular weight of the non-grafted polymer determined by SEC vs. polystyrene standards and corrected with a correction factor of 0.57, 0.73 or 0.88 based on size measured<sup>262</sup>. [f] Dispersity of the non-grafted polymer determined by SEC.

amount of grafting at the cost of efficiency<sup>246,263</sup>. Dispersity of the non-grafted polymer was found at an acceptable value of 1.8 that is significantly higher than usual values obtained for typical polymerizations with an alcohol<sup>148</sup>. The broader distribution can be explained because it is a side reaction involving water and ethanol as co-initiators that are still entrapped in the CNCs after purification. In addition, water and ethanol can also be involved in hydrolysis and transcarbonatation reactions respectively.

Using similar reaction conditions, BEMP (entries 3-5), a phosphazene catalyst, showed quite different results. Full conversion was not reached, and after increasing the reaction time from 3 to 5 hours, the conversion only reached 52%. Further increasing the reaction time to 16 hours did not increase monomer conversion. Despite the lower conversion values, grafting on cellulose was achieved with this catalyst, and up to 37% grafts were achieved in the modified CNCs, showing that this catalyst, while less efficient than TBD using similar parameters, leads to substantial grafting.

The reactions catalyzed with DMAP (entries 6-8) and DBU (entries 9-10) did not perform as well as the one with the other catalysts under the same reaction conditions (room temperature, 5h), with NMR analysis showing very low conversion (<10%). The resulting grafting was rather low for both catalyst (18% maximum) under these conditions, and no oligomers could be recovered by precipitation to allow for SEC analysis. This is believed to be due to their likely very low molecular weight.

The superior results and increased reactivity obtained with TBD can potentially be explain by the presence of the secondary amine group. Unlike DBU, which can operate by a basic and a nucleophilic mechanism, TBD can catalyze transesterification reactions by dual activation *via* H-bonding<sup>167,226</sup>. Having a catalyst that can use both mechanisms may result in a better reaction due to the ability of the catalyst to go in between intermolecular bonding (similarly to how a protic solvent gives a better dispersion of CNCs). In addition, DBU and DMAP may favor side initiation reaction due to their ability to perform a nucleophilic attack on the monomer, which is not the case for the BEMP phosphazene, that leads to an intermediary grafting ratio around 50%.

When looking at results for polymerization of trimethylene carbonate with alcohols<sup>117</sup>, it is worth noting that TBD is also the most active catalyst in bulk, and full conversion is achieved much faster at lower temperatures when compared to DMAP and DBU. As the work presented here is carried

out in solvent but at room temperature, it is possible that the activity of some of the catalysts (except for TBD) is reduced as the activation requires more energy. However, further testing at higher temperature with all the catalyst was not explored as we observed browning of the CNC at temperatures as low as 40 °C in the presence of THF and TBD.

Comparing the  $\text{pK}_a\text{H}^+$  of all four bases, TBD in acetonitrile does not come up as the strongest base (25.96), with BEMP having a higher  $\text{pK}_a\text{H}^+$  (27.5), despite its superiority when it comes to grafting TMC on cellulose. TBD is however a stronger base than DMAP and DBU, which could explain partially the better results obtained when comparing these three bases. As for BEMP, it is a much bulkier catalyst, therefore steric hindrance may be the cause for the lower activity when compared to TMC, in particular for the grafting onto CNC. Despite the subpar grafting efficiency on CNCs with BEMP, the extracted non-grafted polymer showed a higher  $M_n$  than the non-grafted polymer recovered after full conversion with TBD. As the screening of catalysts showed a more efficient grafting with TBD, this reaction was studied further, in order to assess the influence of the reaction conditions.

#### V.1.1.2. Influence of experimental parameters for the TBD catalyzed grafting

THF was used as the main solvent as it had shown to dissolve well TBD, TMC, poly(trimethylene carbonate) (PTMC), and to be a good solvent for CNC dispersion<sup>264</sup>. Some other common solvents were assessed, but a lower amount of PTMC grafting was obtained as can be seen in **Table 9**.

**Table 9:** Ring-opening polymerization of TMC initiated in different solvents on the surface of CNC in the presence of TBD over 5 hours, 25 °C, at a ratio of TMC/Catalyst/OH of 500/1/50. Solvent added outside the glovebox under inert atmosphere.

Entry	Solvent	Grafting <sup>[a]</sup> (wt%)	Conversion <sup>[b]</sup> (%)	Grafting Yield <sup>[c]</sup> (%)	$M_n$ non-grafted polymer <sup>[d]</sup> ( $\text{g}\cdot\text{mol}^{-1}$ )	$\text{Đ}_M$ <sup>[e]</sup>
1.	THF 1.5 mL	52	99	17.3	13,200	1.8
2.	$\text{CH}_2\text{Cl}_2$ 1.5 mL	30	99	6.8	21,300	1.9
3.	Toluene 1.5 mL	00	99	0	62,300	2.1

[a] Determined by elemental analysis (calculation based on hydrogen content (%H) and carbon content (%C)) and corrected for adsorbed water using TGA. [b] Calculated via  $^1\text{H}$  NMR to determine monomer/polymer ratio and corrected to include monomer grafted [c] Ratio of initial monomer to monomer grafted. [d] Number-average molecular weight of the non-grafted polymer determined by SEC vs. polystyrene standards and corrected with a correction factor of 0.57, 0.73 or 0.88 based on size measured<sup>262</sup>. [e] Dispersity of the non-grafted polymer determined by SEC.

As the polymerization of TMC has also been performed in bulk<sup>117</sup>, the grafting reaction on the surface on CNCs was also carried in bulk as comparison (entry 6, **Table 10**). Despite non-grafted

polymerization of TMC being very quick under bulk conditions, the reaction with cellulose did not go to full conversion within an hour. However, the polycarbonate content of modified CNCs did reach 47%, a value comparable to the content obtained by grafting in THF. The viscosity is a major issue in bulk reactions as the melted monomer is not a good medium to disperse CNCs, resulting in poor homogeneity of the final material and a greater difficulty to redisperse the modified cellulose in solvent, rendering its use more complicated. The high viscosity is also likely a cause for the lower conversion, as the reaction slows down considerably with non-grafted polymer production. Lastly, the bulk reaction, as expected, shows a much higher dispersity for the synthesized non-grafted polymer, indicating some loss of control over the polymerization reaction.

As shown previously the polymerization of TMC was total after 5 hours, however a reaction in similar conditions was also performed over 24 hours (entry 7, **Table 10**) to evaluate the activity of TBD over longer period of time, as it has been reported to be capable of depolymerization<sup>166</sup>. In the case of poly(trimethylene carbonate) grafted CNCs, a small increase in grafting content can be measured after 24 hours of reaction (60% vs. 51%), however the average molecular weight of the produced non-grafted polymer started decreasing, showing potential signs of depolymerization or transcarbonation reactions. Therefore 5 hours was the favored reaction time for most reaction, as it allowed for a good control over grafting while having good conversion, and a very good reproducibility, as can be seen when comparing entry 4 and 5 in **Table 10**. Indeed, both reactions done in the same conditions lead to a 51% grafting content when measured by EA, and nearly identical non-grafted polymer.

The effect of temperature on the grafting reaction was evaluated in order to see if kinetics could help favor the grafting reaction vs. the side initiation reactions. As can be seen from entry 8, cooling down the reaction to 0 °C did not lead to a significant difference over 5 hours, as the grafting obtained was found to be 3% higher to the same reaction at RT (entry 4). When increasing the temperature to 40 and 60 °C (entries 9 and 10), a similar grafting could also be obtained. However the molecular weight of the non-grafted polymer obtained decreased by half at 60 °C compared to the same reaction done at RT, showing signs of potential depolymerization induced by the TBD due to the increased reactivity at higher temperatures. Moreover, reaction performed above 40 °C led to a browning of the produced cellulose.

**Table 10:** Ring-opening polymerization of TMC initiated from the surface of CNC in the presence of TBD in THF for 5 hours.

Entry	TMC / Catalyst / OH <sup>[a]</sup>	T (°C)	Grafting <sup>[b]</sup> (wt%)	Conversion <sup>[c]</sup> (%)	Grafting Yield <sup>[d]</sup> (%)	$M_n$ non-grafted polymer <sup>[e]</sup> (g.mol <sup>-1</sup> )	$\bar{M}_w$ <sup>[f]</sup>
4.	500/1/50	25	51	99	16.5	19,700	1.8
5.	500/1/50	25	51	99	16.5	18,000	1.9
6. <sup>[g]</sup>	500/1/50	65	47	33	14.1	11,200	3.0
7. <sup>[h]</sup>	500/1/50	25	60	99	23.8	16,900	1.9
8.	500/1/50	0	54	99	18.7	16,500	2.0
9.	500/1/50	40	51	99	16.5	14,100	2.3
10.	500/1/50	60	52	99	17.2	9,700	1.8
11. <sup>[i]</sup>	500/1/50	25	7	99	1.2	n.d.	n.d.
12.	500/1/40	25	49	99	12.2	18,700	1.7
13.	500/1/30	25	49	99	9.2	23,100	1.7
14. <sup>[j]</sup>	500/1/50	25	53	99	17.9	12,100	2.0
15.	500/2/50	25	9	99	1.6	26,700	1.8
16.	500/5/50	25	9	99	1.6	2,200	1.3
17.	500/0.5/50	25	74	99	45.2	7,100	1.8
18.	500/0.25/50	25	64	78	28.2	11,400	1.6
19.	250/0.5/50	25	57	99	42.1	11,100	1.7
20.	125/0.5/50	25	47	99	56.3	4,600	1.8
21.	62.5/0.5/50	25	23	99	37.9	n.d.	n.d.
22.	250/1/50	25	50	99	31.8	13,700	1.9
23.	125/1/50	25	41	99	44.1	12,900	1.8

[a] Primary hydroxy group of CNC (1/glucose unit) [b] Determined by elemental analysis (calculation based on hydrogen content (%H) and carbon content (%C)) and corrected for adsorbed water using TGA. [c] Calculated via <sup>1</sup>H NMR to determine monomer/polymer ratio and corrected to include monomer grafted [d] Ratio of initial monomer to monomer grafted. [e] Number-average molecular weight of the non-grafted polymer determined by SEC vs. polystyrene standards and corrected with a correction factor of 0.57, 0.73 or 0.88 based on size measured<sup>262</sup>. [f] Dispersity of the non-grafted polymer determined by SEC. [g] Bulk reaction. [h] Reaction done over 24 hours instead of 5. [i] Reaction performed outside the glovebox. [j] Stirred for 24h and sonicated prior to reaction to maximize dispersion of CNC. NA: not available as oligomers, i.e. too short to precipitate in cold methanol.

A reaction was then performed under inert atmosphere, but not under glovebox conditions, to evaluate how sensitive the efficiency of the grafting was regarding the presence of water and other impurities (entry 11). Prior to the reaction, CNCs and TMC were dried using a vacuum and an argon line rather than ultra-high vacuum. THF was used after purification over alumina, similarly to experiments performed inside the glovebox. Multiple argon/vacuum cycles were used to ensure inert atmosphere was achieved. Under these conditions, a low amount of grafting (7 vs. 51% in entry 4) as well as the short chain length of the non-grafted polymer (impossible to precipitate) showed the prevalence of initiation by traces of water and ethanol. Due to CNCs being hydrophilic, it is hard to remove significant traces of water without extreme conditions ( $10^{-6}$  bar of vacuum), as well as ethanol from the purification steps of preparing CNCs. This reaction shows that in order to maximize grafting efficiency, purification of the different chemicals and a thorough drying of the cellulose is required.

In an attempt to increase grafting on cellulose, reactions were then performed with an increased ratio of TMC/CNC by decreasing the quantity of cellulose used. Surprisingly, increasing the quantity of monomer did not lead to a significant improvement in the grafting amount on cellulose (entries 12-13), which seems to reach a maximum at around 50%, a result similar to other reactions (entry 4). This shows that simply increasing the quantity of monomer used in the reaction is an ineffective way to increase the maximum amount of grafting on the surface of CNC.

To determine if the availability of the hydroxy groups on the surface of cellulose is an important factor, a reaction was performed on a batch of CNC in THF with increased effort at individualization of CNCs. The mixture of cellulose and solvent was prepared in the glovebox, then closed tightly and stirred at room temperature over 24 hours vs. 30 min previously used. A sonication bath was also used in burst of 5 minutes over the 24 hours. The results obtained (entry 14) when compared to a “typical” reaction showed that increased effort for maximum individualization of CNCs did not have a significant impact as the grafting obtained was also around the 50% mark.

The influence of catalyst loading was further assessed. Using a typical ratio TMC/TBD/OH of 500/1/50 showed good results and a grafting of around 50%. Increasing the catalyst ratio to 2 equivalents vs. OH (entry 15) however lowered the grafting percent on CNCs by a significant amount (9%), whereas the length of the non-grafted polymer increased, indicating that increasing

the TBD amount favors non-grafted polymerization. By increasing the amount of catalyst further to 5 equivalents (entry 16), the molecular weight of the non-grafted polymer was lowered significantly however ( $< 3,000 \text{ g.mol}^{-1}$ ). As mentioned previously, TBD is not only capable of polymerization, but also depolymerization under the right conditions *via* a nucleophilic attack on the carbonyl moieties<sup>166</sup>. In the case of polylactide, the use of 5 equivalents of TBD decreased the average molecular weight of the resulting polymer more than tenfold, a result very similar to what is observed in this work for the polycarbonate.

As opposed to increasing the catalyst quantity, lowering the amount of TBD used for the reaction to 0.5 equivalents showed an improvement in the grafting on CNCs with a material composed of up to 74% polycarbonate grafts by weight and a grafting yield of 46% (entry 17).  $M_n$  of the non-grafted polymer obtained was lower, which can simply be explained by the increased quantity of monomer turned into grafts rather than non-grafted polymer.

Decreasing the quantity of catalyst further resulted in a decrease in the amount of grafting onto 64% (entry 18), which is an improvement over the result obtained with 1 equivalent (entry 4) but a setback compared to reactions performed with 0.5 equivalent (entry 17). Moreover, the low concentration of TBD did not lead to full conversion after 5 hours.

To improve the grafting efficiency with respect to the total amount of monomer used, reactions with 0.5 equivalents of TBD (shown to have the best results) and successively lower amounts of monomer were carried out.

The grafting percent decreased from 74% to 57% (entry 17 *vs.* 19) when the monomer concentration was halved, but the grafting yield stayed within the same range at 42%. While this is not an improvement, this however allows one to obtain CNCs with around 50% grafts with significantly less monomer loss than some previous experiments (*e.g.* entry 4). Lowering the amount of monomer further continued to reduce the percent grafting (47%) but led to an increased yield of 56% (entry 20) which is a good value for grafting of a polymer on cellulose, as this parameter is usually overlooked in favor of trying to reach a maximum amount of grafting.

Similar reactions were also performed with a typical 1 equivalent TBD to compare to the grafting yield obtained with 0.5 equivalents. As with the previous reactions, a lower amount of catalyst led to a higher amount of grafting, as can be seen when comparing entries 19 to 22 and 20 to 23. For

both reactions, a similar loss of about 6-7% of grafting can be measured, which is also a significant decrease in grafting yield.

Overall, this shows that a wide range of grafting percent is possible, and specific values can be targeted using the right amount of catalyst (typically 0.5 eq) without having to use a large excess of monomer, while keeping the grafting yield as high as possible.

#### V.1.2. Characterization of the poly(trimethylene carbonate)-grafted CNC as a function of the grafting ratio

In addition to elemental analysis, FT-IR was used to determine the success of the grafting reaction (**Figure 51**). As expected, both modified and unmodified cellulose spectra look quite similar at first glance. However, two characteristic bands to our grafts are visible for modified cellulose. First, the band at  $1754\text{ cm}^{-1}$  can be identified as a carbonyl stretch  $\nu(\text{C}=\text{O})$ , thus confirming the successful incorporation of the carbonate moieties onto CNCs. A second characteristic band is observed at  $1229\text{ cm}^{-1}$  corresponding to  $\nu(\text{C}-\text{O})$  stretching<sup>265</sup>. As shown in **Figure 51**, the relative intensity of both bands increased with the grafting content, thus confirming the results determined by elemental analysis and TGA. Lastly, the ratio of absorption band at  $1059\text{ cm}^{-1}$  corresponding to  $\nu(\text{C}3-\text{OH})$  to C-O-C stretching at  $1160\text{ cm}^{-1}$ ,<sup>266</sup> decreases with increasing grafting ratio which shows the successful esterification of the secondary alcohol in the C3 position, thus confirming the successful grafting of PTMC (**Table 11**). The band at  $1032\text{ cm}^{-1}$  corresponding to  $\nu(\text{C}6-\text{OH})$  increases with increasing grafting ratio, as terminal OH of the polycarbonate chains appear in this region as well. As a consequence, grafting on the C6 position is not “visible” by FT-IR, as both primary and secondary C-OH of cellulose are replaced by the primary terminal C-OH of the polymer at  $1032\text{ cm}^{-1}$ . For the third hydroxy  $\nu(\text{C}2-\text{OH})$ , no conclusion can be drawn as PTMC has a band in the area as well.

**Table 11:** intensity ratio of C6-OH and C3-OH peak to C-O-C in FT-IR for unmodified cellulose and grafted cellulose. Grafted CNCs corresponding to reference in **Table 10**: entry 21 (23%), entry 20 (47%), and entry 19 (57%), entry 17 (74%).

	C <sub>6</sub> -OH (1035)	C <sub>3</sub> -OH (1060)
Unmodified CNC	2.581	3.427
23 wt% PTMC-grafted CNC	2.546	2.872
47 wt% PTMC-grafted CNC	2.718	2.654
57 wt% PTMC-grafted CNC	2.761	2.237
74 wt% PTMC-grafted CNC	2.942	1.879

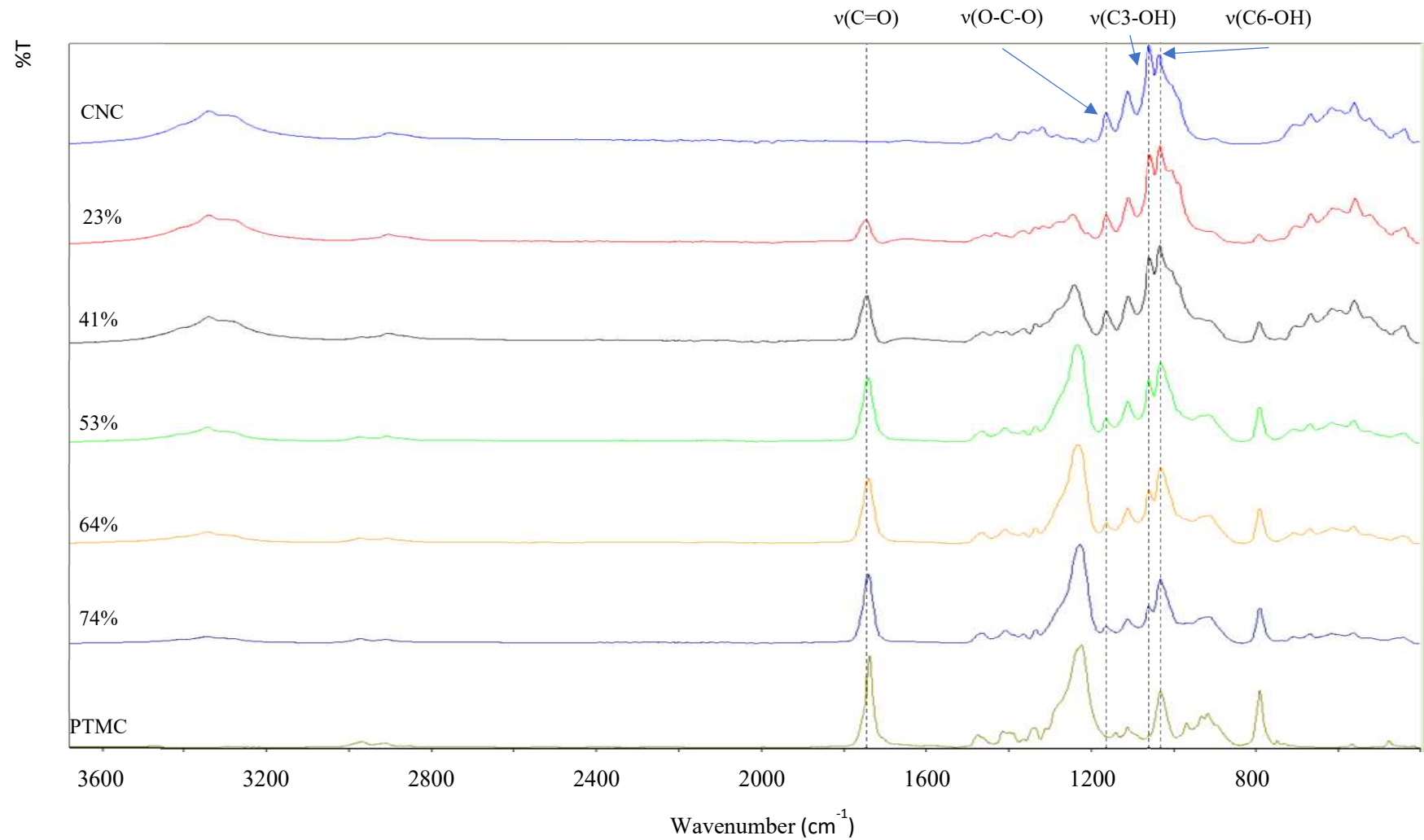


**Figure 51:** FT-IR spectra of unmodified cellulose nanocrystals (CNC) and grafted one with different graft content after purification by Soxhlet extraction. PTMC of 15,400 g.mol<sup>-1</sup> extracted from Soxhlet and purified by precipitation.

Proton NMR was used as a complementary technique to SEC to determine the extent of polymerization of trimethylene carbonate and to calculate the conversion of the monomer. Crude non-grafted polymer samples were separated from CNCs by filtration after quenching of the reaction with benzoic acid.

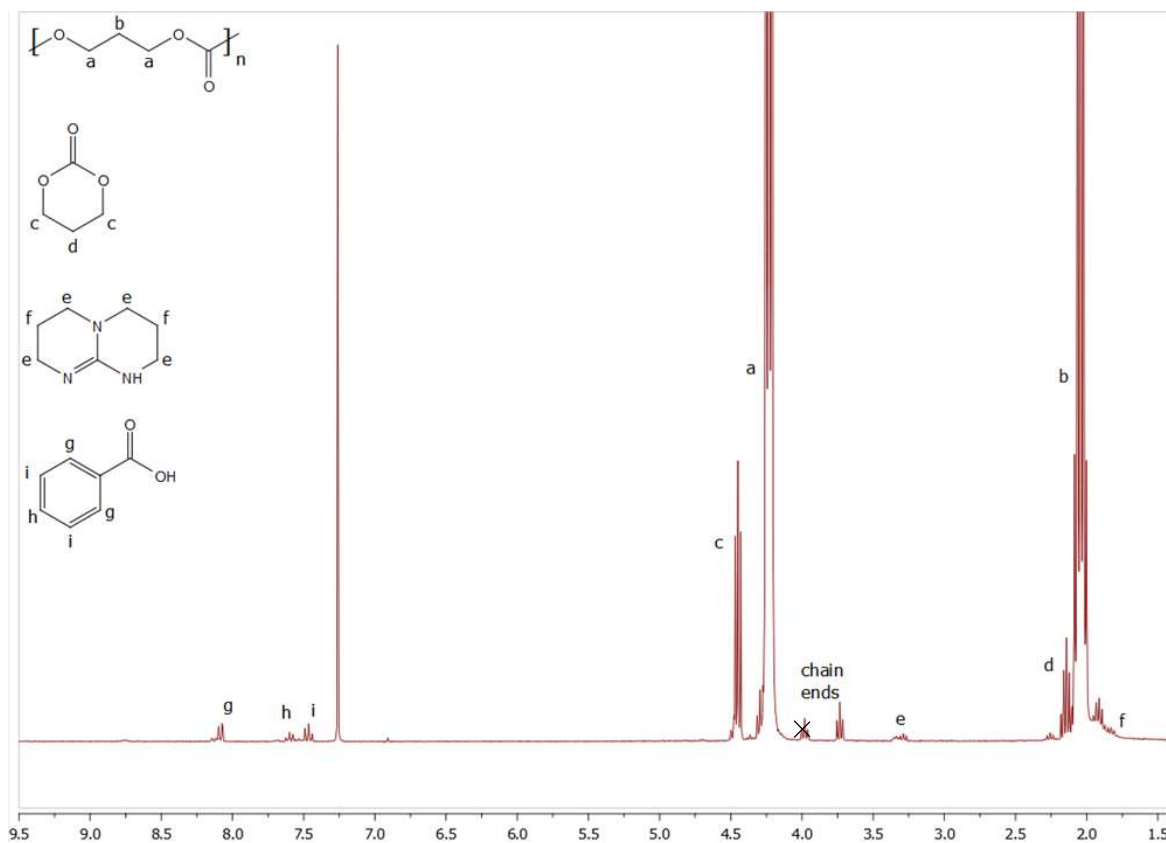


**Figure 52:**  $^1\text{H}$  NMR spectra of the crude mixture after quenching with benzoic acid and separation of CNC in  $\text{CDCl}_3$  (300 MHz).

$^1\text{H}$  NMR ( $\text{CDCl}_3$ , 300 MHz)  $\delta$  (ppm): 8.07, 7.60, 7.47 (m, 6H,  $\text{Ar-COOH}$ ), 4.45 (t, 4H,  $\text{CH}_2\text{OCOOCH}_2\text{CH}_2$ ), 4.23 (t, 4H,  $-\text{OCH}_2\text{CH}_2\text{CH}_2\text{OCO-polymer}$ ), 3.73 (t, 2H,  $-\text{CH}_2\text{OH}$  end), 3.31 (m, 8H,  $\text{NCH}_2\text{CH}_2\text{CH}_2\text{N-}$ ), 2.14 (qi, 2H,  $\text{CH}_2\text{OCOOCH}_2\text{CH}_2$ ), 2.04 (qi,  $\text{CH}_2\text{OCOOCH}_2\text{CH}_2\text{-polymer}$ ), 1.83 (m, 4H,  $\text{NCH}_2\text{CH}_2\text{CH}_2\text{N-}$ )

m: multiplet ; t: triplet ; qi: quintet

Characteristic peaks for benzoic acid are observed in **Figure 52** at 8.07 (g), 7.60 (h) and 7.47 ppm (i) as it is used to quench the reaction. TBD is also observed with a weak signal due to its low concentration, visible at 3.31 (e) and 1.83 ppm (f).

At 4.45 ppm (c), a triplet characteristic of trimethylene carbonate is found. This peak corresponds to the protons closer to the carbonate function of the cyclic monomer, and integrating it shows a value twice as high as the signal at 2.14 ppm (d), another characteristic peak for TMC. This confirms that the signal at 4.45 ppm corresponds to the protons next to the oxygen, whereas the protons at 2.14 ppm are from an aliphatic carbon.

Similar observations can be made for the signals at 4.23 (a) and 2.04 ppm (b), which are more intense as they correspond to poly(trimethylene carbonate). Due to the structure of the polymer compared to the monomer, the chemical shifts are at slightly different values, but the signal can also be integrated to show a ratio of 2. By integrating one of these peaks and comparing to its corresponding monomer peak, a “soluble fraction conversion” can be determined, corresponding to how much monomer has been turned into non-grafted polymer. However, the real conversion is calculated taking into account all of the converted, therefore it is necessary to correct the conversion obtained by NMR with the amount of the monomer grafted onto CNCs. Lastly, a triplet can be observed at 3.73 ppm corresponding to the chain ends of the polymer.

X-ray photoelectron spectroscopy can give additional insight into the composition of the modified CNCs at a surface level. In the C1s high resolution scan (**Figure 53**), the C-C carbon contribution (C1) at 285 eV is shown to increase rapidly with grafting, as cellulose units do not contain carbons without neighboring oxygen atoms, unlike trimethylene carbonate. With an increasing amount of graft content, the relative intensity of the C1 contribution increases and then appears to reach a maximum, at the contribution amount expected for pure poly(trimethylene carbonate) chains indicating that no cellulose contribution is visible anymore. As opposed to C1, the C2 and C3 contributions to the C1s signal, corresponding to C-O and O-C-O environments respectively, both decreased with an increasing amount of grafts, as poly(trimethylene carbonate) contributes less to the C-O signal than cellulose, and does not contribute to the O-C-O signal. Finally, the O-C(O)=O contribution (C4) increased with grafting content, similarly to C1 as the carbonate function is the only contribution to this peak.

The results obtained from elemental analysis are therefore confirmed with the XPS data. Additionally, the samples with a high amount of grafting showed almost no signal corresponding to CNCs, but rather a composition similar to that of pure PTMC, which has a ratio 1/2/1 of C-C/C-

O/OC(O)=O units. This indicated that the surface of the CNCs (10 nm) was fully covered by PTMC, forming a layer over the cellulose core.

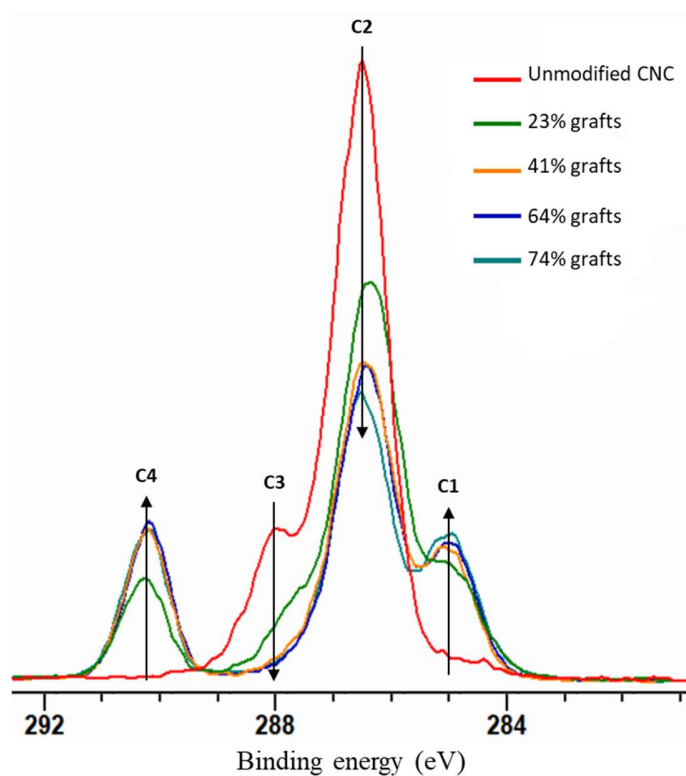


**Figure 53:** Carbon 1s X-ray photoelectron spectroscopy (XPS) scan of cellulose nanocrystals grafted with different poly(trimethylene carbonate content). Grafted CNCs corresponding to reference in **Table 10**: entry 21 (23%) entry 23 (41%), entry 18 (64%), entry 17 (74%).

As sulphur and nitrogen could not be measured by elemental analysis due to the extremely small content detected, XPS data was also used on unmodified and grafted cellulose. As can be seen in **Figure 55**, no significant signal can be found in the sulphur 2p region, indicating that the starting CNCs contained no sulphur, or negligible trace amount of it after purification.

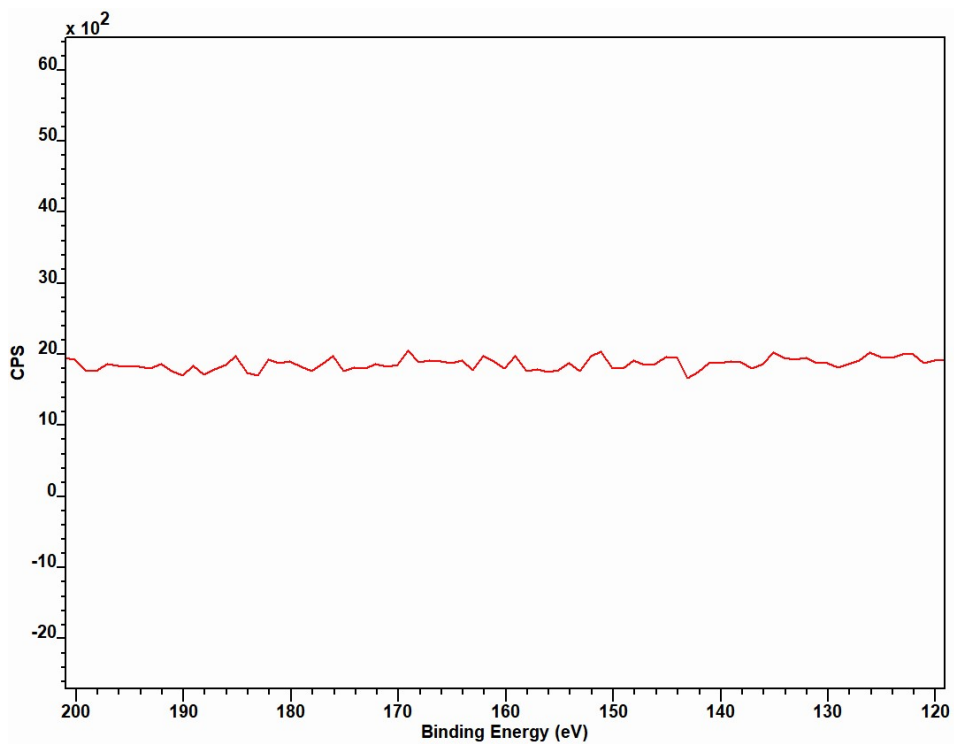


**Figure 55:** X-ray photoelectron spectroscopy (XPS) scan of unmodified cellulose nanocrystals in the region of Sulfur 2p peak.

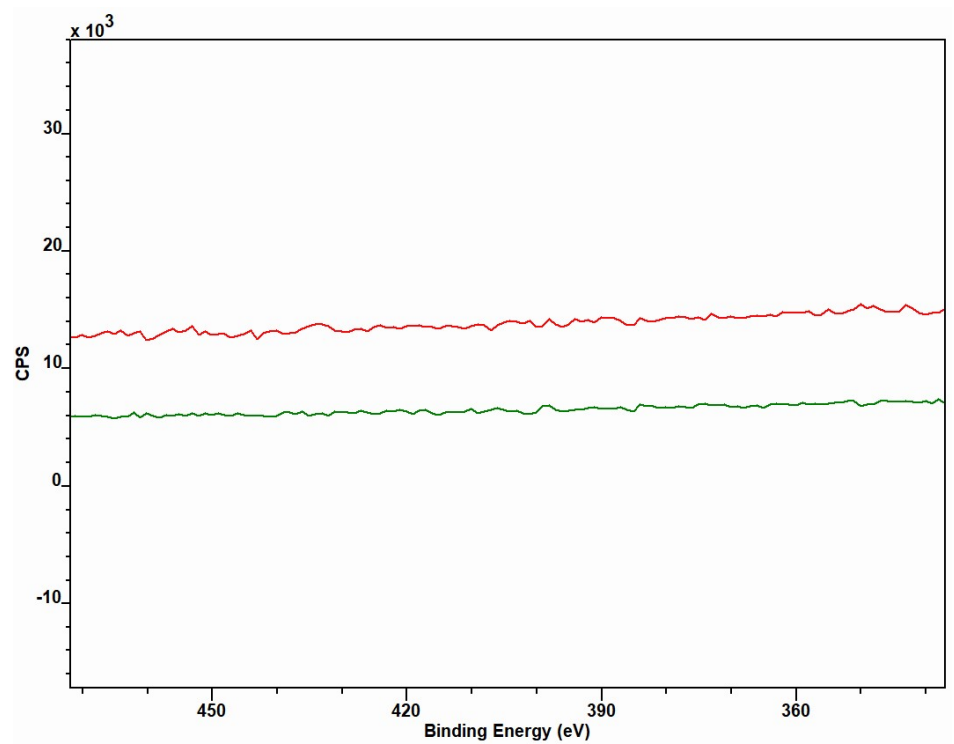


**Figure 54:** X-ray photoelectron spectroscopy (XPS) scan of unmodified CNC (red) and 74% grafted CNC (green) in the region of Nitrogen 1s peak.

A similar observation was done for nitrogen to determine if TBD was still present in the grafted cellulose, but looking at the region of nitrogen 1s revealed no significant difference between the unmodified CNC and grafted ones. Soxhlet extraction therefore showed to be an efficient method of removing the catalyst from the product, a benefit of using organic catalysts (**Figure 54**).

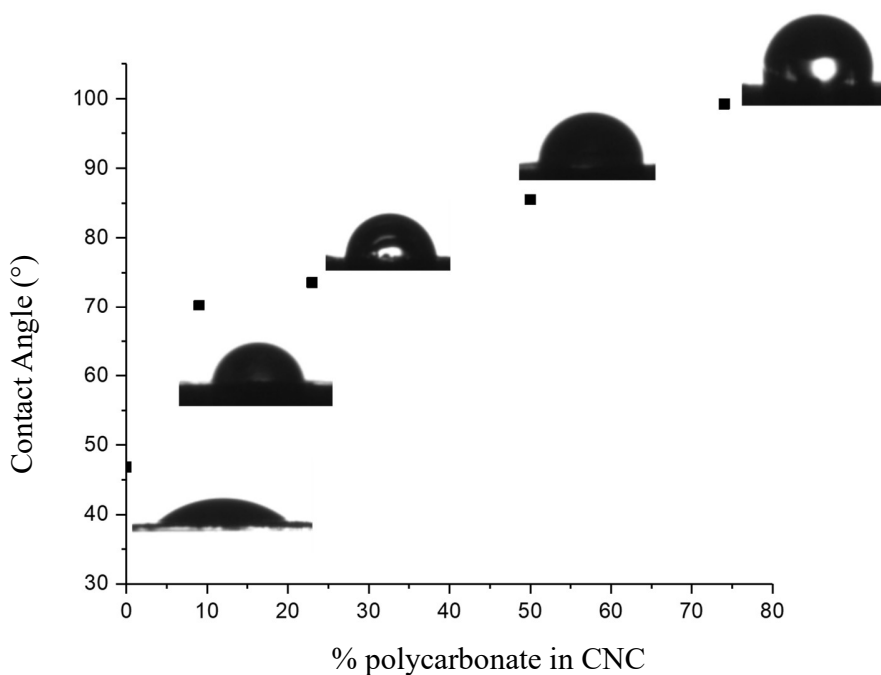


**Figure 56:** Contact angle of a water droplet on the surface of CNC modified with different polycarbonate content. Grafted CNCs corresponding to reference in **Table 10**: entry 15 (9%), entry 21 (23%), entry 4 (51%), and entry 17 (74%).

Since poly(trimethylene carbonate) is a highly hydrophobic material, grafting CNCs with it should change its interaction with water significantly. To quantify this, grafted CNCs were used in contact angle measurements with water (**Figure 56**). For a poly(trimethylene carbonate) content as low as 9%, the increase in hydrophobicity is significant, which then increases more slowly as the synthetic polymer content increased, up to a value close to that of pure PTMC reported in the range 90-110°<sup>267,268</sup>. This might be related to an increasing coverage of the CNC by PTMC, ranging from partial to almost full. It is noteworthy that the contact angle and thus the wettability can be controlled by targeting the proper polycarbonate grafting ratio. As a result, we believe that this increase in

hydrophobicity shows good signs for the potential incorporation of these nanoparticles in a polymer matrix for composite applications.

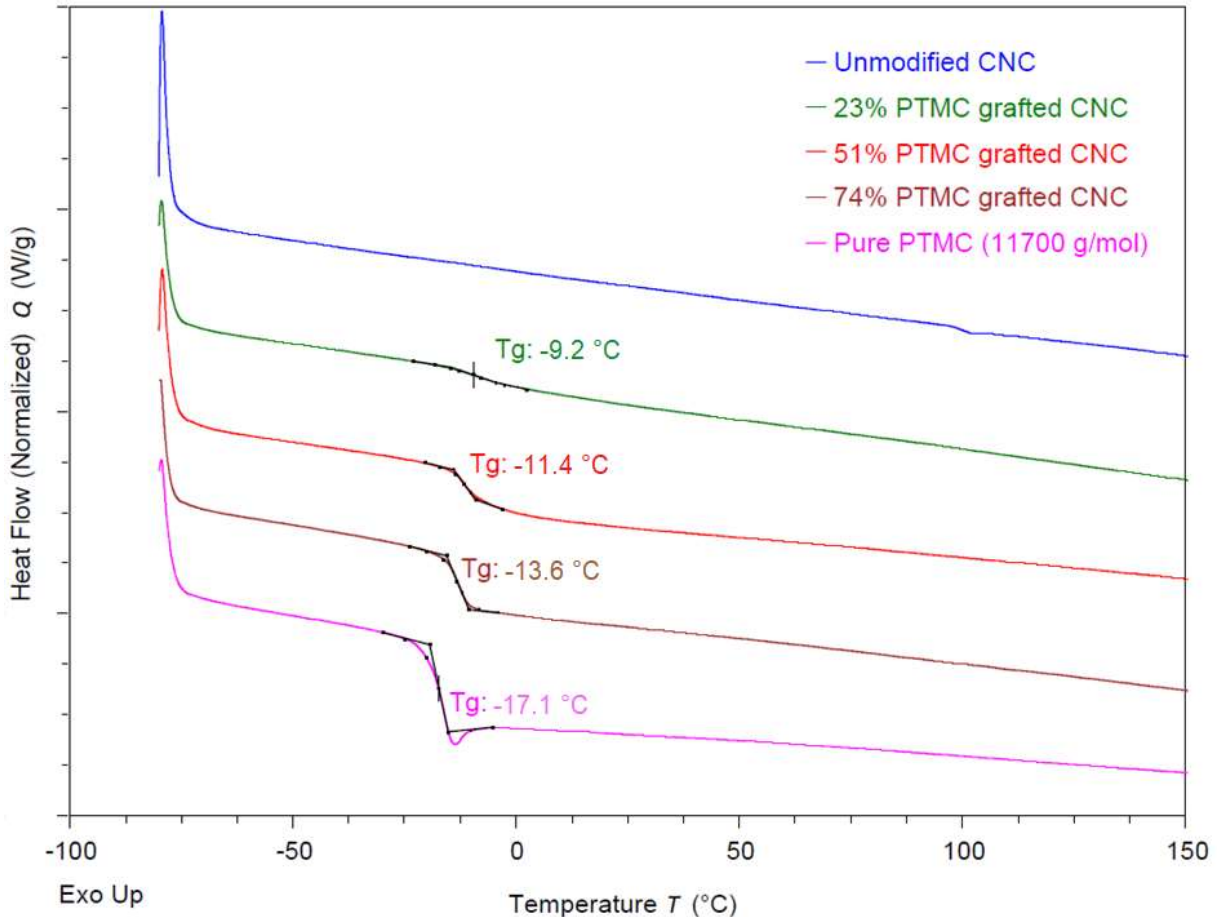


**Figure 57:** Differential Scanning Calorimetry (DSC) graphs of CNC, poly(trimethylene carbonate) (PTMC) and modified CNC during the second heating at 10°C/min. . Grafted CNCs corresponding to reference in **Table 10:** entry 21 (23%), entry 4 (51%), and entry 17 (74%)

DSC analysis were conducted to obtain more information on the thermal behavior of the grafts. The samples were heated from -80 to 190 °C, as the glass transition temperature ( $T_g$ ) of poly(trimethylene carbonate) is below 0 °C. For unmodified CNCs, no  $T_g$  or melting point were observed, as expected (**Figure 57**). For grafted CNCs, a glass transition was observed for all samples in the same range as the  $T_g$  of pure poly(trimethylene carbonate), but with slightly higher values. With a graft content as low as 23%, a  $T_g$  at -9 °C can be recorded, indicative of the presence of poly(trimethylene carbonate) grafts. As the PTMC content increased, the  $T_g$  decreased and progressively moved towards the value for poly(trimethylene carbonate) non-grafted polymer

(11,700 g.mol<sup>-1</sup>) at -17 °C, without ever reaching it. This phenomenon could be attributed to a lower mobility of the chain closer to the CNC backbone, their relative amount decreasing with higher grafting values. Overall, this shows that polymer grafts on cellulose nanocrystals are of sufficient length to showcase polymeric behavior.

As an additional proof of grafting of PTMC on cellulose, and not adsorption of non-grafted polymer, DSC analysis were also performed on CNCs with different PTMC graft wt%, along with the non-grafted polymer produced during the same reaction. These reactions were chosen specifically due the non-grafted polymer having similar molecular weight. As can be seen in **Figure 58**, all three non-grafted polymer have a relatively similar  $T_g$ , but the CNCs exhibit different glass transition temperatures, decreasing with an increasing amount of graft content. If the PTMC was purely adsorbed on the surface of the CNCs, then all three of these modified CNCs should exhibit the same  $T_g$ , as the resulting non-grafted polymers have similar average molecular weight for all three reactions. Furthermore, this shows that the  $T_g$  of the grafted CNCs depends on the grafting percent of PTMC, and is not linked to the size of the non-grafted polymer produced.

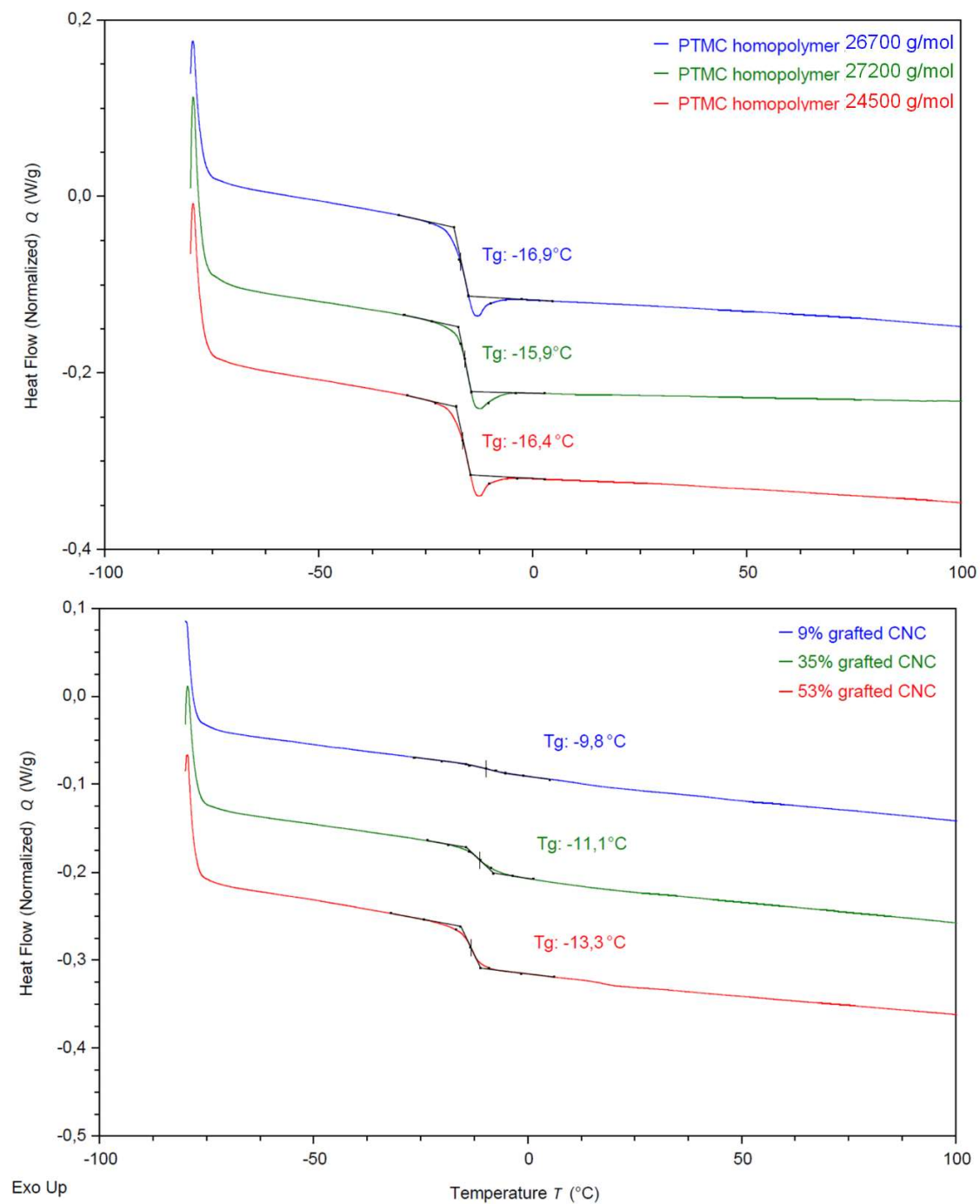


**Figure 58:** Thermogram of PTMC non-grafted polymer and grafted CNCs, each polymer and CNC of the same color coming from the same reaction.

TGA was also performed on the materials, primarily to determine the water content of each sample to apply a correction to the EA data obtained, but also to determine if the modification of the CNC had an impact of their thermal resistance.

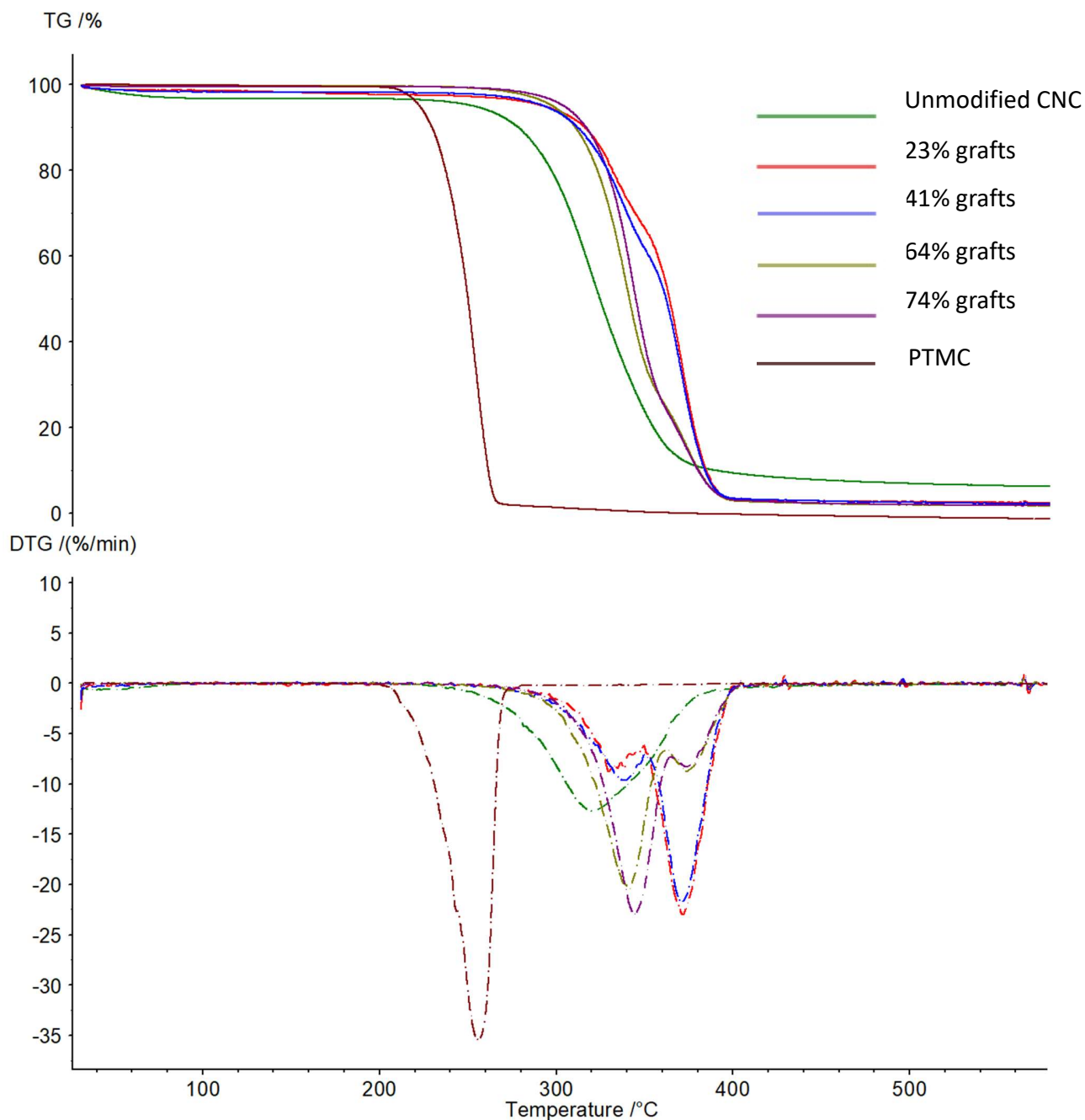


**Figure 59:** Thermograms of unmodified and grafted CNCs from 30 to 600°C as well as pure PTMC. Grafted CNCs corresponding to reference in **Table 10:** entry 21 (23%) entry 23 (41%), entry 18 (64%), entry 17 (74%).

As can be seen in **Figure 59**, the temperature of degradation of unmodified CNCs starts around 240 °C, as is quite typical for CNCs<sup>58</sup>, while the degradation temperature of pristine poly(trimethylene carbonate) is lower at 200°C. However, grafting of PTMC on CNCs did not decrease the degradation temperature, as could have been expected, but rather increased it up to about 275°, improving the thermal resistance properties of the CNCs. This shows that that despite the lower degradation temperature of the grafts, the resulting material thermal resistance is significantly improved, obtaining a degradation temperatures superior to both pure CNCs and PTMC.

In order to know whether or not the cellulose nanocrystals retain their structure following grafting, wide-angle X-ray scattering was used to determine the crystallinity of the pristine and PTMC grafted CNC samples. The X-ray scattering data was fitted with the crystal structure of cellulose I $\beta$ , and the amorphous contribution to the scattering determined. As no melting peak was seen in the DSC data, we know that the PTMC will be included in the amorphous contribution to the scattering data. Therefore, considering the amount of PTMC in the sample, changes in crystallinity of the cellulose ( $\Delta\chi_{c, \text{cellulose}}$ ) can be determined as the difference in crystallinity between the starting material and the product ( $\Delta\chi_{c, \text{sample}}$ ), minus the expected contribution from PTMC ( $\phi_{\text{PTMC}}$  – the volume fraction of PTMC) as shown in **Table 12**.

**Table 12:** The calculated sample crystallinity based on WAXS measurements for all samples.

Sample	$\chi_{c, \text{sample}}$	$\Delta\chi_{c, \text{sample}}$	$\phi_{\text{PTMC}}$	$\Delta\chi_{c, \text{cellulose}}$
Unmodified CNC	0.99	-	0	0
23% PTMC-g-CNC	0.68	-0.31	0.27	-0.04
41% PTMC-g-CNC	0.56	-0.43	0.46	0.03
51% PTMC-g-CNC	0.37	-0.62	0.56	-0.06
64% PTMC-g-CNC	0.26	-0.73	0.69	-0.04
74% PTMC-g-CNC	0.14	-0.85	0.78	-0.07

The data on the grafted samples shows only around 5% change in cellulose crystallinity when the contribution from amorphous PTMC is removed. This change could be due to peeling of the surface chains of the CNC during grafting, however, given the lack of trend in  $\Delta\chi_{c, \text{cellulose}}$ , and the wide

standard deviation in the values, it is possible that this reflects the error in the calculation of the sample crystallinity by this methodology.

Lastly, two samples have been characterized by mass spectrometry in order to get structural information on the non-grafted polymer formed during the grafting procedure. Matrix assisted Laser Desorption/Ionization mass spectrometry (MALDI-MS) were performed on non-grafted polymers of low molecular weight extracted after CNC grafting (**Figure 60**).

MALDI analyzes unambiguously confirm the presence of non-grafted polymers initiated by residual protic species (water and ethanol molecules) even after the drastic drying procedures used. Indeed, sample 25 shows the presence of polymer initiated by ethanol as major product (*i.e.*  $m/z$  1599.5) while sample 29 is mainly composed of PTMC initiated by water (leading to propanediol as initiator after decarboxylation reaction,  $m/z$  1629.5). Interestingly, no significant contribution of cyclic oligomers is observed although high conversions reached.

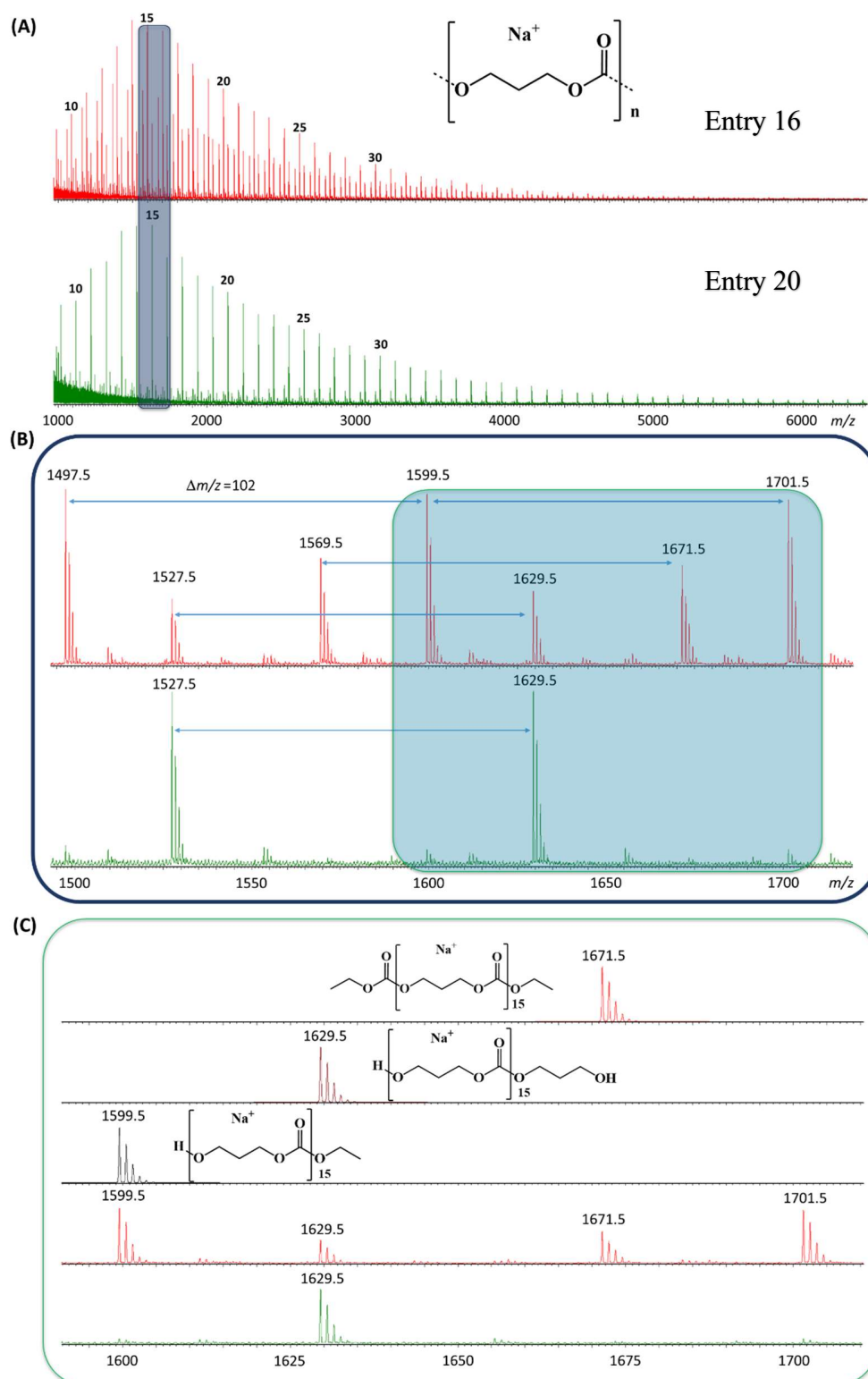


**Figure 60:** MALDI-MS spectra for entry 25 and 29, (A) global mass spectrum, (B) magnification from  $m/z$  1,500 to  $m/z$  1,700 and (C) comparison between experimental data and theoretical isotopic models.

### V.1.3. ROP of TMC by CNC-Supported TBD trial experiments

The results presented here were obtained by using modified CNCs grafted with TBD moieties of their surface. The catalyst was obtained thanks to the work of Nouaamane El Idrissi, a PhD student of the group, therefore its synthesis will not be described here. A degree of substitution (DS) of 0.14 has been found based on elemental analysis calculation with in principle only the primary OH (position C6) functionalized.

**Table 13:** Ring-opening polymerization of TMC using TBD-grafted CNC as catalyst, at 25 °C in THF for 5 hours.

Entry	TMC /Catalyst/ OH	Cat	Time (h)	Conversion <sup>[a]</sup> (%)	$M_n$ non-grafted polymer <sup>[b]</sup> (g.mol <sup>-1</sup> )	$\mathcal{D}_M$ <sup>[c]</sup>
1.	60/1/6 <sup>[d]</sup>	CNC-TBD	5	47	15,000	1.4
2.	30/1/6 <sup>[d]</sup> + 1 <sup>[e]</sup>	CNC-TBD	5	52	19,100	1.4
3.	500/1/50	TBD	5	99	18,100	1.9
4.	100/1/1	mTBD	1	58	12,300	1.7

[a] Calculated via <sup>1</sup>H NMR to determine monomer/polymer ratio. [b] Number-average molecular weight of the non-grafted polymer determined by SEC vs. polystyrene standards and corrected with a correction factor of 0.57, 0.73, or 0.88 based on size measured<sup>262</sup>. [c] Number-average molecular weight of the non-grafted polymer determined by SEC vs. polystyrene standards and corrected with a correction factor of 0.57, 0.73 or 0.88 based on size measured<sup>262</sup>. [d] Based on a ratio of 1/6 of TBD/primary corresponding to a DS of 0.14. [e] BnOH added as co-initiator.

A first reaction was performed in similar conditions to that of conditions described in V.1.1 to try to use the functionalized nanocrystals as both the catalyst and the co-initiator. As can be seen in **Table 13**, entry 1, the trimethylene carbonate was partially converted after five hours, leading to a conversion of 47%, and a non-grafted polymer with an average molecular weight of 15,000 g.mol<sup>-1</sup>. It is interesting to note that no co-initiator other than cellulose was used for this first reaction, yet non-grafted polymer was obtained, likely initiated by protic impurities such as water and ethanol from CNC purification. Despite this, the reaction exhibits good control with an acceptable polydispersity of 1.4. When comparing the activity of the supported catalyst to a similar experiment done with TBD (entry 3), a decrease in conversion can be noted despite the higher equivalents of catalyst used. This result however is not surprising as grafted TBD has a structure similar to that of 7-methyl-1,5,7-triazabicyclo[4.4.0]dec-5-ene (mTBD), which is known to have a lower activity due to the loss of an hydrogen atom participating in H-bonding<sup>141</sup>. In addition, the conversion obtained with TBD-CNC is closer to the one obtained with mTBD than with TBD. A second reaction was then performed, using benzyl alcohol (BnOH) as a co-initiator to evaluate the activity of the supported catalyst for the polymerization of TMC in the presence of a protic initiator, and not to graft it to cellulose. For that reaction, the ratios of monomer, catalyst, and initiator used were

similar to the one found in the literature for the ROP of TMC by TBD (entry 2). Using these parameters, partial conversion was reached as well, this time 52%. Interestingly, the dispersity obtained was similar than in the absence of BnOH, but the average molecular weight was slightly higher. When compared to a reaction performed with mTBD for the ROP of TMC for only 1h (entry 4), a similar conversion can be noted, despite the supported catalysis reaction lasting over 5 hours, showing the lower turnover frequency of the supported catalyst. Regardless of this slower reaction time, a possibility to perform the ROP with a supported organic catalyst and to keep a low polydispersity is an interesting perspective.

To determine if grafting had occurred on the supported catalyst, due to the presence of unmodified surface OH able to participate in the co-initiation of the reaction, FT-IR analysis were performed on the recovered cellulose used as supported catalyst. As can be seen in **Figure 61**, a small signal of C=O can be observed on the TBD-grafted cellulose after the polymerization reaction, showing the presence of a small amount of polycarbonate grafts on the supported catalyst after the reaction. This indicated that the grafting of PTMC on the surface of cellulose bearing catalytic moieties is possible, but with the parameters used, only a small fraction of PTMC is grafted. In the presence of an additional co-initiator such as BnOH, this signal can also be observed, indicating that a small amount of grafting occurs on the cellulose regardless of the presence of an additional co-initiator or not.

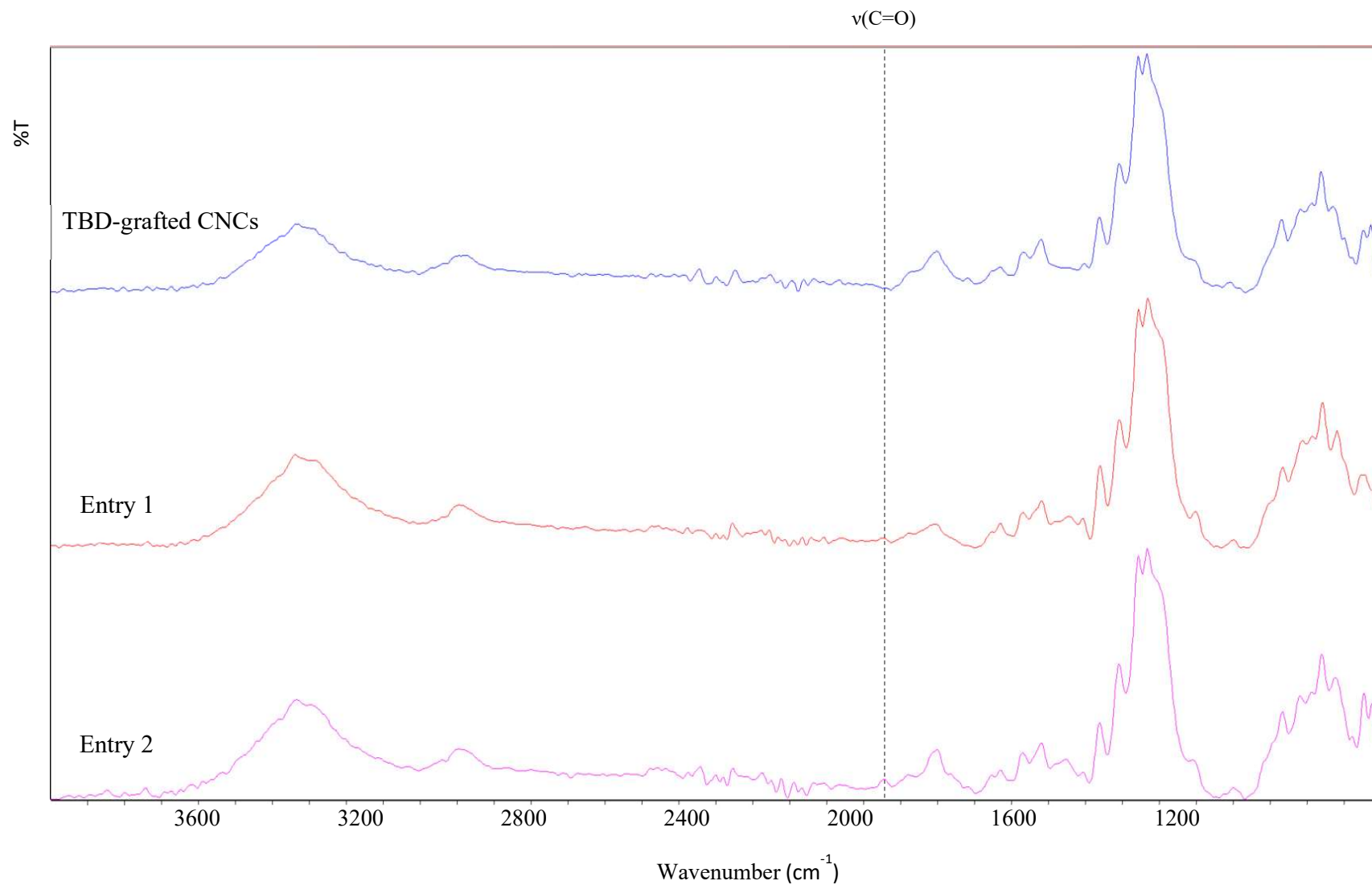


**Figure 61:** FT-IR spectra of TBD-functionalised CNCs before and after polymerization of TMC

**Table 14:** Water and elemental composition for unmodified CNCs and TBD-grafted CNCs before and after reaction.

Entry	Nitrogen content (%)	Carbon content (%)	Hydrogen content (%)	Water content (%)
CNC	0.22	42.49	6.17	2.9
TBD-CNCs	2.60	44.74	6.22	5.9
5.	0.79	41.30	5.98	5.8
6.	1.78	43.60	6.09	5.9

Elemental analysis was also used to characterize the supported catalyst after the reaction, to determine possibly the graft wt% of PTMC, as well as if there was any loss of TBD grafts (**Table 14**). As can be seen from entry 5 for the reaction with only TBD-CNC as co-initiator, an important loss of nitrogen content is noticed, going from 2.60% before reaction to 0.79% after. This shows the likely loss of some of the functions attached to the cellulose nanocrystals before, which could be a problem for recovering and reusing the supported catalyst. This loss of TBD functions was also confirmed by NMR as can be seen in **Figure 62**, where the reaction media was separated from the CNCs by filtration and analyzed. In this mixture, characteristic signals for TBD can be detected at 3.21 and 3.09 ppm, indicating that some was detached from the functionalized CNCs during the reaction. In comparison, entry 6, the reaction performed in the presence of benzyl alcohol, shows a higher nitrogen content, indicating of a better retention of the grafted catalyst on the surface of the cellulose. This was also confirmed by NMR, where the signals of the TBD in the post reaction mixture were very difficult to detect, and a smaller fraction seemed to have been lost, nitrogen content going from 2.60 to 1.78% after reaction.

A range of possible grafting was calculated to determine whether or not the loss in Nitrogen content was caused by a grafting reaction or loss of the grafted TBD. The following calculation is done considering leaching negligible. Reaction 1 was carried out using 1000 mg of TMC, and 214 mg of TBD-CNC, corresponding to 190 mg of CNC, 24 mg of TBD, and 1214 of product in total, TMC representing 82 wt%. TBD is composed of 26 wt% of N, 24 mg of TBD represents 6.25 mg of N. If 100 % of the TMC is grafted on the CNCs, N content would be 0.5 % (24 g / 1214 g), whereas it would be 2.6 % if no grafting occurred. N content of 0.78 wt% would correspond to 800 g of grafted PTMC, which would correspond to 73 wt% grafts. As seen in FT-IR, only a very weak C=O stretching signal is observed, unlike the one observed for a 74 wt% grafted CNCs described in **Figure 51**. For reaction 2, the same calculation would correspond to 39 wt%, which would be more realistic, but still does not correspond to what is observed in FT-IR.

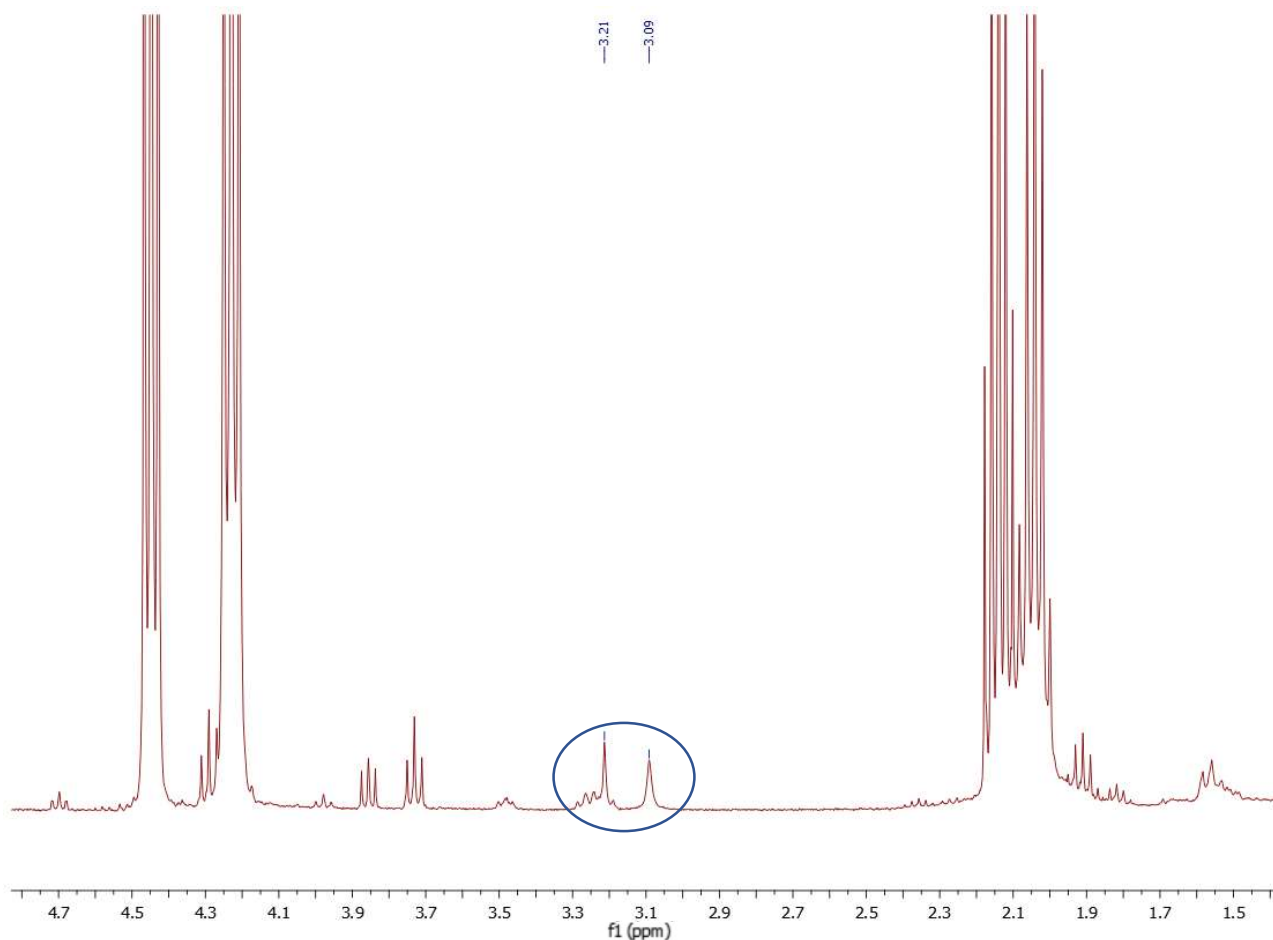


**Figure 62:**  $^1\text{H}$  NMR spectra of the crude mixture after quenching with benzoic acid and separation of CNC in  $\text{CDCl}_3$  (300 MHz).

In regards to the amount of PTMC grafted to the cellulose nanocrystals, this amount could not be quantified using the method described in V.1.1 due to the loss of TBD grafts as well as addition of grafts, making calculation impossible, similarly to resolving a equation system with too many unknown variables as is described in II.5. However, elemental analysis and FT-IR indicate that the wt% of PTMC on the CNCs would be very small, in particular in the case of the reaction done in the presence of BnOH as co-initiator.

## V.2. Conclusion

Ring-opening polymerization of trimethylene carbonate was performed using cellulose nanocrystals as a co-initiator in the presence of four organocatalysts, *i.e.* DMAP, DBU, TBD and BEMP). The overall performances considering conversion, grafting ratio and yield are TBD > BEMP > DBU, DMAP. After optimization, a grafting ratio as high as 74% could be reached using

TBD, corresponding to a material composed by weight of almost  $\frac{3}{4}$  polycarbonate grafts. The reaction was performed at room temperature with a low concentration of the catalyst, 0.5% vs. TMC and 500 equiv. of TMC per glucose unit. This led to a material with  $T_g$  and contact angle close to that of poly(trimethylene carbonate). The use of a single step reaction, under mild conditions while keeping grafting yield high is of great interest to produce CNC with a controlled amount of grafts. In addition, the catalyst could be removed by Soxhlet extraction and no traces of it could be detected in the purified material. Furthermore, we were able to show some of the most influential parameters with respect to grafting content, providing some insight on the chemistry behind cellulose modification. As determined by TGA and WAXS, no loss of properties of the cellulose nanocrystals were recorded after surface modification. Moreover, XPS showed a surface composition almost identical to pure PTMC at higher grafting content, indicating the almost full coverage of the grafts on the CNCs nanoparticle in core-shell like structure. The water contact angle of the resulting material ranged from *ca.* 50 to 100° and could be tuned by adjusting the grafting ratio. Lastly, DSC results revealed the polymeric behavior of the grafts, confirming the successful grafting of polycarbonate chains of sufficient length to have high potential as reinforcement fillers in composite materials. To our knowledge, this is the first reported chemical modification of cellulose nanocrystals with trimethylene carbonate, and the first example of a ROP-based “grafting from” process attaching polycarbonate chains onto CNCs.

The use of TBD-grafted cellulose nanocrystals as a supported catalyst was also tested for the polymerization of trimethylene carbonate. In the absence of another co-initiator, the ability to graft PTMC of the CNCs was evaluated, and only a very small amount of grafting was detected on the CNCs. Full conversion was also not reached after five hours, likely due to the lower reactivity of the supported catalyst when compared to TBD. In addition, an important decrease in nitrogen content of the supported catalyst after recovery was measured by elemental analysis for this reaction, showing that a part of the TBD groups had been detached during the experiment. This was later confirmed by proton NMR analysis where free TBD signal could be detected in the reaction mixture. In comparison, a reaction of polymerization of TMC in the presence of BnOH as a co-initiator was also performed to try to obtain purely non-grafted polymer. With parameters closer to that of similar work reported in the literature, PTMC of narrow dispersity could be obtained as well, and an almost negligible amount of grafts were detected on the recovered catalyst by FT-IR. When compared to a similar reaction performed with mTBD, a lower activity of the supported

catalyst was showed, with a similar conversion obtained at the five hour mark for the supported catalyst *vs.* one hour for mTBD. The loss of functional group of the supported catalyst was determined by elemental analysis, and while some decrease in nitrogen content was noticed, it was not as important as for the reaction performed without BnOH. Overall, while some optimization is needed and re-usability of the supported catalyst was not yet tested, the ability to use a bio-based supported catalyst for the simple polymerization by ROP of cyclic carbonate is an interesting development towards greener catalytic systems.

The methodology developed for the SI-ROP of TMC using TBD proved efficient at obtaining highly grafted CNCs, especially in comparison to the grafting obtained on CNF described in chapter III. Therefore, grafting of PLA and other lactones on CNCs will be explored in the next chapter, as TBD has been reported to be an efficient catalyst for the ROP of many cyclic monomers. Due to the very different mechanical properties of PLA and PTMC, but their common advantages such as biocompatibility, copolymers grafts of both would be particularly interesting, especially if this can be done with the same catalytic system. Therefore, grafting of copolymers onto CNCs will be described to demonstrate the high versatility of this method.

## VI. Block and Statistical Copolymer Grafted CNC by organocatalysis

### VI.1. Introduction

The ever-growing concern over the replacement of fossil fuel-based chemistry has been at the forefront of research over the past years, leading both industry and academia to increasingly invest in developing a biobased resourced industry. This interest has brought forward different materials to replace the currently used polymers such as aliphatic polyesters and polycarbonates with renewable alternatives. Indeed, cyclic esters and carbonates, which constitute a substantial portion of the monomers available to synthesize such polymers, can be obtained from renewable sources. For example, lactic acid can be made commercially by fermentation of carbohydrates, which leads to an optically pure product that can be polymerized to give poly(lactid acid) (PLA)<sup>269</sup>. As for carbonates, a lot of work has focused on producing them through greener pathways, most commonly by combining epoxides with CO<sub>2</sub> to obtain cyclic carbonates, which can be polymerized by ring-opening polymerization (ROP)<sup>104,270</sup>. More recently, the use of biosourced feedstocks to produce organic carbonates has also seen a surge in interest, leading to some new potential applications<sup>271</sup>. However, as with most polymers, a high level of control over the properties of the final material is required for high end applications. These high-value materials usually require a well-defined molecular weight as well as a narrow dispersity, and sometime a high level of control over the chain ends and the sequence of the monomer units<sup>116,272</sup>.

A large amount of work has been carried out to obtain sufficient control over polymerization reaction, and ROP has been the most promising approach to satisfy all of the criteria mentioned previously<sup>223,273</sup>. Among the catalysts used for this type of polymerization, metal alkoxides have been widely used, and their mechanism to catalyze these reactions has been studied thoroughly. Among such systems, magnesium, zinc, calcium, and many others have been developed as efficient and non-toxic catalysts to facilitate their use in as many application as possible<sup>274-276</sup>. However, they can sometime be used with toxic ligands, trace amounts of catalyst are often very difficult to eliminate, and these metal centers can create issues for some applications such as for microelectronic. Moreover, these catalysts are often very sensitive to impurities and used for bulk polymerization which requires high temperatures. This has therefore motivated many researcher to look for metal-free alternatives<sup>253</sup>. Research into organic catalysis for ring-opening polymerization has over time produced and wide variety of catalytic system including the use of enzymes and

mono or bi-component catalysts<sup>155,277</sup>. While these catalysts may not be as efficient with regards to stereo- and regioselectivity, many organic catalysts have been shown to have a high activity and offer a good control over the ROP of common monomer such as cyclic esters and carbonates. Alkaline catalysts have recently risen as one of the most promising group of organic catalysts for such reactions, with species such as guanidines (1,5,7-triazabicyclo[4.4.0]dec-5-ene (TBD), 7-methyl-1,5,7-triazabicyclo[4.4.0]dec-5-ene (mTBD))<sup>167,278</sup>, amidines (1,8-diazabicyclo[5.4.0]undec-7-ene (DBU))<sup>279,280</sup>, and pyridine derivatives (4-dimethylaminopyridine (DMAP))<sup>281</sup>. A great benefit of these catalysts is that they can be used with a protic co-initiator such as an alcohol which allows for greater control over the molecular weight of the final product. Using an alcohol to fine-tune the ratio of initiator/monomer is a great asset as this allows for a very small quantity of catalyst to be used<sup>282</sup>. More recently, phosphazene bases such as 2-(*tert*-butylimino)-2-(diethylamino)-1,3-dimethylperhydro-1,3,2-diazaphosphorinane (BEMP) have also been identified as good candidates for the ring-opening polymerization of cyclic esters, with high activity even under mild conditions and a good stereocontrol when polymerizing *rac*-lactide<sup>283</sup>. In addition, this catalyst has also been used successfully for the ROP of cyclic carbonates<sup>117</sup>.

As good a material as aliphatic polycarbonates and polyesters can be, both of them however present limitations for uses in some applications. Aliphatic polycarbonates (PC) such as poly(trimethylene carbonate) (PTMC) have poor mechanical properties due to a low glass transition temperature (around -17 °C), which hinders their use for practical applications<sup>284,285</sup>. As for polyesters, PLA for example is a very brittle material and shows a poor resistance to oxygen and water permeation, which is an issue in typical applications such as packaging<sup>286</sup>.

An interesting solution to overcome these limitations is to reinforce them with fillers such as cellulose to obtain composite, or to combine different polymers together, or alternatively, materials<sup>287</sup>. In the work presented previously, the grafting of these polymers onto cellulose nanofibers (CNF) and cellulose nanocrystals (CNC) has been explored as a way to make suitable fillers for composite materials.

Regarding the combination of these polymers, copolymers of PLA and PTMC have been described in the literature before using different catalysts. In 2014, Flidel *et al.* described the use of a N-heterocyclic carbene zinc alkoxides to obtain well defined block copolymers of PTMC and PLA by sequential addition of the monomers<sup>288</sup>. Similarly, diblock and triblock copolymers were

described by Socka *et al.* using an aluminum alkoxide catalyst with bulky ligands. Using this system, the authors were able to obtain various combination of PTMC and PLA block such as ABA and BAB by sequential addition of the monomers, and also successfully prepared random copolymers. Copolymers obtained this way exhibited interesting thermal properties and microstructures<sup>289</sup>. As with homopolymerization of these monomers, metal-based catalyst have seen the most amount of work to prepare copolymers, but some work has also been done using organic catalyst such as TBD and methanesulfonic acid (MSA), as described by Toshikj *et al.*. Interestingly, the authors observed that the copolymerization of lactide and TMC with TBD did not work well when starting with a polylactide block, and two homopolymers were obtained this way. Similar results were also observed with a tin-based catalyst<sup>290</sup>.

An interesting perspective would be to combine both approach: graft copolymers onto the surface of cellulose to obtain nanofillers with unique properties. Copolymer-grafted cellulose nanocrystals have already been documented using different methods and monomers. In the work of Carlmark *et al.*<sup>291</sup>, atom transfer radical polymerization (ATRP) was used to modify the surface of a cellulose filter paper. In this work, a first step of surface modification was done using 2-bromoisobutyrylbromide to obtain efficient initiators for ATRP reaction. Following this reaction, “grafting from” polymerization of methyl acrylate was done on the surface of the cellulose using copper bromide. A sequential addition of 2-hydroxyethyl methacrylate was done, and after full conversion, a block-copolymer was observed on the surface of the cellulose fiber. “Grafting from” copolymerization with cellulose was also reported using a metal-free approach by Lu *et al.*<sup>292</sup>. Starting from ethyl cellulose, a first modification was again done to obtain bromide moieties on the surface of cellulose as initiators for ATRP reaction. 10-phenylphenothiazine was used as a photoredox organic catalyst for the sequential copolymerization of lauryl meth-acrylate and furfuryl methacrylate. Under low intensity ultraviolet (UV) light emitting diodes (LED), polymerization of both monomers was successfully done, and “deactivation” of the polymerization could be done by turning the light off. The modified cellulose obtained showed microphase separation as evidence by transmission electron microscopy (TEM) and differential scanning calorimetry (DSC). Another technique that has been used to graft copolymer on cellulose is the “grafting to” approach, as reported by Mano *et al.*<sup>293</sup>. Sequential ROP of  $\epsilon$ -caprolactone (CL) and *L*-lactide (LLA) was first performed using a tin-based catalyst ( $\text{Sn}(\text{Oct})_2$ ) and an alcohol co-initiator. Then, using toluene-2,4-diisocyanate (TDI) and  $\text{Sn}(\text{Oct})_2$ , the copolymer chain ends were

modified to obtain TDI-end capped copolymer. As the final step, CNCs were added to the copolymer in dry toluene, and after 7 days at 90 °C, P(CL-b-LLA)-g-CNC were obtained. Two copolymers with different molecular weight were grafted using this method, and the lower molecular weight copolymer appeared to give a greater surface modification as seen in TEM, resulting in a higher hydrophobicity and better separation of the modified CNCs.

Interestingly, organocatalyzed “grafting from” ROP has not been reported as a method of grafting copolymers on the surface of CNCs yet to the best of our knowledge. In addition, copolymers made from lactide and TMC have yet to be grafted on cellulose.

We hereby report the organocatalyzed ring-opening copolymerization of TMC and lactide on the surface of cellulose nanocrystals. To our knowledge, such copolymers grafts on cellulose have not been reported in the literature, therefore the findings of this study should shed some light on the chemistry behind the obtention of such materials, how to characterize them, and their resulting properties.

## VI.2. Results and discussion

### VI.2.1. PTMC/PLLA Copolymers

Due to PTMC generally having low glass transition temperature, and PLA’s brittleness, graft copolymers of both could make interesting additive for composite materials. For this purpose, grafting of both polymers on CNC was performed in different conditions. In order to compare the reactions involving multiple monomers, grafting reactions were first performed with each monomer separately. First, two different reactions were used with the different catalytic system described previously: a short reaction with a catalytic amount of TBD (similar to reactions with TMC described in Chapter V), and a long reaction with a large amount of DMAP (similar to reactions with lactide described in Chapter III).

**Table 15:** Ring-opening polymerization of *L*-LA initiated from the surface of CNC using TBD and DMAP, at 25 °C in THF.

Entry	Cat.	<i>L</i> -LA / Cat / OH <sup>[a]</sup>	Time (h)	Grafting <sup>[b]</sup> (w%)	Conversion <sup>[c]</sup> (%)	Grafting Yield <sup>[d]</sup> (%)	<i>M<sub>n</sub></i> non-grafted polymer (g.mol <sup>-1</sup> )	<i>D<sub>M</sub></i> <sup>[e]</sup>
1.	TBD	500 / 1 / 50	1	0	7	0.0	24,700	2.3
2.	DMAP	500 / 50 / 50	72	57	99	14.9	94,400	1.4

[a] Calculated using moles of glucose rings (162.14 g/mol), and considering 1 primary OH per ring. [b] Determined by elemental analysis (calculation based on hydrogen content (%H) and carbon content (%C)) and corrected for adsorbed water using TGA. [c] Calculated via <sup>1</sup>H NMR to determine monomer/polymer ratio and corrected to include monomer grafted. [d] Ratio of monomer grafted to initial monomer. [e] Dispersity of the non-grafted polymer determined by SEC.

As can be seen in **Table 15** entry 1, grafting of PLLA on unmodified cellulose nanocrystals did not yield any grafting with the system using TBD, and conversion was low after 1 h of reaction when using CNCs as co-initiator. When compared to previous experiments with TMC, the conversion was also found to be slower, as a conversion of at least 80% should be expected after 1 h for this monomer. It is also interesting to note that the reactivity is much lower when using CNCs

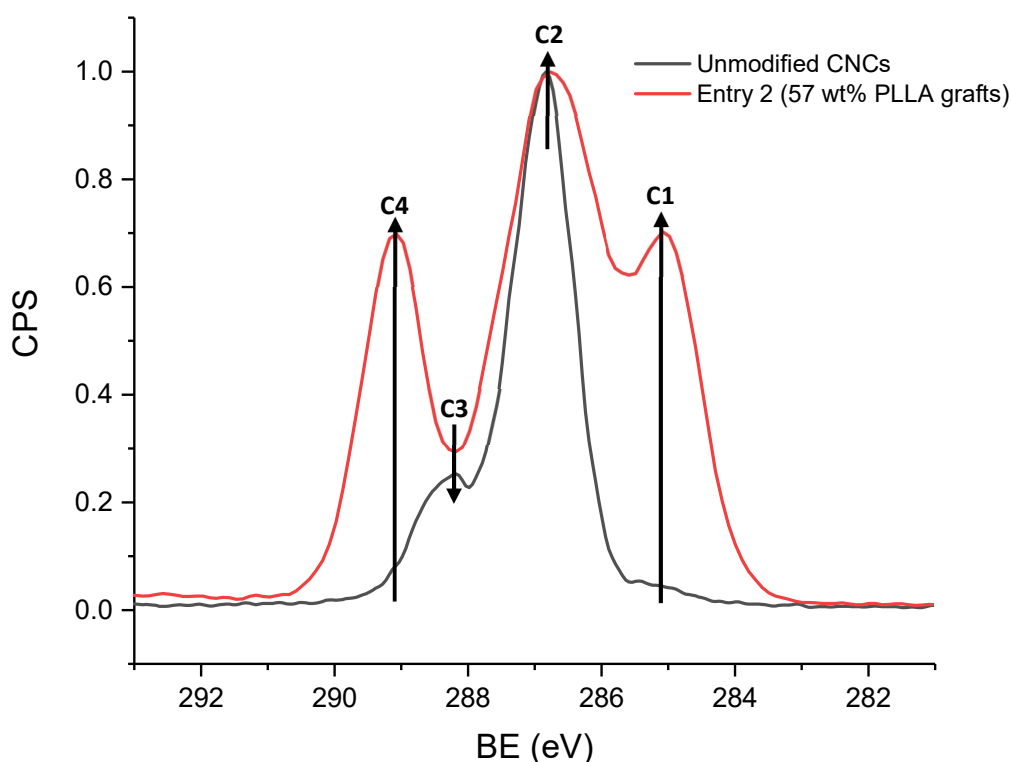


**Figure 63:** Carbon 1s X-ray photoelectron spectroscopy (XPS) normalized spectrogram of unmodified CNCs and PLLA-grafted CNCs. Grafted CNCs corresponding to entry 2 in **Table 15**

as co-initiators, as similar reactions reported using alcohols with TBD showed a much faster conversion, potentially due to a strong H-bonding interaction with CNCs<sup>141</sup>. The second reaction, using DMAP at a ratio of 1 per primary OH on cellulose, lead to full conversion after 72 h, and a very high molecular weight and low dispersity for the non-grafted polymer. Elemental analysis coupled with TGA was used and a grafting of 57 wt% was determined, a result much higher than results reported in Chapter III using CNFs, likely due to the more controlled environment when reactions are done in a glovebox.

Grafting was confirmed by XPS (**Figure 63**) and C-C (C1) and OC=O (C4) contribution increase significantly, to the point where the cellulose C3 contribution could not be seen, showing the complete coating of the cellulose nanocrystals by the PLLA chains. The sample was also characterized by DSC, and a  $T_g$  typical of PLLA could be measured at 59 °C, but melting enthalpy could not be detected. The crystallization may be hampered by the presence of the rigid CNCs. A comparison of different thermograms comparing grafted and non grafted polymers as well as a discussion on the results will be provided later in this chapter.

#### VI.2.1.1. Block Copolymers

For grafting of PTMC on unmodified cellulose nanocrystals, as shown in **Table 10** (Chapter V), it can be successfully carried out using different catalyst, and TBD can lead to a high amount of grafting (up to 74% PTMC by weight). Therefore these reactions will serve as the reference for grafting of PTMC on CNCs throughout the next part.

Isolated CNCs grafted with different amount of polycarbonate (obtained as described in Chapter V) were first used, and TBD was used as the catalyst for the polymerization of *L*-lactide. Despite DMAP yielding better results for the grafting of PLLA on unmodified cellulose, PLLA grafting on PTMC-grafted CNCs was found to be more efficient with TBD. In order to keep the ratio of monomer / catalyst / OH, all values used for cellulose OH content were recalculated to take into account the grafted wt% of PTMC. Therefore 100 mg of 73% grafted CNCs was calculated to correspond to 0.167 mmol of glucose ring repeating units, whereas 59% grafted CNCs would be 0.253 mmol of glucose units. As shown in **Table 16**, the initial amount of PTMC grafted on the CNCs seems to be an important factor in the amount of PLLA grafted, as starting from 73% grafted CNCs yields a grafting of 50 wt% of PLLA on the CNCs, resulting in a material with only 13 wt% of cellulose in the end. Interestingly, due to the difference in molecular weight of both monomers,

this gives an almost equimolar ratio of PTMC/PLLA grafted on cellulose (0.96). When carrying out a similar reaction with modified CNCs containing less PTMC, the grafting obtain for PLLA is also lower, and this trend can be observed all the way to 23% grafted CNC-PTMC. Due to the CNCs with lower PTMC grafting possessing more cellulose, therefore more surface OH, higher amounts of lactide are used to keep the same ratio of monomer to initiator. This result in a drastic drop of yield for reaction performed with less grafted CNCs, going from 41.6 to 13.5% when the initial PTMC content of the CNCs goes from 73 wt% to 59 wt%.

**Table 16:** Ring-opening polymerization of *L*-LA initiated from the surface of PTMC-grafted CNCs using TBD, at 25 °C in THF over 1 hour. Full conversion was reached for all reactions.

Entry	<i>L</i> -LA / TBD / OH <sup>[a]</sup>	Initial PTMC content (wt%)	Grafting by weight <sup>[b]</sup> wt% PLLA / PTMC	Grafting Yield <sup>[c]</sup> (%)	$M_n$ non-grafted polymer (g.mol <sup>-1</sup> )	$D_M$ <sup>[d]</sup>
3.	500 / 1 / 50	73	50 / 37	41.6	49,000	2.8
4.	500 / 1 / 50	59	33 / 40	13.5	43,500	2.4
5.	500 / 1 / 50	35	30 / 25	7.4	33,100	2.5
6.	500 / 1 / 50	23	10 / 21	1.6	26,600	3.3
7. <sup>[e]</sup>	500 / 0.5 / 50	73 <sup>[g]</sup>	37 <sup>[g]</sup> / 46	6.8	47,400	1.3

*[a]* Calculated using moles of glucose rings (162.14 g/mol), and considering 1 primary OH per ring. *[b]* Determined by elemental analysis (calculation based on hydrogen content (%H) and carbon content (%C)) and corrected for adsorbed water using TGA. *[c]* Ratio of PLLA grafted to initial lactide. *[d]* Dispersity of the non-grafted polymer determined by SEC. *[e]* one pot 2 step reaction, with an initial conversion of 500 eq TMC over 5 hours followed by an addition of *L*-LA. *[g]* Calculated based on results obtained in **Table 10**.

Taking into account the difficulty to graft PLLA on unmodified CNCs with this catalytic system (**Table 15**), seeing a decrease in grafting of PLLA with lower grafting of PTMC as seen before would be in agreement with the fact that native CNC hydroxy group are not very reactive with TBD and *L*-lactide, whereas hydroxy end groups of PTMC grafts have a higher reactivity. This also shows the likelihood of the PLLA grafts being attached through the PTMC chain ends rather than to unreacted hydroxy on the surface of CNCs. It is worth noting that CNCs with a higher PTMC content are also more hydrophobic, and non-grafted polymers obtained for these reactions show a trend of being shorter for lower PTMC content. This could indicate that trace amounts of water is also to takes into account, despite every sample going through the same intense drying before reaction ( $10^{-6}$  bar of vacuum over a week).

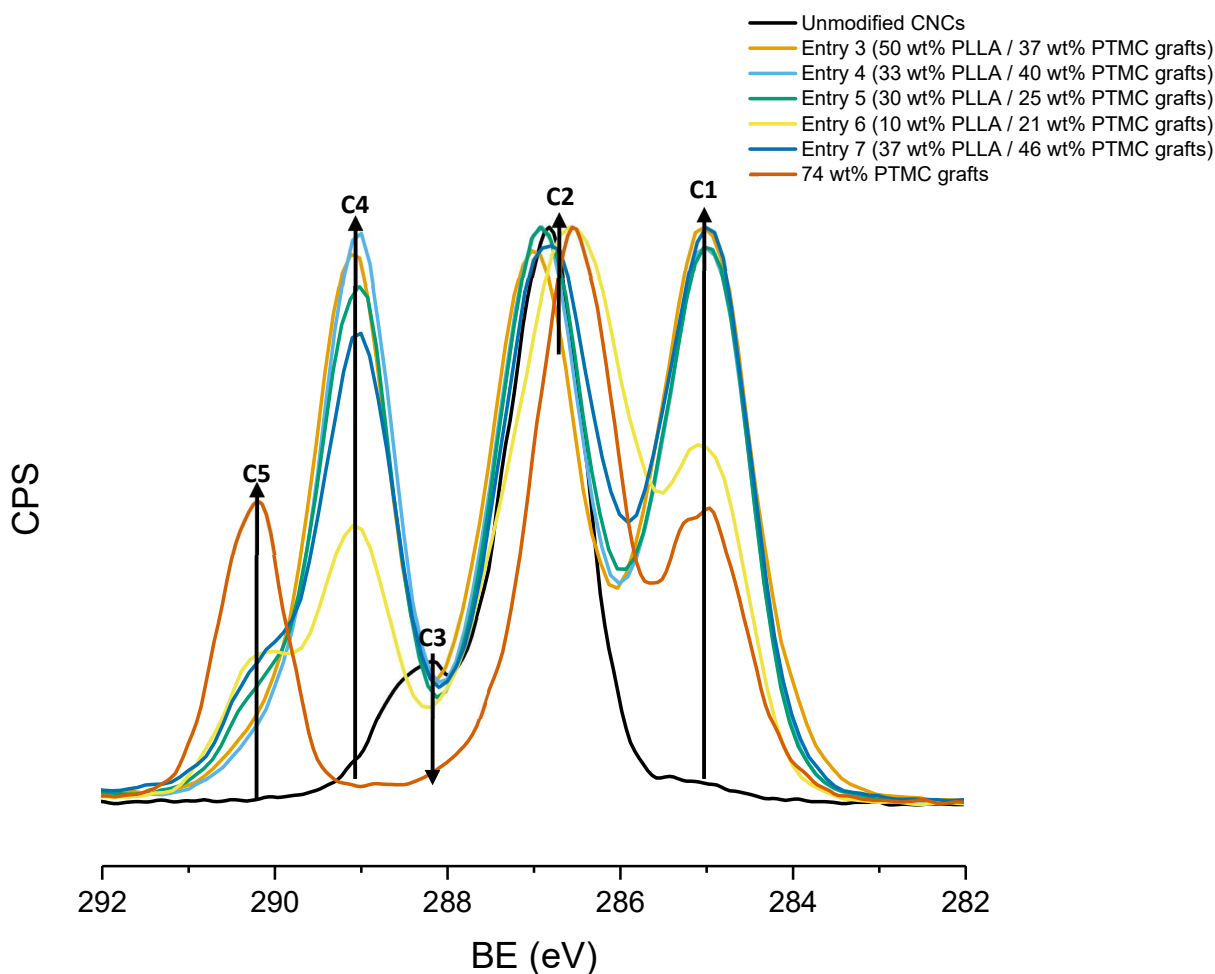


**Figure 64:** Carbon 1s X-ray photoelectron spectroscopy (XPS) normalized spectrogram of unmodified CNCs, PLLA and PTMC blocks grafted CNCs. Modified CNCs corresponding to entries 3 to 7 in **Table 16** and entry 26 in **Table 10**.

As TBD is able to polymerize both TMC and *L*-LA, a one pot, two steps approach was tested to see if similar results could be obtained without the needs for extra steps (entry 7). Catalyst loading was reduced to 0.5 eq as this gave the best results for grafting PTMC on CNCs (73%), and after complete conversion of the first monomer (5 hours), *L*-lactide was added. The grafting of PLLA was calculated once again by elemental analysis, but not having any isolated CNC after the first polymerization, the calculation was obtained assuming 73% grafting of PTMC (similar to a reaction performed with very consistent results). Proceeding like this, the overall grafting obtained was slightly lower, 83% vs. 87%, and the non-grafted polymer obtained had a much lower dispersity, showing a more controlled reaction (possibly due to the lower catalyst load). However, the grafting yield was low at 7%.

XPS analysis on the modified cellulose was performed to compare the surface composition, in particular for the CNCs that were modified to try to obtain block copolymer vs. the one aimed to be statistical. As XPS only provides analyzes of the first 10 nm layers of the material, this method of analysis can provide an interesting insight on the surface of modified CNCs.

As can be seen in **Figure 64**, the sample with the highest amount of PLLA grafted (entry 3) looks almost identical to that of pure PLLA<sup>294</sup>, while the contribution C5 of the trimethylene moieties was very small (XPS data provided in **Table 39**). This not only confirmed the successful grafting of PLLA on the modified CNCs, but it also gave an indication that the PLLA blocks are more likely grafted onto the PTMC blocks rather than directly on unreacted hydroxy functionalities present on the surface of the cellulose. In the dry state, PLLA forms a surface layer on top of the modified nanocrystals. As the amount of PLLA grafted on the surface of the PTMC-grafted CNCs increased, the contribution of the carbonate C5 could be seen increasing, while the contribution of the ester C4 signal decreased. However, even for samples with a higher amount of PTMC than PLLA, the dominant signals was still that of the ester, showing that the surface was made of a PLLA layer, and the PTMC layer was below it. Interestingly, the modified CNCs obtained by a one pot two-steps process (entry 7) had a slightly higher carbonate contribution. This could be an indication of some transesterification/transcarbonation having taken place but could also be attributed to the fact that the PTMC-grafted CNCs were never dried before grafting of PLLA, thus making the PLLA and PTMC interaction different.

Overall XPS indicated that CNC obtained from attempts at block copolymer grafting were mostly composed of PLLA on the surface 10 nm if sufficient grafting was reached, with the sample containing lower PLLA grafting amounts showing that the PTMC block could be found underneath.

FT-IR analysis was also performed, to gain complementary information to XPS analysis due the higher depth of penetration for this technique. For the block copolymer-grafted CNCs, XPS showed mostly PLLA signals in the first 10 nm layer, with carbonate signals representing less than 1% of the surface composition (entry 3). However, as can be seen in **Figure 65**, FT-IR revealed the presence of strong carbonate bands at 788, 1028, 1220 and 1740  $\text{cm}^{-1}$  for the same modified cellulose. As some of these peaks belonged to C=O and C-O stretching, they were in the same region as PLLA bands, but a clear difference could be seen between the PTMC and PLLA signals.

This confirmed the presence of PTMC blocks on the grafted CNCs, as well as the PLLA covering the surface.

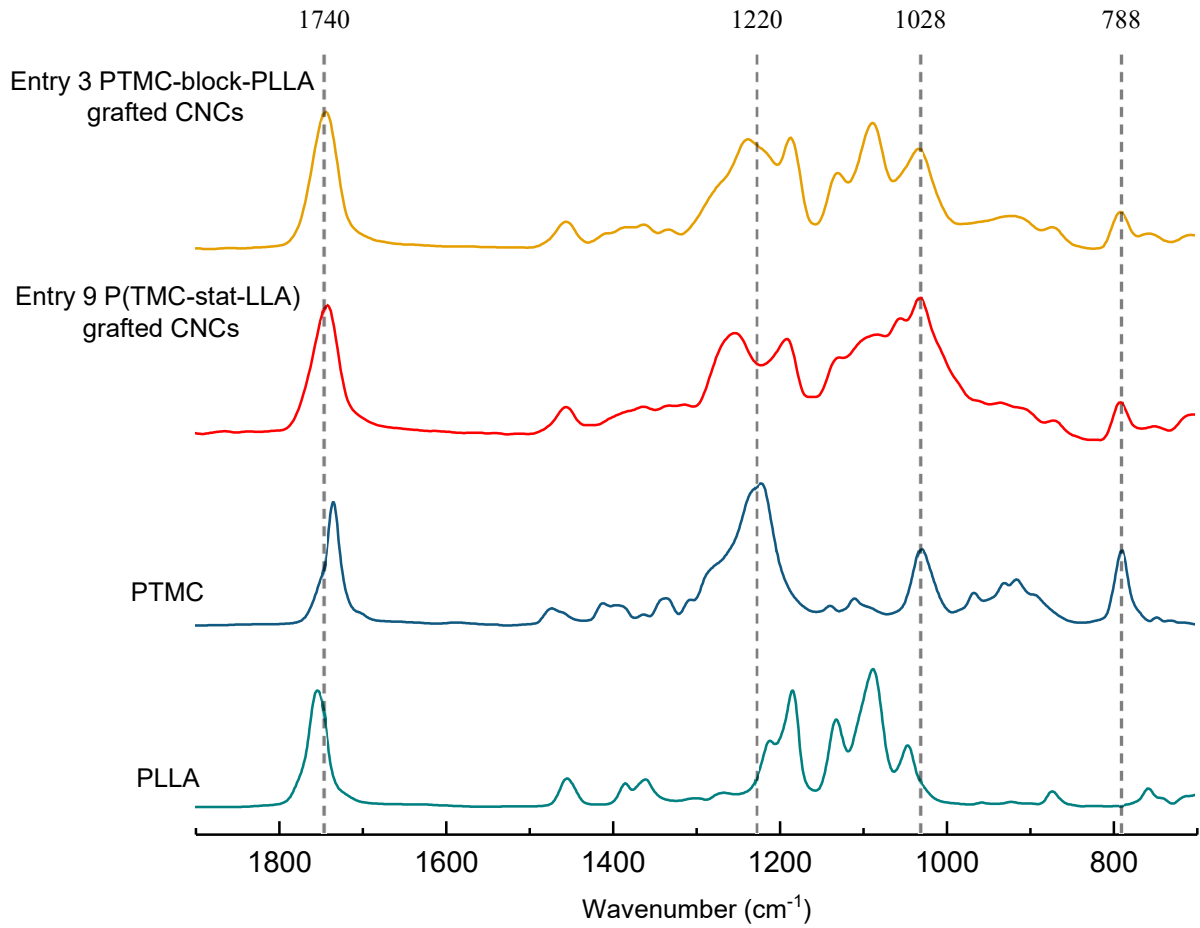


**Figure 65:** FT-IR spectra of copolymer-grafted CNC and non-grafted PTMC and PLLA.

### VI.2.1.2. Statistical Copolymers

**Table 17:** Ring-opening copolymerization of *L*-LA and TMC initiated from the surface of CNCs using TBD, at 25 °C in THF over 5 hours.

Entry	TMC / <i>L</i> -LA / TBD / OH <sup>[a]</sup>	Conversion <sup>[b]</sup> (%)	$M_n$ non-grafted polymer (g.mol <sup>-1</sup> )	$\overline{D}_M$ <sup>[c]</sup>
8. <sup>[d]</sup>	250 / 250 / 0.5 / 5	88% TMC, 90% <i>L</i> -LA	15,200	2.0
9.	250 / 250 / 0.5 / 50	87% TMC, 99% <i>L</i> -LA	5,500	1.8
10.	350 / 150 / 0.5 / 50	96% TMC, 99% <i>L</i> -LA	22,600	2.7
11.	150 / 350 / 0.5 / 50	40% TMC, 0% <i>L</i> -LA	n.d.	n.d.

[a] Calculated using moles of glucose rings (162.14 g/mol) and considering 1 primary OH per ring. [b] Calculated via <sup>1</sup>H NMR to determine monomer/polymer ratio and corrected to include monomer grafted. [c] Dispersity of the non-grafted polymer determined by SEC. [d] Reaction performed with BnOH as co-initiator instead of cellulose.

In an attempt to obtain different materials, CNCs grafts were prepared by mixing both monomers at the beginning of the reaction in the presence of CNCs. However, due to the unknown chemical composition of the grafts, the wt% grafts could not be directly determined by elemental analysis. Moreover, quantification of the grafts using weight of the modified CNCs after reaction was not reliable as some materials were easier to separate from the non-grafted polymer than others. Despite this, interesting comparisons can be done between the CNCs obtained with this method as compared to the blocks described in the previous section, which will be done in the next section.

First, a reaction with benzyl alcohol (BnOH) instead of CNCs was performed to evaluate the reactivity of the monomers (entry 8, **Table 17**). For this reaction conversion for both monomers was similar at 90% when an equimolar quantity of monomer was used at the beginning of the reaction.

As can be seen in **Figure 66**, characteristic signals of PLA (5.10 to 4.97 ppm and 1.52 to 1.48 ppm) obtained after this reaction were different than that of pure PLLA and in the form of multiplets. This could be attributed to the junction between lactide and TMC units, and could be observed for the characteristic PTMC signals as well (4.18 and 1.99 ppm), indicating of the potential statistical nature of the copolymer.

With similar conditions using CNCs as the co-initiator, the same conversion for both monomers could be calculated. When increasing the ratio of PTMC, the conversion increased to reach almost full conversion for both monomers. Interestingly, conversion of lactide on PTMC-grafted CNCs

was much faster than on unmodified cellulose with TBD. When performing a reaction with a majority of lactide however, the opposite was observed and the conversion after five hours was much lower at 40% for TMC and no conversion observed for lactide.

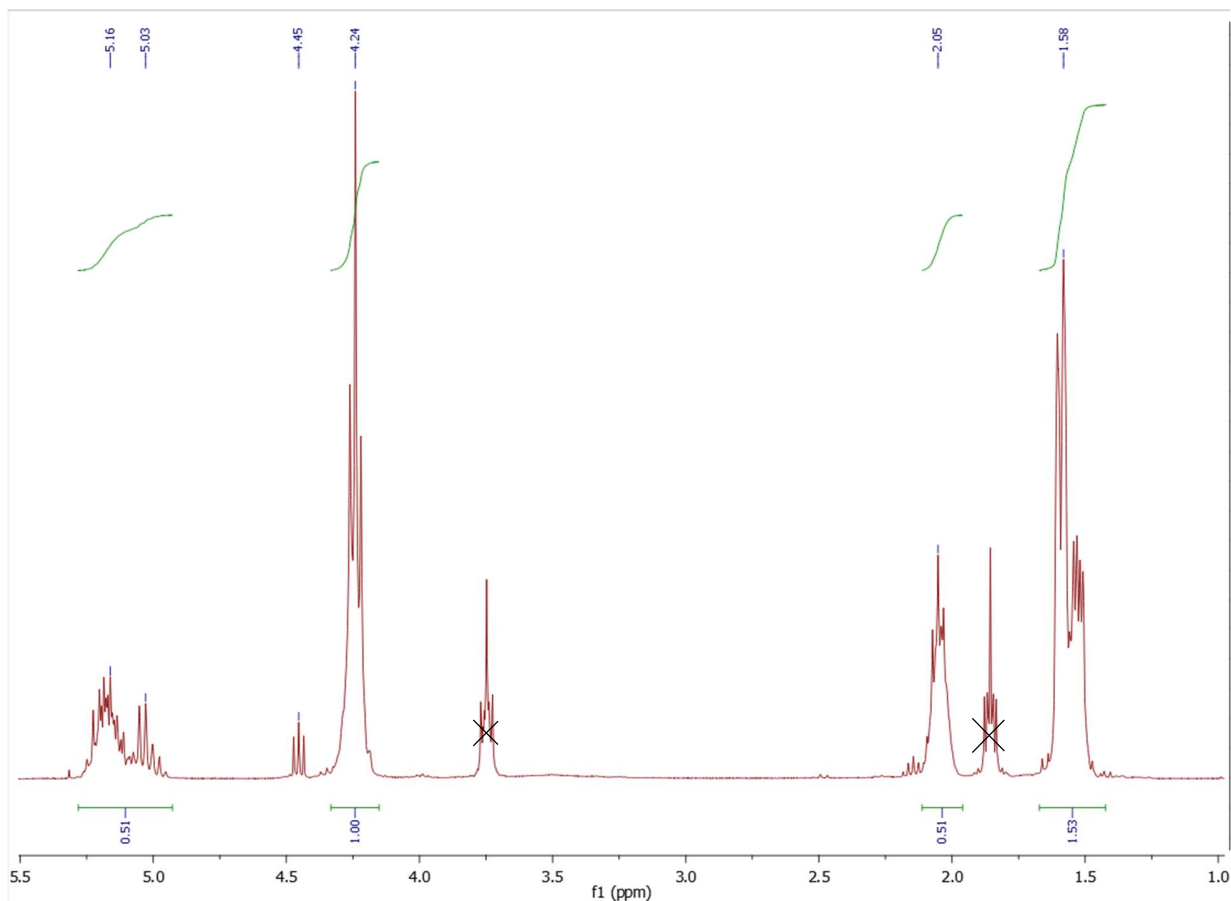


**Figure 66:** <sup>1</sup>H NMR spectra of the crude mixture obtained after equimolar reaction of TMC and *L*-lactide with BnOH as initiator (entry 8, **Table 17**) TBD and Toluene at 110°C for 60 seconds in CDCl<sub>3</sub> (300 MHz). Crossed signals correspond to THF as the NMR can be carried out right after quenching of the reaction.

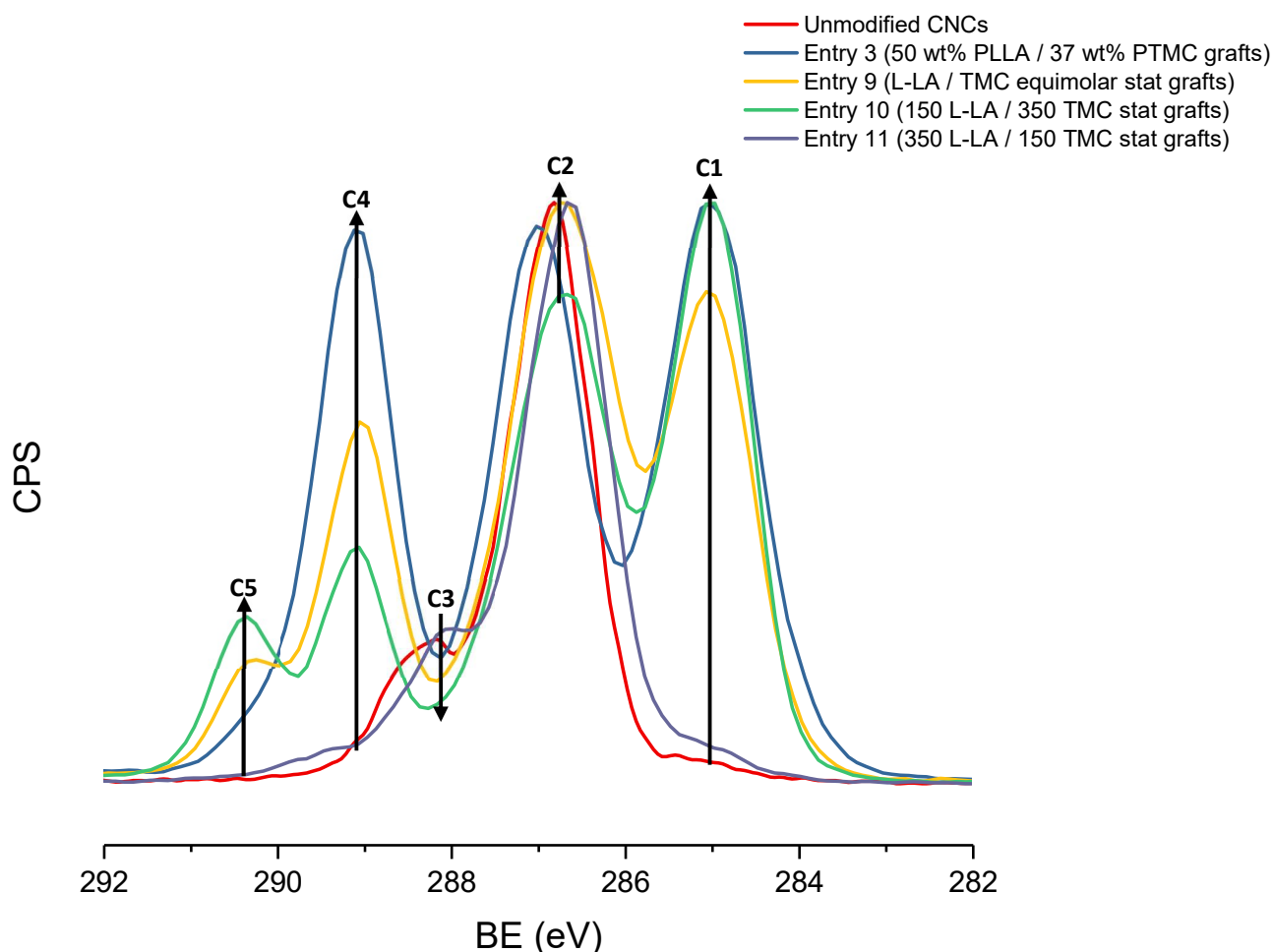


**Figure 67:** Carbon 1s X-ray photoelectron spectroscopy (XPS) normalized spectrogram of unmodified CNCs and P(*L*-LA-*stat*-TMC) grafted CNCs. Modified CNCs corresponding to entry 9 to 11 in **Table 17** and entry 3 in **Table 16**.

For the XPS of the grafts formed with both monomers present at the same time, the surface composition of the modified CNCs was quite different (**Figure 67**). For the equimolar mixture (entry 9), both ester (C4) and carbonate (C5) moieties could be observed, but the OC-O contribution of cellulose found on either side of the  $\beta$ -(1-4) glucosidic bonds was not well defined, showing once more that the graft covered most if not all of the surface of the CNCs. Compared to the block copolymer described in **Figure 64**, the ratio of the contribution C5/C4 was more important, showing the likeliness of a more statistical copolymer composition, with possibly more lactide units integrated in the surface grafts as the ester contribution was higher than the carbonate one. When using a higher ratio of TMC/LLA (entry 10), the surface composition was slightly different, with more carbonate contribution (C5) compared to the equimolar reaction. However,

lactide signals were still stronger, and the ratio of PTMC/LLA units was close to 1, indicating an almost equimolar composition of the copolymer on the surface of the CNCs. The last reaction done, this time with a TMC/LLA ratio of 3/7, gave a material with a composition close to that of unmodified CNCs, showing very little grafting, as expected due to the low conversion of monomers for this reaction. On the contrary, attempts at grafting statistical copolymer of PTMC and PLLA showed a surface composed of both monomer units. This was a good indication of the success of these reactions and of the nature of the copolymers grafted on the surface of the CNCs.

For the statistical grafts on CNCs, a slightly different FT-IR spectra was obtained, likely due to the difference in ratio of PTMC/PLLA grafted after this reaction (**Figure 65**).

#### VI.2.1.3. Differential scanning calorimetry (DSC)

DSC analysis was also performed on a variety of materials to determine their glass transition temperature as well as the presence or absence of crystallinity (as PLLA is usually a semi-crystalline polymer on its own). As can be seen in **Figure 68**, unmodified CNCs showed no signals despite their crystalline nature, due to their degradation temperature being lower than their melting point (around 250 °C for the degradation). When grafted with poly(trimethylene carbonate), a  $T_g$  appeared in the DSC trace. For PLLA-grafted CNCs, a similar  $T_g$  between the non-grafted polymer and PLLA-grafted CNCs was found as well (around 60 °C), however crystallinity of PLLA was not observed on the grafted CNCs. This would indicate that the brush copolymer formed by grafting PLLA was not able to crystallize, possibly due to restricted chain mobility as a result of attachment to the CNC surface.

In order to characterize the copolymers, the miscibility of PLLA and PTMC was evaluated by making and characterizing a blend of both polymers (50/50 wt% of a PTMC of 30,000 g.mol<sup>-1</sup> and a PLLA of 40,000 g.mol<sup>-1</sup>) (**Figure 69**). For this sample, the glass transition temperature of both polymers was measured to be -17 °C for PTMC and 54 °C for PLLA. These values are close to those for both polymers characterized separately, but a slight decrease of the  $T_g$  was noticed for PLLA, which could indicate a partial, yet low miscibility of both polymers.

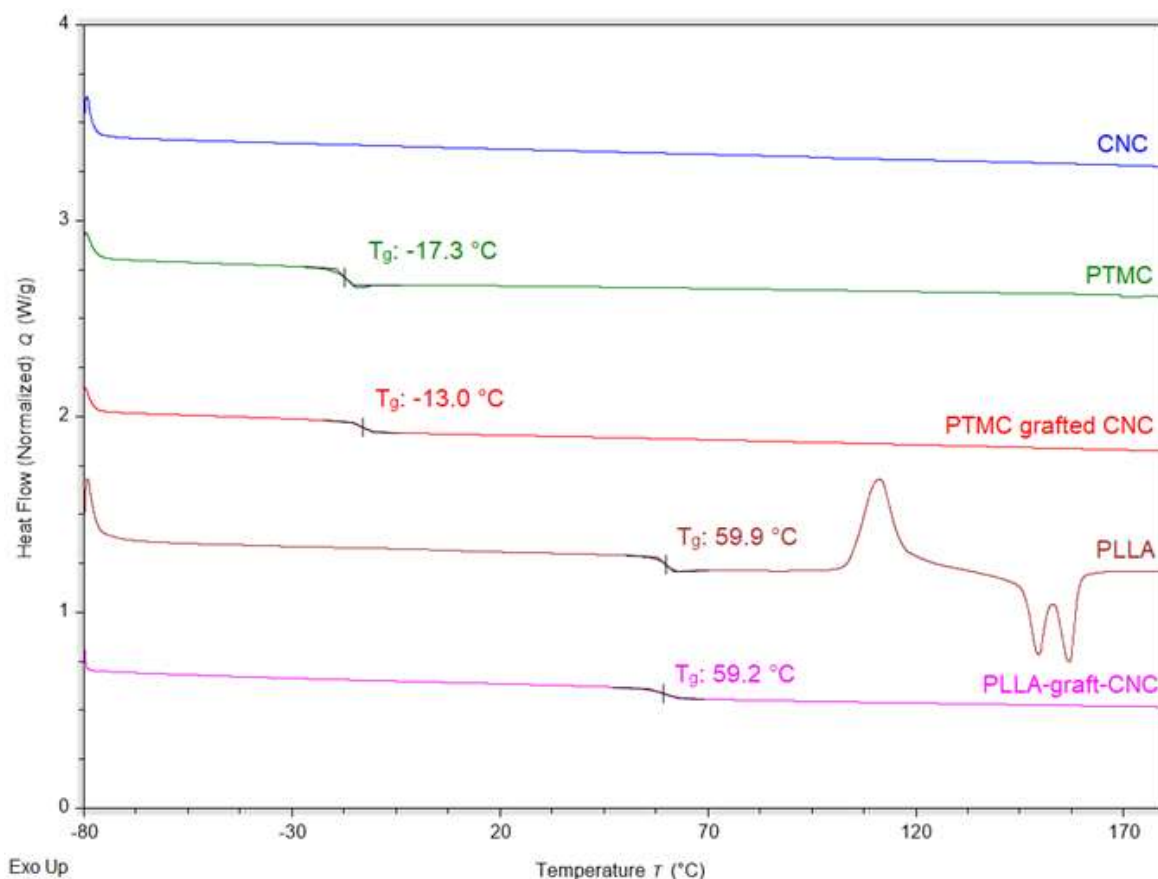


**Figure 68:** DSC thermograms of PTMC, PLLA, unmodified CNCs, and grafted CNCs between -80°C and 180°C.

Interestingly, the melting of PLLA could still be observed. In the case of a PTMC-block-PLLA (**Figure 69**), two glass transition temperatures could still be observed as was expected for a block copolymer with not fully miscible phases. However, an increase in the  $T_g$  of PTMC could be observed at -10 °C, whereas the  $T_g$  of PLLA was decreased to 40 °C. Despite this change in the glass transition temperature observed, the crystallinity of the PLLA block is still visible with a melting peak around 110 °C, which should be noted is also lower than that of pure PLLA (at 120 °C). Thus, it seemed that in these conditions, there was partial miscibility of the two polymers.

A modified cellulose with PTMC and PLLA block was then characterized (corresponding to entry 3 in **Table 16**), and some important differences could be noticed with the non-grafted copolymer. The first thing observed was the absence of a melting point, the rigidity of the cellulose nanocrystals potentially preventing PLLA to crystallize, as was seen for PLLA-grafted CNCs. As for the glass transition temperature of the copolymer-grafted CNCs, signs of both PTMC and PLLA

$T_g$  could be observed around  $-8\text{ }^\circ\text{C}$  and  $62\text{ }^\circ\text{C}$  respectively, which would correspond to the two polymers with partial miscibility (**Figure 69**). Interestingly, the  $T_g$  signal were not as clear as for the non-grafted copolymer. While indicative of the likely presence of a block structure, this could indicate a complex microstructure for the product obtained.

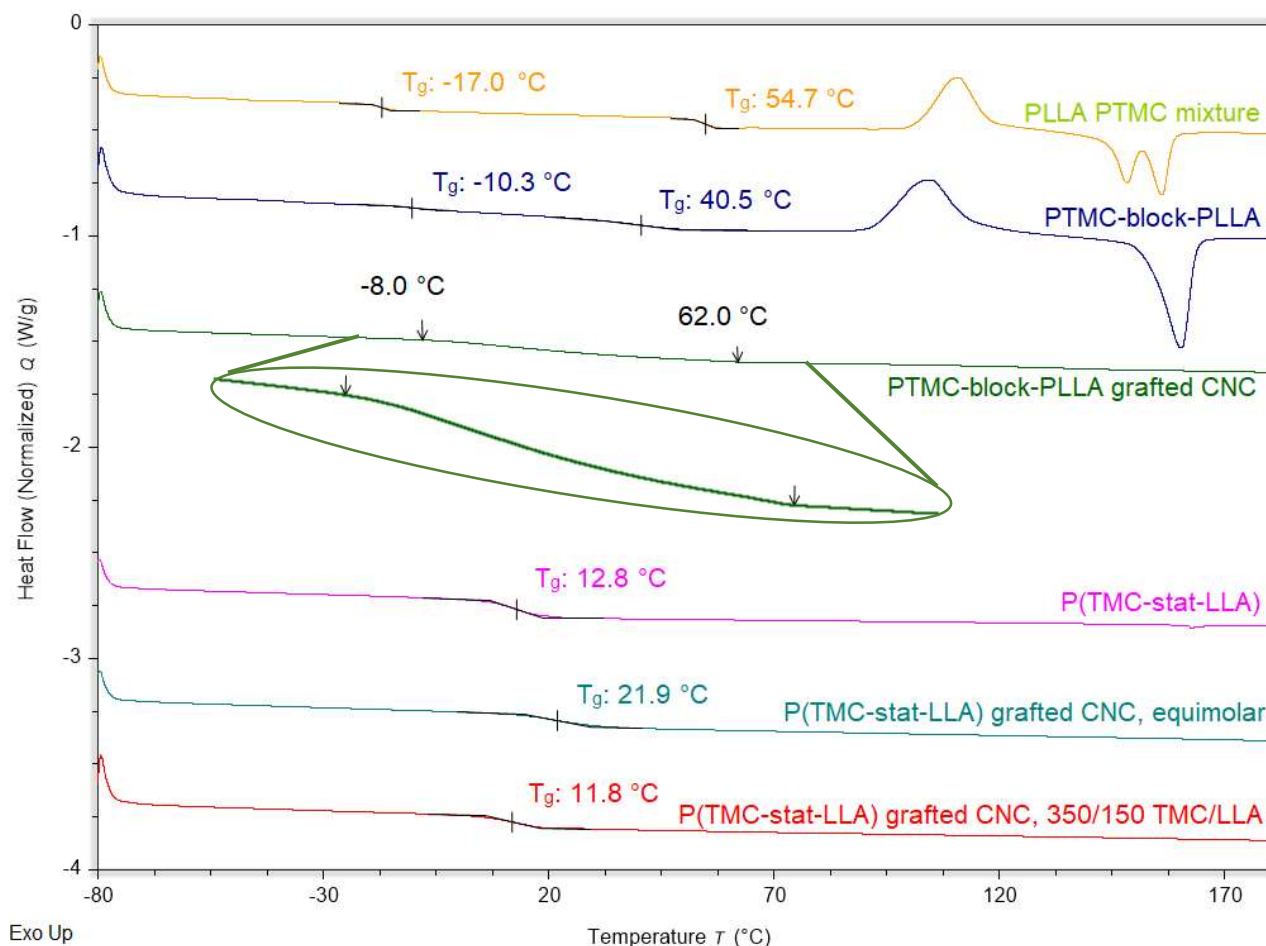


**Figure 69:** DSC thermograms of PTMC, PLLA, unmodified CNCs, and grafted CNCs between  $-80\text{ }^\circ\text{C}$  and  $180\text{ }^\circ\text{C}$ .

Further DSC analysis was performed in order to confirm the block structure of the modified CNCs and to compare the material property with statistical copolymers of PTMC and PLLA. As shown in **Figure 69**, a copolymer obtained by adding both monomers at the beginning of the reaction in equimolar proportion (entry 8) has a  $T_g$  around  $12\text{ }^\circ\text{C}$ , situated between that of both PTMC and PLLA, as expected for a statistical copolymer. The lack of melting peak for PLLA is also quite typical as long chains constituted of only lactide units are unlikely to be present, therefore preventing the crystallization of PLLA. For the similar reaction that was performed with CNCs as the co-initiator, a similar thermogram is obtained, but the  $T_g$  measured is again higher, likely due

to the rigidity of the CNCs the polymer chains are grafted onto. The CNCs produced with a higher ratio of PTMC/PLLA were also characterized, and their glass transition temperature was found to be lower, confirming the presence of more TMC units in the copolymer. The thermograms of the different copolymers and copolymer-grafted CNCs showed different characteristics for the different types of modified CNCs. Coupled with all the analyses described previously, this gives some good indications of having successfully grafted block and statistical copolymers on the surface of cellulose nanocrystals.

#### VI.2.1.1. Degrafting / depolymerization of the modified CNCs

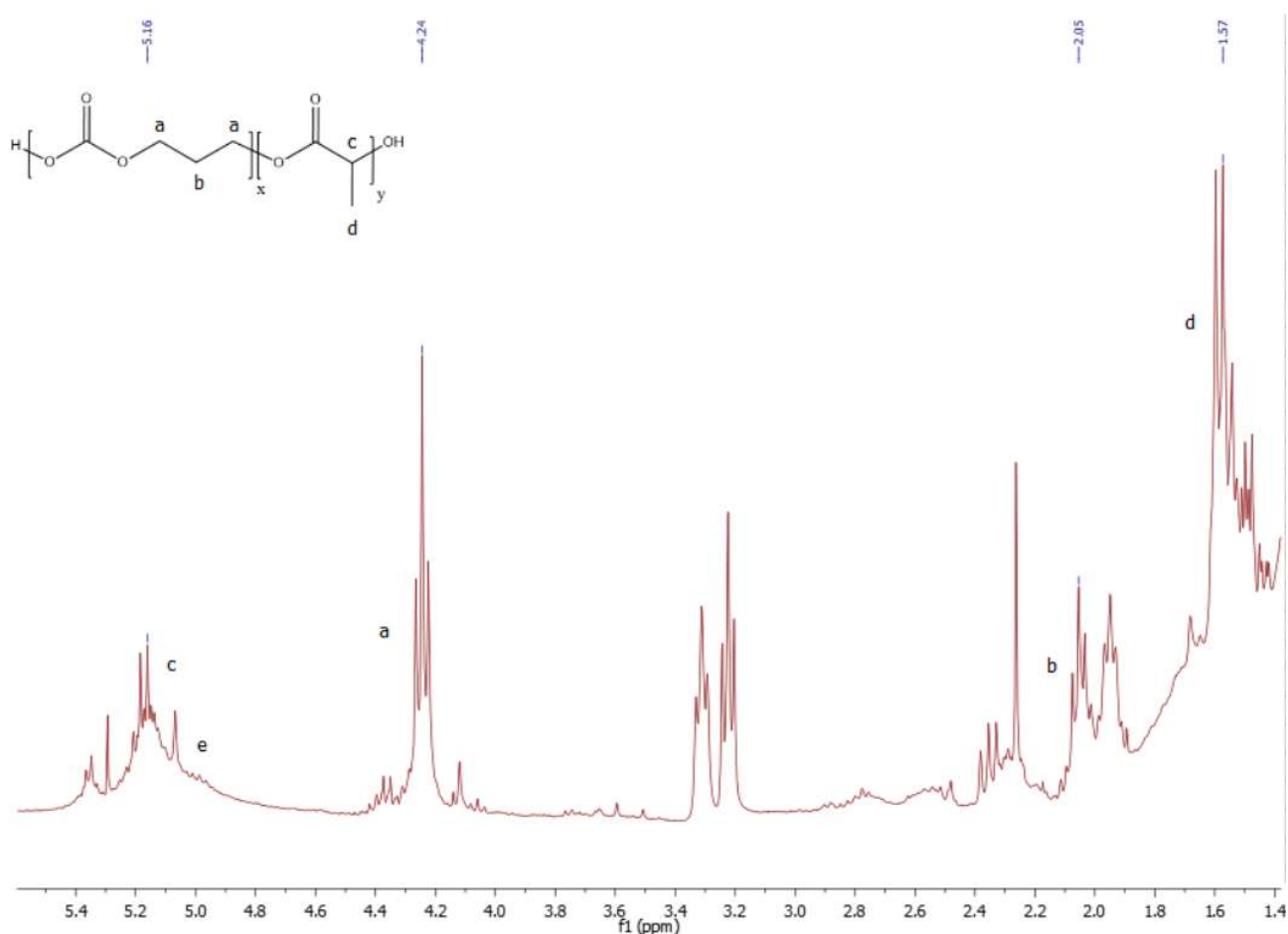


**Figure 70:** <sup>1</sup>H NMR spectra of the crude mixture of grafted CNCs (corresponding to entry 7, **Table 16**) in the presence of TBD and toluene at 110°C for 60 seconds in CDCl<sub>3</sub> (300 MHz).

In order to confirm the structure of the copolymers hypothesized after DSC, XPS and FT-IR analysis, NMR analysis were also performed. However due to the insoluble nature of cellulose nanocrystals, analyses were performed on polymer obtained through a degrafting /

depolymerization reaction of the modified cellulose. TBD has been reported before to be able to depolymerize various polyesters<sup>166</sup> and polycarbonates<sup>295</sup> at high temperatures, therefore a similar reaction was performed on grafted cellulose to attempt a de-grafting of the copolymers on the surface of CNCs. After the cellulose was separated from the rest, proton NMR was performed in  $\text{CDCl}_3$ .

In the case of the copolymer that was grafted by doing 2 different reactions (**Figure 70**): first PTMC grafting and purification, then PLLA grafting (entry 16), the presence of PLLA could be seen around 5.16 ppm (peak “c”) as well as 1.57 ppm (peak “d”), respectively for CH and  $\text{CH}_3$ . Similarly, typical PTMC signals were observed at 4.24 ppm (peak “a”) and 2.05 ppm (peak “b”). In the case of signal “e”, belonging to lactide monomer unit linked to a TMC monomer unit, this signal was this time much smaller than the one described before for the statistical copolymer, which confirmed the block tendency of the grafts obtained on CNC through a two-steps method. It is important to note however that transesterification / transcarbonatation reactions can also occur in the course of this degrafting / depolymerization reaction.

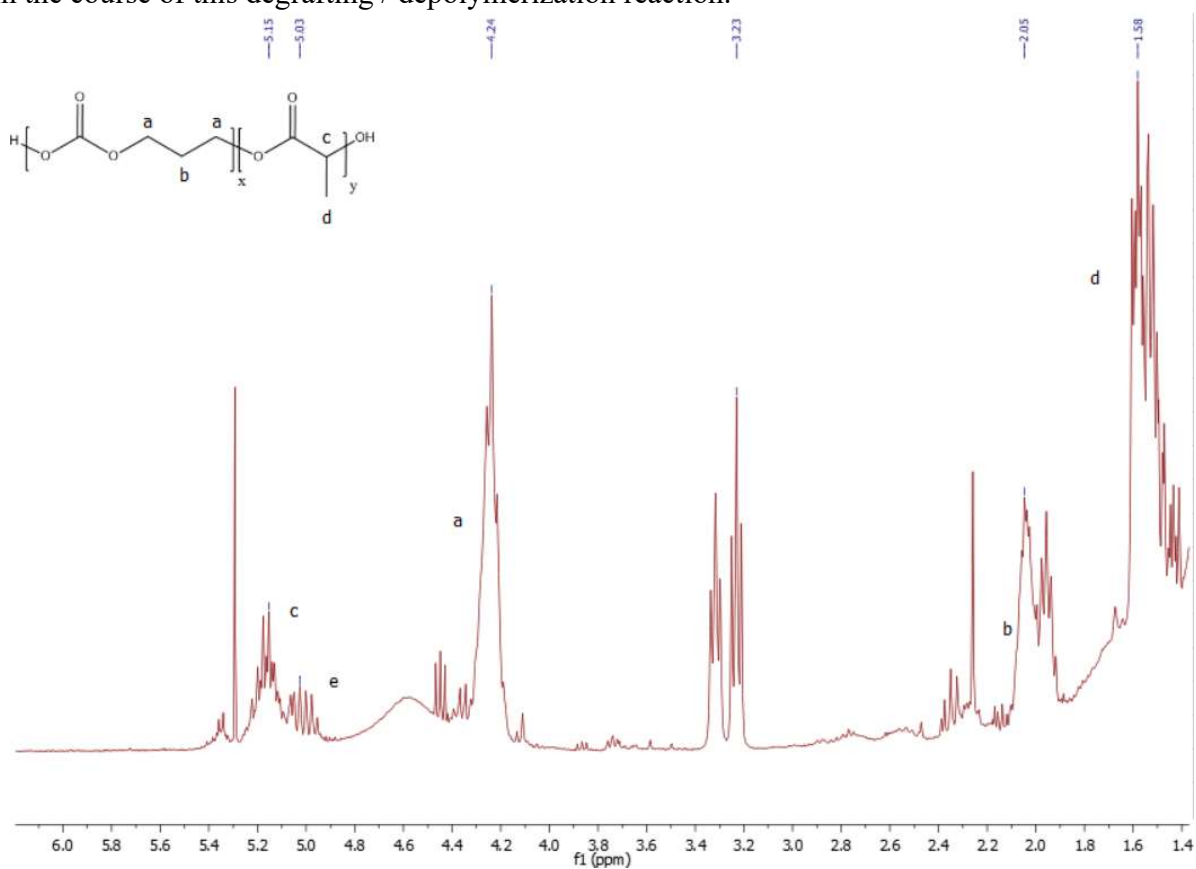


**Figure 71:**  $^1\text{H}$  NMR spectra of the crude mixture of grafted CNCs (corresponding to entry 9, **Table 17**) in the presence of TBD and toluene at  $110^\circ\text{C}$  for 60 seconds in  $\text{CDCl}_3$  (300 MHz).

As shown in **Figure 71**, the degrafting of the chains obtained from the polymerization reaction on CNCs with equimolar ratios of TMC and PLLA (entry 9), gave polymers that could be separated successfully using TBD as well. However, signals of both polymers are not as well defined as could be expected, and some widening of the peaks can be observed. Additionally, peak “e” can be observed around 5.02 ppm, which can be attributed to CH peaks from lactide monomer units that are linked to a TMC monomer unit. When integrating both peak “c” and peak “e”, a ratio of 2/1 is measured, indicating that many of the lactide units are linked to a carbonate unit, thus giving another indication that this grafted copolymer could be a statistical and not a block.

Overall, all the characterization methods used, coupled with the difficult grafting of PLLA on unmodified CNCs with TBD, give strong indications that both statistical and block copolymers of PTMC and PLLA can be grafted on CNCs using TBD. Moreover, while the blocks of PLLA could be attached to the CNCs directly rather than the PTMC units, this was shown to be very unlikely, in particular due to the very different composition observed on the surface by XPS and deeper in the material by FT-IR.

#### VI.2.2. Poly(methyl methacrylate) (PMMA) grafting with phosphazene

##### **Grafting of PMMA with phosphazene base**

While most of the experiments described here focused on producing copolymers with trimethylene carbonate, *L*-lactide (*L*-LA) and  $\delta$ -valerolactone ( $\delta$ -VL), some other monomers available were tested and despite the lack of success, these attempts will first be presented before diving into the more successful results. Due to the overall low success of these attempts at grafting, characterization has not been as thorough, but some analyses will be provided.

As can be seen in **Table 18**, the performance of a phosphazene, namely tBuP<sub>4</sub>, was tested in the presence of modified and unmodified cellulose nanocrystals in order to obtain poly(methyl methacrylate) (PMMA) grafts. This catalyst has been studied before and was reported to polymerize MMA under different conditions, therefore it seemed a good candidate for grafting<sup>296</sup>. In addition, while most of the work presented was focused on ROP and MMA is polymerized *via* a radical polymerization, tBuP<sub>4</sub> has been reported to be able to make copolymer with cyclic lactones<sup>139</sup>.

**Table 18:** Ring-opening polymerization of MMA initiated from the surface of CNC using tBu-P<sub>4</sub>, at 25 °C in THF.

Entry	MMA / tBu-P <sub>4</sub> / OH <sup>[a]</sup>	Time (min)	Grafting by <sup>[b]</sup> (wt%)	Conversion <sup>[c]</sup> (%)	Grafting Yield <sup>[d]</sup> (%)	M <sub>n</sub> non-grafted polymer (g.mol <sup>-1</sup> )	Đ <sub>M</sub> <sup>[e]</sup>
12.	100/ 1.6 / 10	15	9	99	1.6	29,500	3.4
13.	100/ 1.6 / 10	30	7	99	1.2	25,600	2.9
14.	100/ 1.6 / 10	60	9	99	1.5	43,100	2.9
15.	100/ 0.5 / 10	15	3	99	0.5	36,200	2.8
16.	100/ 0.1 / 10	15	1	97	0.2	36,800	2.7
17.	100/ 1.6 / 5	15	13	82	1.5	58,200	2.5
18. <sup>[f]</sup>	100 / 1 / 10	15	0	99	0.0	n.d.	n.d.
19. <sup>[g]</sup>	100 / 1 / 10	5	0	99	0.0	32,300	3.3

*[a]* Calculated using moles of glucose rings (162.14 g/mol) and considering 1 primary OH per ring. *[b]* Determined by elemental analysis (calculation based on hydrogen content (%H) and carbon content (%C)) and corrected for adsorbed water using TGA. wt% of new grafts, pre-modifications not included. *[c]* Calculated via <sup>1</sup>H NMR to determine monomer/polymer ratio and corrected to include monomer grafted. *[d]* Ratio of monomer grafted to initial monomer. *[e]* Dispersity of the non-grafted polymer determined by SEC. *[f]* Reaction performed on 73% PTMC-grafted CNC (by weight). *[g]* Reaction performed on 59% PTMC-grafted CNC (by weight).

As is seen in entries 12-14, polymerization was successful in the presence of cellulose nanocrystals, however a poor control can be noted by the relatively high dispersity of the non-grafted polymer produced during the reaction (>2). With regards to the grafting on the surface on CNCs, elemental analyses revealed a relatively low amount of grafting for all experiments performed rarely exceeding 10%. The conversion for most reactions was total as no more than traces amount of monomer could be detected by NMR after 15 minutes, and longer reaction times did not improve the grafted amount significantly. As tBu-P<sub>4</sub> is a catalyst with a very high activity, lowering catalyst loading was tested as well, with ratios as low as 100/0.1 (monomer/catalyst) still giving a near full conversion after 15 minutes of reaction time. Grafting content on the CNCs did not improve with lowering the catalyst loading. Lastly, a similar reaction was performed with a lower amount of CNCs, resulting in a higher grafting of 13% (entry 17). However this improvement was too low, and lowering the amount of CNCs is equivalent to doubling the amount of monomer used, therefore the grafting yield obtained did not increase.

To confirm the elemental analysis results, XPS was performed on the modified CNCs corresponding to entry 17. As can be seen in **Figure 72**, the surface of the nanocrystals after modification changed. The contribution C1 and C4 corresponding respectively to the C1s C-C and OC=O signals increased significantly, confirming the presence of MMA moieties on the surface.

However, due to the low amount of grafting, cellulose signals (C2 and C3 corresponding to C-O and O-C-O respectively) could still be observed, as the thickness of the grafted polymer was not sufficient to fully cover the surface of the nanocrystals from the probing X-Ray beam. The observations made with XPS were also confirmed by FT-IR, where a C=O stretching band could be observed around  $1750\text{ cm}^{-1}$  region.

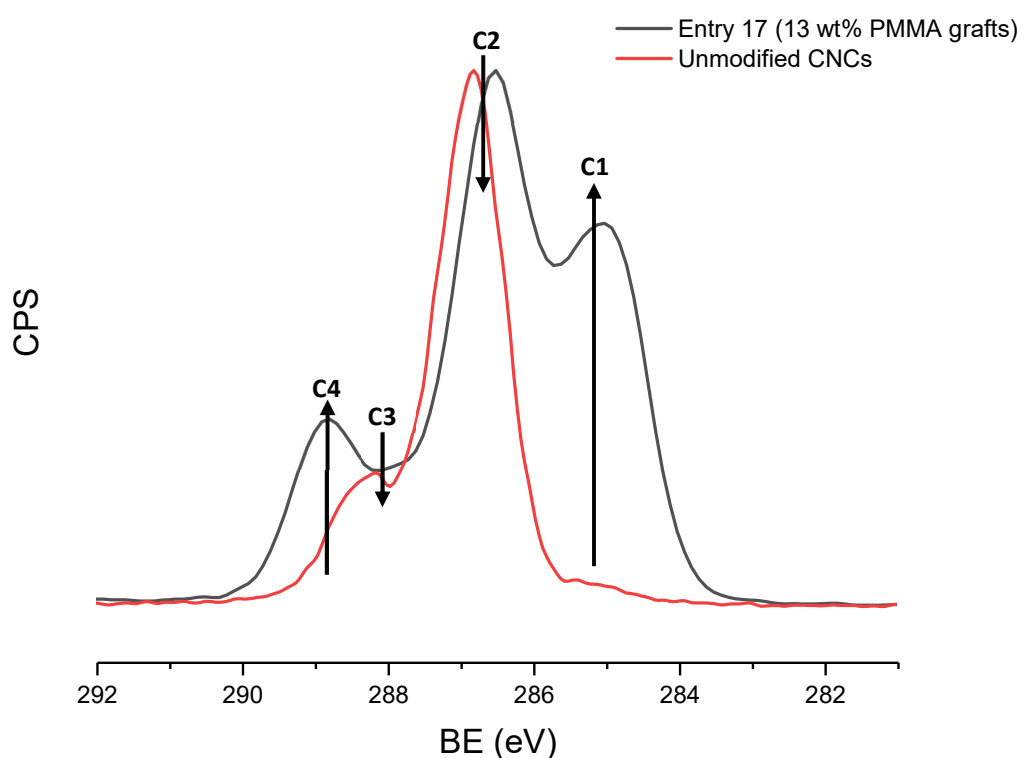


**Figure 72:** Carbon 1s X-ray photoelectron spectroscopy (XPS) normalized spectrogram of unmodified CNCs and PMMA-grafted CNCs. Grafted CNCs corresponding to entry 17 in **Table 18**.

Considering the difference in reactivity between the hydroxy groups available on unmodified cellulose and the hydroxy group chain ends of a polycarbonate chain, additional reactions were performed on already modified, purified, and dried CNCs. MMA was polymerized in the presence of the poly(trimethylene carbonate)-grafted CNC under similar conditions as previously described (entry 18 and 19). PMMA grafts were not observed on the modified cellulose by elemental analysis, and the non-grafted polymer formed had a high dispersity (3.3) and similar molecular weight to the one produced in the presence of unmodified CNCs ( $>30,000$ ). Due to the high activity of this catalyst, it seems likely that the polymerization occurred too quickly without cellulose playing a

part in it, leading to a quick conversion of all the monomer into homogeneous dissolved PMMA. Therefore, this system does not seem well suited for a “grafting from” approach of PMMA on cellulose nanocrystals, especially when compared to a radical approach such as ATRP<sup>297</sup>.

### VI.2.1. Poly( $\epsilon$ -caprolactone) (PCL) grafting

Grafting of poly( $\epsilon$ -caprolactone) was also tested using TBD as previously described for PTMC. Reactions from unmodified CNCs were tried at first, but due to the low reactivity of  $\epsilon$ -caprolactone in these conditions, conversion of the monomer was very slow and did not lead to particularly interesting materials<sup>141</sup>. However, for reactions initiated from PTMC-grafted CNCs (obtained as described in Chapter V), conversion of the lactone was found to be faster. As can be seen in

**Table 19**, 61% conversion was reached after 16h, compared to 5% after 1 hour. However, non-grafted polymer could not be isolated by precipitation for either of the reactions, likely due to a low molecular weight. Despite the important increase in conversion, the increase in grafted amount determined by elemental analysis was not very significant, and only 8% of poly( $\epsilon$ -caprolactone) was grafted to the CNCs. Reactions over longer periods of time were also tested, but for these reactions in particular, technical difficulties were encountered during the separation of the non-grafted polymer and the CNCs, which is why the results are not reported here.

**Table 19:** Ring-opening polymerization of  $\epsilon$ -CL initiated from the surface of PTMC-grafted CNCs (20: 73 wt%, 21: 59%)

Entry	CL / TBD / OH <sup>[a]</sup>	Time	Grafting <sup>[b]</sup>	Conversion <sup>[c]</sup>	Grafting Yield <sup>[d]</sup>
		(h)	wt% PCL / PTMC	(%)	(%)
20.	500 / 1 / 50	1	5 / 69	5	2.7
21.	500 / 1 / 50	16	8 / 54	61	3.0

[a] Calculated using moles of glucose rings (162.14 g/mol) and considering 1 primary OH per ring. PTMC graft content taken into consideration. [b] Determined by elemental analysis (calculation based on hydrogen content (%H) and carbon content (%C)) and corrected for adsorbed water using TGA. PTMC content based on analysis done on the starting modified CNCs [c] Calculated via <sup>1</sup>H NMR to determine monomer/polymer ratio and corrected to include monomer grafted. [d] Ratio of monomer grafted to initial monomer.

The grafted cellulose sample obtained for reaction 21 was also investigated by XPS to confirm the presence of PCL grafts.

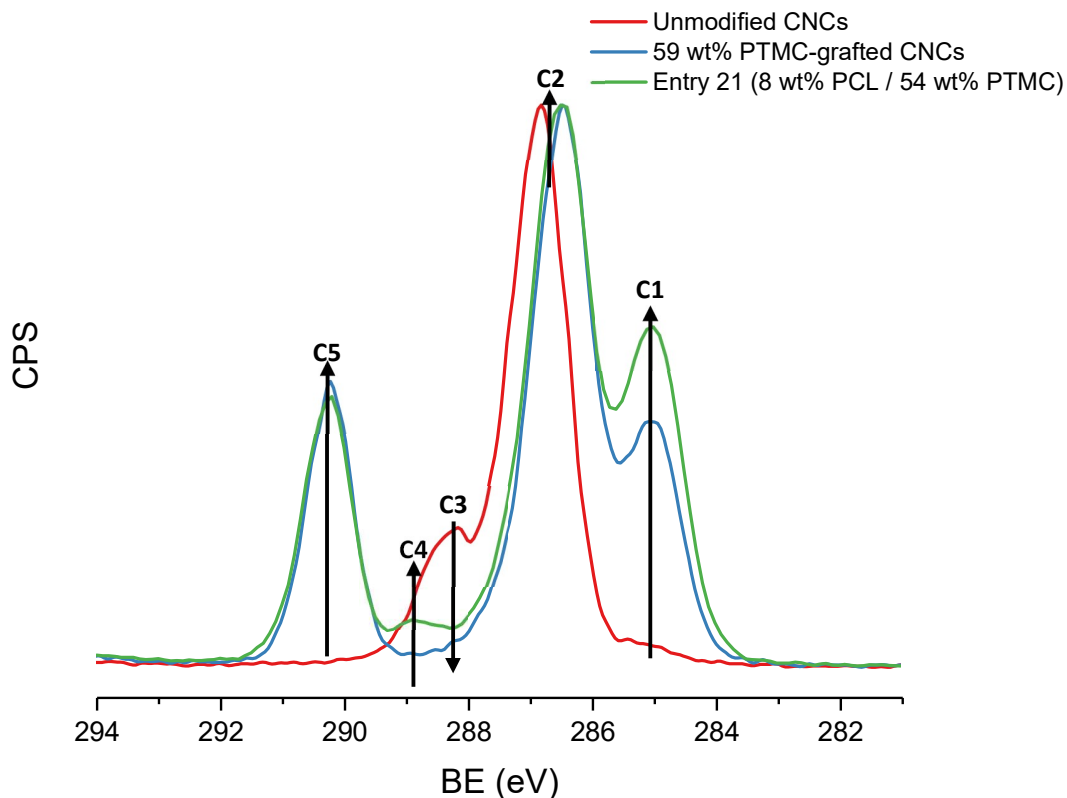


**Figure 73:** Carbon 1s X-ray photoelectron spectroscopy (XPS) normalized spectrogram of unmodified CNCs, PTMC-CNCs and PCL grafted PTMC-CNCs. PCL-grafted CNCs corresponding to entry 21 in **Table 19**.

As can be seen in **Figure 73**, the cellulose obtained after the grafting of PCL has a very similar surface structure as that of PTMC-grafted cellulose (the starting material), with a high C-C (C1), C-O (C2), and OC(O)=O (C5) contribution. Due to the low amount of grafting, the surface of the modified CNCs is still mostly composed of polycarbonate, hence the similarity in the C1s signal appearance. However, the presence of PCL can be seen as the signal C4, corresponding to OC=O, starts to appear, confirming the results obtained in elemental analysis.

Lastly, DSC was used to measure the glass transition temperature of the modified CNC with PCL (**Figure 74**). As the CNC- grafted with PCL are still mostly composed of PTMC, the  $T_g$  measured was close to that of PTMC-grafted CNCs (-9 to -13 °C as seen in **Figure 57**). However, a small decrease is observed after the reaction, which could be an indication of the  $\epsilon$ -caprolactone moieties, as PCL has a much lower  $T_g$  (-60 °C)<sup>298</sup> than PTMC, hence a small amount could be enough to lower the  $T_g$  from -13.1 to -14.8 °C if a miscible blend is obtained under such conditions.

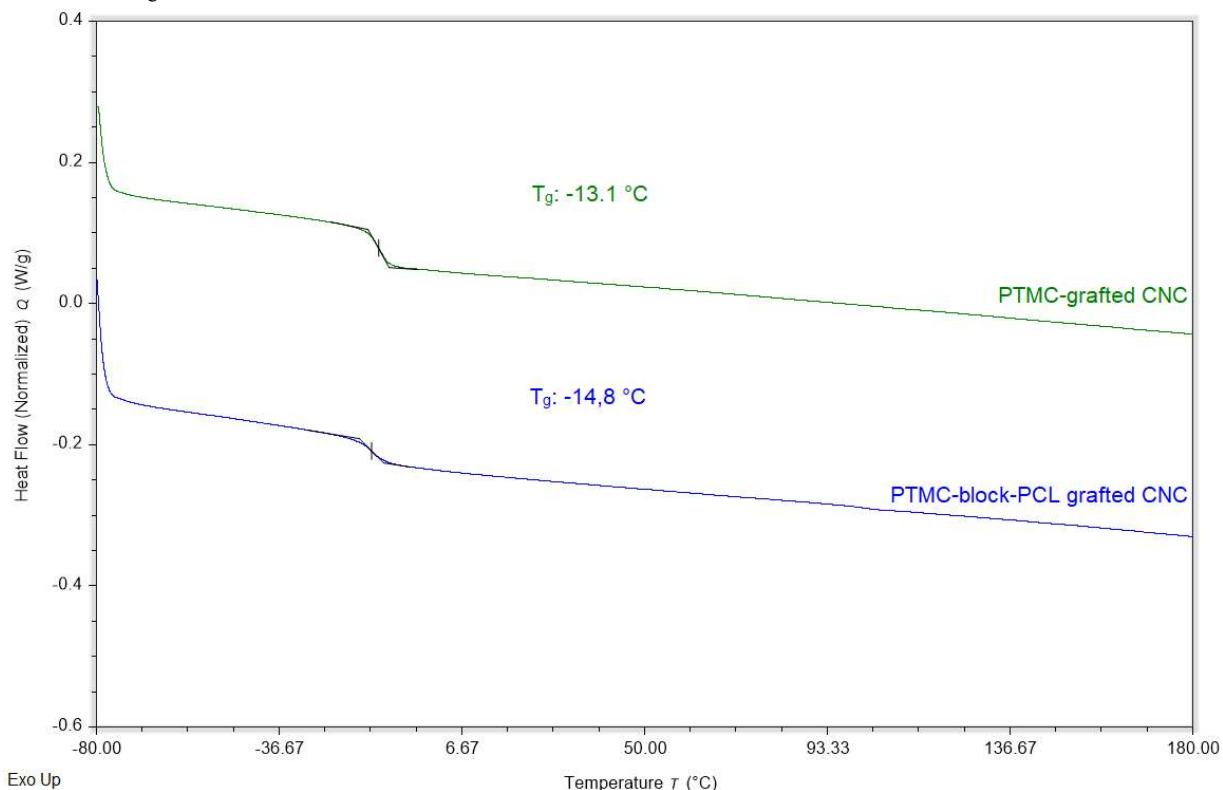


**Figure 74:** DSC thermograms of PTMC-grafted CNCs and PCL-grafted PTMC-CNCs between -80°C and 180°C.

### VI.2.2. PTMC/PVL Copolymers

Due to the difficulties encountered for grafting PCL,  $\delta$ -valerolactone was tested to obtain polymer and copolymer grafts on CNCs due to its higher reactivity with TBD<sup>141</sup>. Moreover, poly( $\delta$ -valerolactone) (PVL) shares many characteristics with PCL such as biocompatibility.

**Table 20:** Ring-opening copolymerization of  $\delta$ -VL on the surface of unmodified and PTMC-grafted CNCs using TBD, at 25 °C in THF.

Entry	TMC / $\delta$ -VL / TBD / OH <sup>[a]</sup>	Time (h)	Grafting by weight <sup>[b]</sup> wt% PVL / PTMC	Conversion <sup>[c]</sup>	Grafting Yield <sup>[e]</sup>	$M_n$ non-grafted polymer	$\mathcal{D}_M$ <sup>[d]</sup>
				(%)	(%)	(g.mol <sup>-1</sup> )	
22.	0 / 500 / 0.5 / 50	6	0 / 0	3	0.0	n.d.	n.d.
23.	0 / 500 / 0.5 / 50	72	37 / 0	97	23.5	75,100	2.1
24. <sup>[c]</sup>	0 / 500 / 1 / 50	6	16 / 50	98	13.5	n.d.	n.d.
25.	250 / 250 / 1 / 50	6	n.d.	47 $\delta$ -VL, 95 TMC	n.d.	23,000	1.8

[a] Calculated using moles of glucose rings (162.14 g/mol) and considering 1 primary OH per ring. [b] Determined by elemental analysis (calculation based on hydrogen content (%H) and carbon content (%C)) and corrected for adsorbed water using TGA. [c] Ratio of monomer grafted to initial monomer. [d] Dispersity of the non-grafted polymer determined by SEC. [e] Reaction done with grafted CNCs containing 59 wt% of PTMC.

Grafting on CNCs of PVL only was first tested with TBD. Due to the lower reactivity of this lactone compared to TMC or *L*-LA, a reaction over 6 hours (entry 13) lead to a very low conversion and no grafting on the CNCs. Following this, another reaction was performed over three days to reach near full conversion (97%, 14) at room temperature. For this reaction, a grafting of up to 37 wt% was obtained according to EA and TGA analysis, and a high molecular weight non-grafted polymer was obtained after this reaction (75,100 g.mol<sup>-1</sup>). In comparison, a grafting reaction on 59 wt% PTMC-grafted CNCs was also performed, and near full conversion was obtained in only 6 hours, as opposed to the reaction on unmodified CNCs. Interestingly, this was similar to what was observed with lactide, for which grafting on grafted CNCs with TBD was much faster than on unmodified nanocrystals. The now twice modified CNCs had a PVL content of 16 wt% and 50 wt% PTMC, corresponding to a molar ratio close to 1/3. Lastly, a reaction with both monomers introduced at the beginning was carried out to try to obtain more statistical copolymer grafts, similarly to what was described before with PLLA. As can be seen for entry 25, conversion of TMC was almost total after 6 hours, but less than half of the  $\delta$ -valerolactone was converted. However, this was a much higher conversion than that observed for entry 22, showing that the reactivity in the presence of PTMC-grafted CNCs was much higher than that of unmodified CNCs for this lactone, as was the case for lactide.

XPS analysis was used to get more information on the composition of the modified CNCs and confirm the grafting calculated with elemental analysis (**Figure 75**). For the CNCs grafted with 37 wt% PVL, a small contribution for the OC-O (C3) could be detected, but the surface composition

was mostly that of PVL, with an important C-C (C1) contribution and a characteristic ester signal (C4) confirming the surface modification of the cellulose.

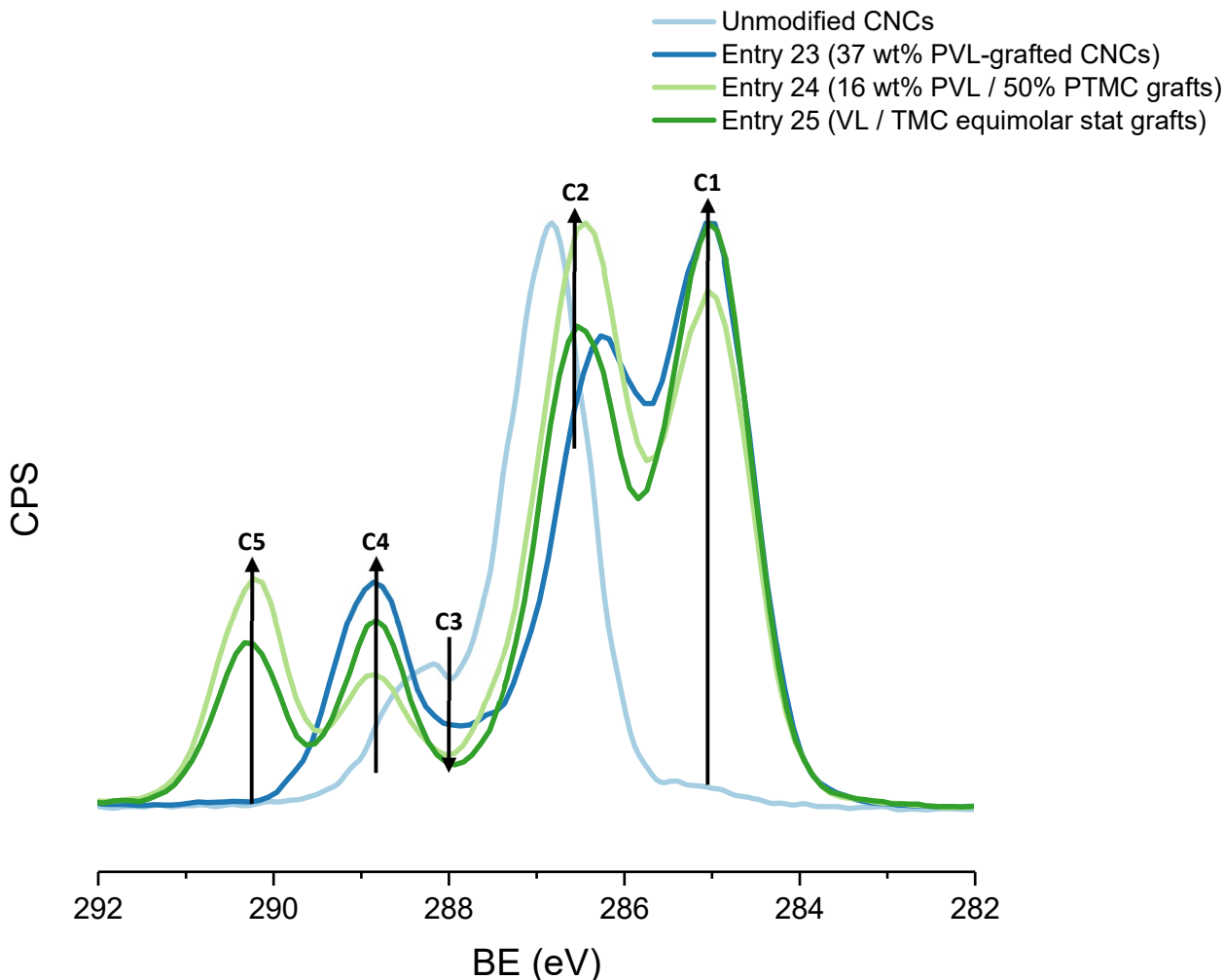


**Figure 75:** Carbon 1s X-ray photoelectron spectroscopy (XPS) normalized spectrogram of unmodified CNCs, PVL and PTMC copolymer grafted CNCs. Modified CNCs corresponding to entry 23 to 25 in **Table 20**.

For the copolymer grafted CNCs corresponding to entry 24, only a small amount of PVL was grafted, and XPS showed a carbonate contribution (C5) stronger than ester contribution (C4). However despite the molar ratio of 1/3 PVL/PTMC, the ratio of C4/C5 signal was 0.7, indicating the presence of PVL grafts mostly on the surface, and the likeliness of PVL blocks grafted onto the PTMC chain. On the other hand, the CNCs modified in a one-step one-pot reaction (entry 25) contained more ester than carbonate on the surface and had a ratio of C4/C7 of 1.4, despite the much higher conversion of TMC. In this case, it is harder to give a conclusion on the structure of the grafts from just XPS characterization. This could indicate a block tendency, with first

integration of a majority of TMC, then  $\delta$ -VL, leading to a surface composition with more ester, or simply be due to a statistical copolymerization with slightly more  $\delta$ -valerolactone content.

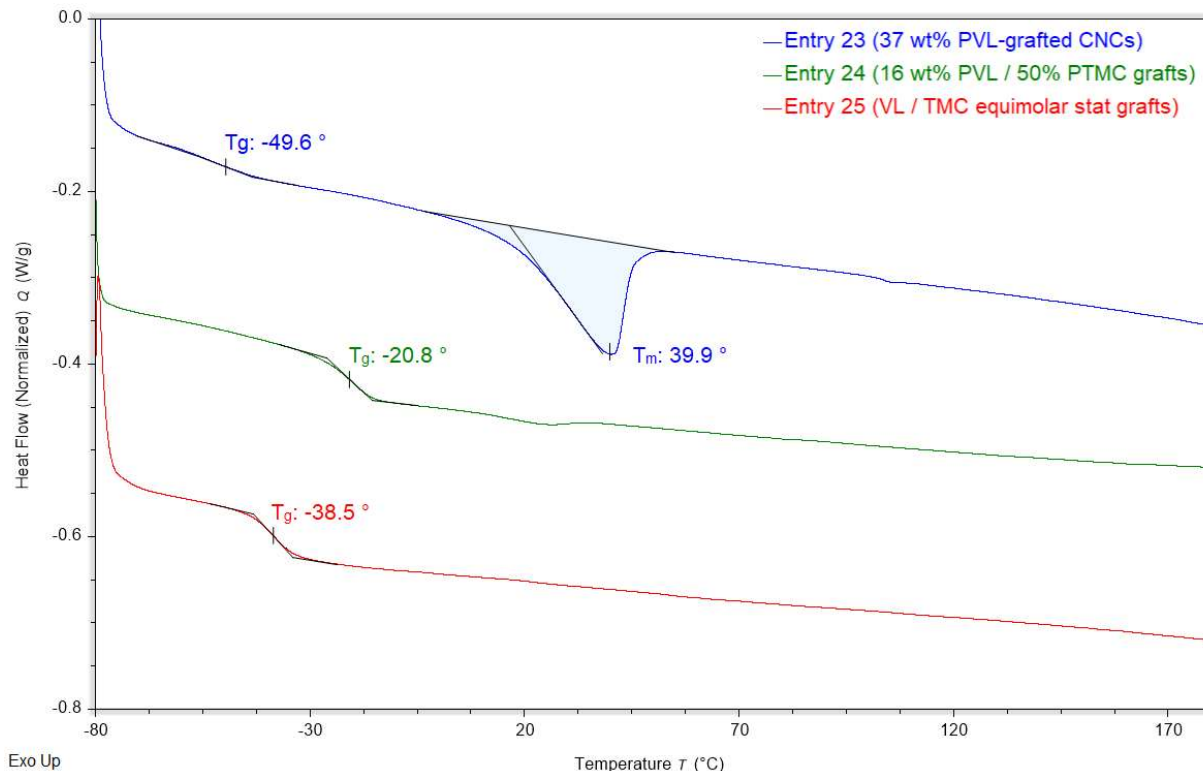


**Figure 76:** DSC thermograms of unmodified CNCs, and PVL/PTMC grafted CNCs between  $-80^{\circ}\text{C}$  and  $180^{\circ}\text{C}$ .

To have more information on the nature of the grafts, DSC of the modified nanocrystals was used once more **Figure 76**. For the PVL-grafted CNCs, a glass transition temperature could be measured at  $-49.6^{\circ}\text{C}$  as well as a melting temperature at  $-39.9^{\circ}\text{C}$ , both values different to value typical for poly( $\delta$ -valerolactone)<sup>299</sup>. The higher value of the  $T_g$  of the graft was similar to previous observations for different polymers grafted on CNCs, however, the presence of a  $T_m$  was more surprising, as other polyesters grafts described previously have not displayed the ability to crystallize. The lower  $T_m$ , similarly to the  $T_g$ , could potentially be attributed to the constraint due to the attachment to the surface of CNCs. For the copolymer made from PTMC-grafted CNCs, the  $T_g$  of PVL was not observed, but the glass transition temperature of PTMC was found at  $-20.8^{\circ}\text{C}$ , a value lower than that of pure PTMC. This could indicate that the presence of a small amount of PVL may not be enough to observe two distinct  $T_g$ 's, and/or to a partial miscibility that lowers the  $T_g$  of the PTMC block. Lastly, the CNCs modified with a mixture of both monomers exhibited a

glass transition temperature at -38.5 °C, potentially indicating the presence of statistical grafts as this  $T_g$  was situated between the  $T_g$  of PTMC and PVL homopolymers, or of partial miscibility.

It is interesting to note that despite their difference in reactivity, the observations made from the grafting of PVL and PLLA are quite similar, with a much easier grafting obtained from PTMC-grafted CNCs than from unmodified CNCs. Similarly, the polymerization of both monomers at once in the presence of CNCs leads to a higher surface content of ester in both cases.

### VI.2.3. PTMC/PLA/PVL terpolymers

Due to the overall successful grafting with different monomers, and copolymer grafts of different nature, some trial experiments were also carried out to obtain different terpolymers containing TMC, *L*-LA and  $\delta$ -VL units. Grafting wt% could not be calculated for any of these modified CNCs due to the unknown composition of the grafts as described previously.

**Table 21:** Ring-opening copolymerization of TMC,  $\delta$ -VL and *L*-LA initiated from the surface of CNCs using TBD, at 25 °C in THF.

Entry	TMC / <i>L</i> -LA / $\delta$ -VL / TBD / OH <sup>[a]</sup>	Conversion %	Time (h)	$M_n$ non-grafted polymer (g.mol <sup>-1</sup> )	$\mathcal{D}_M$ <sup>[b]</sup>
26. <sup>[c]</sup>	0 / 250 / 250 / 0.5 / 50	99 <i>L</i> -LA, 97 $\delta$ -VL	1+5	39,100	4.4
27. <sup>[d]</sup>	0 / 250 / 250 / 0.5 / 50	95 <i>L</i> -LA, 90 $\delta$ -VL	6	16,600	2.0
28.	133 / 133 / 133 / 0.5 / 50	99 PTMC, 99 <i>L</i> -LA, 89 $\delta$ -VL	24	37,600 <sup>[e]</sup>	1.9

[a] Calculated using moles of glucose rings (162.14 g/mol) and considering 1 primary OH per ring. [b] Dispersity of the non-grafted polymer determined by SEC. [c] Reaction done with grafted CNCs containing 59 wt% of PTMC in two steps, initial polymerization of lactide for one hour, then addition of  $\delta$ -VL and polymerization for five hours. [d] Reaction done with grafted CNCs containing 69 wt% of PTMC and simultaneous addition of *L*-LA and  $\delta$ -VL. [e] multimodal signal in SEC

A first reaction was performed using PTMC-grafted CNCs, and PLLA and PVL were grafted as a two-steps one-pot process, with first the addition of lactide, followed by an addition of  $\delta$ -VL one hour later (entry 26). Full conversion was reached using this method, and a high average molecular weight of 39,100 for the non-grafted polymer was obtained. However, the non-grafted polymer did show a multimodal and wide distribution with a dispersity >4. Doing a reaction with both monomers mixed at the beginning also lead to near full conversion, and narrower dispersity of 2 was observed for the non-grafted polymer. Starting from unmodified CNCs, a reaction was carried out by mixing all three monomers with TBD, however due to the low reactivity of both lactide and  $\delta$ -valerolactone with unmodified CNCs, a longer reaction time was used to obtain full conversion.

With this method the non-grafted polymer recovered had a dispersity of 1.9, and a fairly high molecular weight of almost 38,000 g.mol<sup>-1</sup> was obtained. However, a second small peak could be detected, with a very high dispersity (8.8), and possibly a very high average molecular weight (Annex VIII.5).

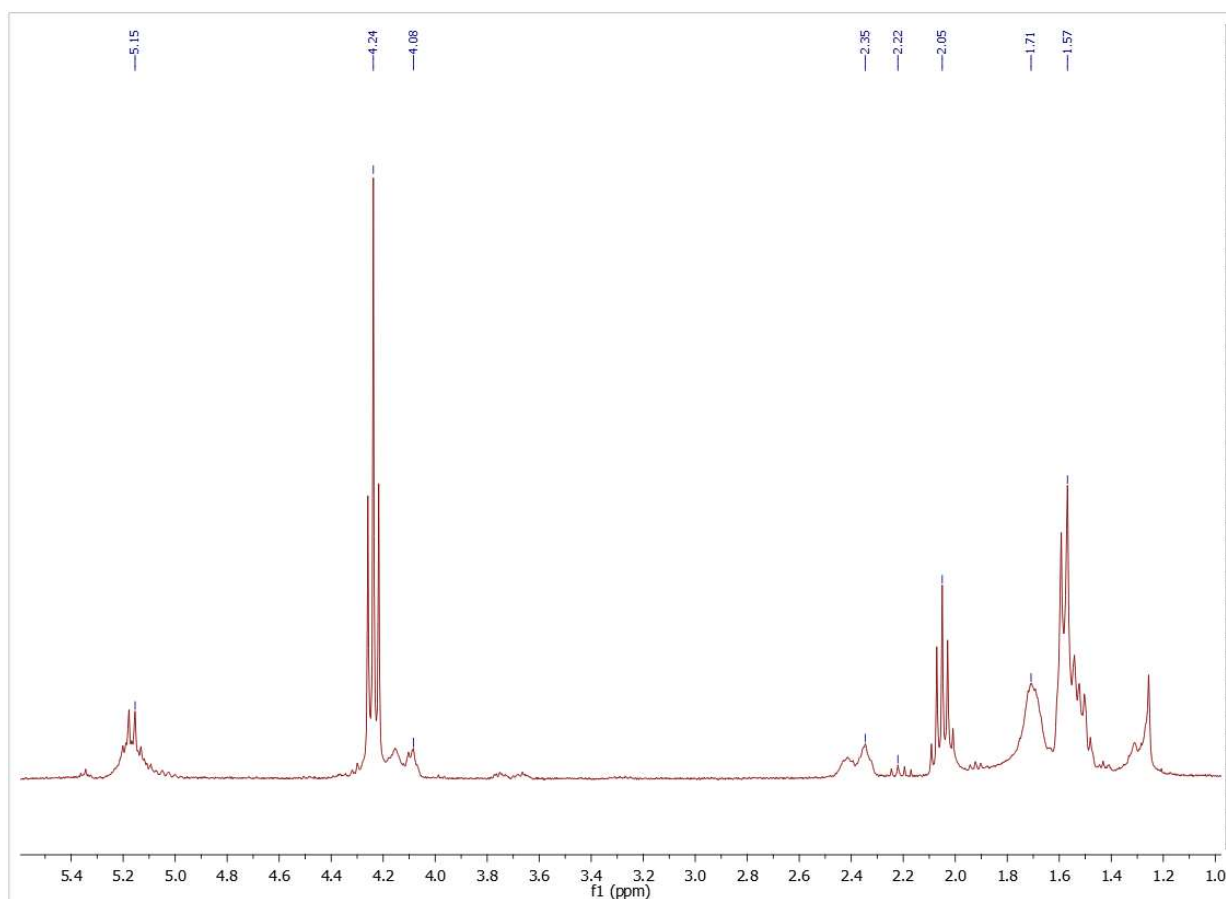


**Figure 77:** <sup>1</sup>H NMR spectra of the crude mixture after polymerization with TMC, *L*-lactide and  $\delta$ -valerolactone corresponding to corresponding to entry 28 (**Table 21**) in CDCl<sub>3</sub> (300 MHz).

As can be seen in **Figure 77**, proton NMR of the polymerization with an equal amount of all monomers shows the characteristic signals of PLA (5.15 and 1.57 ppm), PTMC (4.24 and 2.05 ppm), and PVL (2.35 and 1.71 ppm), however most of the multiplets are slightly more complex than that of their corresponding pure homopolymers. While not as complex as what was observed for the statistical copolymerization of TMC and lactide, this increase in the multiplicity of the peaks could be indicative of a statistical copolymer.

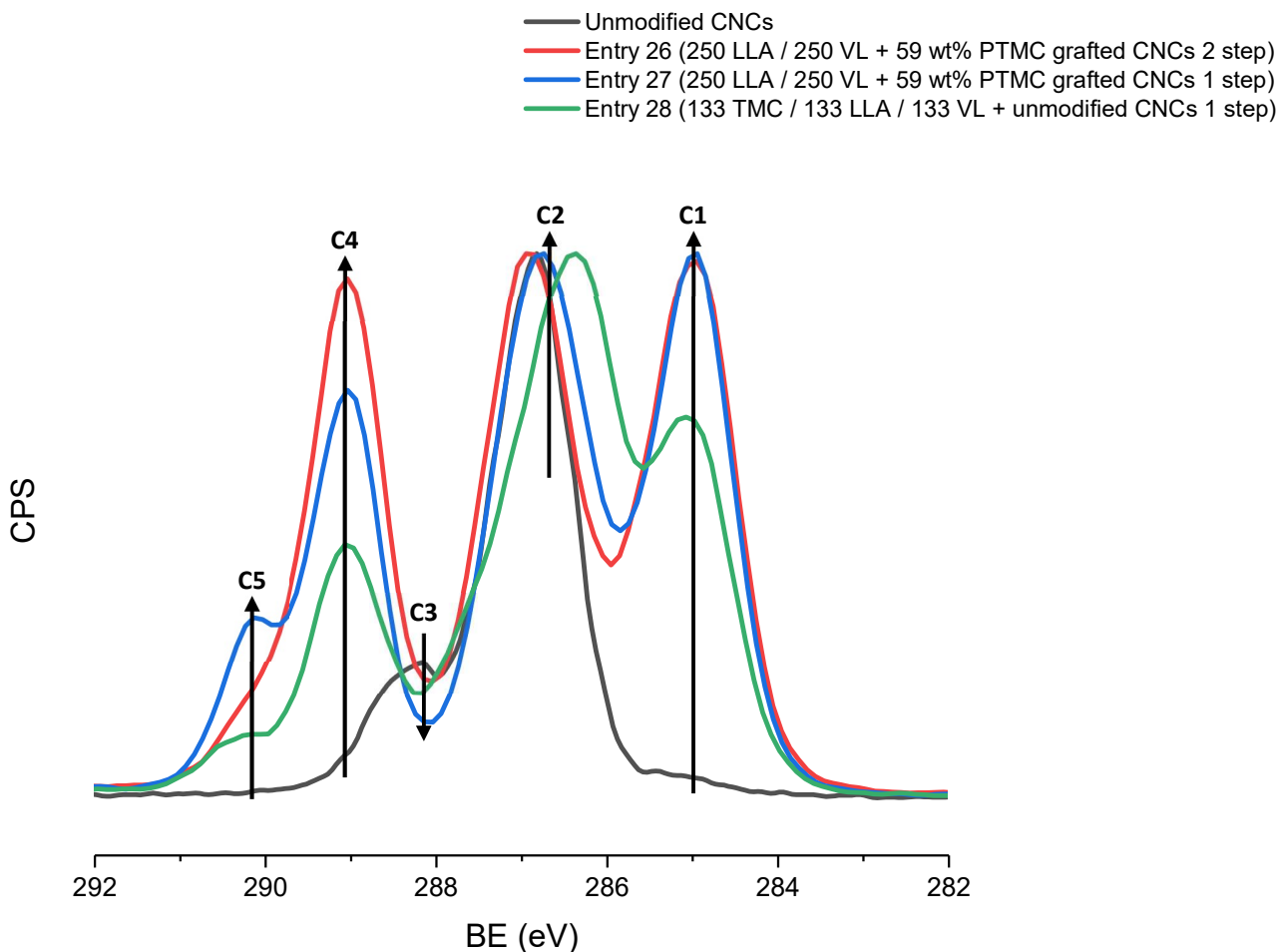


**Figure 78:** Carbon 1s X-ray photoelectron spectroscopy (XPS) normalized spectrogram of unmodified CNCs and modified CNCs corresponding to entries 26 to 28 in **Table 21**.

XPS was used to obtain some information on the surface composition of the modified CNCs obtained for all these reactions **Figure 71**. For the CNCs corresponding to entry 26, a surface composition almost identical to the PTMC-block-PLA grafts corresponding to entry 3 in **Table 16** was found, showing the potentially low amount of  $\delta$ -VL monomer units in the grafts. While the reactivity of  $\delta$ -VL on PTMC chains was shown to be higher than for unmodified CNCs, the reactivity of  $\delta$ -VL toward PLLA could be quite lower, hence the lack of PVL grafts on the CNCs. When lactide and  $\delta$ -VL are introduced at the same time (entry 27), a higher carbonate content is visible on the surface of the CNCs, characteristic of a lower grafting. The contribution C-C (C1) is quite high despite the lower grafting, and when comparing to entry 6 in **Table 16**, possibly due to the integration of some  $\delta$ -VL units which have a high C-C content. Lastly, in the presence of all

the monomers and CNCs (entry 28), the spectra is similar to entry 9 in **Figure 67**, giving another indication that the lower reactivity of  $\delta$ -VL makes its integration in the graft copolymer unlikely.

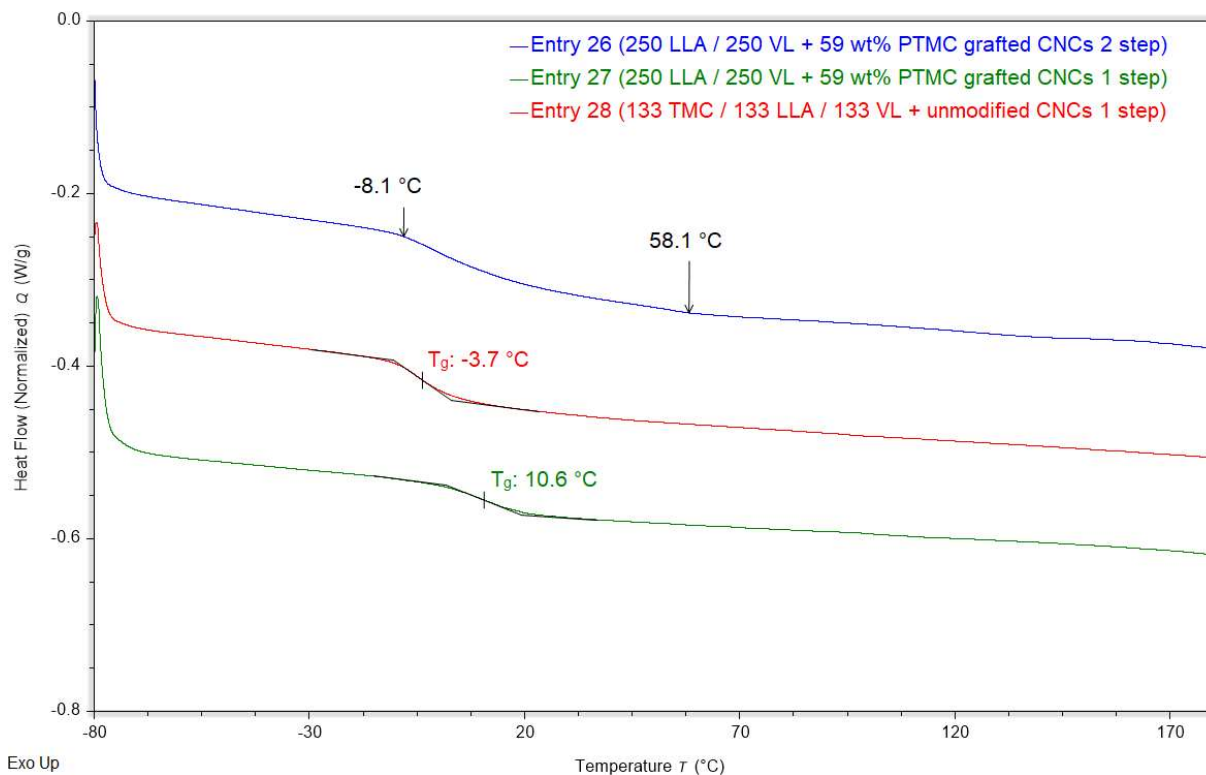


**Figure 79:** DSC thermograms of unmodified of grafted CNCs corresponding to reactions in **Table 21** between  $-80\text{ °C}$  and  $180\text{ °C}$ .

Looking at DSC thermograms (**Figure 79**), the indication of block copolymer grafts can only be seen for entry 26, with the  $T_g$  of only PTMC and PLLA present. Surprisingly, the CNCs first modified with PTMC prior to the reaction with lactide and  $\delta$ -VL have a unique  $T_g$  at  $-3.7\text{ °C}$ , similarly to the one obtained after the reaction done with a mixture of all monomers which have  $T_g$  at  $10.6\text{ °C}$ . Compatibility studies are however clearly required before drawing any firm conclusion.

## VI.1. Conclusion

The polymerization of multiple heterocyclic monomers was done in the presence of cellulose nanocrystals using organic catalysts. With the method developed previously to graft PTMC onto cellulose, copolymers of different structure and composition were grafted onto CNCs. Some runs with MMA were also carried out using a phosphazene, but only a small amount of grafting could be obtained (13 wt%) within the conditions probed despite the high conversion of the monomer.

When trying to obtain PMMA grafts on the surface of PTMC-grafted CNCs however, no PMMA grafting could be observed. Several trial experiments with  $\epsilon$ -caprolactone and PTMC-grafted CNCs also led to a low amount of grafting with TBD (8%), this time due to the low reactivity of  $\epsilon$ -CL. For grafting with lactide, an important difference for the rate of conversion with TBD was observed between using unmodified CNCs and PTMC-grafted CNCs. Starting from CNCs with a high PTMC content, a high amount of PLLA could be grafted, and modified CNCs with up to 87 wt% grafts (50% PLLA / 37% PTMC) were obtained. Reactions with a mixture of TMC and lactide were also performed to obtain statistical copolymer grafts using different ratios of TMC/L-LA. Similar reactions with  $\delta$ -valerolactone were carried out, but a lower amount of grafts was obtained compared to the reactions with lactide. Lastly, reactions with the three different monomers were done, however no quantification could be provided for these grafts. Using XPS, FT-IR and DSC, the composition of the different grafts could be confirmed, and both block and statistical copolymer of PTMC and PLLA could be obtained, with characteristic glass transition temperatures measured. Moreover, strong indication towards the structure of the copolymer grafts could be found, and the grafts on the surface of CNCs were seen as a bilayer shell around a CNC core. For PVL grafting, statistical copolymers were obtained, but PVL and PTMC block copolymers contained a majority of PTMC and no  $T_g$  for a PVL-block could be found by DSC. As for the grafting reactions with three different monomers, determining the exact nature of the grafts was more difficult due to the similar chemical composition of the different monomers. However, similar XPS and DSC spectra to PTMC and PLLA copolymers indicated that  $\delta$ -valerolactone was likely not present in a significant amount in the grafts. Despite the low grafting of some polymers, this catalytic methodology proves useful as a multitude of grafted CNCs could be obtained, with different compositions as well as tuneable glass transition temperatures. These modified celluloses could therefore be useful for composite applications, not only acting as a reinforcing fiber in the polymer matrix, but potentially as a source of soft blocks at the same time. This is to our knowledge the first report of these blocks and statistical copolymers grafts on cellulose nanocrystals by ring-opening polymerization.

## VII. General conclusion and Perspectives

The overall goal of this thesis was the functionalization of nanocellulose by grafting polymer chains on its surface using mainly a “grafting from” approach by organocatalyzed ring-opening polymerization.

Chapter I served as overview of the state of the art for the different parts involved in the project. First, the interest for cellulose based material was highlighted and the production of nanomaterials made from it was detailed in order to give an understanding of the major difference between nanocrystals and nanofibrils. This project being the coupling of nanocellulose and polymers, the latter were also given an introduction, with a focus on polyesters and polycarbonates, as these polymer are good candidates to produce biobased and biocompatible materials, and are the main subject of the work. Among the motivation to use these polymers is the fact that they can be produced in a controlled way by using an alcohol co-initiator and an organic catalyst due to recent development in the advance of metal-free catalysis. This approach was showed to present several advantages such as the possibility to obtain structures sometime difficult to obtain with organometallic species, usability in mild condition, lower sensibility to impurities, and the possibility to obtain polymers free of metal traces for sensitive applications. In particular, organocatalyzed immortal ring-opening polymerization had all of the aforementioned benefits, and allowed for the use of very low amount of catalyst. Lastly, some of the different reports of surface grafting of polymers on cellulose found in the literature were given to show the work that had been done previously, as well as the areas that deserved more attention such as aliphatic carbonate grafting and ROP copolymerization grafting on the surface if CNCs.

In Chapter II, details about the different chemicals used were provided, with details about the purification used for the different monomers, catalysts and initiators used. The different methodologies developed for grafting of cellulose nanofibrils and nanocrystals were described, as well as some of the other reactions used. Details about the characterization techniques used, the calculation resulting from elemental analysis, as well as the methodology and model used for density-functional theory (DFT) were also provided.

The grafting of polylactide (PLA) on the surface of cellulose nanofibrils (CNF) was explored by organic catalysis in Chapter III. While this material had been described in the literature before, details on the organocatalyzed reaction were not as thoroughly studied. PLA grafts were obtained

starting from both freeze dried and never dried CNFs, and the grafting amount could be quantified using elemental analysis and thermogravimetric analysis (TGA). The influence of different parameters was tested as well, and a maximum amount of grafting of 24 wt% was obtained using 4-dimethylaminopyridine (DMAP) at room temperature (RT), a result comparable to that of tin-based ( $\text{Sn}(\text{Oct}_2)$ ) catalyst used at higher temperatures.

In Chapter IV, we investigated the ring-opening polymerization (ROP) on trimethylene carbonate (TMC), a cyclic carbonate of interest, initiated by methanol and catalyzed by DMAP and 1,5,7-triazabicyclo[4.4.0]dec-5-ene (TBD) by computational methods. Indeed, if the mechanisms had been well discussed for cyclic esters with these catalysts, we did not find such studies for cyclic carbonates. This showed that the ring-opening polymerization of trimethylene carbonate with both catalysts occurs *via* a dual mechanism of activation of the alcohol co-initiator and H-bonding between the catalyst and the monomer. Ring-opening was found to be the highest energy barrier at 25.7 and 90.3 kcal.mol<sup>-1</sup> for TBD and DMAP respectively, making it the limiting step, and the higher efficiency was confirmed by experiment with TBD.

Following the DFT study of the ROP of trimethylene carbonate, Chapter V presented reactions of grafting of poly(trimethylene carbonate) (PTMC) on the surface of cellulose nanocrystals (CNC) using both catalysts described previously, as well as 2-(*tert*-butylimino)-2-(diethylamino)-1,3-dimethylperhydro-1,3,2-diazaphosphorinane (BEMP) and 1,8-diazabicyclo[5.4.0]undec-7-ene (DBU). TBD showed the best result for conversion, grafting amount and efficiency. A high grafting content on cellulose nanocrystals of 74 wt% PTMC could be obtained after optimization, in mild conditions (RT, 5 hours) and with a low concentration of TBD. The modified CNCs were characterized using different methods which revealed the obtention of hydrophobic, core-shell nanoparticles as a result of the surface grafting of PTMC. Moreover, no trace amount of the catalyst was detected *via* elemental analysis or X-ray photoelectron spectroscopy (XPS) showing its complete removal. This is, as far as we know, the first example of grafting of PTMC on the surface of CNCs. Following these results, some trials for the ROP of TMC using CNCs supported were done. Despite some problems related to leaching of TBD under some conditions, partial conversion of the monomer was observed, showing some promises for this type of system for ring-opening polymerization.

In Chapter VI, we examined the potential of those nitrogen cyclic bases catalyzed ROP, mainly TBD, to graft statistical and block copolymers onto CNCs. In particular, using PTMC-grafted CNCs as initiator for the TBD catalyzed ring-opening polymerization of lactide led to very high amounts of grafting for block copolymer grafting (87 wt% grafts). The structure of the grafts was confirmed by XPS, Fourier-Transform infra-red (FT-IR) and differential scanning calorimetry (DSC), and a comparison with PTMC-grafted CNCs showed a surface composed almost exclusively of lactide units, making the block copolymer grafted CNCs a multi-layered material. Poly(lactide-co-trimethylene carbonate) statistical copolymeric graft could also be obtained using a mixture of the monomers in the feed, with a glass transition temperature in agreement with the statistical microstructure. Polymerization reaction using  $\delta$ -valerolactone instead of lactide were also tested, and despite the lower reactivity of this monomer, the analyses suggested that both statistical and block copolymeric CNCs grafts were obtained as well. Attempts at obtaining copolymers containing all three monomers were tested, but the few grafted CNCs obtained did not seem contain much  $\delta$ -valerolactone units, requiring further investigation and optimization.

Overall, TBD was demonstrated to be a very versatile catalyst for the production of different grafts on cellulose by ring-opening polymerization. Interestingly, TBD showed a much higher activity towards the grafting of TMC units than lactones on unmodified CNCs, but a higher activity was observed when using PTMC-grafted CNCs as initiator. The various modified CNCs have interesting properties such as different glass transition temperature, surface composition and hydrophobicity. The reactions were all done under mild conditions, and TBD could completely be removed from the finished product, accomplishing the goal of having an efficient yet easily removable catalyst for the reactions of grafting.

While some other catalysts have been tested throughout this work, seeing the potential of TBD raises the question of the use of other combination of monomers and organic catalyst, in particular due to all the recent developments in the latter. For ring-opening polymerization alone, plenty of monomers could be of interest, and future work on different carbonates could be interesting. In addition, a lot of them have been produced making use of CO<sub>2</sub> which presents an interesting alternative for greener monomer, but could also offer different structures. More work could also be done on lactones, as the work presented here only briefly covered some of them, and high amounts of grafting were not achieved. For this purpose, other catalytic systems could be used, with example

such as dual catalysis using thiourea reported as efficient systems for some lactones. For the structure of the grafts, the work presented for copolymer shows very promising results, but more could certainly be explored, in particular for block copolymers. As PLLA and PTMC have been shown to work together, structure such as ABA blocks could have interesting potential for material such as thermoplastic elastomers. Of course, increasing the complexity of the grafts leads to an increased difficulty for characterization, an area that could also be improved. For this, nuclear magnetic resonance (NMR) could provide useful information, however detecting things such as chain ends and linkage between different monomer units in solid NMR can be challenging at best. Thus, recent development in the characterization of polysaccharide have made liquid state NMR possible for cellulose by using particular ionic liquids, allowing for the use of many NMR methods, including 2d spectra with high resolution. A collaborative work with Alistair King, from the University of Helsinki, has been started in regards to this work. The initial application in mind for these materials was reinforcement for composites, therefore if more work were to be done with these materials, testing their compatibility with different polymer matrixes as opposed to native cellulose would be very interesting. A collaborative work with Aurélie Taguet, from Ecole des Mines is currently planned to develop this aspect. Differently grafted CNCs produced as described in this work could be tested, and their impact on the thermo-mechanical properties of the composite would hopefully show a significant improvement.

## VIII. Annexes

### VIII.1. Elemental analysis

Below are compiled tables of the samples described in the publication with their EA and TGA data.

**Table 22:** EA and TGA data obtained for samples in **Table 4:** Ring-opening polymerization of *rac*-lactide initiated from the surface of freeze-dried CNF in the presence of DBU/TBD in DCM for 48 hours at 35 °C.

Entry	Carbon content (%)	Hydrogen content (%)	Water content (%)	Grafted PLA (wt%)
1	40.76	5.90	1.45	0
2	40.38	5.68	2.43	0
3	40.28	5.69	1.22	0
4	42.12	5.95	2.24	0
5	42.09	5.87	3.08	0
6	42.33	5.98	2.56	0
7	42.65	6.06	3.08	7
8	41.71	5.78	2.42	6
9	42.56	5.74	2.30	17

**Table 23:** EA and TGA data obtained for samples in **Table 5:** Ring-opening polymerization of *rac*-lactide initiated from the surface of freeze-dried CNF in the presence of DMAP in DCM for 48 hours at 35 °C.

Entry	Carbon content (%)	Hydrogen content (%)	Water content (%)	Grafted PLA (wt%)
8	41.71	5.78	2.42	6
10	41.61	5.77	2.65	6
11	41.78	5.80	2.54	8
12	41.47	5.83	3.24	8
13	42.01	5.77	2.53	11
14	43.01	5.77	1.60	19
15	41.95	5.68	2.90	12
9	42.56	5.74	2.30	17

**Table 24:** EA and TGA data obtained for samples in **Table 6:** Ring-opening polymerization of *rac*-lactide initiated from the surface of never-dried CNF in the presence of DMAP in DCM.

Entry	Carbon content (%)	Hydrogen content (%)	Water content (%)	Grafted PLA (wt%)
1	41.83	6.08	4.40	7
2	41.87	6.09	3.48	13
3	41.62	6.05	4.78	7
4	43.69	6.18	2.47	18
5	42.49	6.13	3.60	16
6	41.36	5.98	4.05	5

7	42.11	6.03	2.97	9
8	42.16	6.08	3.60	11
9	41.98	6.16	3.62	9
10	42.13	6.19	3.89	12
11	40.27	5.94	5.87	6
12	43.55	6.21	2.77	17
13	43.01	6.05	1.65	12
14	42.28	6.17	3.39	18
15	44.07	6.07	2.48	24
16 <sup>a</sup>	42.15	5.88	4.55	13

**Table 25:** EA and TGA data obtained for samples in **Table 8:** Ring-opening polymerization of TMC initiated from the surface of CNC in the presence of various organocatalysts at 25 °C in THF.

Entry	Carbon content (%)	Hydrogen content (%)	Water content (%)	Grafted PTMC (wt%)
1	42.95	6.21	1.44	2
2	44.87	6.00	1.24	51
3	44.30	6.05	0.76	24
4	44.68	6.05	0.71	35
5	44.57	6.02	0.39	37
6	45.26	6.04	2.98	13
7	42.37	6.07	3.05	3
8	42.70	6.14	2.94	12
9	43.07	6.21	3.08	18
10	42.98	6.16	2.91	12

**Table 26:** EA and TGA data obtained for samples in **Table 9:** Ring-opening polymerization of TMC initiated in different solvents on the surface of CNC in the presence of TBD over 5 hours, 25 °C, at a ratio of TMC/Catalyst/OH of 500/1/50. Solvent added outside the glovebox under inert atmosphere.

Entry	Carbon content (%)	Hydrogen content (%)	Water content (%)	Grafted PTMC (wt%)
11	45.43	5.94	0.54	52
12	44.04	6.03	1.36	30
13	42.72	6.05	1.97	0

**Table 27:** EA and TGA data obtained for samples in **Table 10:** Ring-opening polymerization of TMC initiated from the surface of CNC in the presence of TBD in THF for 5 hours.

Entry	Carbon content (%)	Hydrogen content (%)	Water content (%)	Grafted PTMC (wt%)
2	44.87	6.00	1.24	51
14	45.12	6.01	0.79	51
15	44.81	5.98	0.92	47
16	45.36	5.99	0.96	60
17	45.29	5.96	0.98	54

18	45.08	6.01	0.60	51
19	45.31	5.95	0.22	52
20	42.60	6.10	2.80	7
21	45.05	6.03	0.75	49
22	44.98	5.98	0.85	49
23	45.27	5.87	0.17	53
24	43.37	6.11	1.77	9
25	43.40	6.11	1.71	9
26	45.97	5.88	0.44	74
27	45.81	6.00	0.24	64
28	45.51	6.00	0.38	57
29	45.01	6.09	0.79	47
30	43.77	6.05	1.36	23
32	44.74	6.09	1.17	50
32	44.42	6.11	1.67	41

**Table 28:** EA and TGA data obtained for samples in **Table 13:** Ring-opening polymerization of TMC using TBD-grafted CNC as catalyst, at 25 °C in THF for 5 hours.

Entry	Carbon content (%)	Hydrogen content (%)	Water content (%)	Nitrogen content (t%)
1	41.30	5.98	5.88	0.78
2	43.60	6.09	5.88	1.78

**Table 29:** EA and TGA data obtained for samples in **Table 15:** Ring-opening polymerization of *L-LA* initiated from the surface of CNC using TBD and DMAP, at 25 °C in THF.

Entry	Carbon content (%)	Hydrogen content (%)	Water content (%)	Grafted PLLA (wt%)
1	43.26	6.12	2.11	0
2	46.98	5.70	0.85	57

**Table 30:** EA and TGA data obtained for samples in **Table 16:** Ring-opening polymerization of *L-LA* initiated from the surface of PTMC-grafted CNCs using TBD, at 25 °C in THF over 1 hour. Full conversion was reached for all reactions.

Entry	Carbon content (%)	Hydrogen content (%)	Water content (%)	Grafted PLLA (wt%)
3	48.03	5.82	0.16	50
4	46.96	5.87	0.43	33
5	46.23	5.95	0.60	30
6	44.30	6.05	1.45	10
7	47.33	5.92	0.60	37

**Table 31:** EA and TGA data obtained for samples in **Table 18:** Ring-opening polymerization of MMA initiated from the surface of CNC using tBu-P<sub>4</sub>, at 25 °C in THF.

Entry	Carbon content (%)	Hydrogen content (%)	Water content (%)	Grafted PMMA (wt%)
12	43.57	6.19	2.85	9
13	43.51	6.12	2.24	7
14	43.97	6.22	2.03	9
15	43.64	6.21	0.89	3
16	43.31	6.17	0.91	1
17	44.65	6.27	2.09	13
18	45.86	6.07	0.53	0
19	45.56	6.12	1.23	0

**Table 32:** EA and TGA data obtained for samples in **Table 19:** Ring-opening polymerization of  $\epsilon$ -CL initiated from the surface of PTMC-grafted CNCs (20: 73 wt%, 21: 59%).

Entry	Carbon content (%)	Hydrogen content (%)	Water content (%)	Grafted PCL (wt%)
20	46.89	6.10	0.29	5
21	46.87	6.26	0.57	8

**Table 33:** EA and TGA data obtained for samples in **Table 20:** Ring-opening copolymerization of  $\delta$ -VL on the surface of unmodified and PTMC-grafted CNCs using TBD, at 25 °C in THF.

Entry	Carbon content (%)	Hydrogen content (%)	Water content (%)	Grafted PVL (wt%)
22	46.24	6.33	2.16	0
23	50.70	6.10	0.29	37
24	48.58	6.39	0.37	16
25	49.36	6.64	0.92	n.d.

**Table 34:** EA and TGA data obtained for samples in **Table 21:** Ring-opening copolymerization of TMC,  $\delta$ -VL and *L*-LA initiated from the surface of CNCs using TBD, at 25 °C in THF.

Entry	Carbon content (%)	Hydrogen content (%)	Water content (%)
26	47.03	5.85	0.48
27	45.97	6.08	0.1
28	46.53	5.95	0.86

## VIII.2. NMR spectra

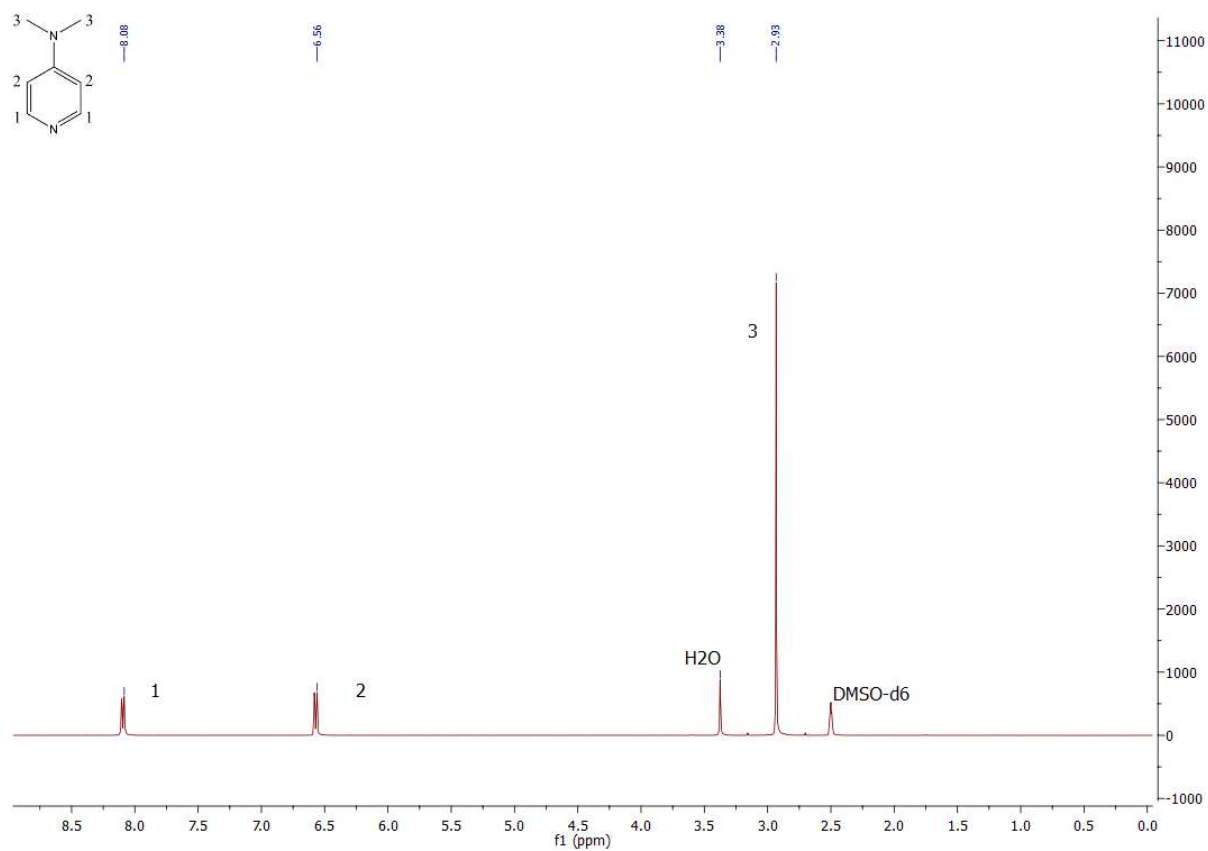


**Figure 80:**  $^1\text{H}$  NMR spectra of 4-dimethylaminopyridine in  $\text{DMSO-d}_6$  (300 MHz).

$^1\text{H}$  NMR ( $\text{DMSO-d}_6$ , 300 MHz)  $\delta$  (ppm) 8.08 (d, 2H), 6.56 (d, 2H), 2.93 (s, 6H)

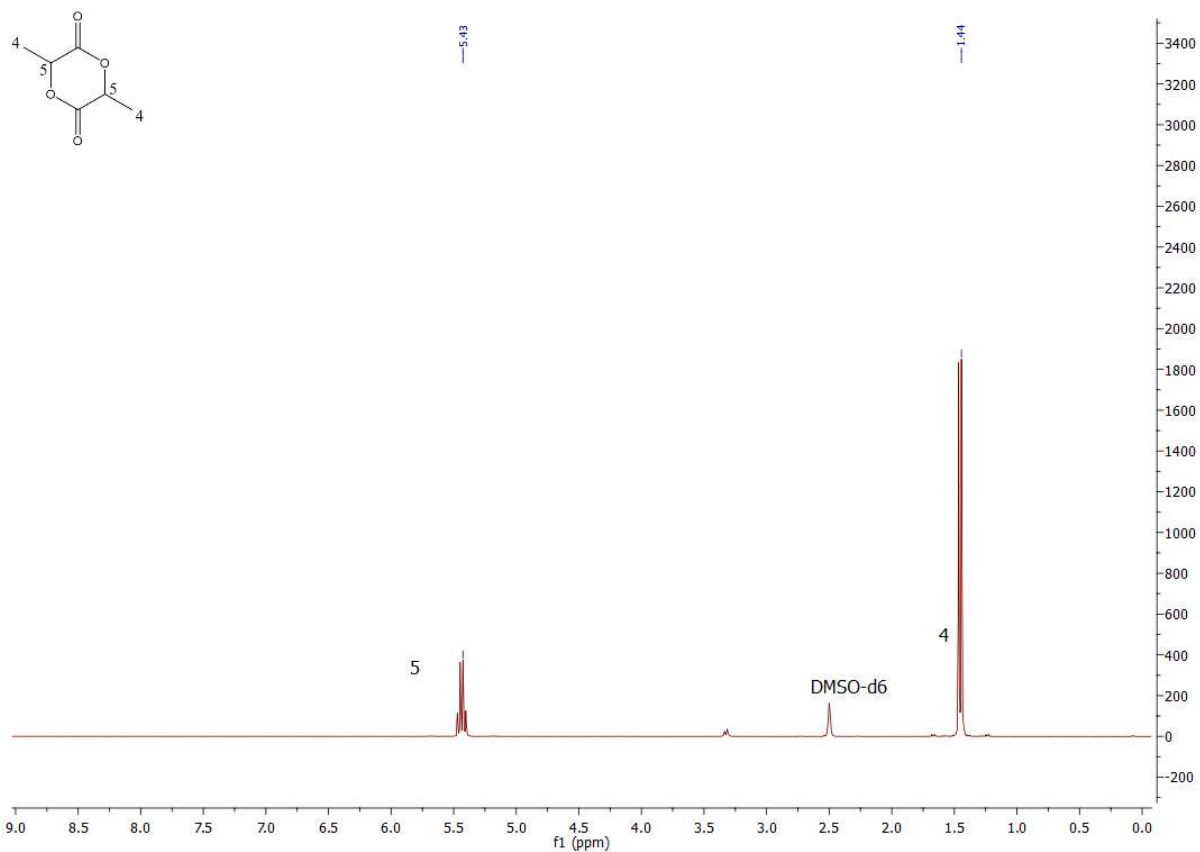


**Figure 81:** <sup>1</sup>H NMR spectra of lactide in DMSO-d<sub>6</sub> (300 MHz).

<sup>1</sup>H NMR (DMSO-d<sub>6</sub>, 300 MHz)  $\delta$  (ppm) 5.43 (q, 2H), 1.44 (d, 6H)

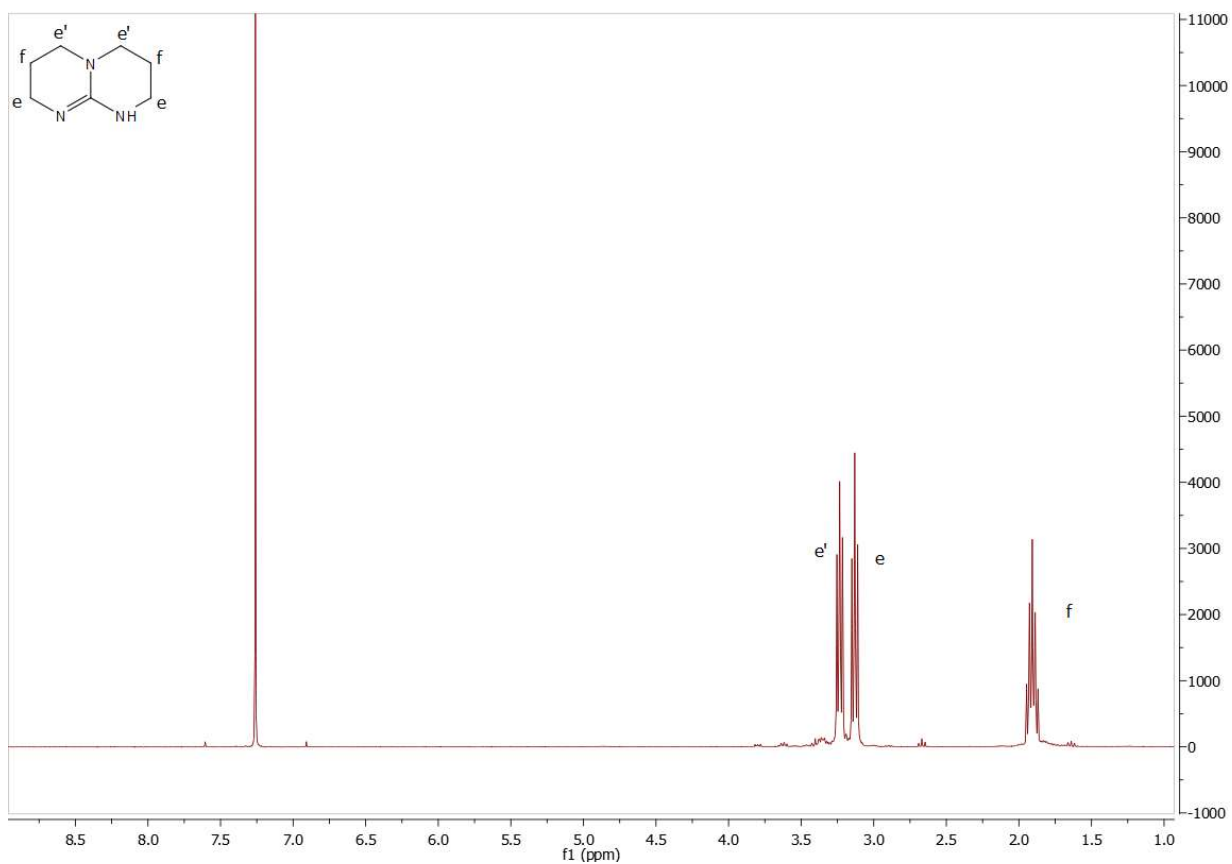


**Figure 82:** <sup>1</sup>H NMR spectra of TBD in CDCl<sub>3</sub> (300 MHz)

<sup>1</sup>H NMR (CDCl<sub>3</sub>, 300 MHz) δ (ppm): 3.23 (t, 4H, -NCH<sub>2</sub>CH<sub>2</sub>CH<sub>2</sub>N-), 3.13 (t, 4H, -HNCH<sub>2</sub>CH<sub>2</sub>CH<sub>2</sub>N-) 1.91 (m, 4H, -NCH<sub>2</sub>CH<sub>2</sub>CH<sub>2</sub>N-)

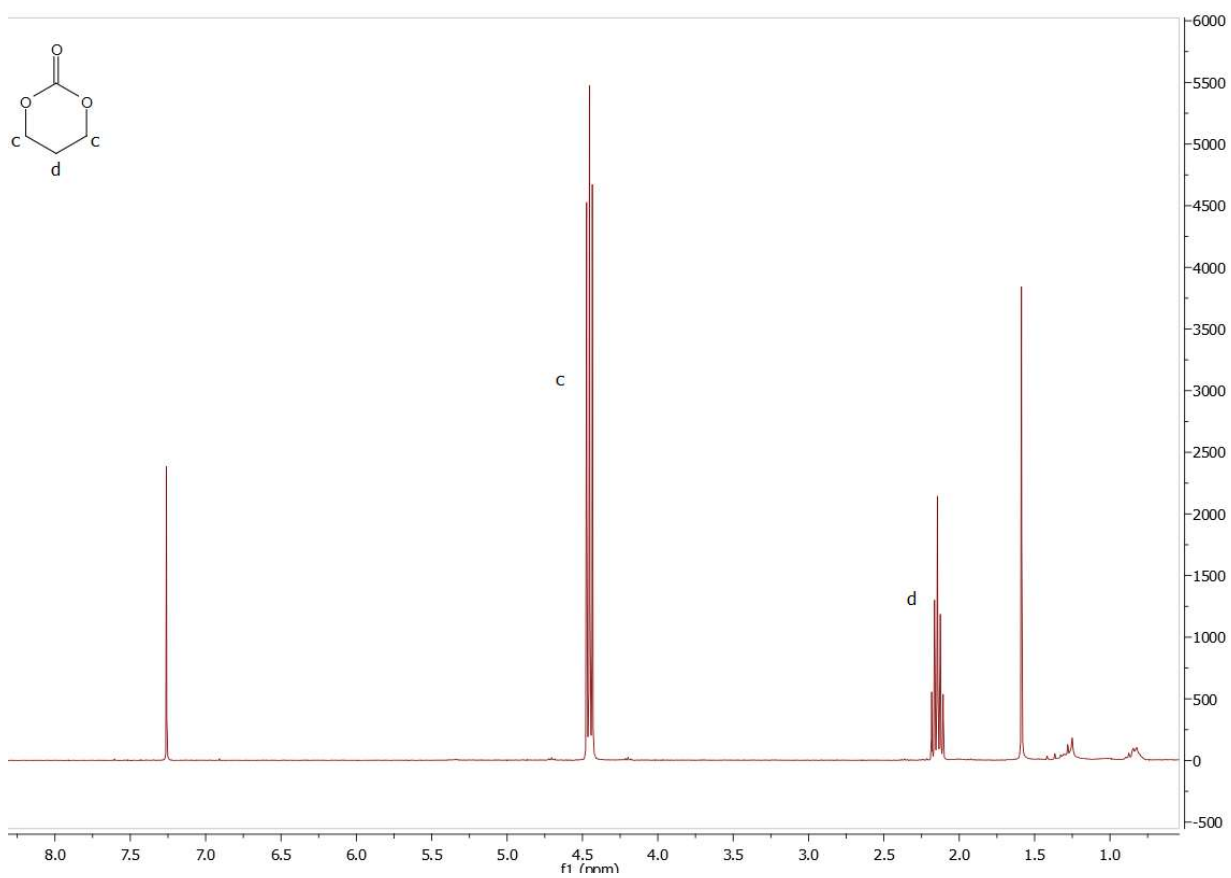


**Figure 83:** <sup>1</sup>H NMR spectra of TMC in CDCl<sub>3</sub> (300 MHz).

<sup>1</sup>H NMR (CDCl<sub>3</sub>, 300 MHz) δ (ppm): 4.45 (t, 4H, CH<sub>2</sub>OCOOCH<sub>2</sub>CH<sub>2</sub>), 2.14 (qi, 2H, CH<sub>2</sub>OCOOCH<sub>2</sub>CH<sub>2</sub>)

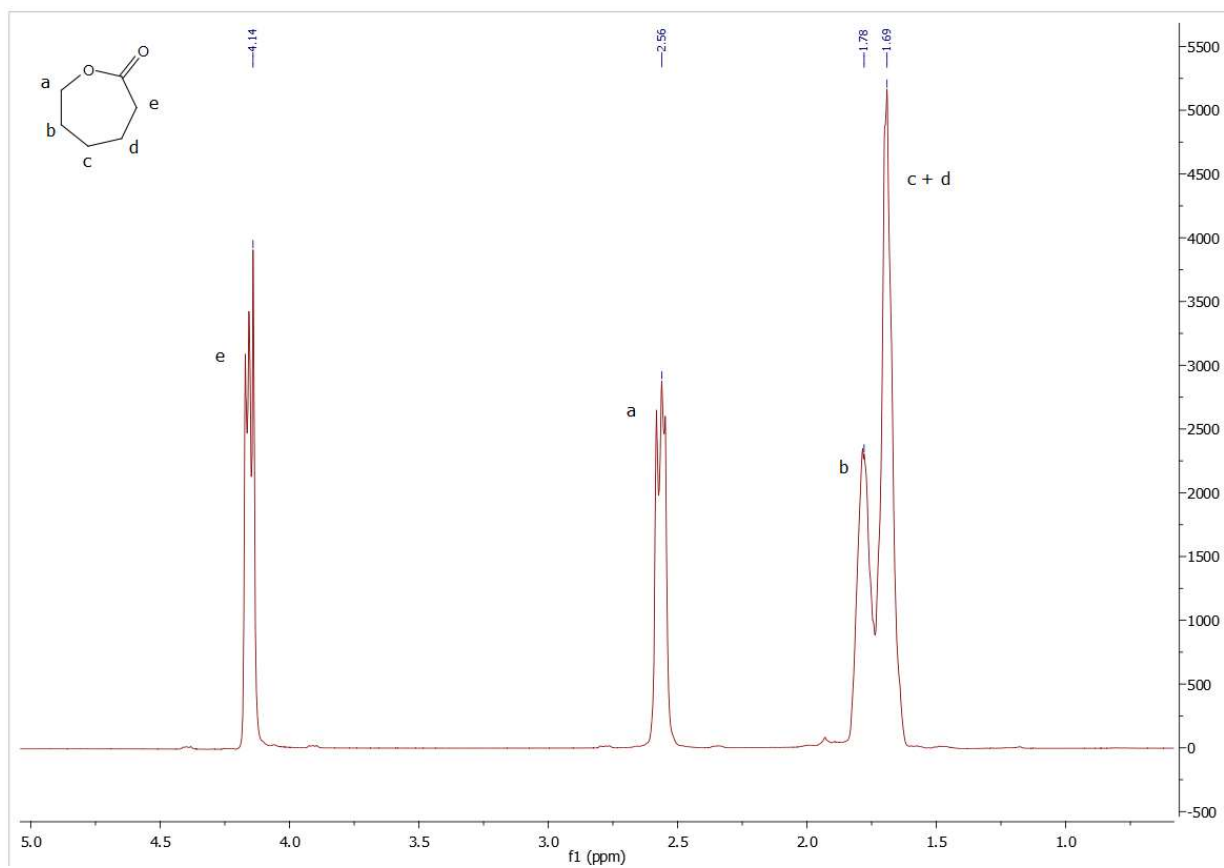


**Figure 84:**  $^1\text{H}$  NMR spectra of  $\epsilon$ -CL in  $\text{CDCl}_3$  (300 MHz).

$^1\text{H}$  NMR ( $\text{CDCl}_3$ , 300 MHz)  $\delta$  (ppm): 4.14 (m, 2H), 2.56 (m, 2H), 1.78 (m, 2H), 1.69 (s, 4H)

### VIII.3. Infrared

**Table 35:** FT-IR signals detected for unmodified and modified CNFs, with their corresponding functions.

<b>Bond</b>	<b>wave number cm<sup>-1</sup></b>	
	<b>unmodified CNF</b>	<b>modified CNF</b>
$\nu$ (O-H)	3342	3335
$\nu$ (C-H)	2899	2899
$\nu$ (C=O)		1743
$\delta$ (H <sub>2</sub> O)	1639	1646
$\delta$ (C-O-H)	1428	1428
$\delta$ (C-O-H)	1369	1369
$\delta$ (C-O-H)	1317	1316
$\nu$ (C-O, ester)		1201
$\nu$ (C-O-C, glucose ring asym.)	1160	1160
$\nu$ (C-OH)	1107	1105
$\nu$ (C-OH)	1056	1055
$\omega$ (C-OH)	665-561	663-560

#### VIII.4. XPS Data

**Table 36:** X-ray Photoelectron Spectroscopy data obtained for different signals, material analyzed corresponding to **Table 5**.

	Orbital	Component	Binding energy (eV)	FWHM (eV)	% Area
<i>Unmodified CNF</i>	C 1s	C-C	285.00	1.13	4.21
		C-O	286.86	1.13	76.81
		O-C-O	288.32	1.13	17.86
		O=C-O	289.48	1.13	1.13
	O 1s	O-C	533.06	1.36	59.88
		O-C-O	533.36	1.36	40.12
Entry 8	C 1s	C-C	285.00	1.11	10.68
		C-O	286.50	1.11	69.63
		O-C-O	287.91	1.11	16.48
		O=C-O	289.20	1.11	3.21
	O 1s	O-C	532.89	1.41	95.05
		O-C=O	534.05	1.41	4.95
Entry 10	C 1s	C-C	285.00	1.16	7.20
		C-O	286.62	1.16	70.19
		O-C-O	288.02	1.16	17.16
		O=C-O	289.46	1.16	5.45
	O 1s	O-C	532.92	1.41	92.08
		O-C=O	534.15	1.41	7.92
Entry 11	C 1s	C-C	285.00	1.18	5.99
		C-O	286.46	1.18	67.89
		O-C-O	287.82	1.18	18.53
		O=C-O	289.36	1.18	7.59
	O 1s	O-C	532.72	1.41	88.39
		O-C=O	534.00	1.41	11.61
Entry 12	C 1s	C-C	285.00	1.18	6.13
		C-O	286.40	1.18	66.59
		O-C-O	287.76	1.18	18.79
		O=C-O	289.31	1.18	8.49
	O 1s	O-C	532.71	1.40	87.11

		O-C=O	533.93	1.40	12.89
Entry 13	Orbital	Component	Binding energy (eV)	FWHM (eV)	% Area
	C 1s	C-C	285.00	1.22	19.65
		C-O	286.41	1.22	43.41
		O-C-O	287.45	1.22	18.12
		O=C-O	289.16	1.22	18.83
	O 1s	O-C	532.52	1.43	70.38
O-C=O		533.74	1.43	29.62	
Entry 14	Orbital	Component	Binding energy (eV)	FWHM (eV)	% Area
	C 1s	C-C	285.00	1.15	23.59
		C-O	286.37	1.15	28.41
		O-C-O	287.17	1.15	22.64
		O=C-O	289.04	1.15	25.37
	O 1s	O-C	532.38	1.38	59.43
O-C=O		533.60	1.38	40.57	
Entry 15	Orbital	Component	Binding energy (eV)	FWHM (eV)	% Area
	C 1s	C-C	285.00	1.18	21.79
		C-O	286.39	1.18	35.67
		O-C-O	287.25	1.18	18.76
		O=C-O	289.02	1.18	23.77
	O 1s	O-C	532.41	1.40	63.06
O-C=O		533.63	1.40	36.94	
Entry 9	Orbital	Component	Binding energy (eV)	FWHM (eV)	% Area
	C 1s	C-C	285.00	1.18	21.96
		C-O	286.34	1.18	33.61
		O-C-O	287.22	1.18	21.48
		O=C-O	289.04	1.18	22.94
	O 1s	O-C	532.42	1.41	63.45
O-C=O		533.64	1.41	36.55	

**Table 37:** X-ray Photoelectron Spectroscopy data obtained for different signals, material analyzed corresponding to **Table 6**.

Entry 4	Orbital	Component	Binding energy (eV)	FWHM (eV)	% Area
	C 1s	C-C	285.00	1.14	10.57
		C-O	286.76	1.14	70.08
		O-C-O	288.19	1.14	16.56
		O=C-O	289.44	1.14	2.79

	O 1s	O-C	532.97	1.41	59.30
		O-C-O	533.27	1.41	39.73
		O-C=O	533.77	1.41	0.49
		O-C=O	532.37	1.41	0.49
Entry 12	Orbital	Component	Binding energy (eV)	FWHM (eV)	% Area
	C 1s	C-C	285.00	1.12	9.12
		C-O	286.80	1.12	71.63
		O-C-O	288.23	1.12	16.94
		O=C-O	289.57	1.12	1.83
	O 1s	O-C	533.00	1.37	59.53
		O-C-O	533.30	1.37	39.89
		O-C=O	533.80	1.37	0.29
O-C=O		532.40	1.37	0.29	
Entry 15	Orbital	Component	Binding energy (eV)	FWHM (eV)	% Area
	C 1s	C-C	285.00	1.13	6.21
		C-O	286.75	1.13	72.85
		O-C-O	288.15	1.13	17.06
		O=C-O	289.41	1.13	3.01
	O 1s	O-C	532.95	1.38	59.26
		O-C-O	533.25	1.38	39.71
		O-C=O	533.75	1.38	0.52
O-C=O		532.35	1.38	0.52	

**Table 38:** X-ray Photoelectron Spectroscopy data obtained for different signals, material analyzed corresponding to **Table 10**.

Unmodified CNC	Orbital	Component	Binding energy (eV)	FWHM (eV)	% Area
	C 1s	C-C	285.00	1.05	1.95
		C-O	286.84	1.04	76.81
		O-C-O	288.24	1.32	17.86
CNC 23% PTMC grafts	Orbital	Component	Binding energy (eV)	FWHM (eV)	% Area
	C 1s	C-C	285.00	1.17	16.32
		C-O	286.43	1.13	60.22
		O-C-O	287.70	1.22	10.89
OC(O)=O		290.35	0.94	12.57	
CNC 41% PTMC grafts	Orbital	Component	Binding energy (eV)	FWHM (eV)	% Area
	C 1s	C-C	285.00	1.06	21.43
		C-O	286.46	1.16	52.39

		O-C-O	287.52	1.71	6.24
		OC(O)=O	290.26	0.91	19.94
CNC 64% PTMC grafts	Orbital	Component	Binding energy (eV)	FWHM (eV)	% Area
	C 1s	C-C	285.00	1.04	21.60
		C-O	286.46	1.10	52.10
		O-C-O	287.41	1.32	4.97
		OC(O)=O	290.23	0.91	21.32
CNC 74% PTMC grafts	Orbital	Component	Binding energy (eV)	FWHM (eV)	% Area
	C 1s	C-C	285.00	1.05	25.94
		C-O	286.46	1.16	45.92
		O-C-O	287.41	1.75	6.66
		OC(O)=O	290.23	0.93	21.47

**Table 39:** X-ray Photoelectron Spectroscopy data obtained for different signals, material analyzed corresponding to **Table 16**.

Entry 3	Orbital	Component	Binding energy (eV)	FWHM (eV)	% Area
	C 1s	C-C	285.00	1.21	35.77
		C-O	286.98	1.21	33.01
		OC=O	289.12	1.21	30.60
		OC(O)=O	290.66	1.21	0.63
Entry 4	Orbital	Component	Binding energy (eV)	FWHM (eV)	% Area
	C 1s	C-C	285.00	1.17	33.56
		C-O	286.91	1.17	34.09
		OC=O	289.05	1.17	31.31
		OC(O)=O	290.47	1.17	1.03
Entry 5	Orbital	Component	Binding energy (eV)	FWHM (eV)	% Area
	C 1s	C-C	285.00	1.18	33.84
		C-O	286.89	1.18	34.46
		OC=O	289.06	1.18	28.88
		OC(O)=O	290.37	1.18	2.82
Entry 6	Orbital	Component	Binding energy (eV)	FWHM (eV)	% Area
	C 1s	C-C	285.00	1.13	25.83
		C-O	286.38	1.13	30.03
		OC-O	287.15	1.13	18.28
		OC=O	289.05	1.13	18.99
		OC(O)=O	290.20	1.13	6.88
Entry 7	Orbital	Component	Binding energy (eV)	FWHM (eV)	% Area

C 1s	C-C	285.00	1.18	33.14
	C-O	286.86	1.18	35.65
	O-C-O	289.06	1.18	27.07
	OC(O)=O	290.32	1.18	4.14

**Table 40:** Xray Photoelectron Spectroscopy data obtained for different signals, material analyzed corresponding to **Table 17**.

	Orbital	Component	Binding energy (eV)	FWHM (eV)	% Area
Entry 9	C 1s	C-C	285.00	1.26	32.52
		C-O	286.79	1.26	40.65
		OC=O	289.10	1.26	23.15
		OC(O)=O	290.44	1.26	3.69
	Orbital	Component	Binding energy (eV)	FWHM (eV)	% Area
Entry 10	C 1s	C-C	285.00	1.10	38.66
		C-O	286.55	1.10	26.27
		OC-O	287.21	1.10	13.35
		OC=O	289.11	1.10	14.21
		OC(O)=O	290.41	1.10	7.50
	Orbital	Component	Binding energy (eV)	FWHM (eV)	% Area
Entry 11	C 1s	C-C	285.00	1.10	3.59
		C-O	286.68	1.10	75.22
		OC-O	288.11	1.10	17.83
		OC=O	289.48	1.10	3.36

**Table 41:** Xray Photoelectron Spectroscopy data obtained for different signals, material analyzed corresponding to **Table 18**.

	Orbital	Component	Binding energy (eV)	FWHM (eV)	% Area
Entry 17	C 1s	C-C	285.00	1.24	33.05
		C-O	286.50	1.24	46.34
		OC-O	287.76	1.24	6.64
		OC=O	288.83	1.24	13.98

**Table 42:** Xray Photoelectron Spectroscopy data obtained for different signals, material analyzed corresponding to **Table 19**.

Entry 21	Orbital	Component	Binding energy (eV)	FWHM (eV)	% Area
----------	---------	-----------	---------------------	-----------	--------

C 1s	C-C	285.00	1.05	26.80
	C-O	286.44	1.05	40.69
	OC-O	287.09	1.05	10.21
	OC=O	288.49	1.05	2.91
	OC(O)=O	290.27	1.05	19.40

**Table 43:** Xray Photoelectron Spectroscopy data obtained for different signals, material analyzed corresponding to **Table 20**.

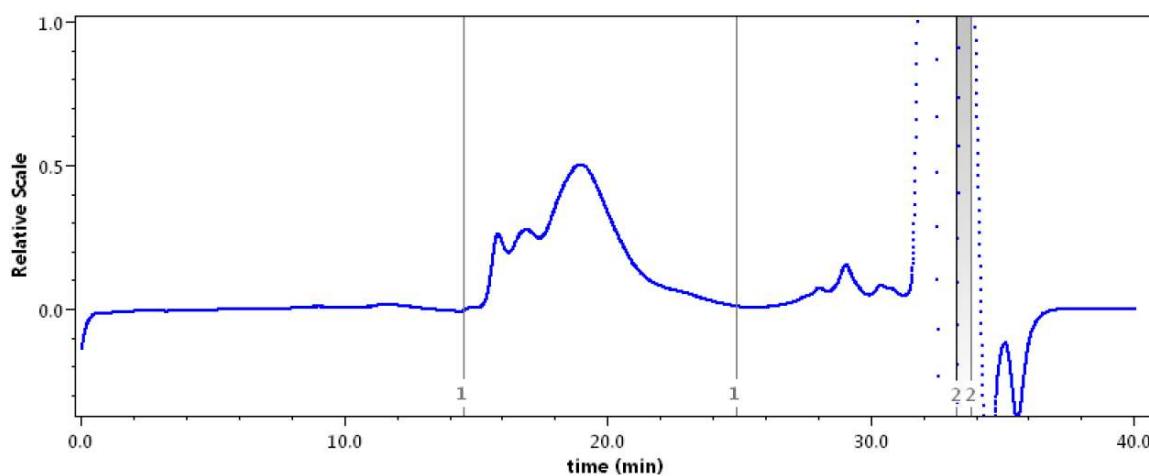
	Orbital	Component	Binding energy (eV)	FWHM (eV)	% Area
Entry 23	C 1s	C-C	285.00	1.10	44.11
		C-O	286.28	1.10	34.32
		OC-O	287.38	1.10	16.58
		OC=O	288.85	1.10	4.99
Entry 24	C 1s	C-C	285.00	1.09	42.30
		C-O	286.42	1.09	30.67
		OC-O	286.98	1.09	6.24
		OC=O	288.84	1.09	11.89
		OC(O)=O	290.31	1.09	8.89
Entry 25	C 1s	C-C	285.00	1.11	36.73
		C-O	286.49	1.11	42.04
		OC=O	288.80	1.11	8.38
		OC(O)=O	290.27	1.11	12.85

**Table 44:** Xray Photoelectron Spectroscopy data obtained for different signals, material analyzed corresponding to **Table 21**.

	Orbital	Component	Binding energy (eV)	FWHM (eV)	% Area
Entry 26	C 1s	C-C	285.00	1.19	34.04
		C-O	286.89	1.19	34.26
		OC=O	289.06	1.19	30.09
		OC(O)=O	290.33	1.19	1
Entry 27	C 1s	C-C	285.00	1.19	34.36
		C-O	286.76	1.19	36.54
		OC=O	289.09	1.19	24.25
		OC(O)=O	290.27	1.19	4.85

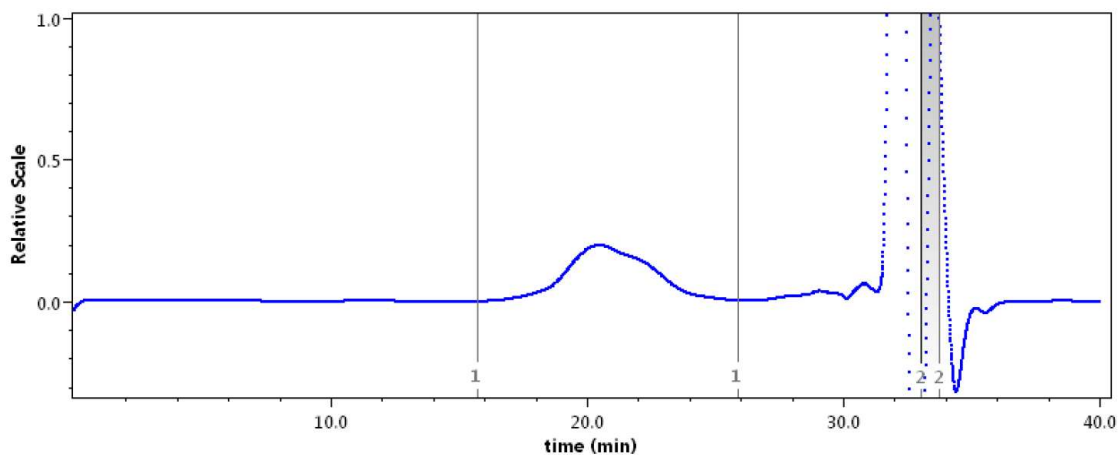
Entry 28	Orbital	Component	Binding energy (eV)	FWHM (eV)	% Area
	C 1s	C-C	285.00	1.20	32.79
		C-O	286.50	1.20	36.73
		OC-O	287.45	1.20	11.89
		OC=O	289.16	1.20	16.93
		OC(O)=O	290.259	1.20	1.67

### VIII.5. Size exclusion chromatography



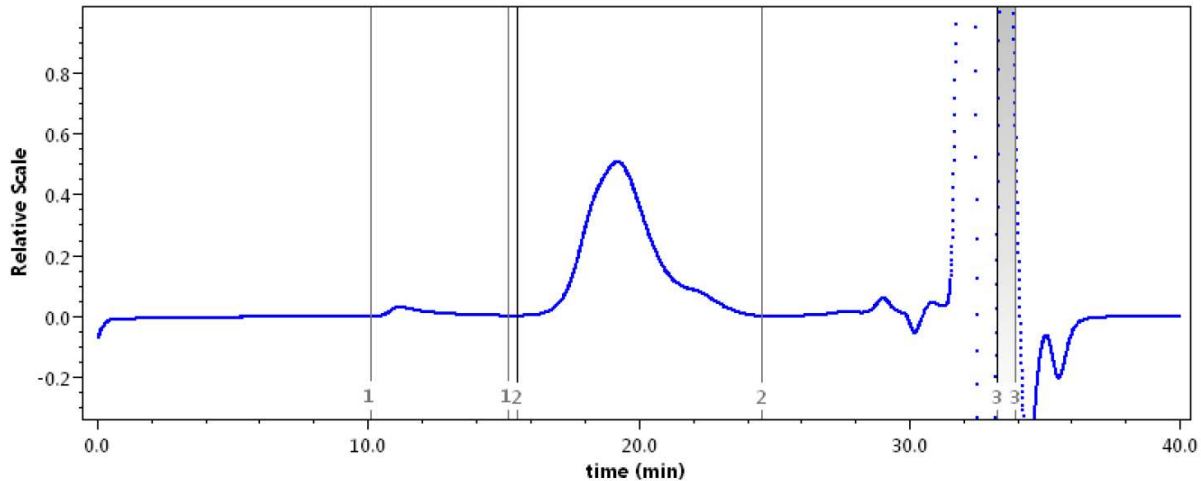
Peak Results		
	Peak 1	MARKER
<b>Masses</b>		
Calculated Mass ( $\mu\text{g}$ )	68.42	50.76
<b>Molar mass moments (g/mol)</b>		
Mn	$3.919 \times 10^4$ ( $\pm 8.656\%$ )	$9.688 \times 10^1$ ( $\pm 8.656\%$ )
Mw	$1.737 \times 10^5$ ( $\pm 8.656\%$ )	$9.709 \times 10^1$ ( $\pm 8.656\%$ )
Mz	$4.851 \times 10^5$ ( $\pm 19.356\%$ )	$9.730 \times 10^1$ ( $\pm 19.356\%$ )
M(avg)	$5.455 \times 10^3$ ( $\pm 0.418\%$ )	$9.906 \times 10^1$ ( $\pm 1.093\%$ )
<b>Polydispersity</b>		
Mw/Mn	4.433 ( $\pm 12.242\%$ )	1.002 ( $\pm 12.242\%$ )
Mz/Mn	12.379 ( $\pm 21.203\%$ )	1.004 ( $\pm 21.203\%$ )

**Figure 85:** SEC analyses data of the non-grafted copolymer obtained from reaction 26 in **Table 21**.



Peak Results		
	Peak 1	MARKER
<b>Masses</b>		
Calculated Mass ( $\mu\text{g}$ )	76.44	39.79
<b>Molar mass moments (g/mol)</b>		
Mn	$1.660 \times 10^4$ ( $\pm 4.262\%$ )	$1.012 \times 10^1$ ( $\pm 4.262\%$ )
Mw	$3.390 \times 10^4$ ( $\pm 4.262\%$ )	$1.030 \times 10^1$ ( $\pm 4.262\%$ )
Mz	$8.467 \times 10^4$ ( $\pm 9.530\%$ )	$1.048 \times 10^1$ ( $\pm 9.530\%$ )
M(avg)	$4.341 \times 10^3$ ( $\pm 0.196\%$ )	$1.125 \times 10^1$ ( $\pm 0.475\%$ )
<b>Polydispersity</b>		
Mw/Mn	2.042 ( $\pm 6.028\%$ )	1.017 ( $\pm 6.028\%$ )
Mz/Mn	5.101 ( $\pm 10.440\%$ )	1.035 ( $\pm 10.440\%$ )

Figure 87: SEC analyses data of the non-grafted copolymer obtained from reaction 27 in Table 21.



Peak Results			
	Peak 1	Peak 2	MARKER
<b>Masses</b>			
Calculated Mass ( $\mu\text{g}$ )	3.02	92.99	67.27
<b>Molar mass moments (g/mol)</b>			
Mn	$4.242 \times 10^7$ ( $\pm 4.262\%$ )	$3.762 \times 10^4$ ( $\pm 4.262\%$ )	9.438 ( $\pm 4.262\%$ )
Mw	$3.736 \times 10^8$ ( $\pm 4.262\%$ )	$7.148 \times 10^4$ ( $\pm 4.262\%$ )	9.724 ( $\pm 4.262\%$ )
Mz	$8.595 \times 10^8$ ( $\pm 9.530\%$ )	$1.281 \times 10^5$ ( $\pm 9.530\%$ )	$1.001 \times 10^1$ ( $\pm 9.530\%$ )
M(avg)	$3.587 \times 10^6$ ( $\pm 0.319\%$ )	$7.608 \times 10^3$ ( $\pm 0.202\%$ )	8.949 ( $\pm 0.506\%$ )
<b>Polydispersity</b>			
Mw/Mn	8.806 ( $\pm 6.028\%$ )	1.900 ( $\pm 6.028\%$ )	1.030 ( $\pm 6.028\%$ )
Mz/Mn	20.260 ( $\pm 10.440\%$ )	3.405 ( $\pm 10.440\%$ )	1.060 ( $\pm 10.440\%$ )

Figure 86: SEC analyses data of the non-grafted copolymer obtained from reaction 28 in Table 21.

## IX. References

- (1) Azab, S. M. A Comprehensive Structural Comparison between Cellulose and Starch Polymers Functionalized Cobalt Nanoparticles Sensors for the Nanomolar Detection of Paracetamol. *Journal of Electroanalytical Chemistry* **2019**, *840*, 319–327. <https://doi.org/10.1016/j.jelechem.2019.04.011>.
- (2) Ramesh, H. P.; Tharanathan, R. N. Carbohydrates—The Renewable Raw Materials of High Biotechnological Value. *Critical Reviews in Biotechnology* **2003**, *23* (2), 149–173. <https://doi.org/10.1080/713609312>.
- (3) Heux, L.; Dinand, E.; Vignon, M. R. Structural Aspects in Ultrathin Cellulose Microfibrils Followed by <sup>13</sup>C CP-MAS NMR. *Carbohydrate Polymers* **1999**, *40* (2), 115–124. [https://doi.org/10.1016/S0144-8617\(99\)00051-X](https://doi.org/10.1016/S0144-8617(99)00051-X).
- (4) Eichhorn, S. J.; Dufresne, A.; Aranguren, M.; Marcovich, N. E.; Capadona, J. R.; Rowan, S. J.; Weder, C.; Thielemans, W.; Roman, M.; Renneckar, S.; Gindl, W.; Veigel, S.; Keckes, J.; Yano, H.; Abe, K.; Nogi, M.; Nakagaito, A. N.; Mangalam, A.; Simonsen, J.; Benight, A. S.; Bismarck, A.; Berglund, L. A.; Peijs, T. Review: Current International Research into Cellulose Nanofibres and Nanocomposites. *J Mater Sci* **2010**, *45* (1), 1–33. <https://doi.org/10.1007/s10853-009-3874-0>.
- (5) Favier, V.; Chanzy, H.; Cavaille, J. Y. Polymer Nanocomposites Reinforced by Cellulose Whiskers. *Macromolecules* **1995**, *28* (18), 6365–6367. <https://doi.org/10.1021/ma00122a053>.
- (6) Azizi Samir, M. A. S.; Alloin, F.; Dufresne, A. Review of Recent Research into Cellulosic Whiskers, Their Properties and Their Application in Nanocomposite Field. *Biomacromolecules* **2005**, *6* (2), 612–626. <https://doi.org/10.1021/bm0493685>.
- (7) Nordgren, N.; Lönnberg, H.; Hult, A.; Malmström, E.; Rutland, M. W. Adhesion Dynamics for Cellulose Nanocomposites. *ACS Appl. Mater. Interfaces* **2009**, *1* (10), 2098–2103. <https://doi.org/10.1021/am900381t>.
- (8) Morandi, G.; Heath, L.; Thielemans, W. Cellulose Nanocrystals Grafted with Polystyrene Chains through Surface-Initiated Atom Transfer Radical Polymerization (SI-ATRP). *Langmuir* **2009**, *25* (14), 8280–8286. <https://doi.org/10.1021/la900452a>.
- (9) Habibi, Y.; Goffin, A.-L.; Schiltz, N.; Duquesne, E.; Dubois, P.; Dufresne, A. Bionanocomposites Based on Poly( $\epsilon$ -Caprolactone)-Grafted Cellulose Nanocrystals by Ring-Opening Polymerization. *J. Mater. Chem.* **2008**, *18* (41), 5002. <https://doi.org/10.1039/b809212e>.
- (10) Hafrén, J.; Córdova, A. Direct Organocatalytic Polymerization from Cellulose Fibers: Direct Organocatalytic Polymerization from Cellulose Fibers. *Macromol. Rapid Commun.* **2005**, *26* (2), 82–86. <https://doi.org/10.1002/marc.200400470>.
- (11) Ottou, W. N.; Sardon, H.; Mecerreyes, D.; Vignolle, J.; Taton, D. Update and Challenges in Organo-Mediated Polymerization Reactions. *Progress in Polymer Science* **2016**, *56*, 64–115. <https://doi.org/10.1016/j.progpolymsci.2015.12.001>.
- (12) Fèvre, M.; Vignolle, J.; Gnanou, Y.; Taton, D. Organocatalyzed Ring-Opening Polymerizations. In *Polymer Science: A Comprehensive Reference*; Elsevier, 2012; pp 67–115. <https://doi.org/10.1016/B978-0-444-53349-4.00119-9>.
- (13) Klemm, D.; Heublein, B.; Fink, H.-P.; Bohn, A. Cellulose: Fascinating Biopolymer and Sustainable Raw Material. *Angew. Chem. Int. Ed.* **2005**, *44* (22), 3358–3393. <https://doi.org/10.1002/anie.200460587>.

- (14) Komuriah, A.; Kumar, N. S.; Prasad, B. D. Chemical Composition of Natural Fibers and Its Influence on Their Mechanical Properties. *Mech Compos Mater* **2014**, *50* (3), 359–376. <https://doi.org/10.1007/s11029-014-9422-2>.
- (15) Bakri, M. K. B.; Rahman, M. R.; Chowdhury, F. I. Sources of Cellulose. In *Fundamentals and Recent Advances in Nanocomposites Based on Polymers and Nanocellulose*; Elsevier, 2022; pp 1–18. <https://doi.org/10.1016/B978-0-323-85771-0.00012-9>.
- (16) Comprehensive Cellulose Chemistry. Volume 1. Fundamentals and Analytical Methods By D. Klemm, B. Philipp, T. Heinze, U. Heinze, and W. Wagenknecht. Wiley: Weinheim, Germany. 1998. 260 Pp. \$236.25. ISBN 3-527-29413-9. *J. Am. Chem. Soc.* **1999**, *121* (37), 8677–8677. <https://doi.org/10.1021/ja9857514>.
- (17) Wolfs, J.; Meier, M. A. R. A More Sustainable Synthesis Approach for Cellulose Acetate Using the DBU/CO<sub>2</sub> Switchable Solvent System. *Green Chem.* **2021**, *23* (12), 4410–4420. <https://doi.org/10.1039/D1GC01508G>.
- (18) Heinze, T.; Liebert, T. Unconventional Methods in Cellulose Functionalization. *Progress in Polymer Science* **2001**, *26* (9), 1689–1762. [https://doi.org/10.1016/S0079-6700\(01\)00022-3](https://doi.org/10.1016/S0079-6700(01)00022-3).
- (19) Fox, S. C.; Li, B.; Xu, D.; Edgar, K. J. Regioselective Esterification and Etherification of Cellulose: A Review. *Biomacromolecules* **2011**, *12* (6), 1956–1972. <https://doi.org/10.1021/bm200260d>.
- (20) Mormann, W.; Demeter, J. Silylation of Cellulose with Hexamethyldisilazane in Liquid Ammonia First Examples of Completely Trimethylsilylated Cellulose. *Macromolecules* **1999**, *32* (5), 1706–1710. <https://doi.org/10.1021/ma9814393>.
- (21) Rahn, K.; Diamantoglou, M.; Klemm, D.; Berghmans, H.; Heinze, T. Homogeneous Synthesis of Cellulose P-Toluenesulfonates in N,N-Dimethylacetamide/LiCl Solvent System. *Angew. Makromol. Chemie* **1996**, *238* (1), 143–163. <https://doi.org/10.1002/apmc.1996.052380113>.
- (22) Ju, F. A Novel Efficient Enzyme Immobilization Reaction on NH<sub>2</sub> Polymers by Means of Lascorbic Acid. **1999**, *8*.
- (23) Tiller, J.; Klemm, D.; Berlin, P. Designed Aliphatic Aminocellulose Derivatives as Transparent and Functionalized Coatings for Enzyme Immobilization. *Designed Monomers and Polymers* **2001**, *4* (4), 315–328. <https://doi.org/10.1163/156855501753210808>.
- (24) Chinga-Carrasco, G. Cellulose Fibres, Nanofibrils and Microfibrils: The Morphological Sequence of MFC Components from a Plant Physiology and Fibre Technology Point of View. *Nanoscale Res Lett* **2011**, *6* (1), 417. <https://doi.org/10.1186/1556-276X-6-417>.
- (25) Nechyporchuk, O.; Belgacem, M. N.; Bras, J. Production of Cellulose Nanofibrils: A Review of Recent Advances. *Industrial Crops and Products* **2016**, *93*, 2–25. <https://doi.org/10.1016/j.indcrop.2016.02.016>.
- (26) Moon, R. J.; Martini, A.; Nairn, J.; Simonsen, J.; Youngblood, J. Cellulose Nanomaterials Review: Structure, Properties and Nanocomposites. *Chem. Soc. Rev.* **2011**, *40* (7), 3941. <https://doi.org/10.1039/c0cs00108b>.
- (27) Turbak, A. F.; Snyder, F. W. Microfibrillated Cellulose, a New Cellulose Product: Properties, Uses, and Commercial Potential. *Journal of Applied Polymer Science* **1983**, *37*, 815–827.
- (28) Svagan, A. J.; Azizi Samir, M. A. S.; Berglund, L. A. Biomimetic Polysaccharide Nanocomposites of High Cellulose Content and High Toughness. *Biomacromolecules* **2007**, *8* (8), 2556–2563. <https://doi.org/10.1021/bm0703160>.
- (29) Alemdar, A.; Sain, M. Biocomposites from Wheat Straw Nanofibers: Morphology, Thermal and Mechanical Properties. *Composites Science and Technology* **2008**, *68* (2), 557–565. <https://doi.org/10.1016/j.compscitech.2007.05.044>.

- (30) Dufresne, A.; Cavaille, J.-Y.; Vignon, M. R. Mechanical Behavior of Sheets Prepared from Sugar Beet Cellulose Microfibrils. *J. Appl. Polym. Sci.* **1997**, *64* (6), 1185–1194. [https://doi.org/10.1002/\(SICI\)1097-4628\(19970509\)64:6<1185::AID-APP19>3.0.CO;2-V](https://doi.org/10.1002/(SICI)1097-4628(19970509)64:6<1185::AID-APP19>3.0.CO;2-V).
- (31) Goussé, C.; Chanzy, H.; Cerrada, M. L.; Fleury, E. Surface Silylation of Cellulose Microfibrils: Preparation and Rheological Properties. *Polymer* **2004**, *45* (5), 1569–1575. <https://doi.org/10.1016/j.polymer.2003.12.028>.
- (32) Dufresne, A.; Dupeyre, D.; Vignon, M. R. Cellulose Microfibrils from Potato Tuber Cells: Processing and Characterization of Starch-Cellulose Microfibril Composites. *J. Appl. Polym. Sci.* **2000**, *76* (14), 2080–2092. [https://doi.org/10.1002/\(SICI\)1097-4628\(20000628\)76:14<2080::AID-APP12>3.0.CO;2-U](https://doi.org/10.1002/(SICI)1097-4628(20000628)76:14<2080::AID-APP12>3.0.CO;2-U).
- (33) Malainine, M. E.; Mahrouz, M.; Dufresne, A. Thermoplastic Nanocomposites Based on Cellulose Microfibrils from *Opuntia Ficus-Indica* Parenchyma Cell. *Composites Science and Technology* **2005**, *65* (10), 1520–1526. <https://doi.org/10.1016/j.compscitech.2005.01.003>.
- (34) Henriksson, M.; Henriksson, G.; Berglund, L. A.; Lindström, T. An Environmentally Friendly Method for Enzyme-Assisted Preparation of Microfibrillated Cellulose (MFC) Nanofibers. *European Polymer Journal* **2007**, *43* (8), 3434–3441. <https://doi.org/10.1016/j.eurpolymj.2007.05.038>.
- (35) Besbes, I.; Vilar, M. R.; Boufi, S. Nanofibrillated Cellulose from Alfa, Eucalyptus and Pine Fibres: Preparation, Characteristics and Reinforcing Potential. *Carbohydrate Polymers* **2011**, *86* (3), 1198–1206. <https://doi.org/10.1016/j.carbpol.2011.06.015>.
- (36) Liimatainen, H.; Visanko, M.; Sirviö, J.; Hormi, O.; Niinimäki, J. Sulfonated Cellulose Nanofibrils Obtained from Wood Pulp through Regioselective Oxidative Bisulfite Pre-Treatment. *Cellulose* **2013**, *20* (2), 741–749. <https://doi.org/10.1007/s10570-013-9865-y>.
- (37) Zimmermann, T.; Pöhler, E.; Geiger, T. Cellulose Fibrils for Polymer Reinforcement. *Adv. Eng. Mater.* **2004**, *6* (9), 754–761. <https://doi.org/10.1002/adem.200400097>.
- (38) Eriksen, Ø.; Syverud, K.; Gregersen, Ø. The Use of Microfibrillated Cellulose Produced from Kraft Pulp as Strength Enhancer in TMP Paper. *Nordic Pulp & Paper Research Journal* **2008**, *23* (3), 299–304. <https://doi.org/10.3183/npprj-2008-23-03-p299-304>.
- (39) Lindström, T.; Aulin, C. Market and Technical Challenges and Opportunities in the Area of Innovative New Materials and Composites Based on Nanocellulosics. *Scandinavian Journal of Forest Research* **2014**, *29* (4), 345–351. <https://doi.org/10.1080/02827581.2014.928365>.
- (40) Taniguchi, T.; Okamura, K. New Films Produced from Microfibrillated Natural Fibres. *Polym. Int.* **1998**, *47* (3), 291–294. [https://doi.org/10.1002/\(SICI\)1097-0126\(199811\)47:3<291::AID-PI11>3.0.CO;2-1](https://doi.org/10.1002/(SICI)1097-0126(199811)47:3<291::AID-PI11>3.0.CO;2-1).
- (41) Gane, P. A. C.; Schoellkopf, J.; Gantenbein, D.; Oftringen, S. Pohl, Villach (AT). Beat Kübler, 15.
- (42) Bardet, R.; Belgacem, M. N.; Bras, J. Different Strategies for Obtaining High Opacity Films of MFC with TiO<sub>2</sub> Pigments. *Cellulose* **2013**, *20* (6), 3025–3037. <https://doi.org/10.1007/s10570-013-0025-1>.
- (43) Karande, V. S.; Bharimalla, A. K.; Hadge, G. B.; Mhaske, S. T.; Vigneshwaran, N. Nanofibrillation of Cotton Fibers by Disc Refiner and Its Characterization. *Fibers Polym* **2011**, *12* (3), 399–404. <https://doi.org/10.1007/s12221-011-0399-3>.
- (44) Ho, T. T. T.; Abe, K.; Zimmermann, T.; Yano, H. Nanofibrillation of Pulp Fibers by Twin-Screw Extrusion. *Cellulose* **2015**, *22* (1), 421–433. <https://doi.org/10.1007/s10570-014-0518-6>.

- (45) Wang, S.; Cheng, Q. A Novel Process to Isolate Fibrils from Cellulose Fibers by High-Intensity Ultrasonication, Part 1: Process Optimization. *J. Appl. Polym. Sci.* **2009**, *113* (2), 1270–1275. <https://doi.org/10.1002/app.30072>.
- (46) Cherian, B. M.; Leão, A. L.; de Souza, S. F.; Thomas, S.; Pothan, L. A.; Kottaisamy, M. Isolation of Nanocellulose from Pineapple Leaf Fibres by Steam Explosion. *Carbohydrate Polymers* **2010**, *81* (3), 720–725. <https://doi.org/10.1016/j.carbpol.2010.03.046>.
- (47) Zhang, L.; Tsuzuki, T.; Wang, X. Preparation of Cellulose Nanofiber from Softwood Pulp by Ball Milling. *Cellulose* **2015**, *22* (3), 1729–1741. <https://doi.org/10.1007/s10570-015-0582-6>.
- (48) Kose, R.; Mitani, I.; Kasai, W.; Kondo, T. “Nanocellulose” As a Single Nanofiber Prepared from Pellicle Secreted by *Gluconacetobacter Xylinus* Using Aqueous Counter Collision. *Biomacromolecules* **2011**, *12* (3), 716–720. <https://doi.org/10.1021/bm1013469>.
- (49) Davis, N. J.; Flitscb, S. L. Selective Oxidation of Monosaccharide Derivatives to Uranic Acids. 4.
- (50) Tejado, A.; Alam, Md. N.; Antal, M.; Yang, H.; van de Ven, T. G. M. Energy Requirements for the Disintegration of Cellulose Fibers into Cellulose Nanofibers. *Cellulose* **2012**, *19* (3), 831–842. <https://doi.org/10.1007/s10570-012-9694-4>.
- (51) Aulin, C.; Ahola, S.; Josefsson, P.; Nishino, T.; Hirose, Y.; Österberg, M.; Wågberg, L. Nanoscale Cellulose Films with Different Crystallinities and Mesostructures—Their Surface Properties and Interaction with Water. *Langmuir* **2009**, *25* (13), 7675–7685. <https://doi.org/10.1021/la900323n>.
- (52) Saito, T.; Isogai, A. Introduction of Aldehyde Groups on Surfaces of Native Cellulose Fibers by TEMPO-Mediated Oxidation. *Colloids and Surfaces A: Physicochemical and Engineering Aspects* **2006**, *289* (1–3), 219–225. <https://doi.org/10.1016/j.colsurfa.2006.04.038>.
- (53) Rånby, B. G. Fibrous Macromolecular Systems. Cellulose and Muscle. The Colloidal Properties of Cellulose Micelles. *Discuss. Faraday Soc.* **1951**, *11* (0), 158–164. <https://doi.org/10.1039/DF9511100158>.
- (54) Habibi, Y.; Lucia, L. A.; Rojas, O. J. Cellulose Nanocrystals: Chemistry, Self-Assembly, and Applications. *Chem. Rev.* **2010**, *110* (6), 3479–3500. <https://doi.org/10.1021/cr900339w>.
- (55) Araki, J.; Wada, M.; Kuga, S.; Okano, T. Influence of Surface Charge on Viscosity Behavior of Cellulose Microcrystal Suspension. *J. Wood Sci.* **1999**, *45* (3), 258–261. <https://doi.org/10.1007/BF01177736>.
- (56) Filponnen, I. Filponnen Thesis CNC.Pdf. Ph.D. Thesis, North Carolina State University, Raleigh, 2009.
- (57) Sharples, A. The Hydrolysis of Cellulose and Its Relation to Structure. **1957**, 5.
- (58) Roman, M.; Winter, W. T. Effect of Sulfate Groups from Sulfuric Acid Hydrolysis on the Thermal Degradation Behavior of Bacterial Cellulose. *Biomacromolecules* **2004**, *5* (5), 1671–1677. <https://doi.org/10.1021/bm034519+>.
- (59) Mariano, M.; El Kissi, N.; Dufresne, A. Cellulose Nanocrystals and Related Nanocomposites: Review of Some Properties and Challenges. *J. Polym. Sci. Part B: Polym. Phys.* **2014**, *52* (12), 791–806. <https://doi.org/10.1002/polb.23490>.
- (60) Elazzouzi-Hafraoui, S.; Nishiyama, Y.; Putaux, J.-L.; Heux, L.; Dubreuil, F.; Rochas, C. The Shape and Size Distribution of Crystalline Nanoparticles Prepared by Acid Hydrolysis of Native Cellulose. *Biomacromolecules* **2008**, *9* (1), 57–65. <https://doi.org/10.1021/bm700769p>.

- (61) Bai, W.; Holbery, J.; Li, K. A Technique for Production of Nanocrystalline Cellulose with a Narrow Size Distribution. *Cellulose* **2009**, *16* (3), 455–465. <https://doi.org/10.1007/s10570-009-9277-1>.
- (62) Lahiji, R. R.; Xu, X.; Reifengerger, R.; Raman, A.; Rudie, A.; Moon, R. J. Atomic Force Microscopy Characterization of Cellulose Nanocrystals. *Langmuir* **2010**, *26* (6), 4480–4488. <https://doi.org/10.1021/la903111j>.
- (63) Hanley, S. J.; Revol, J.-F. O.; Godbout, L.; Gray, D. G. Atomic Force Microscopy and Transmission Electron Microscopy of Cellulose from *Micrasterias Denticulata*; Evidence for a Chiral Helical Micro@bril Twist. *12*.
- (64) Tashiro, K.; Kobayashi, M. Theoretical Evaluation of Three-Dimensional Elastic Constants of Native and Regenerated Celluloses: Role of Hydrogen Bonds. *Polymer* **1991**, *32* (8), 1516–1526. [https://doi.org/10.1016/0032-3861\(91\)90435-L](https://doi.org/10.1016/0032-3861(91)90435-L).
- (65) El Halal, S. L. M.; Kringel, D. H.; Zavareze, E. da R.; Dias, A. R. G. Methods for Extracting Cereal Starches from Different Sources: A Review. *Starch - Stärke* **2019**, *71* (11–12), 1900128. <https://doi.org/10.1002/star.201900128>.
- (66) Pérez, S.; Baldwin, P. M.; Gallant, D. J. Structural Features of Starch Granules I. In *Starch*; Elsevier, 2009; pp 149–192. <https://doi.org/10.1016/B978-0-12-746275-2.00005-7>.
- (67) Jane, J. Structural Features of Starch Granules II. In *Starch*; Elsevier, 2009; pp 193–236. <https://doi.org/10.1016/B978-0-12-746275-2.00006-9>.
- (68) Dai, L.; Zhang, J.; Cheng, F. Effects of Starches from Different Botanical Sources and Modification Methods on Physicochemical Properties of Starch-Based Edible Films. *International Journal of Biological Macromolecules* **2019**, *132*, 897–905. <https://doi.org/10.1016/j.ijbiomac.2019.03.197>.
- (69) Volpe, V.; De Feo, G.; De Marco, I.; Pantani, R. Use of Sunflower Seed Fried Oil as an Ecofriendly Plasticizer for Starch and Application of This Thermoplastic Starch as a Filler for PLA. *Industrial Crops and Products* **2018**, *122*, 545–552. <https://doi.org/10.1016/j.indcrop.2018.06.014>.
- (70) Blohm, S.; Heinze, T. Synthesis and Properties of Thermoplastic Starch Laurates. *Carbohydrate Research* **2019**, *486*, 107833. <https://doi.org/10.1016/j.carres.2019.107833>.
- (71) El Knidri, H.; Belaabed, R.; Addaou, A.; Laajeb, A.; Lahsini, A. Extraction, Chemical Modification and Characterization of Chitin and Chitosan. *International Journal of Biological Macromolecules* **2018**, *120*, 1181–1189. <https://doi.org/10.1016/j.ijbiomac.2018.08.139>.
- (72) Pillai, C. K. S.; Paul, W.; Sharma, C. P. Chitin and Chitosan Polymers: Chemistry, Solubility and Fiber Formation. *Progress in Polymer Science* **2009**, *34* (7), 641–678. <https://doi.org/10.1016/j.progpolymsci.2009.04.001>.
- (73) Nešić, A.; Cabrera-Barjas, G.; Dimitrijević-Branković, S.; Davidović, S.; Radovanović, N.; Delattre, C. Prospect of Polysaccharide-Based Materials as Advanced Food Packaging. *Molecules* **2019**, *25* (1), 135. <https://doi.org/10.3390/molecules25010135>.
- (74) Obianom, C.; Romanazzi, G.; Sivakumar, D. Effects of Chitosan Treatment on Avocado Postharvest Diseases and Expression of Phenylalanine Ammonia-Lyase, Chitinase and Lipxygenase Genes. *Postharvest Biology and Technology* **2019**, *147*, 214–221. <https://doi.org/10.1016/j.postharvbio.2018.10.004>.
- (75) Wang, A.; Ao, Q.; Wei, Y.; Gong, K.; Liu, X.; Zhao, N.; Gong, Y.; Zhang, X. Physical Properties and Biocompatibility of a Porous Chitosan-Based Fiber-Reinforced Conduit for Nerve Regeneration. *Biotechnol Lett* **2007**, *29* (11), 1697–1702. <https://doi.org/10.1007/s10529-007-9460-0>.

- (76) Yamane, S.; Iwasaki, N.; Kasahara, Y.; Harada, K.; Majima, T.; Monde, K.; Nishimura, S.; Minami, A. Effect of Pore Size Onin Vitro Cartilage Formation Using Chitosan-Based Hyaluronic Acid Hybrid Polymer Fibers. *J. Biomed. Mater. Res.* **2007**, *81A* (3), 586–593. <https://doi.org/10.1002/jbm.a.31095>.
- (77) Shao, X.; Hunter, C. J. Developing an Alginate/Chitosan Hybrid Fiber Scaffold for Annulus Fibrosus Cells. *J. Biomed. Mater. Res.* **2007**, *82A* (3), 701–710. <https://doi.org/10.1002/jbm.a.31030>.
- (78) Rinaudo, M. Chitin and Chitosan: Properties and Applications. *Progress in Polymer Science* **2006**, *31* (7), 603–632. <https://doi.org/10.1016/j.progpolymsci.2006.06.001>.
- (79) Carothers, W.; Arvin, J. A. Studies on Polymerization and Ring Formation. II. Poly-Esters. *Contribution N°11 from the experimental station of E.I Du Pont de Nemours and Company* **1929**, Vol. 51, 2560.
- (80) Lunt, J. Large-Scale Production, Properties and Commercial Applications of Polylactic Acid Polymers. *Polymer Degradation and Stability* **1998**, *59* (1–3), 145–152. [https://doi.org/10.1016/S0141-3910\(97\)00148-1](https://doi.org/10.1016/S0141-3910(97)00148-1).
- (81) Farrington, D.; Lunt, J.; Davies, S.; Blackburn, R. S. In *Poly(lactic acid) fibers; Biodegradable and sustainable fibres*.
- (82) *Biopolymers from Renewable Resources*; Kaplan, D. L., Ed.; Springer Berlin Heidelberg: Berlin, Heidelberg, 1998. <https://doi.org/10.1007/978-3-662-03680-8>.
- (83) Jamshidian, M.; Tehrany, E. A.; Imran, M.; Jacquot, M.; Desobry, S. Poly-Lactic Acid: Production, Applications, Nanocomposites, and Release Studies. *Comprehensive Reviews in Food Science and Food Safety* **2010**, *9* (5), 552–571. <https://doi.org/10.1111/j.1541-4337.2010.00126.x>.
- (84) Moon, S.-I.; Lee, C.-W.; Taniguchi, I.; Miyamoto, M.; Kimura, Y. Melt/Solid Polycondensation of l-Lactic Acid: An Alternative Route to Poly(l-Lactic Acid) with High Molecular Weight. *Polymer* **2001**, *42* (11), 5059–5062. [https://doi.org/10.1016/S0032-3861\(00\)00889-2](https://doi.org/10.1016/S0032-3861(00)00889-2).
- (85) Ishii, D.; Ying, T. H.; Mahara, A.; Murakami, S.; Yamaoka, T.; Lee, W.; Iwata, T. In Vivo Tissue Response and Degradation Behavior of PLLA and Stereocomplexed PLA Nanofibers. *Biomacromolecules* **2009**, *10* (2), 237–242. <https://doi.org/10.1021/bm8009363>.
- (86) Karamanlioglu, M.; Robson, G. D. The Influence of Biotic and Abiotic Factors on the Rate of Degradation of Poly(Lactic) Acid (PLA) Coupons Buried in Compost and Soil. *Polymer Degradation and Stability* **2013**, *98* (10), 2063–2071. <https://doi.org/10.1016/j.polyimdegradstab.2013.07.004>.
- (87) Auras, R. A.; Harte, B.; Selke, S.; Hernandez, R. Mechanical, Physical, and Barrier Properties of Poly(Lactide) Films. *Journal of Plastic Film & Sheeting* **2003**, *19* (2), 123–135. <https://doi.org/10.1177/8756087903039702>.
- (88) Jacobsen, S.; Fritz, H. G. Plasticizing Polylactide? The Effect of Different Plasticizers on the Mechanical Properties. *Polym. Eng. Sci.* **1999**, *39* (7), 1303–1310. <https://doi.org/10.1002/pen.11517>.
- (89) Södergård, A.; Stolt, M. Properties of Lactic Acid Based Polymers and Their Correlation with Composition. *Progress in Polymer Science* **2002**, *27* (6), 1123–1163. [https://doi.org/10.1016/S0079-6700\(02\)00012-6](https://doi.org/10.1016/S0079-6700(02)00012-6).
- (90) Van de Velde, K.; Kiekens, P. Biopolymers: Overview of Several Properties and Consequences on Their Applications. *Polymer Testing* **2002**, *21* (4), 433–442. [https://doi.org/10.1016/S0142-9418\(01\)00107-6](https://doi.org/10.1016/S0142-9418(01)00107-6).

- (91) Lehermeier, H. J.; Dorgan, J. R.; Way, J. D. Gas Permeation Properties of Poly(Lactic Acid). *Journal of Membrane Science* **2001**, *190* (2), 243–251. [https://doi.org/10.1016/S0376-7388\(01\)00446-X](https://doi.org/10.1016/S0376-7388(01)00446-X).
- (92) Labuza, T. P.; Breene, W. M. APPLICATIONS OF “ACTIVE PACKAGING” FOR IMPROVEMENT OF SHELF-LIFE AND NUTRITIONAL QUALITY OF FRESH AND EXTENDED SHELF-LIFE FOODS 1. 70.
- (93) Vermeiren, L.; Devlieghere, F.; van Beest, M.; de Kruijf, N.; Debevere, J. Developments in the Active Packaging of Foods. **1999**, 10.
- (94) Maharana, T.; Mohanty, B.; Negi, Y. S. Melt–Solid Polycondensation of Lactic Acid and Its Biodegradability. *Progress in Polymer Science* **2009**, *34* (1), 99–124. <https://doi.org/10.1016/j.progpolymsci.2008.10.001>.
- (95) Lasprilla, A. J. R.; Martinez, G. A. R.; Lunelli, B. H.; Jardini, A. L.; Filho, R. M. Poly-Lactic Acid Synthesis for Application in Biomedical Devices — A Review. *Biotechnology Advances* **2012**, *30* (1), 321–328. <https://doi.org/10.1016/j.biotechadv.2011.06.019>.
- (96) Azimi, B.; Nourpanah, P.; Rabiee, M.; Arbab, S. Poly (ε-Caprolactone) Fiber: An Overview. *Journal of Engineered Fibers and Fabrics* **2014**, *9* (3), 17.
- (97) Li, Z.; Tan, B. H. Towards the Development of Polycaprolactone Based Amphiphilic Block Copolymers: Molecular Design, Self-Assembly and Biomedical Applications. *Materials Science and Engineering: C* **2014**, *45*, 620–634. <https://doi.org/10.1016/j.msec.2014.06.003>.
- (98) Sachan, R.; Warkar, S. G.; Purwar, R. An Overview on Synthesis, Properties and Applications of Polycaprolactone Copolymers, Blends & Compo. *Polymer-Plastics Technology and Materials* **2022**, 33. <https://doi.org/10.1080/25740881.2022.2113890>.
- (99) Wang, H.; Ding, G.; Li, X.; She, H.; Zhu, Y.; Li, Y. Sustainable Production of γ-Valerolactone and δ-Valerolactone through the Coupling of Hydrogenation and Dehydrogenation. *Sustainable Energy Fuels* **2021**, *5* (4), 930–934. <https://doi.org/10.1039/D0SE01776K>.
- (100) Acharya, A. K.; Chang, Y. A.; Jones, G. O.; Rice, J. E.; Hedrick, J. L.; Horn, H. W.; Waymouth, R. M. Experimental and Computational Studies on the Mechanism of Zwitterionic Ring-Opening Polymerization of δ-Valerolactone with N-Heterocyclic Carbenes. *J. Phys. Chem. B* **2014**, *118* (24), 6553–6560. <https://doi.org/10.1021/jp500200b>.
- (101) Legrand, D. G.; Bendler, J. T. *Handbook of Polycarbonate Science and Technology*, Marcel Dekker.; New York/Basel, 2000.
- (102) Serini, V. Polycarbonates. In *Ullmann's Encyclopedia of Industrial Chemistry*; Wiley-VCH Verlag GmbH & Co. KGaA, Ed.; Wiley-VCH Verlag GmbH & Co. KGaA: Weinheim, Germany, 2000; p a21\_207. [https://doi.org/10.1002/14356007.a21\\_207](https://doi.org/10.1002/14356007.a21_207).
- (103) Kember, M. R.; Buchard, A.; Williams, C. K. Catalysts for CO<sub>2</sub> /Epoxide Copolymerisation. *Chem. Commun.* **2011**, *47* (1), 141–163. <https://doi.org/10.1039/C0CC02207A>.
- (104) North, M.; Pasquale, R.; Young, C. Synthesis of Cyclic Carbonates from Epoxides and CO<sub>2</sub>. *Green Chem.* **2010**, *12* (9), 1514. <https://doi.org/10.1039/c0gc00065e>.
- (105) Matsuda, H.; Ninagawa, A.; Nomura, R. Reaction of Carbon Dioxide with Epoxides in the Presence of Pentavalent Organoantimony Compounds. *Chem. Lett.* **1979**, 1261–1262.
- (106) Cokoja, M.; Wilhelm, M. E.; Anthofer, M. H.; Herrmann, W. A.; Kühn, F. E. Synthesis of Cyclic Carbonates from Epoxides and Carbon Dioxide by Using Organocatalysts. *ChemSusChem* **2015**, *8* (15), 2436–2454. <https://doi.org/10.1002/cssc.201500161>.
- (107) Rokicki, G. Aliphatic Cyclic Carbonates and Spiroorthocarbonates as Monomers. *Progress in Polymer Science* **2000**, *25* (2), 259–342. [https://doi.org/10.1016/S0079-6700\(00\)00006-X](https://doi.org/10.1016/S0079-6700(00)00006-X).

- (108) Baba, A.; Kashiwagi, H.; Matsuda, H. Cycloaddition of Oxetane and Carbon Dioxide Catalyzed by Tetraphenylstibonium Iodide. *Tetrahedron Letters* **1985**, *26* (10), 1323–1324. [https://doi.org/10.1016/S0040-4039\(00\)94883-4](https://doi.org/10.1016/S0040-4039(00)94883-4).
- (109) Clements, J. H. Reactive Applications of Cyclic Alkylene Carbonates. *Ind. Eng. Chem. Res.* **2003**, *42* (4), 663–674. <https://doi.org/10.1021/ie020678i>.
- (110) Baba, Akio.; Kashiwagi, Hiroki.; Matsuda, Haruo. Reaction of Carbon Dioxide with Oxetane Catalyzed by Organotin Halide Complexes: Control of Reaction by Ligands. *Organometallics* **1987**, *6* (1), 137–140. <https://doi.org/10.1021/om00144a024>.
- (111) Hosseinian, A.; Farshbaf, S.; Mohammadi, R.; Monfared, A.; Vessally, E. Advancements in Six-Membered Cyclic Carbonate (1,3-Dioxan-2-One) Synthesis Utilizing Carbon Dioxide as a C1 Source. *RSC Adv.* **2018**, *8* (32), 17976–17988. <https://doi.org/10.1039/C8RA01280F>.
- (112) Vogdanis, L.; Heitz, W. The Polymerization of Ethylene Carbonate. *Makromol. Chem., Rapid Commun.* **1986**, *7* (9), 543–547. <https://doi.org/10.1002/marc.1986.030070901>.
- (113) Helou, M.; Miserque, O.; Brusson, J.-M.; Carpentier, J.-F.; Guillaume, S. M. Ultraproductive, Zinc-Mediated, Immortal Ring-Opening Polymerization of Trimethylene Carbonate. *Chem. Eur. J.* **2008**, *14* (29), 8772–8775. <https://doi.org/10.1002/chem.200801416>.
- (114) Wei, J.; Riffel, M. N.; Diaconescu, P. L. Redox Control of Aluminum Ring-Opening Polymerization: A Combined Experimental and DFT Investigation. *Macromolecules* **2017**, *50* (5), 1847–1861. <https://doi.org/10.1021/acs.macromol.6b02402>.
- (115) Zhu, K. J.; Hendren, R. W.; Jensen, K.; Pitt, C. G. Synthesis, Properties, and Biodegradation of Poly(1,3-Trimethylene Carbonate). *Macromolecules* **1991**, *24* (8), 1736–1740. <https://doi.org/10.1021/ma00008a008>.
- (116) Feng, J.; Zhuo, R.-X.; Zhang, X.-Z. Construction of Functional Aliphatic Polycarbonates for Biomedical Applications. *Progress in Polymer Science* **2012**, *37* (2), 211–236. <https://doi.org/10.1016/j.progpolymsci.2011.07.008>.
- (117) Helou, M.; Miserque, O.; Brusson, J.-M.; Carpentier, J.-F.; Guillaume, S. M. Organocatalysts for the Controlled “Immortal” Ring-Opening Polymerization of Six-Membered-Ring Cyclic Carbonates: A Metal-Free, Green Process. *Chem. Eur. J.* **2010**, *16* (46), 13805–13813. <https://doi.org/10.1002/chem.201001111>.
- (118) Konwar, D. B.; Satapathy, B. K.; Jacob, J. Influence of Aliphatic Polycarbonate Middle Block on Mechanical and Microstructural Behaviour of Triblock Copolymers Based on Poly(L-Lactide) and Polycarbonate: Influence of Polycarbonate Middle Block on Behaviour of Triblock Copolymers. *Polym. Int.* **2019**, *68* (3), 400–409. <https://doi.org/10.1002/pi.5723>.
- (119) Nobuoka, H.; Ajiro, H. Novel Synthesis Method of Ester Free Trimethylene Carbonate Derivatives. *Tetrahedron Letters* **2019**, *60* (2), 164–170. <https://doi.org/10.1016/j.tetlet.2018.12.002>.
- (120) Jenkins, A. D.; Kratochvíl, P.; Stepto, R. F. T.; Suter, U. W. Glossary of Basic Terms in Polymer Science (IUPAC Recommendations 1996). *Pure and Applied Chemistry* **1996**, *68* (12), 2287–2311. <https://doi.org/10.1351/pac199668122287>.
- (121) Leuchs, H. Ueber die Glycin-carbonsäure. *Ber. Dtsch. Chem. Ges.* **1906**, *39* (1), 857–861. <https://doi.org/10.1002/cber.190603901133>.
- (122) Dainton, F. S.; Devlin, T. R. E.; Small, P. A. The Thermodynamics of Polymerization of Cyclic Compounds by Ring Opening. *Trans. Faraday Soc.* **1955**, *51*, 1710. <https://doi.org/10.1039/TF9555101710>.
- (123) Kulkarni, R. K.; Pani, K. C.; Neuman, C.; Leonard, F. LACTIC ACTIC Acid in Its Racemic or Optically Active Form Can Undergo Acid Catalyzed Homopolymerization to

Yield a Polymer of Lower Molecular Weight, Which Is Not Suitable for Plastic or Fibers.1  
However, the Cyclic Diester, the Lactide 2 of Lactic Acid, Can. 5.

- (124) Albertsson, A.-C.; Varma, I. K. Recent Developments in Ring Opening Polymerization of Lactones for Biomedical Applications. *Biomacromolecules* **2003**, *4* (6), 1466–1486. <https://doi.org/10.1021/bm034247a>.
- (125) Fontaine, L. Handbook of Ring-Opening Polymerization. Edited by Philippe Dubois, Olivier Coulembier and Jean-Marie Raquez. *Angew. Chem. Int. Ed.* **2009**, *48* (52), 9780–9780. <https://doi.org/10.1002/anie.200904840>.
- (126) Penczek, S.; Kubisa, P.; Matyjaszewski, K. Monomer Structures, Ring Strains and Nucleophilicities (Basicities). In *Cationic Ring-Opening Polymerization of Heterocyclic Monomers*; Cantow, H.-J., Dall'Asta, G., Dušek, K., Ferry, J. D., Fujita, H., Gordon, M., Kennedy, J. P., Kern, W., Okamura, S., Overberger, C. G., Saegusa, T., Schulz, G. V., Slichter, W. P., Stille, J. K., Series Eds.; Springer Berlin Heidelberg: Berlin, Heidelberg, 1980; Vol. 37, pp 3–7. <https://doi.org/10.1007/BFb0023045>.
- (127) Hashimoto, K. Ring-Opening Polymerization of Lactams. Living Anionic Polymerization and Its Applications. *Progress in Polymer Science* **2000**, *25* (10), 1411–1462. [https://doi.org/10.1016/S0079-6700\(00\)00018-6](https://doi.org/10.1016/S0079-6700(00)00018-6).
- (128) Kubisa, P.; Penczek, S. Cationic Activated Monomer Polymerization of Heterocyclic Monomers. *Progress in Polymer Science* **1999**, *24* (10), 1409–1437. [https://doi.org/10.1016/S0079-6700\(99\)00028-3](https://doi.org/10.1016/S0079-6700(99)00028-3).
- (129) Fuchise, K.; Chen, Y.; Satoh, T.; Kakuchi, T. Recent Progress in Organocatalytic Group Transfer Polymerization. *Polym. Chem.* **2013**, *4* (16), 4278. <https://doi.org/10.1039/c3py00278k>.
- (130) Gazeau-Bureau, S.; Delcroix, D.; Martín-Vaca, B.; Bourissou, D.; Navarro, C.; Magnet, S. Organo-Catalyzed ROP of  $\epsilon$ -Caprolactone: Methanesulfonic Acid Competes with Trifluoromethanesulfonic Acid. *Macromolecules* **2008**, *41* (11), 3782–3784. <https://doi.org/10.1021/ma800626q>.
- (131) Oshimura, M.; Tang, T.; Takasu, A. Ring-opening Polymerization of  $\epsilon$ -caprolactone Using Perfluoroalkanesulfonates and Perfluoroalkanesulfonimides as Organic Catalysts. *J. Polym. Sci. A Polym. Chem.* **2011**, *49* (5), 1210–1218. <https://doi.org/10.1002/pola.24539>.
- (132) Delcroix, D.; Martín-Vaca, B.; Bourissou, D.; Navarro, C. Ring-Opening Polymerization of Trimethylene Carbonate Catalyzed by Methanesulfonic Acid: Activated Monomer versus Active Chain End Mechanisms. *Macromolecules* **2010**, *43* (21), 8828–8835. <https://doi.org/10.1021/ma101461y>.
- (133) Bourissou, D.; Martín-Vaca, B.; Dumitrescu, A.; Graullier, M.; Lacombe, F. Controlled Cationic Polymerization of Lactide. *Macromolecules* **2005**, *38* (24), 9993–9998. <https://doi.org/10.1021/ma051646k>.
- (134) Kakuchi, R.; Tsuji, Y.; Chiba, K.; Fuchise, K.; Sakai, R.; Satoh, T.; Kakuchi, T. Controlled/Living Ring-Opening Polymerization of  $\delta$ -Valerolactone Using Triflylimide as an Efficient Cationic Organocatalyst. *Macromolecules* **2010**, *43* (17), 7090–7094. <https://doi.org/10.1021/ma100798u>.
- (135) Casas, J.; Persson, P. V.; Iversen, T.; Córdova, A. Direct Organocatalytic Ring-Opening Polymerizations of Lactones. *Advanced Synthesis & Catalysis* **2004**, *346* (910), 1087–1089. <https://doi.org/10.1002/adsc.200404082>.
- (136) Labet, M.; Thielemans, W. Citric Acid as a Benign Alternative to Metal Catalysts for the Production of Cellulose-Grafted-Polycaprolactone Copolymers. *Polym. Chem.* **2012**, *3* (3), 679. <https://doi.org/10.1039/c2py00493c>.

- (137) Zhang, L.; Nederberg, F.; Pratt, R. C.; Waymouth, R. M.; Hedrick, J. L.; Wade, C. G. Phosphazene Bases: A New Category of Organocatalysts for the Living Ring-Opening Polymerization of Cyclic Esters. *Macromolecules* **2007**, *40* (12), 4154–4158. <https://doi.org/10.1021/ma070316s>.
- (138) Zhang, L.; Nederberg, F.; Messman, J. M.; Pratt, R. C.; Hedrick, J. L.; Wade, C. G. Organocatalytic Stereoselective Ring-Opening Polymerization of Lactide with Dimeric Phosphazene Bases. *J. Am. Chem. Soc.* **2007**, *129* (42), 12610–12611. <https://doi.org/10.1021/ja074131c>.
- (139) Yang, H.; Xu, J.; Pispas, S.; Zhang, G. Hybrid Copolymerization of  $\epsilon$ -Caprolactone and Methyl Methacrylate. *Macromolecules* **2012**, *45* (8), 3312–3317. <https://doi.org/10.1021/ma300291q>.
- (140) Dove, A. P.; Pratt, R. C.; Lohmeijer, B. G. G.; Waymouth, R. M.; Hedrick, J. L. Thiourea-Based Bifunctional Organocatalysis: Supramolecular Recognition for Living Polymerization. *J. Am. Chem. Soc.* **2005**, *127* (40), 13798–13799. <https://doi.org/10.1021/ja0543346>.
- (141) Lohmeijer, B. G. G.; Pratt, R. C.; Leibfarth, F.; Logan, J. W.; Long, D. A.; Dove, A. P.; Nederberg, F.; Choi, J.; Wade, C.; Waymouth, R. M.; Hedrick, J. L. Guanidine and Amidine Organocatalysts for Ring-Opening Polymerization of Cyclic Esters. *Macromolecules* **2006**, *39* (25), 8574–8583. <https://doi.org/10.1021/ma0619381>.
- (142) Pratt, R. C.; Nederberg, F.; Waymouth, R. M.; Hedrick, J. L. Tagging Alcohols with Cyclic Carbonate: A Versatile Equivalent of (Meth)Acrylate for Ring-Opening Polymerization. *Chem. Commun.* **2008**, No. 1, 114–116. <https://doi.org/10.1039/B713925J>.
- (143) Connor, E. F.; Nyce, G. W.; Myers, M.; Möck, A.; Hedrick, J. L. First Example of N-Heterocyclic Carbenes as Catalysts for Living Polymerization: Organocatalytic Ring-Opening Polymerization of Cyclic Esters. *J. Am. Chem. Soc.* **2002**, *124* (6), 914–915. <https://doi.org/10.1021/ja0173324>.
- (144) Nyce, G. W.; Glauser, T.; Connor, E. F.; Möck, A.; Waymouth, R. M.; Hedrick, J. L. In Situ Generation of Carbenes: A General and Versatile Platform for Organocatalytic Living Polymerization. *J. Am. Chem. Soc.* **2003**, *125* (10), 3046–3056. <https://doi.org/10.1021/ja021084+>.
- (145) Jensen, T. R.; Breyfogle, L. E.; Hillmyer, M. A.; Tolman, W. B. Stereoelective Polymerization of d,l-Lactide Using N-Heterocyclic Carbene Based Compounds. *Chem. Commun.* **2004**, No. 21, 2504. <https://doi.org/10.1039/b405362a>.
- (146) Coulembier, O.; Kiesewetter, M. K.; Mason, A.; Dubois, P.; Hedrick, J. L.; Waymouth, R. M. A Distinctive Organocatalytic Approach to Complex Macromolecular Architectures. *Angew. Chem. Int. Ed.* **2007**, *46* (25), 4719–4721. <https://doi.org/10.1002/anie.200700522>.
- (147) Dove, A. P.; Li, H.; Pratt, R. C.; Lohmeijer, B. G. G.; Culkin, D. A.; Waymouth, R. M.; Hedrick, J. L. Stereoselective Polymerization of Rac- and Meso-Lactide Catalyzed by Sterically Encumbered N-Heterocyclic Carbenes. *Chem. Commun.* **2006**, No. 27, 2881. <https://doi.org/10.1039/b601393g>.
- (148) Nederberg, F.; Lohmeijer, B. G. G.; Leibfarth, F.; Pratt, R. C.; Choi, J.; Dove, A. P.; Waymouth, R. M.; Hedrick, J. L. Organocatalytic Ring Opening Polymerization of Trimethylene Carbonate. *Biomacromolecules* **2007**, *8* (1), 153–160. <https://doi.org/10.1021/bm060795n>.
- (149) Nederberg, F.; Connor, E. F.; Möller, M.; Glauser, T.; Hedrick, J. L. New Paradigms for Organic Catalysts: The First Organocatalytic Living Polymerization. *Angew. Chem.* **2001**, *113* (14), 2784–2787. [https://doi.org/10.1002/1521-3757\(20010716\)113:14<2784::AID-ANGE2784>3.0.CO;2-B](https://doi.org/10.1002/1521-3757(20010716)113:14<2784::AID-ANGE2784>3.0.CO;2-B).

- (150) Miao, Y.; Rousseau, C.; Mortreux, A.; Martin, P.; Zinck, P. Access to New Carbohydrate-Functionalized Polylactides via Organocatalyzed Ring-Opening Polymerization. *Polymer* **2011**, *52* (22), 5018–5026. <https://doi.org/10.1016/j.polymer.2011.08.040>.
- (151) Feng, H.; Dong, C.-M. Preparation and Characterization of Chitosan- Graft -Poly ( $\epsilon$ -Caprolactone) with an Organic Catalyst. *J. Polym. Sci. A Polym. Chem.* **2006**, *44* (18), 5353–5361. <https://doi.org/10.1002/pola.21625>.
- (152) Penczek, S.; Cypryk, M.; Duda, A.; Kubisa, P.; Slomkowski, S. Living Ring-Opening Polymerizations of Heterocyclic Monomers. *Progress in Polymer Science* **2007**, *32* (2), 247–282. <https://doi.org/10.1016/j.progpolymsci.2007.01.002>.
- (153) Domínguez de María, P. Minimal Hydrolases: Organocatalytic Ring-Opening Polymerizations Catalyzed by Naturally Occurring Carboxylic Acids. *ChemCatChem* **2010**, *2* (5), 487–492. <https://doi.org/10.1002/cctc.201000030>.
- (154) Molenberg, A.; Moller, M. A Fast Catalyst System for the Ring-Opening Polymerization of Cyclosiloxanes. *5*.
- (155) Kiesewetter, M. K.; Shin, E. J.; Hedrick, J. L.; Waymouth, R. M. Organocatalysis: Opportunities and Challenges for Polymer Synthesis. *Macromolecules* **2010**, *43* (5), 2093–2107. <https://doi.org/10.1021/ma9025948>.
- (156) Bonduelle, C.; Martín-Vaca, B.; Cossío, F. P.; Bourissou, D. Monomer versus Alcohol Activation in the 4-Dimethylaminopyridine-Catalyzed Ring-Opening Polymerization of Lactide and LacticO-Carboxylic Anhydride. *Chem. Eur. J.* **2008**, *14* (17), 5304–5312. <https://doi.org/10.1002/chem.200800346>.
- (157) Nederberg, F.; Connor, E. F.; Glausser, T.; Hedrick, J. L. Organocatalytic Chain Scission of Poly(Lactides): A General Route to Controlled Molecular Weight, Functionality and Macromolecular Architecture. *Chem. Commun.* **2001**, No. 20, 2066–2067. <https://doi.org/10.1039/b106125a>.
- (158) Brignou, P.; Priebe Gil, M.; Casagrande, O.; Carpentier, J.-F.; Guillaume, S. M. Polycarbonates Derived from Green Acids: Ring-Opening Polymerization of Seven-Membered Cyclic Carbonates. *Macromolecules* **2010**, *43* (19), 8007–8017. <https://doi.org/10.1021/ma1014098>.
- (159) Guerin, W.; Helou, M.; Carpentier, J.-F.; Slawinski, M.; Brusson, J.-M.; Guillaume, S. M. Macromolecular Engineering Viaring-Opening Polymerization (1): L -Lactide/Trimethylene Carbonate Block Copolymers as Thermoplastic Elastomers. *Polym. Chem.* **2013**, *4* (4), 1095–1106. <https://doi.org/10.1039/C2PY20859H>.
- (160) Ishikawa, T. *Superbases for Organic Synthesis: Guanidines, Amidines and Phosphazenes and Related Organocatalysts*; Wiley: Chichester, West Sussex, U.K., 2009.
- (161) Brown, H. A.; De Crisci, A. G.; Hedrick, J. L.; Waymouth, R. M. Amidine-Mediated Zwitterionic Polymerization of Lactide. *ACS Macro Lett.* **2012**, *1* (9), 1113–1115. <https://doi.org/10.1021/mz300276u>.
- (162) Coulembier, O.; Dubois, P. 4-Dimethylaminopyridine-Based Organoactivation: From Simple Esterification to Lactide Ring-Opening “Living” Polymerization. *J. Polym. Sci. A Polym. Chem.* **2012**, *50* (9), 1672–1680. <https://doi.org/10.1002/pola.25949>.
- (163) Miao, Y.; Stanley, N.; Favrelle, A.; Bousquet, T.; Bria, M.; Mortreux, A.; Zinck, P. New Acid/Base Salts as Co-Catalysts for the Organocatalyzed Ring Opening Polymerization of Lactide. *J. Polym. Sci. Part A: Polym. Chem.* **2015**, *53* (5), 659–664. <https://doi.org/10.1002/pola.27488>.

- (164) Sherck, N. J.; Kim, H. C.; Won, Y.-Y. Elucidating a Unified Mechanistic Scheme for the DBU-Catalyzed Ring-Opening Polymerization of Lactide to Poly(Lactic Acid). *Macromolecules* **2016**, *49* (13), 4699–4713. <https://doi.org/10.1021/acs.macromol.6b00621>.
- (165) Martello, M. T.; Burns, A.; Hillmyer, M. Bulk Ring-Opening Transesterification Polymerization of the Renewable  $\delta$ -Decalactone Using an Organocatalyst. *ACS Macro Lett.* **2012**, *1* (1), 131–135. <https://doi.org/10.1021/mz200006s>.
- (166) Meimoun, J.; Favrelle-Huret, A.; Bria, M.; Merle, N.; Stoclet, G.; De Winter, J.; Mincheva, R.; Raquez, J.-M.; Zinck, P. Epimerization and Chain Scission of Poly lactides in the Presence of an Organic Base, TBD. *Polymer Degradation and Stability* **2020**, *181*, 109188. <https://doi.org/10.1016/j.polymdegradstab.2020.109188>.
- (167) Simón, L.; Goodman, J. M. The Mechanism of TBD-Catalyzed Ring-Opening Polymerization of Cyclic Esters. *J. Org. Chem.* **2007**, *72* (25), 9656–9662. <https://doi.org/10.1021/jo702088c>.
- (168) Asano, S.; Aida, T.; Inoue, S. ‘Immortal’ Polymerization. Polymerization of Epoxide Catalysed by an Aluminium Porphyrin–Alcohol System. *J. Chem. Soc., Chem. Commun.* **1985**, No. 17, 1148–1149. <https://doi.org/10.1039/C39850001148>.
- (169) Ajellal, N.; Carpentier, J.-F.; Guillaume, C.; Guillaume, S.; Helou, M.; Poirier, V.; Sarazin, Y.; Trifonov, A. Metal-Catalyzed Immortal Ring-Opening Polymerization of Lactones, Lactides and Cyclic Carbonates. *Dalton Trans.* **2010**, *39* (36), 8354. <https://doi.org/10.1039/c0dt90044c>.
- (170) Soykeabkaew, N.; Thanomsilp, C.; Suwanton, O. A Review: Starch-Based Composite Foams. *Composites Part A: Applied Science and Manufacturing* **2015**, *78*, 246–263. <https://doi.org/10.1016/j.compositesa.2015.08.014>.
- (171) Othman, S. H. Bio-Nanocomposite Materials for Food Packaging Applications: Types of Biopolymer and Nano-Sized Filler. *Agriculture and Agricultural Science Procedia* **2014**, *2*, 296–303. <https://doi.org/10.1016/j.aaspro.2014.11.042>.
- (172) Sharma, A.; Thakur, M.; Bhattacharya, M.; Mandal, T.; Goswami, S. Commercial Application of Cellulose Nano-Composites – A Review. *Biotechnology Reports* **2019**, *21*, e00316. <https://doi.org/10.1016/j.btre.2019.e00316>.
- (173) Bondeson, D.; Oksman, K. Dispersion and Characteristics of Surfactant Modified Cellulose Whiskers Nanocomposites. *Composite Interfaces* **2007**, *14* (7–9), 617–630. <https://doi.org/10.1163/156855407782106519>.
- (174) Siqueira, G.; Mathew, A. P.; Oksman, K. Processing of Cellulose Nanowhiskers/Cellulose Acetate Butyrate Nanocomposites Using Sol–Gel Process to Facilitate Dispersion. *Composites Science and Technology* **2011**, *71* (16), 1886–1892. <https://doi.org/10.1016/j.compscitech.2011.09.002>.
- (175) Wohlhauser, S.; Delepierre, G.; Labet, M.; Morandi, G.; Thielemans, W.; Weder, C.; Zoppe, J. O. Grafting Polymers from Cellulose Nanocrystals: Synthesis, Properties, and Applications. *Macromolecules* **2018**, *51* (16), 6157–6189. <https://doi.org/10.1021/acs.macromol.8b00733>.
- (176) Thielemans, W.; Belgacem, M. N.; Dufresne, A. Starch Nanocrystals with Large Chain Surface Modifications. *Langmuir* **2006**, *22* (10), 4804–4810. <https://doi.org/10.1021/la053394m>.
- (177) Roy, D.; Semsarilar, M.; Guthrie, J. T.; Perrier, S. Cellulose Modification by Polymer Grafting: A Review. *Chem. Soc. Rev.* **2009**, *38* (7), 2046. <https://doi.org/10.1039/b808639g>.
- (178) Lönnberg, H.; Larsson, K.; Lindström, T.; Hult, A.; Malmström, E. Synthesis of Polycaprolactone-Grafted Microfibrillated Cellulose for Use in Novel Bionanocomposites–

- Influence of the Graft Length on the Mechanical Properties. *ACS Appl. Mater. Interfaces* **2011**, 3 (5), 1426–1433. <https://doi.org/10.1021/am2001828>.
- (179) Labet, M.; Thielemans, W. Improving the Reproducibility of Chemical Reactions on the Surface of Cellulose Nanocrystals: ROP of  $\epsilon$ -Caprolactone as a Case Study. *Cellulose* **2011**, 18 (3), 607–617. <https://doi.org/10.1007/s10570-011-9527-x>.
- (180) Samuel, C.; Chalamet, Y.; Boisson, F.; Majesté, J.-C.; Becquart, F.; Fleury, E. Highly Efficient Metal-Free Organic Catalysts to Design New Environmentally-Friendly Starch-Based Blends. *J. Polym. Sci. Part A: Polym. Chem.* **2014**, 52 (4), 493–503. <https://doi.org/10.1002/pola.27022>.
- (181) Revol, J.-F.; Bradford, H.; Giasson, J.; Marchessault, R. H.; Gray, D. G. Helicoidal Self-Ordering of Cellulose Microfibrils in Aqueous Suspension. *International Journal of Biological Macromolecules* **1992**, 14 (3), 170–172. [https://doi.org/10.1016/S0141-8130\(05\)80008-X](https://doi.org/10.1016/S0141-8130(05)80008-X).
- (182) Eyley, S.; Schütz, C.; Thielemans, W. Surface Chemistry and Characterization of Cellulose Nanocrystals. In *Cellulose Science and Technology*; Rosenau, T., Potthast, A., Hell, J., Eds.; John Wiley & Sons, Inc.: Hoboken, NJ, USA, 2018; pp 223–252. <https://doi.org/10.1002/9781119217619.ch10>.
- (183) Frisch, M. J.; Trucks, G. W.; Schlegel, H. B.; Scuseria, G. E.; Robb, M. A.; Cheeseman, J. R.; Scalmani, G.; Barone, V.; Petersson, G. A.; Nakatsuji, H.; Li, X.; Caricato, M.; Marenich, A. V.; Bloino, J.; Janesko, B. G.; Gomperts, R.; Mennucci, B.; Hratchian, H. P.; Ortiz, J. V.; Izmaylov, A. F.; Sonnenberg, J. L.; Williams; Ding, F.; Lipparini, F.; Egidi, F.; Goings, J.; Peng, B.; Petrone, A.; Henderson, T.; Ranasinghe, D.; Zakrzewski, V. G.; Gao, J.; Rega, N.; Zheng, G.; Liang, W.; Hada, M.; Ehara, M.; Toyota, K.; Fukuda, R.; Hasegawa, J.; Ishida, M.; Nakajima, T.; Honda, Y.; Kitao, O.; Nakai, H.; Vreven, T.; Throssell, K.; Montgomery Jr., J. A.; Peralta, J. E.; Ogliaro, F.; Bearpark, M. J.; Heyd, J. J.; Brothers, E. N.; Kudin, K. N.; Staroverov, V. N.; Keith, T. A.; Kobayashi, R.; Normand, J.; Raghavachari, K.; Rendell, A. P.; Burant, J. C.; Iyengar, S. S.; Tomasi, J.; Cossi, M.; Millam, J. M.; Klene, M.; Adamo, C.; Cammi, R.; Ochterski, J. W.; Martin, R. L.; Morokuma, K.; Farkas, O.; Foresman, J. B.; Fox, D. J. *Gaussian 16 Rev. B.01*; Wallingford, CT, 2016.
- (184) Zhao, Y.; Truhlar, D. G. The M06 Suite of Density Functionals for Main Group Thermochemistry, Thermochemical Kinetics, Noncovalent Interactions, Excited States, and Transition Elements: Two New Functionals and Systematic Testing of Four M06-Class Functionals and 12 Other Functionals. *Theoretical Chemistry Accounts* **2008**, 120 (1–3), 215–241. <https://doi.org/10.1007/s00214-007-0310-x>.
- (185) Marenich, A. V.; Cramer, C. J.; Truhlar, D. G. Universal Solvation Model Based on Solute Electron Density and on a Continuum Model of the Solvent Defined by the Bulk Dielectric Constant and Atomic Surface Tensions. *J. Phys. Chem. B* **2009**, 113 (18), 6378–6396. <https://doi.org/10.1021/jp810292n>.
- (186) Ribeiro, R. F.; Marenich, A. V.; Cramer, C. J.; Truhlar, D. G. Use of Solution-Phase Vibrational Frequencies in Continuum Models for the Free Energy of Solvation. *J. Phys. Chem. B* **2011**, 115 (49), 14556–14562. <https://doi.org/10.1021/jp205508z>.
- (187) Breneman, C. M.; Wiberg, K. B. Determining Atom-Centered Monopoles from Molecular Electrostatic Potentials. The Need for High Sampling Density in Formamide Conformational Analysis. *J. Comput. Chem.* **1990**, 11 (3), 361–373. <https://doi.org/10.1002/jcc.540110311>.
- (188) Siqueira, G.; Bras, J.; Dufresne, A. Cellulosic Bionanocomposites: A Review of Preparation, Properties and Applications. *Polymers* **2010**, 2 (4), 728–765. <https://doi.org/10.3390/polym2040728>.

- (189) Zhao, G.; Du, J.; Chen, W.; Pan, M.; Chen, D. Preparation and Thermostability of Cellulose Nanocrystals and Nanofibrils from Two Sources of Biomass: Rice Straw and Poplar Wood. *Cellulose* **2019**. <https://doi.org/10.1007/s10570-019-02683-8>.
- (190) Dufresne, A. Nanocellulose: A New Ageless Bionanomaterial. *Materials Today* **2013**, *16* (6), 220–227. <https://doi.org/10.1016/j.mattod.2013.06.004>.
- (191) Bondeson, D.; Mathew, A.; Oksman, K. Optimization of the Isolation of Nanocrystals from Microcrystalline Cellulose by Acid Hydrolysis. *Cellulose* **2006**, *13* (2), 171–180. <https://doi.org/10.1007/s10570-006-9061-4>.
- (192) Liu, J.-C.; Moon, R. J.; Rudie, A.; Youngblood, J. P. Mechanical Performance of Cellulose Nanofibril Film-Wood Flake Laminate. *Holzforschung* **2014**, *68* (3), 283–290. <https://doi.org/10.1515/hf-2013-0071>.
- (193) Trache, D.; Hussin, M. H.; Haafiz, M. K. M.; Thakur, V. K. Recent Progress in Cellulose Nanocrystals: Sources and Production. *Nanoscale* **2017**, *9* (5), 1763–1786. <https://doi.org/10.1039/C6NR09494E>.
- (194) Xu, X.; Liu, F.; Jiang, L.; Zhu, J. Y.; Haagenson, D.; Wiesenborn, D. P. Cellulose Nanocrystals vs. Cellulose Nanofibrils: A Comparative Study on Their Microstructures and Effects as Polymer Reinforcing Agents. *ACS Appl. Mater. Interfaces* **2013**, *5* (8), 2999–3009. <https://doi.org/10.1021/am302624t>.
- (195) Xie, H.; Du, H.; Yang, X.; Si, C. Recent Strategies in Preparation of Cellulose Nanocrystals and Cellulose Nanofibrils Derived from Raw Cellulose Materials. *International Journal of Polymer Science* **2018**, *2018*, 1–25. <https://doi.org/10.1155/2018/7923068>.
- (196) Eyley, S.; Thielemans, W. Surface Modification of Cellulose Nanocrystals. *Nanoscale* **2014**, *6* (14), 7764–7779. <https://doi.org/10.1039/C4NR01756K>.
- (197) Habibi, Y. Key Advances in the Chemical Modification of Nanocelluloses. *Chem. Soc. Rev.* **2014**, *43* (5), 1519–1542. <https://doi.org/10.1039/C3CS60204D>.
- (198) Heux, L.; Chauve, G.; Bonini, C. Nonflocculating and Chiral-Nematic Self-Ordering of Cellulose Microcrystals Suspensions in Nonpolar Solvents. *Langmuir* **2000**, *16* (21), 8210–8212. <https://doi.org/10.1021/la9913957>.
- (199) Abitbol, T.; Kloser, E.; Gray, D. G. Estimation of the Surface Sulfur Content of Cellulose Nanocrystals Prepared by Sulfuric Acid Hydrolysis. *Cellulose* **2013**, *20* (2), 785–794. <https://doi.org/10.1007/s10570-013-9871-0>.
- (200) de Nooy, A. E. J.; Besemer, A. C.; van Bekkum, H. Highly Selective Tempo Mediated Oxidation of Primary Alcohol Groups in Polysaccharides. *Recl. Trav. Chim. Pays-Bas* **2010**, *113* (3), 165–166. <https://doi.org/10.1002/recl.19941130307>.
- (201) Isogai, A.; Saito, T.; Fukuzumi, H. TEMPO-Oxidized Cellulose Nanofibers. *Nanoscale* **2011**, *3* (1), 71–85. <https://doi.org/10.1039/C0NR00583E>.
- (202) Yamamoto, H.; Horii, F.; Hirai, A. Structural Studies of Bacterial Cellulose through the Solid-Phase Nitration and Acetylation by CP/MAS 13C NMR Spectroscopy. *Cellulose* **2006**, *13* (3), 327–342. <https://doi.org/10.1007/s10570-005-9034-z>.
- (203) Yang, Z.-Y.; Wang, W.-J.; Shao, Z.-Q.; Zhu, H.-D.; Li, Y.-H.; Wang, F.-J. The Transparency and Mechanical Properties of Cellulose Acetate Nanocomposites Using Cellulose Nanowhiskers as Fillers. *Cellulose* **2013**, *20* (1), 159–168. <https://doi.org/10.1007/s10570-012-9796-z>.
- (204) Hasani, M.; Cranston, E. D.; Westman, G.; Gray, D. G. Cationic Surface Functionalization of Cellulose Nanocrystals. *Soft Matter* **2008**, *4* (11), 2238–2244. <https://doi.org/10.1039/B806789A>.

- (205) Goussé, C.; Chanzy, H.; Excoffier, G.; Soubeyrand, L.; Fleury, E. Stable Suspensions of Partially Silylated Cellulose Whiskers Dispersed in Organic Solvents. *Polymer* **2002**, *43* (9), 2645–2651. [https://doi.org/10.1016/S0032-3861\(02\)00051-4](https://doi.org/10.1016/S0032-3861(02)00051-4).
- (206) Lasseuguette, E. Grafting onto Microfibrils of Native Cellulose. *Cellulose* **2008**, *15* (4), 571–580. <https://doi.org/10.1007/s10570-008-9200-1>.
- (207) Drumright, R. E.; Gruber, P. R.; Henton, D. E. Polylactic Acid Technology. 6.
- (208) Munim, S. A.; Raza, Z. A. Poly(Lactic Acid) Based Hydrogels: Formation, Characteristics and Biomedical Applications. *J Porous Mater* **2019**, *26* (3), 881–901. <https://doi.org/10.1007/s10934-018-0687-z>.
- (209) Avinc, O.; Khoddami, A. OVERVIEW OF POLY(LACTIC ACID) (PLA) FIBRE. 11.
- (210) Gazzotti, S.; Rampazzo, R.; Hakkarainen, M.; Bussini, D.; Ortenzi, M. A.; Farina, H.; Lesma, G.; Silvani, A. Cellulose Nanofibrils as Reinforcing Agents for PLA-Based Nanocomposites: An in Situ Approach. *Composites Science and Technology* **2019**, *171*, 94–102. <https://doi.org/10.1016/j.compscitech.2018.12.015>.
- (211) Stepanova, M.; Averianov, I.; Gofman, I.; Solomakha, O.; Nashchekina, Y.; Korzhikov-Vlakh, V.; Korzhikova-Vlakh, E. Poly( $\epsilon$ -Caprolactone)-Based Biocomposites Reinforced with Nanocrystalline Cellulose Grafted with Poly(L-Lactic Acid); 500 012021; IOP Conf. Ser.: Mater. Sci. Eng., 2019.
- (212) Ouchi, T.; Kontani, T.; Ohya, Y. Modification of Polylactide upon Physical Properties by Solution-Cast Blends from Polylactide and Polylactide-Grafted Dextran. *Polymer* **2003**, *44* (14), 3927–3933. [https://doi.org/10.1016/S0032-3861\(03\)00308-2](https://doi.org/10.1016/S0032-3861(03)00308-2).
- (213) Ohkita, T.; Lee, S.-H. Effect of Aliphatic Isocyanates (HDI and LDI) as Coupling Agents on the Properties of Eco-Composites from Biodegradable Polymers and Corn Starch. *Journal of Adhesion Science and Technology* **2004**, *18* (8), 905–924. <https://doi.org/10.1163/156856104840516>.
- (214) Labet, M. Grafting  $\epsilon$ -Caprolactone from the Surface of Polysaccharide Nanocrystals, University of Nottingham, 2012.
- (215) Dove, A. P. Organic Catalysis for Ring-Opening Polymerization. *ACS Macro Lett.* **2012**, *1* (12), 1409–1412. <https://doi.org/10.1021/mz3005956>.
- (216) Li, H.; Ai, B.-R.; Hong, M. Stereoselective Ring-Opening Polymerization of Rac-Lactide by Bulky Chiral and Achiral N-Heterocyclic Carbenes. *Chin J Polym Sci* **2018**, *36* (2), 231–236. <https://doi.org/10.1007/s10118-018-2071-5>.
- (217) Nogueira, G.; Favrelle, A.; Bria, M.; Prates Ramalho, J. P.; Mendes, P. J.; Valente, A.; Zinck, P. Adenine as an Organocatalyst for the Ring-Opening Polymerization of Lactide: Scope, Mechanism and Access to Adenine-Functionalized Polylactide. *React. Chem. Eng.* **2016**, *1* (5), 508–520. <https://doi.org/10.1039/C6RE00061D>.
- (218) Artham, T.; Doble, M. Biodegradation of Aliphatic and Aromatic Polycarbonates: Biodegradation of Aliphatic and Aromatic Polycarbonates. *Macromol. Biosci.* **2008**, *8* (1), 14–24. <https://doi.org/10.1002/mabi.200700106>.
- (219) Xu, J.; Feng, E.; Song, J. Renaissance of Aliphatic Polycarbonates: New Techniques and Biomedical Applications: Review. *J. Appl. Polym. Sci.* **2014**, *131* (5), n/a-n/a. <https://doi.org/10.1002/app.39822>.
- (220) Yu, W.; Maynard, E.; Chiaradia, V.; Arno, M. C.; Dove, A. P. Aliphatic Polycarbonates from Cyclic Carbonate Monomers and Their Application as Biomaterials. *Chem. Rev.* **2021**, *121* (18), 10865–10907. <https://doi.org/10.1021/acs.chemrev.0c00883>.

- (221) Azemar, F.; Gimello, O.; Pinaud, J.; Robin, J.-J.; Monge, S. Insight into the Alcohol-Free Ring-Opening Polymerization of TMC Catalyzed by TBD. *Polymers* **2021**, *13* (10), 1589. <https://doi.org/10.3390/polym13101589>.
- (222) Lalanne-Tisné, M.; Eyley, S.; De Winter, J.; Favrelle-Huret, A.; Thielemans, W.; Zinck, P. Cellulose Nanocrystals Modification by Grafting from Ring Opening Polymerization of a Cyclic Carbonate. *Carbohydrate Polymers* **2022**, *295*, 119840. <https://doi.org/10.1016/j.carbpol.2022.119840>.
- (223) Chuma, A.; Horn, H. W.; Swope, W. C.; Pratt, R. C.; Zhang, L.; Lohmeijer, B. G. G.; Wade, C. G.; Waymouth, R. M.; Hedrick, J. L.; Rice, J. E. The Reaction Mechanism for the Organocatalytic Ring-Opening Polymerization of L-Lactide Using a Guanidine-Based Catalyst: Hydrogen-Bonded or Covalently Bound? *Journal of the American Chemical Society* **2008**, *130* (21), 6749–6754. <https://doi.org/10.1021/ja0764411>.
- (224) Katiyar, V.; Nanavati, H. Ring-Opening Polymerization of L-Lactide Using N-Heterocyclic Molecules: Mechanistic, Kinetics and DFT Studies. *Polym. Chem.* **2010**, *1* (9), 1491. <https://doi.org/10.1039/c0py00125b>.
- (225) Brown, H. A.; Waymouth, R. M. Zwitterionic Ring-Opening Polymerization for the Synthesis of High Molecular Weight Cyclic Polymers. *Accounts of Chemical Research* **2013**, *46* (11), 2585–2596. <https://doi.org/10.1021/ar400072z>.
- (226) Stanley, N.; Chenal, T.; Jacquél, N.; Saint-Loup, R.; Prates Ramalho, J. P.; Zinck, P. Organocatalysts for the Synthesis of Poly(Ethylene Terephthalate-*Co*-isosorbide Terephthalate): A Combined Experimental and DFT Study. *Macromol. Mater. Eng.* **2019**, *304* (9), 1900298. <https://doi.org/10.1002/mame.201900298>.
- (227) Nifant'ev, I.; Ivchenko, P. DFT Modeling of Organocatalytic Ring-Opening Polymerization of Cyclic Esters: A Crucial Role of Proton Exchange and Hydrogen Bonding. *Polymers* **2019**, *11* (12), 2078. <https://doi.org/10.3390/polym11122078>.
- (228) del Rosal, I.; Brignou, P.; Guillaume, S. M.; Carpentier, J.-F.; Maron, L. DFT Investigations on the Ring-Opening Polymerization of Substituted Cyclic Carbonates Catalyzed by Zinc- $\{\beta$ -Diketimate $\}$  Complexes. *Polym. Chem.* **2015**, *6* (17), 3336–3352. <https://doi.org/10.1039/C5PY00313J>.
- (229) del Rosal, I.; Brignou, P.; Guillaume, S. M.; Carpentier, J.-F.; Maron, L. DFT Investigations on the Ring-Opening Polymerization of Cyclic Carbonates Catalyzed by Zinc- $\{\beta$ -Diiminate $\}$  Complexes. *Polym. Chem.* **2011**, *2* (11), 2564. <https://doi.org/10.1039/c1py00309g>.
- (230) Jitonnom, J.; Meelua, W. Effect of Ligand Structure in the Trimethylene Carbonate Polymerization by Cationic Zirconocene Catalysts: A “Naked Model” DFT Study. *Journal of Organometallic Chemistry* **2017**, *841*, 48–56. <https://doi.org/10.1016/j.jorganchem.2017.04.023>.
- (231) Kazarina, O. V.; Gourlaouen, C.; Karmazin, L.; Morozov, A. G.; Fedushkin, I. L.; Dagorne, S. Low Valent Al(II)–Al(II) Catalysts as Highly Active  $\epsilon$ -Caprolactone Polymerization Catalysts: Indication of Metal Cooperativity through DFT Studies. *Dalton Trans.* **2018**, *47* (39), 13800–13808. <https://doi.org/10.1039/C8DT02614A>.
- (232) Xu, X.; Luo, G.; Mehmood, A.; Zhao, Y.; Zhou, G.; Hou, Z.; Luo, Y. Theoretical Mechanistic Studies on Redox-Switchable Polymerization of Trimethylene Carbonate Catalyzed by an Indium Complex Bearing a Ferrocene-Based Ligand. *Organometallics* **2018**, *37* (24), 4599–4607. <https://doi.org/10.1021/acs.organomet.8b00599>.
- (233) Venkataraman, S.; Ng, V. W. L.; Coady, D. J.; Horn, H. W.; Jones, G. O.; Fung, T. S.; Sardon, H.; Waymouth, R. M.; Hedrick, J. L.; Yang, Y. Y. A Simple and Facile Approach to

- Aliphatic *N*-Substituted Functional Eight-Membered Cyclic Carbonates and Their Organocatalytic Polymerization. *J. Am. Chem. Soc.* **2015**, *137* (43), 13851–13860. <https://doi.org/10.1021/jacs.5b06355>.
- (234) Gregory, G. L.; Jenisch, L. M.; Charles, B.; Kociok-Köhn, G.; Buchard, A. Polymers from Sugars and CO<sub>2</sub>: Synthesis and Polymerization of a D-Mannose-Based Cyclic Carbonate. *Macromolecules* **2016**, *49* (19), 7165–7169. <https://doi.org/10.1021/acs.macromol.6b01492>.
- (235) Shen, Y.; Yang, X.; Song, Y.; Tran, D. K.; Wang, H.; Wilson, J.; Dong, M.; Vazquez, M.; Sun, G.; Wooley, K. L. Complexities of Regioselective Ring-Opening vs Transcarbonylation-Driven Structural Metamorphosis during Organocatalytic Polymerizations of Five-Membered Cyclic Carbonate Glucose Monomers. *JACS Au* **2022**, *2* (2), 515–521. <https://doi.org/10.1021/jacsau.1c00545>.
- (236) Song, Y.; Yang, X.; Shen, Y.; Dong, M.; Lin, Y.-N.; Hall, M. B.; Wooley, K. L. Invoking Side-Chain Functionality for the Mediation of Regioselectivity during Ring-Opening Polymerization of Glucose Carbonates. *J. Am. Chem. Soc.* **2020**, *142* (40), 16974–16981. <https://doi.org/10.1021/jacs.0c05610>.
- (237) Li, S.; Lu, H.; Zhu, L.; Yan, M.; Kang, X.; Luo, Y. Ring-Opening Polymerization of L-Lactide Catalyzed by Food Sweetener Saccharin with Organic Base Mediated: A Computational Study. *Polymer* **2022**, *246*, 124747. <https://doi.org/10.1016/j.polymer.2022.124747>.
- (238) Yamamoto, Y.; Kaihara, S.; Toshima, K.; Matsumura, S. High-Molecular-Weight Polycarbonates Synthesized by Enzymatic ROP of a Cyclic Carbonate as a Green Process: High-Molecular-Weight Polycarbonates Synthesized .... *Macromol. Biosci.* **2009**, *9* (10), 968–978. <https://doi.org/10.1002/mabi.200900039>.
- (239) Niaounakis, M. Definitions of Terms and Types of Biopolymers. In *Biopolymers: Applications and Trends*; Elsevier, 2015; pp 1–90. <https://doi.org/10.1016/B978-0-323-35399-1.00001-6>.
- (240) Xu, J.; Wu, Z.; Wu, Q.; Kuang, Y. Acetylated Cellulose Nanocrystals with High-Crystallinity Obtained by One-Step Reaction from the Traditional Acetylation of Cellulose. *Carbohydrate Polymers* **2020**, *229*, 115553. <https://doi.org/10.1016/j.carbpol.2019.115553>.
- (241) Girouard, N. M.; Xu, S.; Schueneman, G. T.; Shofner, M. L.; Meredith, J. C. Site-Selective Modification of Cellulose Nanocrystals with Isophorone Diisocyanate and Formation of Polyurethane-CNC Composites. *ACS Appl. Mater. Interfaces* **2016**, *8* (2), 1458–1467. <https://doi.org/10.1021/acsami.5b10723>.
- (242) Trinh, B. M.; Mekonnen, T. Hydrophobic Esterification of Cellulose Nanocrystals for Epoxy Reinforcement. *Polymer* **2018**, *155*, 64–74. <https://doi.org/10.1016/j.polymer.2018.08.076>.
- (243) Sahlin, K.; Forsgren, L.; Moberg, T.; Bernin, D.; Rigdahl, M.; Westman, G. Surface Treatment of Cellulose Nanocrystals (CNC): Effects on Dispersion Rheology. *Cellulose* **2018**, *25* (1), 331–345. <https://doi.org/10.1007/s10570-017-1582-5>.
- (244) Anžlovar, A.; Krajnc, A.; Žagar, E. Silane Modified Cellulose Nanocrystals and Nanocomposites with LLDPE Prepared by Melt Processing. *Cellulose* **2020**, *27* (10), 5785–5800. <https://doi.org/10.1007/s10570-020-03181-y>.
- (245) Azzam, F.; Heux, L.; Jean, B. Adjustment of the Chiral Nematic Phase Properties of Cellulose Nanocrystals by Polymer Grafting. *Langmuir* **2016**, *32* (17), 4305–4312. <https://doi.org/10.1021/acs.langmuir.6b00690>.

- (246) Lalanne-Tisné, M.; Mees, M. A.; Eyley, S.; Zinck, P.; Thielemans, W. Organocatalyzed Ring Opening Polymerization of Lactide from the Surface of Cellulose Nanofibrils. *Carbohydrate Polymers* **2020**, *250*, 116974. <https://doi.org/10.1016/j.carbpol.2020.116974>.
- (247) Lendlein, A. Biodegradable, Elastic Shape-Memory Polymers for Potential Biomedical Applications. *Science* **2002**, *296* (5573), 1673–1676. <https://doi.org/10.1126/science.1066102>.
- (248) Engler, A. C.; Chan, J. M. W.; Fukushima, K.; Coady, D. J.; Yang, Y. Y.; Hedrick, J. L. Polycarbonate-Based Brush Polymers with Detachable Disulfide-Linked Side Chains. *ACS Macro Lett.* **2013**, *2* (4), 332–336. <https://doi.org/10.1021/mz400069u>.
- (249) Kluin, O. S.; van der Mei, H. C.; Busscher, H. J.; Neut, D. A Surface-Eroding Antibiotic Delivery System Based on Poly-(Trimethylene Carbonate). *Biomaterials* **2009**, *30* (27), 4738–4742. <https://doi.org/10.1016/j.biomaterials.2009.05.012>.
- (250) Pendergraph, S. A.; Klein, G.; Johansson, M. K. G.; Carlmark, A. Mild and Rapid Surface Initiated Ring-Opening Polymerisation of Trimethylene Carbonate from Cellulose. *RSC Adv.* **2014**, *4* (40), 20737. <https://doi.org/10.1039/c4ra01788a>.
- (251) Park, S.-A.; Eom, Y.; Jeon, H.; Koo, J. M.; Lee, E. S.; Jegal, J.; Hwang, S. Y.; Oh, D. X.; Park, J. Preparation of Synergistically Reinforced Transparent Bio-Polycarbonate Nanocomposites with Highly Dispersed Cellulose Nanocrystals. *Green Chem.* **2019**, *21* (19), 5212–5221. <https://doi.org/10.1039/C9GC02253H>.
- (252) Jerome, C.; Lecomte, P. Recent Advances in the Synthesis of Aliphatic Polyesters by Ring-Opening Polymerization☆. *Advanced Drug Delivery Reviews* **2008**, *60* (9), 1056–1076. <https://doi.org/10.1016/j.addr.2008.02.008>.
- (253) Kamber, N. E.; Jeong, W.; Waymouth, R. M.; Pratt, R. C.; Lohmeijer, B. G. G.; Hedrick, J. L. Organocatalytic Ring-Opening Polymerization. *Chem. Rev.* **2007**, *107* (12), 5813–5840. <https://doi.org/10.1021/cr068415b>.
- (254) Kamel, S.; Khattab, T. A. Recent Advances in Cellulose Supported Metal Nanoparticles as Green and Sustainable Catalysis for Organic Synthesis. *Cellulose* **2021**, *28* (8), 4545–4574. <https://doi.org/10.1007/s10570-021-03839-1>.
- (255) Vekariya, R. L. A Review of Ionic Liquids: Applications towards Catalytic Organic Transformations. *Journal of Molecular Liquids* **2017**, *227*, 44–60. <https://doi.org/10.1016/j.molliq.2016.11.123>.
- (256) Varzi, Z.; Maleki, A. Design and Preparation of ZnS-ZnFe<sub>2</sub>O<sub>4</sub>: A Green and Efficient Hybrid Nanocatalyst for the Multicomponent Synthesis of 2,4,5-triaryl-1*H*-imidazoles. *Appl Organometal Chem* **2019**, *33* (8). <https://doi.org/10.1002/aoc.5008>.
- (257) Gopiraman, M.; Fujimori, K.; Zeeshan, K.; Kim, B. S.; Kim, I. S. Structural and Mechanical Properties of Cellulose Acetate/Graphene Hybrid Nanofibers: Spectroscopic Investigations. *Express Polym. Lett.* **2013**, *7* (6), 554–563. <https://doi.org/10.3144/expresspolymlett.2013.52>.
- (258) Margelefsky, E. L.; Zeidan, R. K.; Davis, M. E. Cooperative Catalysis by Silica-Supported Organic Functional Groups. *Chem. Soc. Rev.* **2008**, *37* (6), 1118. <https://doi.org/10.1039/b710334b>.
- (259) Dai, W.; Mao, J.; Liu, Y.; Mao, P.; Luo, X.; Zou, J. Commercial Polymer Microsphere Grafted TBD-Based Ionic Liquids as Efficient and Low-Cost Catalyst for the Cycloaddition of CO<sub>2</sub> with Epoxides. *Catal Lett* **2019**, *149* (3), 699–712. <https://doi.org/10.1007/s10562-018-02650-1>.

- (260) Barbarini, A.; Maggi, R.; Mazzacani, A.; Mori, G.; Sartori, G.; Sartorio, R. Cycloaddition of CO<sub>2</sub> to Epoxides over Both Homogeneous and Silica-Supported Guanidine Catalysts. *Tetrahedron Letters* **2003**, *44* (14), 2931–2934. [https://doi.org/10.1016/S0040-4039\(03\)00424-6](https://doi.org/10.1016/S0040-4039(03)00424-6).
- (261) Wilson, B. C.; Jones, C. W. A Recoverable, Metal-Free Catalyst for the Green Polymerization of  $\epsilon$ -Caprolactone. *Macromolecules* **2004**, *37* (26), 9709–9714. <https://doi.org/10.1021/ma048239d>.
- (262) Palard, I.; Schappacher, M.; Belloncle, B.; Soum, A.; Guillaume, S. M. Unprecedented Polymerization of Trimethylene Carbonate Initiated by a Samarium Borohydride Complex: Mechanistic Insights and Copolymerization with  $\epsilon$ -Caprolactone. *Chem. Eur. J.* **2007**, *13* (5), 1511–1521. <https://doi.org/10.1002/chem.200600843>.
- (263) Miao, C.; Hamad, W. Y. In-Situ Polymerized Cellulose Nanocrystals (CNC)—Poly(1-Lactide) (PLLA) Nanomaterials and Applications in Nanocomposite Processing. *Carbohydrate Polymers* **2016**, *153*, 549–558. <https://doi.org/10.1016/j.carbpol.2016.08.012>.
- (264) Bruel, C.; Tavares, J. R.; Carreau, P. J.; Heuzey, M.-C. The Structural Amphiphilicity of Cellulose Nanocrystals Characterized from Their Cohesion Parameters. *Carbohydrate Polymers* **2019**, *205*, 184–191. <https://doi.org/10.1016/j.carbpol.2018.10.026>.
- (265) Nyquist, R. A.; Potts, W. J. Infrared Absorptions Characteristic of Organic Carbonate Derivatives and Related Compounds. 19.
- (266) Marechal, Y.; Chanzy, H. The Hydrogen Bond Network in  $\beta$ -D-Glucopyranose as Observed by Infrared Spectrometry. *Journal of Molecular Structure* **2000**, *48*, 1–14.
- (267) Brossier, T.; Volpi, G.; Vasquez-Villegas, J.; Petitjean, N.; Guillaume, O.; Lapinte, V.; Blanquer, S. Photoprintable Gelatin-Graft-Poly(Trimethylene Carbonate) by Stereolithography for Tissue Engineering Applications. *Biomacromolecules* **2021**, *22* (9), 3873–3883. <https://doi.org/10.1021/acs.biomac.1c00687>.
- (268) Yao, H.; Li, J.; Li, N.; Wang, K.; Li, X.; Wang, J. Surface Modification of Cardiovascular Stent Material 316L SS with Estradiol-Loaded Poly(Trimethylene Carbonate) Film for Better Biocompatibility. *Polymers* **2017**, *9* (11), 598. <https://doi.org/10.3390/polym9110598>.
- (269) Datta, R.; Henry, M. Lactic Acid: Recent Advances in Products, Processes and Technologies — a Review. *J. Chem. Technol. Biotechnol.* **2006**, *81* (7), 1119–1129. <https://doi.org/10.1002/jctb.1486>.
- (270) Martín, C.; Fiorani, G.; Kleij, A. W. Recent Advances in the Catalytic Preparation of Cyclic Organic Carbonates. *ACS Catal.* **2015**, *5* (2), 1353–1370. <https://doi.org/10.1021/cs5018997>.
- (271) Furtwengler, P.; Avérous, L. From D-Sorbitol to Five-Membered Bis(Cyclo-Carbonate) as a Platform Molecule for the Synthesis of Different Original Biobased Chemicals and Polymers. *Sci Rep* **2018**, *8* (1), 9134. <https://doi.org/10.1038/s41598-018-27450-w>.
- (272) Farah, S.; Anderson, D. G.; Langer, R. Physical and Mechanical Properties of PLA, and Their Functions in Widespread Applications — A Comprehensive Review. *Advanced Drug Delivery Reviews* **2016**, *107*, 367–392. <https://doi.org/10.1016/j.addr.2016.06.012>.
- (273) Dove, A. P. Controlled Ring-Opening Polymerisation of Cyclic Esters: Polymer Blocks in Self-Assembled Nanostructures. *Chem. Commun.* **2008**, No. 48, 6446. <https://doi.org/10.1039/b813059k>.
- (274) Jacobsen, S.; Degee, P.; Fritz, H. G. Polylactide (PLA)—a New Way of Production. 9.
- (275) O’Keefe, B. J.; Hillmyer, M. A.; Tolman, W. B. Polymerization of Lactide and Related Cyclic Esters by Discrete Metal Complexes. *J. Chem. Soc., Dalton Trans.* **2001**, No. 15, 2215–2224. <https://doi.org/10.1039/b104197p>.

- (276) Bridging the Gap in Catalysis via Multidisciplinary Approaches. *Dalton Trans.* **2010**, 39 (36), 8354. <https://doi.org/10.1039/c0dt90044c>.
- (277) Kundys, A.; Bialecka-Florjańczyk, E.; Fabiszewska, A.; Małajowicz, J. Candida Antarctica Lipase B as Catalyst for Cyclic Esters Synthesis, Their Polymerization and Degradation of Aliphatic Polyesters. *J Polym Environ* **2018**, 26 (1), 396–407. <https://doi.org/10.1007/s10924-017-0945-1>.
- (278) Chuma, A.; Horn, H. W.; Swope, W. C.; Pratt, R. C.; Zhang, L.; Lohmeijer, B. G. G.; Wade, C. G.; Waymouth, R. M.; Hedrick, J. L.; Rice, J. E. The Reaction Mechanism for the Organocatalytic Ring-Opening Polymerization of L -Lactide Using a Guanidine-Based Catalyst: Hydrogen-Bonded or Covalently Bound? *J. Am. Chem. Soc.* **2008**, 130 (21), 6749–6754. <https://doi.org/10.1021/ja0764411>.
- (279) Chan, J. M. W.; Zhang, X.; Brennan, M. K.; Sardon, H.; Engler, A. C.; Fox, C. H.; Frank, C. W.; Waymouth, R. M.; Hedrick, J. L. Organocatalytic Ring-Opening Polymerization of Trimethylene Carbonate To Yield a Biodegradable Polycarbonate. *J. Chem. Educ.* **2015**, 92 (4), 708–713. <https://doi.org/10.1021/ed500595k>.
- (280) Nederberg, F.; Trang, V.; Pratt, R. C.; Mason, A. F.; Frank, C. W.; Waymouth, R. M.; Hedrick, J. L. New Ground for Organic Catalysis: A Ring-Opening Polymerization Approach to Hydrogels. *Biomacromolecules* **2007**, 8 (11), 3294–3297. <https://doi.org/10.1021/bm700895d>.
- (281) Meimoun, J.; Phuphuak, Y.; Miyamachi, R.; Miao, Y.; Bria, M.; Rousseau, C.; Nogueira, G.; Valente, A.; Favrelle-Huret, A.; Zinck, P. Cyclodextrins Initiated Ring-Opening Polymerization of Lactide Using 4-Dimethylaminopyridine (DMAP) as Catalyst: Study of DMAP/ $\beta$ -CD Inclusion Complex and Access to New Structures. *Molecules* **2022**, 27 (3), 1083. <https://doi.org/10.3390/molecules27031083>.
- (282) Mindemark, J.; Hilborn, J.; Bowden, T. End-Group-Catalyzed Ring-Opening Polymerization of Trimethylene Carbonate. *Macromolecules* **2007**, 40 (10), 3515–3517. <https://doi.org/10.1021/ma0629081>.
- (283) Wei, C.; Kou, X.; Liu, S.; Li, Z. Fast, Selective and Metal-Free Ring-Opening Polymerization to Synthesize Polycarbonate/Polyester Copolymers with High Incorporation of Ethylene Carbonate Using an Organocatalytic Phosphazene Base. *Polym. Chem.* **2019**, 10 (43), 5905–5912. <https://doi.org/10.1039/C9PY01319A>.
- (284) Li, H.; Chang, J.; Qin, Y.; Wu, Y.; Yuan, M.; Zhang, Y. Poly(Lactide-Co-Trimethylene Carbonate) and Polylactide/Polytrimethylene Carbonate Blown Films. *IJMS* **2014**, 15 (2), 2608–2621. <https://doi.org/10.3390/ijms15022608>.
- (285) Han, J.; Branford-White, C. J.; Zhu, L.-M. Preparation of Poly( $\epsilon$ -Caprolactone)/Poly(Trimethylene Carbonate) Blend Nanofibers by Electrospinning. *Carbohydrate Polymers* **2010**, 79 (1), 214–218. <https://doi.org/10.1016/j.carbpol.2009.07.052>.
- (286) Qin, Y.; Yang, J.; Yuan, M.; Xue, J.; Chao, J.; Wu, Y.; Yuan, M. Mechanical, Barrier, and Thermal Properties of Poly(Lactic Acid)/Poly(Trimethylene Carbonate)/Talc Composite Films. *J. Appl. Polym. Sci.* **2014**, 131 (6), n/a-n/a. <https://doi.org/10.1002/app.40016>.
- (287) Zhang, X.; Geven, M. A.; Grijpma, D. W.; Gautrot, J. E.; Peijs, T. “Polymer-Polymer Composites for the Design of Strong and Tough Degradable Biomaterials.” *Materials Today Communications* **2016**, 8, 53–63. <https://doi.org/10.1016/j.mtcomm.2016.05.001>.
- (288) Fliedel, C.; Mameri, S.; Dagorne, S.; Avilés, T. Controlled Ring-Opening Polymerization of Trimethylene Carbonate and Access to PTMC-PLA Block Copolymers Mediated by Well-Defined *N*-Heterocyclic Carbene Zinc Alkoxides: *N*-Heterocyclic Carbene Zn(II) Species

- and Polymerization Catalysis. *Appl. Organometal. Chem.* **2014**, *28* (7), 504–511. <https://doi.org/10.1002/aoc.3154>.
- (289) Socka, M.; Duda, A.; Adamus, A.; Wach, R. A.; Ulanski, P. Lactide/Trimethylene Carbonate Triblock Copolymers: Controlled Sequential Polymerization and Properties. *Polymer* **2016**, *87*, 50–63. <https://doi.org/10.1016/j.polymer.2016.01.059>.
- (290) Toshikj, N.; Robin, J.-J.; Blanquer, S. A Simple and General Approach for the Synthesis of Biodegradable Triblock Copolymers by Organocatalytic ROP from Poly(Lactide) Macroinitiators. *European Polymer Journal* **2020**, *127*, 109599. <https://doi.org/10.1016/j.eurpolymj.2020.109599>.
- (291) Carlmark, A.; Malmström, E. E. ATRP Grafting from Cellulose Fibers to Create Block-Copolymer Grafts. *Biomacromolecules* **2003**, *4* (6), 1740–1745. <https://doi.org/10.1021/bm030046v>.
- (292) Lu, C.; Wang, C.; Yu, J.; Wang, J.; Chu, F. Metal-Free ATRP “Grafting from” Technique for Renewable Cellulose Graft Copolymers. *Green Chem.* **2019**, *21* (10), 2759–2770. <https://doi.org/10.1039/C9GC00138G>.
- (293) Mano, V.; Chimenti, S.; Ruggeri, G.; Pereira, F. V.; de Paula, E. L. P(CL-b-LLA) Diblock Copolymers Grafting onto Cellulosic Nanocrystals. *Polym. Bull.* **2017**, *74* (9), 3673–3688. <https://doi.org/10.1007/s00289-017-1919-0>.
- (294) Renò, F.; D’Angelo, D.; Gottardi, G.; Rizzi, M.; Aragno, D.; Piacenza, G.; Cartasegna, F.; Biasizzo, M.; Trotta, F.; Cannas, M. Atmospheric Pressure Plasma Surface Modification of Poly(D,L-Lactic Acid) Increases Fibroblast, Osteoblast and Keratinocyte Adhesion and Proliferation. *Plasma Processes Polym.* **2012**, *9* (5), 491–502. <https://doi.org/10.1002/ppap.201100139>.
- (295) Li, C.; Sablong, R. J.; van Benthem, R. A. T. M.; Koning, C. E. Unique Base-Initiated Depolymerization of Limonene-Derived Polycarbonates. *ACS Macro Lett.* **2017**, *6* (7), 684–688. <https://doi.org/10.1021/acsmacrolett.7b00310>.
- (296) Mundil, R.; Kayser, F.; Favrelle-Huret, A.; Stoclet, G.; Zinck, P. Organocatalytic Sequential Ring-Opening Polymerization of a Cyclic Ester and Anionic Polymerization of a Vinyl Monomer. *Chem. Commun.* **2020**, *56* (58), 8067–8070. <https://doi.org/10.1039/D0CC02906H>.
- (297) Štěpánek, M.; Raus, V.; Uchman, M.; Šlouf, M.; Látalová, P.; Čadová, E.; Netopilík, M.; Kříž, J.; Dybal, J.; Vlček, P. Cellulose-Based Graft Copolymers with Controlled Architecture Prepared in a Homogeneous Phase. *J. Polym. Sci. A Polym. Chem.* **2011**, *49* (20), 4353–4367. <https://doi.org/10.1002/pola.24876>.
- (298) McKeen, L. Renewable Resource and Biodegradable Polymers. In *The Effect of Sterilization on Plastics and Elastomers*; Elsevier, 2012; pp 305–317. <https://doi.org/10.1016/B978-1-4557-2598-4.00012-5>.
- (299) Aubin, M.; Prud’homme, R. E. Preparation and Properties of Poly(Valerolactone). *Polymer* **1981**, *22* (9), 1223–1226. [https://doi.org/10.1016/0032-3861\(81\)90137-3](https://doi.org/10.1016/0032-3861(81)90137-3).